MATHEMATICAL MODELLING AND HYBRID ACO-PSO TECHNIQUE FOR PV PERFORMANCE IMPROVEMENT

ALI MAHMOOD HUMADA

DOCTOR OF PHILOSOPHY (ELECTRICAL AND ELECTRONIC ENGINEERING) UNIVERSITI MALAYSIA PAHANG

UNIVERSITI MALAYSIA PAHANG

DECLARATION OF THESIS AND COPYRIGHT

Author's full name : ALI MAHMOOD HUMADA

Date of birth : 01 APRIL 1982

Title : MATHEMATICAL MODELING AND HYBRID ACO-PSO TECHNIQUE FOR PV PERFORMANCE IMPROVEMENT

Academic Session : 2015/2016

I declare that this thesis is classified as:

☐ **CONFIDENTIAL** (Contains confidential information under the Official Secret Act 1972)

☐ **RESTRICTED** (Contains restricted information as specified by the organization where research was done)

☑ **OPEN ACCESS** I agree that my thesis to be published as online open access (Full text)

I acknowledge that Universiti Malaysia Pahang reserve the right as follows:

1. The Thesis is the Property of Universiti Malaysia Pahang.
2. The Library of Universiti Malaysia Pahang has the right to make copies for the purpose of research only.
3. The Library has the right to make copies of the thesis for academic exchange.

Certified By:

(Student's Signature)	(Signature of Supervisor)
A4650820	Dr. MOJGAN HOJABRI
New IC / Passport Number	Name of Supervisor
Date :	Date :

SUPERVISOR'S DECLARATION

We hereby declare that we have checked this thesis and in our opinion, this thesis is adequate in terms of scope and quality for the award of the degree of Doctor of Philosophy in Electrical Engineering.

Signature	:	
Name of Supervisor	:	DR. MOJGAN HOJABRI
Position	:	SENIOR LECTURER
Date	:	AUGUST 2016

Signature	:	
Name of Co-supervisor	:	DR. MOHD. HERWAN BIN SULAIMAN
Position	:	SENIOR LECTURER
Date	:	AUGUST 2016

STUDENT'S DECLARATION

I hereby declare that the work in this thesis is my own except for quotations and summaries, which have been duly acknowledged. I also declare that it has not been previously or concurrently submitted for any other degree at Universiti Malaysia Pahang or any other institutions.

Signature	:	
Name	:	ALI MAHMOOD HUMADA
ID Number	:	PEE13002
Date	:	AUGUST 2016

MATHEMATICAL MODELLING AND HYBRID ACO-PSO TECHNIQUE FOR PV PERFORMANCE IMPROVEMENT

ALI MAHMOOD HUMADA

Thesis submitted in fulfillment of the requirements
for the award of the degree of
Doctor of Philosophy in Electrical Engineering

Faculty of Electrical and Electronic Engineering
UNIVERSITI MALAYSIA PAHANG

AUGUST 2016

DEDICATION

To
The spirit of my Mother; My Father with all respect; My wife with love; My lovely children;My brothers and My sisters; and My own people

ACKNOWLEDGEMENTS

In the name of ALLAH, the Most Benevolent, the most Merciful. First of all, I wish to record immeasurable gratitude and thankful fullness to the One and The Almighty Creator, the Lord and Sustainer of the universe, and the Mankind, in particular; peace and blessings of Allah be upon the noblest of the Prophets and Messengers, our Prophet Mohammed and upon his family, companion and who follows him until the last day. First of all I would like to thank My Almighty God, who helped me complete a research and this thesis appearance in this form. Moreover, it is ardently desired that this little effort be accepted by Him to be of some service to the cause of humanity. I am truly and deeply indebted to so many people that there is no way to acknowledge all or even any of them properly. Therefore, I offer my sincerest apologies to anyone I ungratefully omitted from explicit mention.

I would like to express my deep and grateful thanks to my supervisors Dr. Mojgan Hojabri, Dr. Mohd Herwan Bin Sulaiman,and Professor Dr. Saad Mekhlief, for have been constant guidance and encouragement to me throughout a doctoral study. It has truly been a pleasure to work with them, and I appreciate the supervision they have given me to accomplish this work.

I would like to express my sincere gratitude Universiti Malaysia Pahang (UMP) for providing laboratory facilities and financial support under project no. RDU, also I cannot forget the supporting from Universiti Malaya for providing laboratory facilities. It was a wonderful place to work, and they are very dedicated people. I gained so much knowledge an experience from here. Furthermore, special thanks to the academic, management and technical staff in Faculty of Electrical Engineering and the staff of Institute of Postgraduate Studies (IPS) in UMP. I thank all my friends and colleagues for every bit of support; I thank to all Malaysian people whom I met, for their openness, friendship and hospitality.

I am also grateful to Iraqi Ministry of Electricity and Electricity Production Directorate of Salahaldeen for giving me the permission for this study. I don’t forget to thank to Dr. Tamer Khatib for his help and support.

Moreover, special recognition is also given to Dr. Tahseen Ahmad Tahssen from the Tikrit Uninversity, Dr. Khalid G. Mohammed from the Dyala University, and My brother Hussien Mahmood Humada for their appreciated assistance and encouraging.

Lastly and most importantly, to my parents, wife, my children and all family members. I just want to say that I love all of you very much and that I dedicated this thesis to all of you. I am also indebted to my lovely wife for all her sacrifices and patience during the past three years.

ABSTRACT

Photovoltaic (PV) solar energy systems have been playing an important role in the field of energy generation for the last few decades. For such systems to attain the maximum efficiency and reliability in power generation, certain factors should be considered to improve the extracted power. For the purpose, this thesis is focused on some of the most important issues, assisting to improve the extracted power status. One of the most important issue for each PV system is the modelling of PV cells and the modules; the accuracy of these models is the main target in building any PV system. Therefore, this study is focused on developing an accurate and reliable PV model, based on five main parameters; the photocurrent, I_{ph}, the reverse diode saturation current, I_o, the ideality factor of diode, n, the series resistance, R_s, and the shunt resistance, R_{sh}. Performance of these five solar cell parameters (I_{ph}, I_o, n, R_S, R_{sh}) and their effect on both the Current–Voltage (I–V) and Power–Voltage (P–V) characteristic curves, were tested and compared with other models, respectively. Firstly, the photocurrent, I_{ph} effect was studied; the results showed that the increase in the I_{ph} leads to an increase in the maximum power point (MPP) in a prominent way. In addition to this increment in MPP, an increase in the values of I_{sc} and V_{oc} were also observed. With an increase in I_o, a regular increasing mode was observed in MPP, the I_{sc} and V_{oc} values in a similar manner. The value of changing n, showed no effect on I_{sc} and V_{oc} values, but increasing n values lead to a decrease in MPP values in the P–V characteristic curve. The increasing R_s values exhibited a decrease in the value of MPP, while not affecting the the I_{sc} and V_{oc} values, in a smiliar pattern with increasing n values. Finally, the effect of R_{sh} value was also tested; showed a barely noticeable effect on MPP, I_{sc} , and V_{oc} values.

Secondly, a hybrid Ant Colony Optimisation-Particle Swarm Optimisation (ACO-PSO) algorithm was proposed to optimally determine the MPPT parameters. To improve the overall performance of the maximum power point (MPPT) system, the efforts of oscillation filtering and noise suppression were taken in this design, as well as the time response and the settling time. The proposed method is employed to track the global MPP under different shadow conditions, based on three different irradiation levels to test the ability and accuracy of the proposed method. The results of tracking MPP by the proposed MPPT technique showed that the improved method tracked the MPP for all the tested cases with a reasonable accuracy and in a very short convergence time as compared to the P&O method.

Thirdly, to develop a new configuration incorporates ACO-PSO and PID to improve the steady state condition after tracking the MPP. The improved PID controller had contributed in attaining the steady state condition and assuring that there is no oscillation around the MPP. In the comparison with the P&O method, it still has a notable oscillation around the MPP, which results in decreasing the efficiency of the extracted power from the PV system. Moreover, in this study, two 5 kWp PV plants from two different PV technologies (mono-crystalline silicon (c-Si) and copper–indium–diselenide (CIS)) were used to validate the PV model performance based on energy generation, energy efficiency, and the performance ratio. Also, two different models from the literature were used to validate the PV model performance. For all of the validation factors, the energy generated, energy efficiency, and performance ratio of the proposed model showed that it is approximately fitting the real results for both of the CIS and c-Si plants with high level of accuracy than the compared models.

ABSTRAK

Sistem tenaga solar fotovoltaik (PV) memainkan peranan penting dalam bidang penjanaan tenaga bagi dekad yang lalu. Bagi memperoleh kecekapan dan keboleh-percayaan yang tinggi, sistem ini telah dibangunkan untuk memenuhi segala keperluan yang memberi kesan dalam proses penjanaan. Untuk tujuan ini, tesis ini memberi tump-uan kepada isu-isu yang paling penting yang dapat membantu meningkatkan kuasa yang diekstrak. salah satu isu yang penting untuk setiap sistem fv adalah model sel dan modul pv serta ketepatan yang boleh menjadi sasaran utama dalam pembinaan sistem PV. Oleh itu, kajian ini memberi tumpuan dan membina model PV yang tepat dan boleh dipercayai yang terdiri daripada lima parameter iaitu arus foto, I_{ph}, arus tepu diod terbalik, I_o, faktor idealiti diod, n, rintangan siri, R_s, dan rintangan pirau, R_{sh}. Prestasi kelima-lima parameter sel solar (I_{ph}, I_o, n, R_s, R_{sh}) dan kesannya ke atas lengkungan ciri arus-voltan (I-V) dan kuasa-voltan (P-V) telah diuji dan dibandingkan dengan model lain. Pertama sekali, kesan arusfoto, I_{ph} telah dicari di mana keputusan menunjukkan bahawa semakin meningkat $I_{ph,}$ peningkatan kepada titik kuasa maksimum, di samping peningkatan dalam i_{ph} membawa kepada peningkatan kedua-dua I_{sc} dan V_{oc}. Untuk menin-gkatkan I_o yang membawa kepada peningkatan titik kuasa maksimum (MPP) dalam mod biasa, disamping ia dipengaruhi kedua-dua I_{sc} dan V_{oc} dan kadar berat yang sama. Selanjutnya, hasil kesan n menunjukkan bahawa ia tidak memberi kesan sama ada kepada I_{sc} dan V_{oc}. Walaubagaimanapun, keputusan untuk meningkatkan R_s menunjukkan bahawa ia membawa kepada mengurangkan nilai MPP, dan juga tidak menjejaskan I_{sc} dan V_{oc}.

Di samping itu, algoritma pengesan titik kuasa maksimum (MPPT) lebih baik menggunakan pengawal PID yang dioptimumkan dilaksanakan dengan merujuk kepada pengeluaran mekanisme algoritma dan tak ciri-ciri linear konvensional P&O fotovolta sebagai input kepada pengawal PID. Untuk meningkatkan prestasi keseluruhan sistem mppt, usaha penapisan ayunan dan penind-asan bunyi telah diambil dalam reka bentuk ini, serta masa tindak balas dan masa menetap. kaedah yang dicadangkan digunakan untuk mengesan mpp global di bawah keadaan bayang-bayang. Dalam maksud ini, tiga syarat bayangan yang berbeza digunakan untuk menguji keupayaan dan ketepatan kaedah yang dicadangkan. Keputusan mengesan MPP dengan teknik mppt yang dicadangkan menunjukkan bahawa kaedah yang lebih baik dikesan mpp untuk semua kes-kes yang diuji dalam ketepatan yang munasabah dan dengan masa pengenapan yang singkat berbanding dengan kaedah P&O.

Di samping itu, ia adalah titik yang lebih penting bahawa kaedah mppt yang digunakan tidak mempunyai apa-apa ayunan sekitar perbandingan mpp dengan P&O kaedah yang masih mempunyai ayunan ketara di sekitar mpp yang menyokong dalam mengurangkan kecekapan kuasa yang dikeluarkan dari sistem pv. Selain itu, dalam kajian ini, dua loji PV 5 kWp daripada dua teknologi PV yang berbeza (silikon mono-kristal (m-Ki) dan tembaga-indium-diselenide (TID)) telah digunakan untuk mengesahkan prestasi model PV berdasarkan penjanaan tenaga, tenaga kecekapan, dan nisbah prestasi. Untuk semua faktor pengesahan, tenaga yang dihasilkan, kecekapan tenaga, dan nisbah prestasi model yang dicadangkan menunjukkan bahawa ia adalah kira-kira yang menepati keputusan sebenar untuk kedua-dua loji TID m-Ki dengan tahap ketepatan yang tinggi daripada model yang dibandingkan.

TABLE OF CONTENTS

LIST OF TABLES

LIST OF FIGURES

LIST OF ABBREVIATIONS AND SYMBOLS

Symbol	Description
A	PV module area
Eq	the energy gap of solar cell
G	solar irradiance (W/m^2)
G_{STC}	solar irradiance at standard test conditions ($1000W/m^2$)
G▽	the ratio of the generic solar irradiance to the irradiance at STC
I	PV output current
Io	reverse saturation current of the diode (A)
Iph	photogenerated current (A)
$Iph,_{STC}$	photogenerated current at standard rating conditions (A)
I*mpp	coordinates of current at the maximum power point (A)
Isc	short circuit current of the module (A)
$Isc,\ _{STC}$	short circuit current of the module at standard test condition (A)
I_{mpp}	a current corresponding to the maximum power point (A)
$Io,\ _{STC}$	reverse saturation current at standard rating conditions (A)
K	Boltzmann constant (1.381E10 – 23 J/K)
MAPE	mean absolute percentage errors
μ_{Isc}	coefficient of the short circuit current (A/1C)
μ_{Voc}	coefficient of the open circuit voltage (V/1C)
N	diode quality factor
$n,\ _{STC}$	diode quality factor at standard rating conditions
P	power generated by the PV panel (W)
PR	performance ratio
Q	electric charge of an electron (1.602E10 –19 C)

R_s	series resistance (Ω)
R_{so}	reciprocal of the gradient at the open-circuit point
R_{oc}	the inverse of the gradients [(dI/dV)-1] under the open circuit conditions
R_{sh}	shunt resistance (Ω)
R_{sho}	the reciprocal of the gradient at the short-circuit point
R_{sc}	inverse of the gradients [(dI/dV)-1] under the short circuit conditions
SSR	sum of square due to regression
SST	sum of squares due to error
T	PV cell Temperature (K)
T_{STC}	the temperature at standard test conditions (25°C)
$T^{\bigtriangledown}$	the ratio of the generic temperature to the irradiance at STC
V_D	voltage across the diode
V*mpp	coordinates of the voltage at the maximum power point (V)
V_{mpp}	a voltage corresponding to at the maximum power point (V)
Vpv	output volatage of PV panel
Voc	open circuit voltage of the panel
Voc,STC	open circuit voltage of the panel at standard test condition (V)
Va	denotes a random value of the voltage
Vt	thermal voltage value which equal to (q/nKT)

CHAPTER I

INTRODUCTION

1.1 Overview

The conversion of photovoltaic (PV) energy is a process of directly-converting light energy into electric energy. PV power can be generated only when specific conditions are fulfilled. Some of the conditions are proper absorption of solar radiation, the creation of the movable electron/hole pairs, connection of oppositely charged contacts, and a collection of charges. Theoretically, a solar cell is an electrical current source that is driven by a flux of radiation. Substantial research efforts have been exerted to enhance PV power's efficiency and reliability because of the widespread application of PV power as an energy source, owing to the large number of merits over other power systems (Cibira Koščová, 2014b). The PV cell has a typical lifespan of over twenty five years (Khan, 2006). Furthermore, as the system is stationary, it does not require maintenance and can be left unmonitored (Leyva et al., 2006). Besides that, PV systems work in almost any weather conditions and respond immediately to solar radiation (Amin et al., 2009).

Energy generated from PV cells is based on a wide variety of device materials, structures and models that have been developed with recently reported energy conversion efficiencies (Ahmed, 1994; Duffie, 2006; Patel, 2005). Consequently, the ultimate goal of this research effort is to develop a model for PV cells operating under shadow conditions, to maximize the power extracted, and to maintain the steady state condition of the power extracted. The first step in establishing a PV system is to aggregate enough PV cells so that the desired total power levels can be produced. In a typical system, PV cells are first aggregated into panels (modules), and then multiple panels are aggregated into an array (Bube, 2012).

Moreover, when PV system operates under different temperature and illumination levels, each PV panel will generate a unique characteristic curve, since the output power of PV panel varies as a function of the output voltage. Each PV panel has a unique Maximum Power Point (MPP). At the MPP, the corresponding voltage changes as environmental temperature or irradiation level varies. Thus, it is necessary to track the PV array's MPP in order to maintain a high power efficiency output of the PV generation system. The steady state condition is also vital to ensure power stability after tracking the MPP. As the installation cost of PV array is high, the process of tracking MPP maximises the efficiency of PV energy systems in the PV conversion process. All in all, the Maximum Power Point Tracking (MPPT) process and the maintained steady state condition help in reducing the cost of system; while enhancing the conversion efficiency and reliability.

This chapter presents the introduction of the thesis. It describes the overview of the study then the problem statements, objectives, scope of study and thesis organisation.

1.2 Problem Statements

Accuracy of PV modelling is an important task for the PV system design, control and planning. To design a PV system, understanding the environmental effects on its performance is important, especially the array's output power under specific climate situations. The main problem in any PV model is building accurate mathematical equations for PV parameters. Many studies have developed PV models based on different operational parameters. However, the five parameter model is the most accurate as compared to the other models (Humada et al., 2016). Therefore, all available PV parameters considered in the current research are applied to enhance the reliability of the developed PV model. Furthermore, the current study is focused on the accuracy of these dependant parameters. The parameters included are I_{ph}; photo generated current, I_o; diode ideality factor, R_s; the diode saturation current, n; series resistance, R_{sh}; shunt resistance.

Furthermore, ensuring that PV modules have an accurate model is also essential in developing the model-based MPPT algorithms (De Brito et al., 2013; Ishaque Salam, 2011a; Villalva Gazoli, 2009). The MPPT controller is required to enhance the PV system's efficiency by ensuring continuous maximum power supply by the PV module although weather condition changes. Many studies have developed different MPPT techniques, but each method has its own restrictions. In some methods, it has very slow convergence speed, whereas some others cannot hold the effect of shadow weather conditions. Shading effect is one of the major problems for PV array within a distributed generation system, especially for large scale installations. In general, the total efficiency of PV generation and conversion will reduce due to partial shading. Therefore, the necessity of employing an efficient MPPT method, which is able to exceed the shadow weather effect, is vital. Apart from that, it is also important to ensure that the extracted power sent to the load side is operating in a steady state condition and without any transient around the MPP to ensure the reliability of the PV system's operation.

1.3 Thesis Objectives

The aim of this study is to develop an accurate PV model that is able to emulate the PV system characteristics and then to develop MPPT method with the sole purpose of improving the extracted power from a PV system. This thesis also aims in maintaining the steady state condition for PV system reliability. Therefore, the objectives of this study are outlined as follow:

I. To develop an accurate mathematical PV model to emulate the PV characteristics under different shadow conditions.
II. To develop ACO-PSO optimization technique for MPPT parameters identifications.
III. To develop a new configuration which incorporates ACO-PSO and PID to improve the steady state condition after tracking the MPP.

1.4 Scope of Study

This thesis attempts to develop an accurate mathematical model for a PV array and charactarise the parameters of this model at different temperature and irradiance levels. It presents an improvement in the performance of the studied parameters and their effects on the P–V and I–V characteristics, by validating and comparing the real results with related models from previous studies. In addition to that, this model was employed to develop a MPPT method. The actual performance of the proposed PV model was validated with two real PV plants (cooper indium diselenide (CIS) PV plant and mono crystalline silicon (c-Si) PV plant, of the same size; 2 × 5kWp) installed at Bangi City,Selangor, and other models from previous studies. The following aspects illustrate the scope of this study.

I. The main five parameters of PV model are considered different from earlier studies; where some parameters were kept constant. In some studies, they were totally ignored. This affected the accuracy of the model.
II. Performance of these parameters in standard test condition (STC) is also studied and their effects on the values of MPP, I_{sc}, and V_{oc} are also calculated.
III. An improved MPPT method is included in this study to demonstrate the ability of extracting the maximum available power point at any climate condition. Three different shadow conditions are included in the analysis.
IV. Realising steady state condition has also been considered in order to achieve system reliability, by employing an optimal PID controller, based on a hybrid ACO-PSO algorithm.
V. Reliability of the proposed model is validated on the basis of energy generated values, energy efficiency curves, and performance ratio. These are considered for all proposed model, real PV system and also two different models from literature to ensure the robustness of the used model.

1.5 Thesis Organization

This thesis is arranged in a manner that clarifies the subject from all aspects; it provides details on the PV modelling, a method to extract the maximum available power, and to maintain the steady state condition of the extracted power. The PV model performance was also validated based on two real PV modules in order to authenticate the objectives. The thesis contains five chapters. Chapter I elaborates introduction of the thesis in the specified manner; introduction, the problem statement, the objectives, and the scope of study.

Chapter II discusses the modelling and characterisation methods as previously studied. This chapter also discusses and reviews PV parameter extraction methods, especially the most used and robust methods, which are classified based on all available number of parameters. In addition to that, the MPPT method's usage based on normal and shadow conditions are also discussed briefly.

Chapter III depicts the method of calculating the mathematical equations of the proposed model, based on all five PV parameters. Secondly, the model is then applied in the proposed MPPT technique. This MPPT technique is later implemented to calculate the MPP for different shadow conditions to prove the robustness of this method. Chapter III also employed an optimal (ACO-PSO) PID controller to carry out the steady state condition for the extracted power. Finally, an effective validation for the proposed model is also discussed in this chapter.

Chapter IV debates the results and discussion of modelling, MPPT technique, and steady state condition. Firstly, methods for finding model parameters are discussed. After this, the I-V and P-V curves of other models are compared. Furthermore, results and discussion of the proposed MPPT method under three different shadow conditions are presented to verify the robustness of the methods used. At the same time, steady state condition is displayed on the output power curve. Finally, this chapter studies the performance of the PV model, based on the two most robust PV modules (CIS and c-Si) and two related PV models from previous studies.

In chapter V, conclusion and recommendations for the future work are discussed. The contributions of current thesis are also presented in this chapter.

CHAPTER II

LITERATURE REVIEW

2.1 Introduction

Significant amounts of research work have been carried out to enhance solar cells' efficiency. This is because solar energy has a widespread use today. Modelling and characterising solar PV arrays are important tasks in the design of solar PV system (Brano et al., 2010). The designs of solar PV system need to ensure the reliability and flexibility of the model used. The most important and effective aspect of the PV model is its electrical characteristics and its reliability with the changing climate conditions (Brano et al., 2010; Kadri et al., 2012; Nguyen Lehman, 2006).

Therefore, the solar PV system's design should understand the environmental effects on performance, particularly the array's output power under numerous shading conditions. The most important issue in each PV model is the ability to simulate the electrical behaviour of solar PV array in different changing environmental factors: temperature and solar irradiance. Moreover, the understanding of PV characteristics helps in implementing accurate and reliable MPPT methods. These MPPT methods are becoming essential in the installation of any PV system due to its contribution in increasing the extracted power from PV module.

2.2 Operation of a PV Module

A PV cell is a PV system's most important power conversion unit (Grätzel, 2005) and is the component that produces electricity from solar energy. Although a single cell is capable of generating significant current, it operates at an insufficient voltage for typical applications. To obtain a higher voltage, the cells should be connected in series and encapsulated into a PV module panel. These modules show similar electrical behaviour of individual cells. Similarly, modules are connected in parallel and series to form a PV array. The arrays generate direct current (DC) power that will be converted to alternating current (AC) power using inverters.

The operation of PV cell is on the basis of the ability of a semiconductor to convert sunlight into electricity through the PV effect (Bube, 2012; Grätzel, 2005). Once the sunlight is incident on the solar cell, the photons can either be reflected, absorbed or passed through it. Only the absorbed photons contribute to the generation of electricity. For a photon to be absorbed, its energy must be larger than the band gap of the solar cell, which is the difference in energy levels between valence and conduction band in the cell. The absorbed photons generate pairs of mobile charged carriers (electrons and holes) which are then separated from the device structure (such as a p-n junction) and produce electrical current.

Therefore, the p-n junction can be made to operate as a PV cell (Tang Sargent, 2011) Figure 2.1. The p-n junction responds to the incident light photons and generates an electric current, as shown in Figure 2.2. The influence of arriving photon energy produces a minority current effect (Tang Sargent, 2011). These photons generate free electron-hole carriers, which are attracted towards the junction. The electron and hole charges travel in opposite directions and set the direction of the PV current as shown in the Figure 2.2 (Tang Sargent, 2011). The electron flow from n-type silicon to p-type silicon in the circuit (Tang Sargent, 2011). The current generated varies with the light intensity.

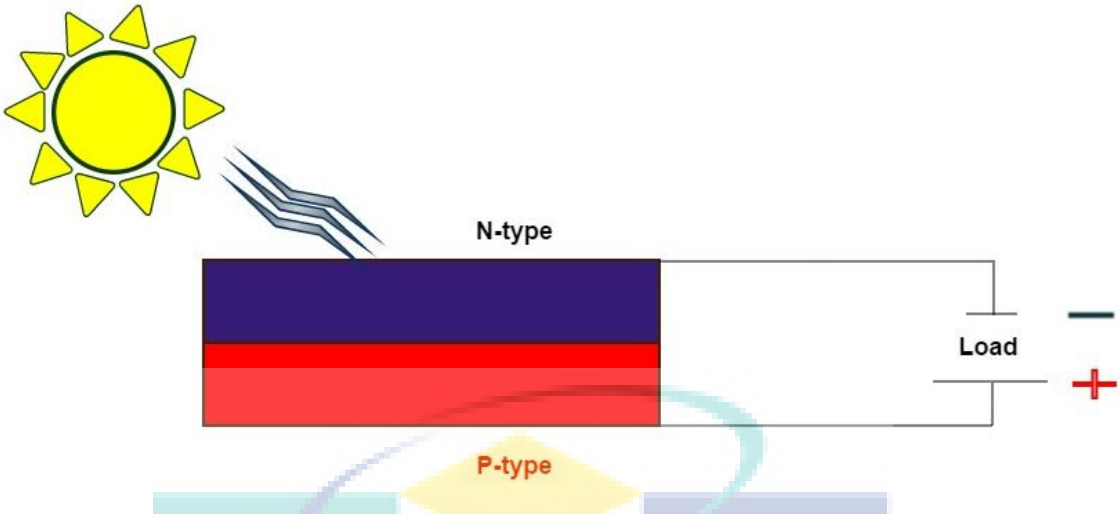

Figure 2.1. Response of PV cell to the incident light and generating the current

The sign convention used for current and voltage in PV is to indicate that the photocurrent is always positive. The light generated current, which is termed as photocurrent, is represented as I_{ph}, the diode current as I_D, the net current and the terminal voltage of solar cells as I_{cell} and V_{cell} respectively. The net current I_{cell} available from the solar cell is the current source.

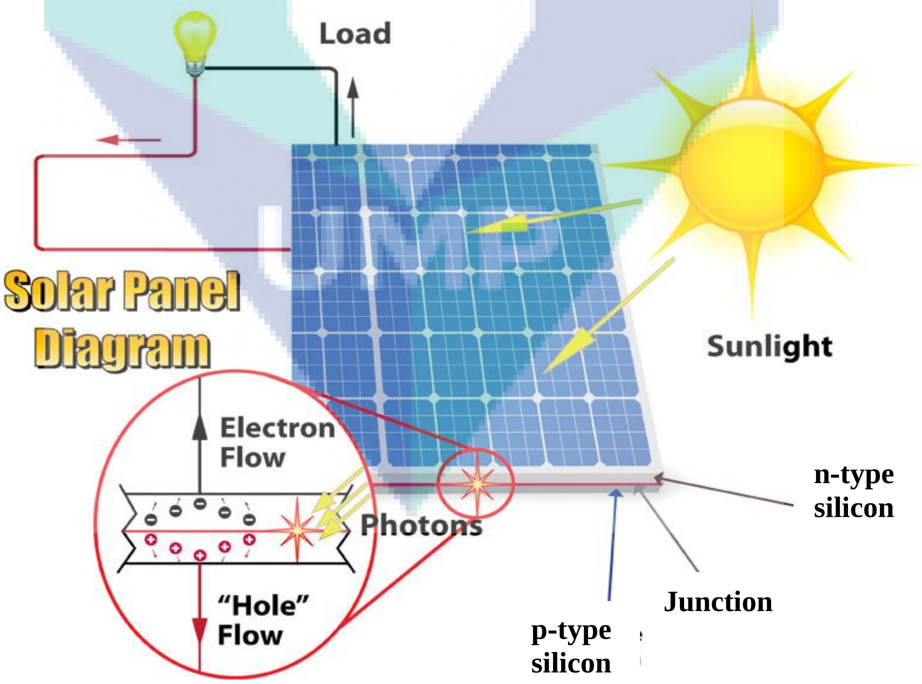

Figure 2.2. Operation of generation electric current and direction of the electrons through a circuit.

2.3 Modelling and Simulation of PV Modules

One of the most important observations is that solar cells exhibit a non-linear output characteristic and this is represented in three quadrants of its I–V curve as shown in Figure 2.3. Practically, the solar cell generates power in the 1st quadrant, but dissipates power as load in the 2nd and 4th quadrants of its I–V curve. In the 1st quadrant, the solar cell's I–V curve varies with solar irradiance and ambient temperature.

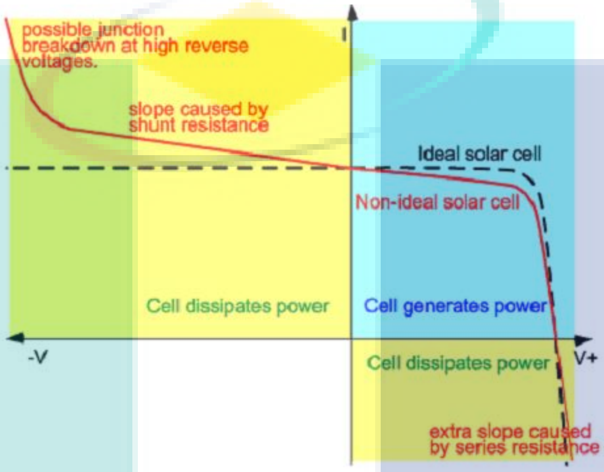

Figure 2.3. General I–V characteristic curve for a PV solar cell.

PV modules are usually comprised of a number of solar cells with identical characteristics. Similarly, a number of PV modules are used to build a PV array and these arrays are connected together to make a PV farm, as shown in Figure 2. 4. Ideally, a PV array will have a similar non-linear I–V curve as shown in Figure 2.3. However, in real working conditions, since PV modules might work at different irradiances, ambient temperatures and even under faulty conditions, the I–V curve of a PV array will be completely different. Also, the interconnection of PV modules becomes difficult to predict. So, these complexities bring challenges to existing modelling approaches of PV arrays.

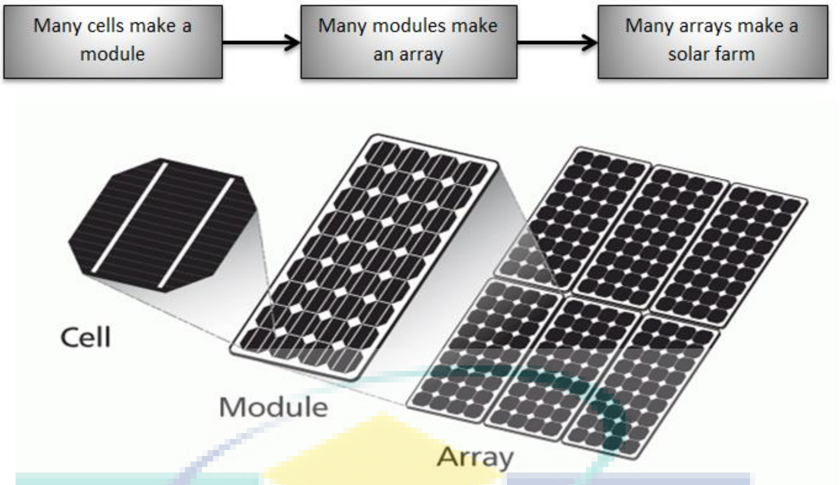

Figure 2.4. A PV array structure and components.

In this purpose, numerous researches used PV system modelling and characterisation (Akkaya Kulaksiz, 2004; Cibira Koščová, 2014a; Dizqah et al., 2014; Ishaque Salam, 2011b; Ismail et al., 2013a; Khezzar et al., 2014; Laudani Fulginei, 2014). However, these models are either too simple to be accurate enough for the power tracking and extraction purposes (Akkaya Kulaksiz, 2004), are not tested in all weather conditions and for a large PV system (Ishaque Salam, 2011b; Khezzar et al., 2014), or are complicated in some studies (Ismail et al., 2013b).

For example, a study devised an approach to find model parameters for PV system's single-diode model (Dizqah et al., 2014). The effect of temperature and irradiation on these parameters was taken into consideration. But, a method to calculate the model parameters in the event of instantaneous variation in temperatures and irradiances were not taken into consideration and argued. PV modelling was built based on simple procedures to obtain PV system parameters quickly and easily (Cibira Koščová, 2014a). This model is mainly used to characterise these parameters by employing MATLAB/Simulink. Nevertheless, this model's employability is restricted since the model didn't take rapid climate change into consideration. Later, in 2014, modelling improvement for four parameter model was conducted by (Khezzar et al., 2014). Consequently, this study aims to build a model that fits the varying current–voltage qualities (I–V) under different working conditions.

However, the absence of pragmatic examination in this research rendered the validation feeble. In addition to that, a circuit-level PV array model is built in SPICE, for power electronics simulation in a study done by (Jiang et al., 2011), but this paper didn't discuss or consider the effect of shadow conditions on the PV modelling and characterisation.

The modelling of a PV module involves the calculation of the I–V and P–V characteristics. Nevertheless, it is complex and difficult to make models representing different temperature and irradiance conditions that can evaluate the parameters in an illustrative manner (Ciulla et al., 2014; Keogh et al., 2004). The understanding of characteristic of solar cells is essential for designing and dimensioning a PV power supply. This also permits the development of creative and high–performances PV systems, matching system-components and approving the assessment of the behaviour of complete system in different conditions. One of the most complicated issues in PV characterisation is the number of dependent PV parameters. Some researchers built their models based on five PV parameters (Brano et al., 2010; Celik Acikgoz, 2007; Orioli Di Gangi, 2013), while others built their models based on four parameters (Celik Acikgoz, 2007; Chegaar et al., 2006; Ishaque Salam, 2011b), three parameters (Garrido-Alzar, 1997; Khatib et al., 2013), two parameters (Bowden Rohatgi, 2001; Ortiz-Conde et al., 2006), and one-parameter model (El-Adawi Al-Nuaim, 2001; Kim Choi, 2010).

2.4 Trends of PV Models

This section gives a summary of the two existing PV models, namely the single- and double-diode model, to depict the property of each model alone. When introducing a streamlined form of the models, certain presumptions were made to design research applications with respect to the solar system. In both models, the number of diodes that represents the immersion current differs.

2.4.1 Single-Diode PV Cell Model

A strong, non-illuminated, single-junction PV cell acts particularly like a semiconductor diode. Equation (2.1) below describes the characteristics of a simple diode, and is shown in Figure 2.5:

$$I_D = I_o\left[\exp\left(\frac{qV_D}{nkT}\right) - 1\right] \tag{2.1}$$

Where q is the electric charge of an electron (1.602×10^{-19} C); I_o is the reverse saturation current of the diode; k is the Boltzmann constant (1.381×10^{-23} J/K); V_D is the voltage across the diode; T is the diode temperature; and n is the ideality factor (emission coefficient or quality factor), that values normally ranging between 1 to 2 (in some occasions, it can be higher than 2), as per the semiconductor material and fabrication process. The ideality factor, n is omitted as it is always approximated to be close to 1. Upon illuminating the semiconductor diode, a photo-generated current, I_{ph} will be created. This will lead to a vertical translation of the I–V curve of an amount that is almost absolutely connected to the incident energy's surface density.

Hence, a perfect cell can be illustrated as a current generator which is connected to a parallel diode, with an I–V characteristic depicted in the equation as follow (Shockley, 1953):

$$I_{pv} = I_{ph} - I_o\left[\exp\left(\frac{qV_D}{nkT}\right) - 1\right] - \frac{V_D}{R_{sh}} \tag{2.2}$$

Where $V_D = V + R_S I_{pv}$, where I_{pv} is the output current.

Equation (2.2) is only a simple theoretical definition because it does take into account the effects brought by the existence of electrodes, the one above and the other below the semiconductor layer, that are needed to gather the charges layering the intercepting surface to a certain level.

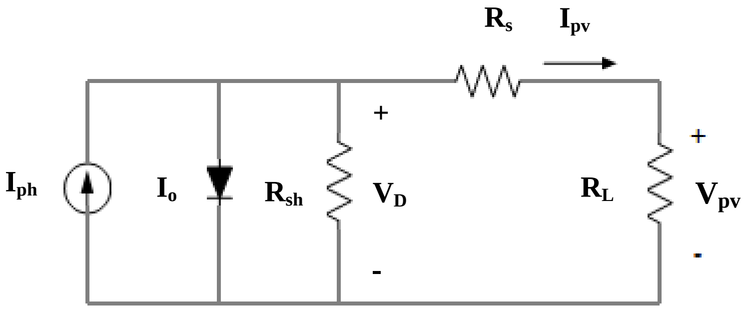

Figure 2.5. One-diode model equivalent circuit.

2.4.2 Double-Diode PV Cell Model

Rauschenbach (Wolf Rauschenbach, 1963), found that the single-diode and the overall impact of multiple elementary diodes that are neighbouring to each other and are dependably distributed along the surface between the two layers of the semiconductor creating a photocurrent in PV cell. Current passes through each elementary diode while flowing over the semiconductor layers along an alternate way, set apart by various electric resistances and lessening in voltage.

The transverse component of the current, I_{ph}, running parallel to the surface of the cell, each elementary diode must differ in order that every diode has a distinct I–V characteristic. Since these diodes are thought to be in parallel, their combination will decide the overall I–V characteristic of the PV cell. The transverse electrical resistance enormously surpasses the electrical resistance with regards to the direct I_{ph} component. The transverse component of the current I_{ph}, that happens only in a real PV cell, which dissipates high energy that extensively decreases the solar cell's conversion efficiency.

Wolf Rauschenbach, (1963), derived a simplified equal circuit, as illustrated in Figure 2.6, which only comprises of two diodes, two resistors and a current generator, mulling over the dissipative impacts depicted above and the presence of any construction defects. Resolving the equivalent circuit above brought about the insinuated expression of current, I_{pv} as follow:

$$I_{pv} = I_{ph} - I_{o1}[\exp(\frac{qV_D}{n_1 kT}) - 1] - I_{o2}[\exp(\frac{qV_D}{n_2 kT}) - 1] - \frac{V_D}{R_{sh}} \quad (2.4)$$

Where I_{ph} is proportional to the irradiance (Shockley, 1953); I_{o1} and I_{o2} are the diode saturation currents of the two diodes, R_s and R_{sh} are the parallel and series resistances, respectively; and n_1 and n_2 are the ideality factors of the two diodes. As it can be clearly seen in Figure 2.6, in order to solve Eq. (2.4), the parameters (I_{ph}; n_1; n_2; I_{o1}; I_{o2}; R_s; and Rsh) should be identified first. In more thorough terms, Figure 2.7, which represents the slope of the curve before and after the "knee" of the I-V characteristic curve, is modified by the resistors R_{sh} and R_s, individually, while the ebb and flow is changed by the proportion amongst I_{o1} and I_{o2} (McEvoy et al., 2003). The calculation of these parameters is challenged by the implicit form of the equation and by the existence of two exponential terms although it that can be solved mathematically. There are couple of extensive models in the scientific literature accessible that permit the algorithm to be coded with a specific end goal to recover these parameters. In addition to that, particular assumptions made while building these are single-cell models limit their application.

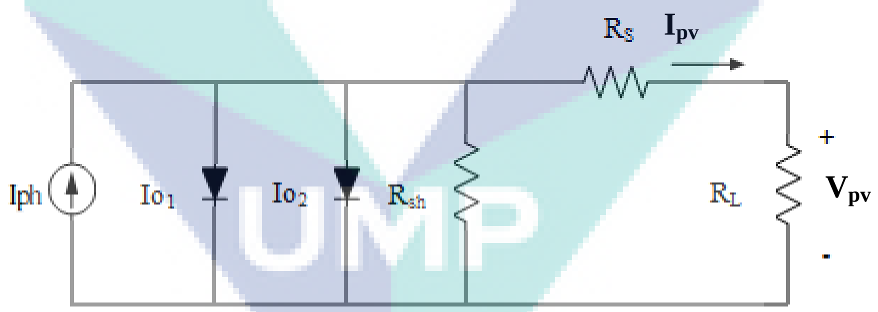

Figure 2.6. Two-diode model equivalent circuit.

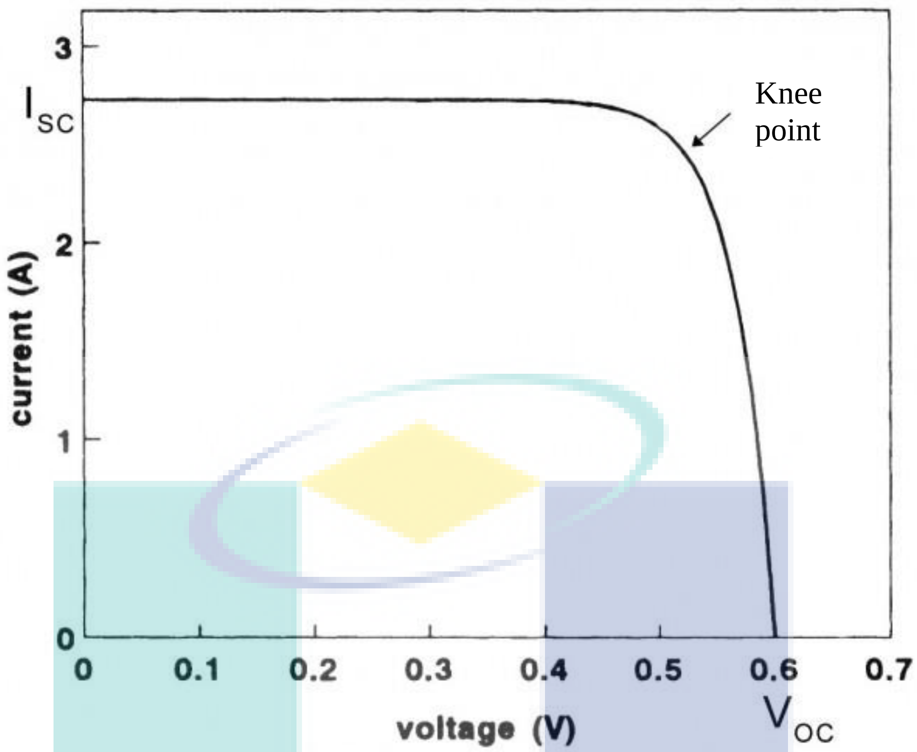

Figure 2.7. I-V characteristic curve and the knee point.

2.5 Extraction of PV Model Parameters

In the process of extracting the PV parameters, some researchers have focused on the application of several correlations which are not based on any particular electrical model (Akbaba Alattawi, 1995; Ortiz-Conde et al., 2006), since there are only five unknown parameters available. As per the traditional technique, the photocurrent, I_{ph} is dictated by the irradiance, I_o, which is impacted by the cell's temperature, while n, R_s and R_{sh} stay steady. A few studies have come up with recommendations for development and/or simplification that allows the five parameters (I_{ph}, n, I_o, R_s, and R_{sh}) to be identified as indicated by the performance data of modules supplied by the manufacturers. However, some other researches have focused on fewer (ranging from four to one) parameters. This study will review the available literature on some of the ideal models in order to assess the electrical behaviour of single and double-diode model based on the number of DC parameters of PV solar cells. Nevertheless, the single-diode model is the one that is used most extensively as it is the simplest model that adequately describes the characteristic behaviour of most solar cells. The methods to extricate the solar cell parameters are briefly reviewed and condensed as follow.

2.5.1 Five-Parameter Models

The solar cell model is usually based on five parameters (I_{ph}, I_o, n, R_s, and R_{sh}). The procedure of extracting the parameters differs from one model to another. Some models were based on the single diode model while others on the double diode model. In this part, some of the best explicated models considered for the assessment of electrical characteristics are based on the quantity of DC parameters of PV cells, in both, single and double-diode.

Brano et al., (2010) devised a single-diode model to determine the parameters of solar cells. The computed I–V characteristics and those given by manufacturers were both utilised to acquire the five parameters, R_s, R_{sh}, n, I_{ph} and I_o. Therefore, in this model, all five parameters had been considered and the effect of irradiance and temperature were clearly shown on the diode's reverse current parameter, I_o rather than other parameters. The fast change in irradiance value, has shown a clear effect on the I-V characteristic curve. The current method produced Eqs. (A.1 to A.5) (appendix A) to develop the model.

As a worthy merit of this model, it considers ebbs and flows in external conditions, which will lead to an exact estimation of the extracted parameters. Another important observation is the ability to determine value of irradiance and temperature of the current I_o (G, T) using Eq. (A.5). On the other hand, the lack of getting irradiance and temperature sample values in any fast changing in weather conditions made the parameters extraction operation more difficult.

The model proposed by (Celik Acikgoz, 2007) to derive the five parameters, I_{ph}, I_o, R_s, R_{sh} and n, at a particular temperature and solar irradiance level being limited by V_{oc}, I_{sc}, V_{mp} and I_{mp}, as per the definitions of R_{so} and R_{sho}, as shown in Eq. (A.6) and (A.7) (appendix A), where R_{so} is the gradient's reciprocal at the open-circuit point, whereas R_{sho} is the gradient's reciprocal at the short-circuit point.

The module manufacturers usually will not provide these resistance values. Blas et al. (2002) proposed R_{so} values between 0.30 to 0.33 and R_{sho} values between 50 to 170 Ω, as per the experimental curves' gradients (De Blas et al., 2002). As per the sensitivity analysis of the five-parameter model for R_{so} and R_{sho}, the model is adequately capable of predicting the existing values for a wide array of range of R_{so} and R_{sho} values. The five important parameters could be computed through Eqs. (A.8) to (A.14) (Appendix A). Apart from the reference values, the values of I_{sc} and V_{oc} at temperatures and solar irradiance levels can be computed from Eqs. (A.13) and (A.14).

Therefore, the model is employed in the following manner: Eq. (A.13) and (A.14) are utilised to calculate I_{sc} and V_{oc} based on the respective reference values, and they are altered concurrently to suit environmental conditions. Eq. (A.8 to A.12) are utilised to compute the five parameters, which are successively used in Eq. (2.2), linking the cell's current to its voltage. From Eq. (2.2), the measured voltage values are employed to compute the cell's current.

The I-V characteristics calculation is used to calculate five parameter values directly. Therefore, the R_{so} and R_{sho} values can be calculated at any sample time. This is the benefit of using this model. However, the approximation of the R_{so} and R_{sho} results in low accuracy level when validating the five parameters.

Chan et al., (1986) devised analytical five-point method to evaluate five parameters of PV cells (Chan et al., 1986). The single-diode model is utilised to determine the parameters, namely I_{ph}, I_o, n, R_s and R_{sh}, under illumination using values of I_{sc}, V_{oc}, I_m, V_m, the gradient at the open-circuit point R_{so}, and the gradient at the short-circuit point R_{sho}, that are obtained through the I–V characteristic. The values of R_{sho} and R_{so}, which are given by Eq. (A.6) and (A.7), (Appendix A), individually, can be computed by fitting the I–V characteristic linearly around the short-circuit current point and the open-circuit voltage point.

The diode's ideality factor, n can be calculated using Eq. (A.15) (Appendix A). The other parameters, namely I_o, R_s and I_{ph}, can be obtained from Eq. (A.14 to A.16) (Appendix A). The I-V characteristic of the PV modules was tested through a microcomputer, based on data logging system. In order to maximise data sampling storing properly, the testing and calculation process needs to have a big memory to store the collected data. This increases the difficulty in getting an accurate value of the extracted parameters by this model.

Brano (2013) designed a technique to identify the solar cell's parameters. (Brano Ciulla, 2013).The strategy needs no further improvements or assumptions for extricating five parameters utilising Eq. (2.2) (Appendix A) and is constructed only in light of the typical technical data for a single-diode model under Standard Test Conditions (STC).

The I_{sc} values can be utilised in this model to generate the first equation. The voltage is zero at the short circuit current point. Substituting these figures into Eq. (2.2) will generate Eq. (A.22). Then, the V_{oc} values can be utilised to arrive at the second equation. The current is zero at the open circuit voltage point. Substituting these values into Eq. (2.2) will produce Eq. (A.23). The data of MPP, where $V = V_{mpp}$ and $I = I_{mpp}$ can be used to derive the third equation, and substituting these values into Eq. (2.2) will produce Eq. (A.24). Then, the fourth equation can be generated from Eq. (A.25) in terms of V, where $V = V_{mpp}$ and $I = I_{mpp}$. Finally, the model's fifth equation can be generated from the power of (V *Eq. (2.2)), also in terms of V, where $V = V_{mpp}$ and $I = I_{mpp}$.

The model is built, starting at a random point and then crossing over the neighbours. The initial estimates of I_L, I_o, R_s, R_{sh} and n may be chosen from a scope of relatively huge arbitrary values. The process can be rehashed until the residuals for the equations, f1(I_{ph}, I_o, R_s, R_{sh} and n) =0,..., f5(I_{ph}, I_o, R_s, R_{sh} and n) = 0, are virtually zero. The automated use of a non-linear optimisation solver, which does not require coding, can be obtained from almost any spreadsheet software (including open source). The Generalised Reduced Gradient (GRG) algorithm is the standout amongst the strongest non-linear programming methods, and is typically utilized by these solvers to work out optimisation problems (Lasdon et al., 1978). This method is selected as it is easy to be used with the system in Eq. (A.27) by using an ordinary office application without having to write out a code line.

Five different mathematical Eq. (A.22) and (A.23) (Appendix A) were devised to compute the correct values for the five parameters. When these equations are solved concurrently, the five unknown parameters can be identified. The significance of applying the standard test condition in the model is beneficial in obtaining the parameter values directly in standard conditions. However, any change in weather conditions is not yet considered in this model, which makes it inactive for all conditions and valid only for standard test condition.

Haouari Merbaha et al., (2005) devised a new method to derive the five parameters of solar cells (R_S, $G_{sh} = (1/R_{sh})$, I_L, n_1 and n_2, and I_{o1} and I_{o2}) through double-diode model (Haouari-Merbah et al., 2005). The line of resistance, having a gradient of V_{oc}/I_{sc}, divides the I–V characteristic of a solar cell, measured under illumination conditions into two locales, with one area being near the short circuit current and the other being near to the open circuit voltage. Therefore, the first area of the I–V characteristic is a function of the current, whereas the second area is a function of the voltage. Eq. (2.3) and can be modelled as Eqs. (A.28) and (A.29) (Appendix A) for the first and second areas, individually.

The first area is represented by the superscript "*f*", the second region by the superscript "*s*", and the curvature of the I–V characteristic by $h^f(I, V)$, with I being for "*s*" (Ouennoughi Chegaar, 1999). In order to find out the coefficients (I_{sc}; G_{fsh}), the first area should be in close proximity with the short circuit with Eq. (A.28), whereas to identify the coefficients (V_{oc}; R_{ss}), the second area should be in close proximity with the open circuit with Eq. (2.29). In order to find out the set of parameters (I_{ph}, G_{sh1}/R_{sh}, I_{od}, I_{or}, and R_s), the system should be solved by utilising five non-linear equations acquired for I_{sc}, G_{shs}, V_{oc}, R_S and I_o, with the curve crossing over the boundary point, which is around the MPP (Haouari-Merbah et al., 2005). The theoretical values n_{di} and n_{r2} employ the value assumed for the ideality factors of the diode. The set of parameters should first be equivalent to zero and the iterative procedure is led once the parameters converge in order to solve the system.

The method is dependent on the calculation of I–V characteristics in the region close to I_{sc} when the V_{oc} is zero at the first time, and in the region close to V_{oc} when the I_{sc} is kept zero at other times. It results in making the extraction operation confined to only two regions, enabling significant extraction of parameters. Nonetheless, resetting the values of I_{sc} or V_{oc} to zero, is active only in case of R_s, R_{sh}, and n. Meanwhile, in the case of I_{ph} and I_o parameters extraction, it provides a very low level of accuracy (Macabebe et al., 2011).

2.5.2 Four-Parameter Models

A four-parameter model designed by (Celik Acikgoz, 2007) was based on the assumption that R_{sh} in Eq. (2.2) (Appendix A), is infinite and therefore, can be disregarded. All things considered, this is a single-diode model that can be acquired from Eq. (2.2). Kou et al., (1998) illustrated a method to determine the four parameters required for equation (2.2) (Kou et al., 1998). When $V = 0$, the short-circuit current can be identified by Eq. (A.30) (Appendix A). The other parameters under the reference conditions (standard test conditions, 25°C and 1000 W/m^2), as per the characteristics of PV module can be computed using Eqs. from (A.31 to A.37) (Appendix A) (Celik Acikgoz, 2007).

By utilising Eqs. (A.30 to A.33) (Appendix A), the values of four parameters under reference conditions can be discovered. Eq. (A.34 to A.37) are utilised to conform these four parameters to coordinate the environmental conditions, and they are then utilized in Eq. (2.2) to provide connection between the cell current and the cell voltage. The cell current or the cell voltage, either one of them, can be computed using Eq. (2.2), depending on the known value. Whereas, the MPP can be used to calculate both the cell current and the cell voltage.

Standing on the worthy merits of applying the current model, it can be concluded that, like the last presented models, it is easy to extract parameter values directly from the used model in standard test conditions. However, any change in weather condition will make the calculation operation worthless, due to the fact that the current method is incapable of adjusting to the change in the weather condition.

A model devised by Tivanov et al. (2005) is favoured to compute the solar cell's parameters, such as R_{sh}, R_s, I_o and n, from the I–V characteristic via a set of illumination level (Tivanov et al., 2005),. Based on equation Eq. (2.2) for the single-diode model, and by approximating $I_{ph} = I_{SC}$ and analysing the I–V characteristic of a solar cell at a set of illumination level, its parameters can be computed using Eqs. (A.38 to A.40) (Appendix A). To confirm the allotted specific value of n, the value is compared to the value obtained by using the Eq. (A.41) (Appendix A).

This model differs from other models that didn't consider the change in the weather conditions and active only at a specific condition. It's dependent on a set of illumination levels. In this case, the possibility of extracting more accurate parameters is higher than in a specific condition. Nonetheless, it still has some weakness, as it measures only specific sets and not the random levels, such as rapid change in the weather conditions.

Chegaar et al. (2006) suggested a simplified model to extract parameters R_{sh}, R_s, I_o and n of the solar cell under illuminated conditions by utilising the I–V characteristic of one-diode model, an auxiliary function $F(V)$ and a fitting routine (Chegaar et al., 2006). Equation (A.47) (Appendix A) was used to derive the shunt resistance. Whereas, the other three parameters were obtained by introducing auxiliary functions in Eqs. (A.43 to A.45) (Appendix A).

Then, Eq. (A.44) is used to find the entire series resistance, the ideality factor of diode and the reverse saturation current. The values of $F(l)$ (from Eq. (A.44)) were calculated for each point (V, I) at a constant temperature and for a value of V_a to plot the curve. Chegaar et al., considered the integer values for V_a from 1 to 5 (Chegaar et al., 2006). The photo-generated current was assumed to be almost similar to the short circuit current in terms of value.

The use of I–V characteristic curve is to aid in extracting the PV parameters in a more prominent way, by dividing the whole area under I–V curve into five zones. This helps in accounting the integer values for the V_a (applied in the equations of parameter calculations) directly for each specific zone. However, the two zones close to I_{sc} and V_{oc} will be affected through the change in illumination levels directly.

Khan's model, (Khan et al., 2014) which uses the single-diode model as reference, was assessed to foresee the impact of the illumination level on solar cell parameters of a c-Si solar cell. The PV cell parameters, namely R_{sh}, R_s, n, and I_o, were acquired mathematically by using the values of I_{sc}, V_{oc}, R_{sc}, R_{oc}, V_m, and I_m. The values of I_{sc} and I_m, that were acquired from researches, increased linearly at various rates as the P_{in} increased. The product of I_{sc}, and V_{oc} determines the performance of PV systems.

The parameter values of this model could be computed using Eqs. (A.46 to A.49) (Appendix A).

F. Khan et al, (2014) have extracted the four PV parameters, namely R_{sh}, R_s, n, and I_o considering the effect of increase in the illumination level gradually, via an analytical and experimental calculations. The model was based on the values of V, I, and R; at three important points (I_{sc}, V_{oc}, and the Knee point) on the I-V characteristic curve. Therefore, the reliability of extracting parameters could be more acceptable, since it considered an open range of irradiance levels, but it still has not considered the effect of varied temperature levels.

Kaminski et al. (1999) utilised the double-diode model in dark environments to discover the solar cell's parameters (I_{od}, I_{or}, n_d, n_r, R_s and R_{sh}) (Kaminski et al., 1999). A study of the I–V characteristic of solar cell in dark environments is done on two areas: the first locale denoting the higher segment where the series resistance and the diffusion mechanism are critical, and the second locale representing the lower segment where the shunt resistance and the recombination mechanism are critical. The parameters I_{od}, n_d and R_s are decided using the first segment, while the linear regression of Eq. (A.49) is utilised to discover the series resistance and the ideality factor of the diode where (V_1, I_1) denotes a point on the first segment of I–V characteristic of the solar cell. Suppose the correlation coefficient is poor, then the value of I_1 should be escalated. In order to assess the saturation current, I_o, l_n and I must be plotted against the function of V- IR_s. The parameters I_{or}, n_r and R_{sh} can be acquired from the second segment of the characteristic curve. The linear part of the lower segment of I–V characteristic is acquired using least square method in Eq. (A.51). Eq. (A.52) is then utilised to compute the shunt resistance.

Different from previously presented models, in this model, the operation of parameter extraction was based on dividing the I–V characteristic curve into two parts. The right section, or lower section, is where the V_{oc} is active and helps in calculating the values of shunt resistance, R_{sh} and the diode ideality factor, n. The left section, or upper section, is where the I_{sc} is active and assists in calculating the rest parameters. Nonetheless, the application of this model still has some obstacles, such as ambiguity in finding these parameter values when the weather condition changes. This is due to change in I_{sc} and V_{oc} when the weather condition changes.

2.5.3 Three-Parameter Models

In order to find out the solar cell's parameters, Zhang et al. (2011) used the single-diode model to design a method that uses single I–V characteristic at a stable illumination level and the function of Lambert W. It can be clearly seen that equation (A.53) is a straightforward equation with just three parameters, n, R_s and R_{sh}, that can be determined by utilising the numerical fitting technique. The shunt resistance's initial value can be acquired by employing Eq. (A.54) and the linear dependency dV/dI as a function of $(I_{sc} + I – V/R_{sh})\ 1\ kT/q$, whereas the values of series resistance and the ideality factor, n, of diode can be acquired from the intercept and gradient. Equations (A.55) and (A.56) are employed to compute the saturation current and the photo-generated current, individually.

Therefore, extracting three parameters, namely n, R_s and R_{sh}, can be done by applying numerical fitting method, and from the single I–V characteristic of PV modules at a steady level of illumination. However, this method did not consider the change in illumination level via calculation process.

Inan, K. (1999) used a method which is also using the single-diode model as a basis, to determine the parameters of a solar cell under illumination conditions (Kiran İnan, 1999). The method based on employing an estimated equation obtained from Eq. (2.2) to eliminate the saturation current, and by regarding the shunt resistance as being infinite, thus formulating Eq. (A.57) (Appendix A). As per this estimation, it is apparent that the outcomes gained using this technique are different from the anticipated values as the cell undergoes aging process. This is critical in researches related to aging of PV cells.

Equation (A.57) has only three parameters, namely R_s, n and I_{sc}, that could be computed from the experimental data. The photo-generated current is defined as $I_{ph} = I_{sc}$. Therefore, in this study, the aging factor is considered in the calculation of PV parameter extraction method.

Arcipiani's model is based on the generalised area method (Arcipiani, 1985). The solar cell parameters, containing the ideality factor, the series resistance and the shunt resistance of diode, can be found using this technique, that includes the computation of area between the V and I axis and the I–V characteristic of solar cell using Eq. (A.58) (Appendix A). The current expression was employed for the solar cell's single-diode model.

This model takes the generally accepted approximations of $gr \ll 1$, $I_o < I_{ph}$ and I_{sc} EI_{ph} into account (Khan et al., 2010). This model depends only on the area under I–V characteristic curve in the parameter extraction operation, and only for standard test conditions. Subsequently, it is totally dependent on the values of I_{sc} and V_{oc}, that could be affected by the changing weather conditions.

In another study (Khatib et al., 2013), three parameters (I_o, I_{ph}, and n) were considered and inferred experimentally before being contrasted with the hypothetical values. Tailing this, the numerical expressions were determined through actual parameters to derive an ideal numerical model for the projected plan. Equation (A.60) depicts these three parameters.

The information of parameters are later detailed out and extracted by using Eqs. (A.61 to A.64). This method uses experimental data in the process of extraction parameters. It firstly extracts the diode ideality factor, n and then employ its value in equations (A.63) and (A.64) to get the photo-generated current, I_{ph} and the diode saturated current, I_o. Therefore, the current method extracts the diode ideality factor experimentally. After that, it employs the extracted coefficient values to calculate the other two parameters.

Garrido-Alzar (1997) designed a new solar cell model by using the two-diode model as a basis, to determine the solar cell's parameters (Garrido-Alzar, 1997). The technique comprises of solving the equation system obtained from Eq. (2.3) for four points, namely i_{1}, $_{2}$, $_{3}$, $_{\text{and}}$ $_{4}$, from the I–V characteristic (V_i, I_i), and n_{d1}, in zero order estimation for n and R_s (Garrido-Alzar, 1997). It later leads to the computation of parameter I_{ph}, I_{od}, I_{or} and R_{sh}. Equation (A.65) is utilised to calculate n, and Eq. (A.66) is utilised to compute the series resistance.

The expression of the Eqs. (A.65) and (A.66) must be carried out over and over until, for example, the value of n_r, with the desired level of precision, is obtained (Garrido-Alzar, 1997), where $n \neq 2$. Therefore, by applying the assumption of dividing I–V characteristic into four specific points, the values of these declared parameters could be extracted. This method could be effective, when the model is operating in normal condition. Also, the optimal value of n_r is achieved only when the I–V characteristic is unique.

2.5.4 Two-Parameter Models

Rohatgi (2001) contrived a strategy for determining two parameters of the solar cell, n and R_s (Bowden Rohatgi, 2001), by utilising two I–V characteristics, one measured for one sun illumination whereas the other one measured for 0.1 sun illumination, or preferably where the illumination level is such that the short circuit current of the solar cell is the same as $I_{sc},1$- I_m, 1. Eq. (A.67) can be utilised to compute the series resistance

The ($V_{m,1}$, $I_{sc,\ 1}$) is derived from the I–V characteristic measured for one sun illumination, and ($V_{oc,\ 0.1}$, $I_{sc,\ 0.1}$) is obtained from the I–V characteristic measured for 0.1 sun illumination. Eq. (A.68) is employed to compute the ideality factor of diode. This method is based on two elementary values of illumination levels applied on the I–V characteristic curve in the extraction process. One value is based on the illumination level in the standard test condition (1 kW/m^2), and another on the value of 0.1 kW/m^2, whose value is close to I_{sc}value.

Singh's model (Lal Singh, 2007), using the one-diode model as a basis, demonstrates that, in the Eq. (A.74), the semi-logarithmic I_{sc} –V_{oc} characteristic can be employed to discover the ideality factor of the diode and the reverse current. The short circuit current and the open circuit voltage should be determined for different illumination levels. The single-diode model is used in this technique by taking into account the estimation of Eq. (A.69).

The semi-logarithmic characteristic can be utilised to figure the ideality factor of the diode, while the interception of the characteristic on the Y-axis is employed to compute the saturation current. This technique was enhanced by Priyanka et al., (2008) by considering the value of shunt resistance. Thus, Eq. (A.69) was employed to extract the value of shunt resistance, R_{sh} parameter. As mentioned above, this model is based on different illumination levels in the extraction process. Therefore, it increases the reliability of the extracted parameters.

El-Adawi and Al-Nuaim (2001) suggested another technique for discovering the series and shunt resistances by using single-diode model (El-Adawi Al-Nuaim, 2001). Equation (2.2) can be utilised to appraise the series resistance, with the estimations shown in Eq. (A. 70), and by choosing two points, (Vi, Ii), i = 1, 2, around the knee of the I–V characteristic of solar cell. Equation (A.73) can also be utilised to compute the shunt resistance.

Differing from last presented models, this model had selected only two points around the knee point of the I–V characteristic curve of PV cell in the calculation process. By applying the current and voltage values on these points in the related equations, the extreme values of the series and shunt resistance will be obtained.

Ortiz-Conde et al. (2006) concocted an enhanced integral method (Ortiz-Conde et al., 2006), which was firstly introduced by Kaminski et al. (1999) (Kaminski et al., 1999). The linear regression of Eq. (A.75), that is obtained from Eq. (A.74) through integration, can be employed to acquire the series resistance and diode's ideality factor. In this research, the single-diode model is used, as the solar cell and the shunt resistance is viewed as infinite. Single point (V_1, I_1) is considered on the I–V characteristic of PV cell, since I is the current under dark conditions. The trapezoidal technique can be employed to find out critical issues.

Like the previously presented models, this model appointed different points on the I–V characteristic curve of PV cell. However, in this method, the selected points were integrated using Eqs. (A.74) and (A.75) to get the series resistance and ideality factor of the diode parameter values.

Jia et al. (1988) formulated a strategy for determining the series resistance and the ideality factor of the diode (Jia et al., 1988), whereby n is viewed as a variable of I–

V characteristic, and therefore bringing about n_1 at V_{oc} and n_2 at I_{sc}. The double-diode model was utilised in this technique with the solar cell being illuminated. The series resistance can be calculated using Eq. (A.76), that is determined using the following estimations where I_{ph}, I_{sc}, Rsh is infinite and I_{sc}, Io. Whereas equation (A.77) can be employed to compute the value of diode's ideality factor at the MPP.

In this method, the double diode model was the base in the operation of PV parameter extraction. The two parameters in concern were the series resistance and the diode ideality factor. The unique feature of this method is that it considered the values of I_{ph}, I_{sc}, and R_{sh} infinite and calculated the series resistance value. Then, in the calculation of diode ideality factor, it appointed three points on the I-V characteristic curves, which are I_{sc}, V_{oc}, and the MPP.

2.5.5 One-Parameter Models

A basic technique, usually referred to as the single-diode model, was formulated by (El-Adawi Al-Nuaim, 2001) taking into account the estimation of Rs from a single I–V characteristic curve of a solar cell. In this research, where it tries to avoid further graphical manipulation, all proposed parameters, except for V and I, are kept constants. To eliminate complex calculations, the method is made on the basis of drawing of a curve in relation to the power and the current or voltage, of which two points, (V_1, I_1) and (V_2, I_2), are chosen on a single I–V characteristic curve as in Eq. (A.78).

In this model, all constant PV parameter values were considered, but the series resistance, whereby the calculation process is based on the photo-generated current (which is proposed as a constant) and the values of V and I. Therefore, this method took the slope of two different values of V and I on the I–V characteristic curve, as depicted in Eq. (A.78).

In this technique, the solar cell's series resistance is determined using measurements under both dark and illumination conditions. Aberle et al., (1993) suggested the utilisation of Eq. (A.79) to ascertain the series resistance value. It was indicated that the dark condition by maximum voltage dark expression, $V_{dark,m}$ is measured under dark conditions in-line with the current, I_m, that is measured under illumination conditions.

Since the effect of series resistance in dark condition is disregarded, the error can be more than 5%. In the present model, to lessen the error, the revised Eq. (A.80) is employed to calculate the series resistance (Cotfas et al., 2013). Whereas, Eq. (A.81) can be used to calculate $R_{s,\,dark}$. Therefore, the difference of this method from the other methods is that it subtracts the voltage value in the short circuit condition (dark condition) from the voltage value in the open circuit condition (illuminated condition) and divides it to the short circuit current.

Cotfas et al. (2008) designed a technique to find out the series resistance using the single-diode model as a basis. There are two I–V characteristics used in this method. One of them is measured and the other is ideal. The ideal I–V characteristic can be computed using n_1 or with the actual values for n and I_o derived from the slope of semi-logarithmic characteristic at I_{sc} point. Equation (A.82) can be employed to compute the series resistance.

Therefore, this model is based on two different I–V characteristic curves, one in the standard test conditions (1000 W/m^2) and another with the short circuit condition. Then, the voltage of ideal case (standard test condition) is subtracted from the voltage of short circuit current, and the total is divided with maximum current.

Sanchez, A. (1982) formulated the area method to determine the series resistance of a solar cell through the use of single-diode model in Eq. (2.2) (Araujo Sanchez, 1982). The R_{sh} parameter is viewed as infinite, while the ideality factor of diode has a value equivalent to one. In this technique, the series resistance is ascertained as per the presented expression in Eq. (A.83).

Therefore, the key point of calculating the series resistance in this method is based on fixing the ideality factor of the diode with a value equal to one, and suppose that the shunt resistance value has an infinite value. Also, the area between the I–V characteristic curve and the I and V axes are fully considered in the calculation process of series resistance, within a specific weather condition. However, any changes in the weather condition will cause unfitting shift in the I–V characteristic curve, which is not considered in this study.

Polman et al. (1986) conceived a strategy for finding out the series resistance of solar cells using double-diode model to depict the solar cell, and by considering the shunt resistance and the ideality factor of diode (Polman et al., 1986). Using Eq. (A.84), the series resistance can be calculated through the average values acquired when n = 1 and n = 2.

In this method, the partial derivative value of the current to voltage, at the open circuit voltage point, is obtained from the gradient of the linear fitting of several points around V= V_{oc}. Like the previously presented method, shunt resistance value is supposed to be infinite, but the ideality factor of diode was taken in one time as a 1 and in another time equal to 2.

2.6 PV Models Accuracy Comparison Based on Number of Parameters

A brief comparison based on a model parameter used is presented in Table 2.1 to show comparison results between models from literature above. The comparison show that the accuracy of parameters based on these criteria indicated that the five parameter model is the most accurate among the others (Humada et al., 2016). In addition to that, models with high number of parameters are considered to have very small errors when compared to the ones with a lower number of parameters.

Table 2.1

A comparison of different models accuracy based on the number of parameters.

Author	**Year**	**2-diode model**	**1-diode model**	**No. Of Parameters used**	**Type of tested parameter**	**MAPE**	**R-square**
A. Polman et al.	1986	√		One parameter used in this model	Series resistance (R_s)	11.4%	0.943
A. Aberle et al..	1993		√	One parameter used in this model	Series resistance (R_s)	10.6%	0.966
Ortiz-Conde	2006	√		Two parameters used in this model	Diode ideality factor (n)	11.3%	0.961
Jia and Anderson	1998		√	Two parameters used in this model	Diode ideality factor (n)	7.35%	0.976
Garrido-Alzar	1997	√		Three parameters used in this model	Parallel resistance(R_{sh})	9.89%	0.976
Zhang et al.	2011		√	Three parameters used in this model	Parallel resistance(R_{sh})	6.67%	0.971
Kaminski et al.	1999	√		Four parameters used in this model	Diode current (I_o)	5.33%	0.974
F. Khan et al.	2014		√	Four parameters used in this model	Diode current (I_o)	4.67%	0.978
Merbaha et al.	2005	√		Five parameters used in this model	Photon current (I_{ph})	3.47%	0.986
Navabi et al.	2015		√	Five parameters used in this model	Photon current (I_{ph})	3.37%	0.987

2.7 Maximum Power Point Tracking Techniques

A PV module only converts a relatively low percentage of its incident solar irradiation into electrical energy, which means its efficiency is modest. Main step in increasing the PV cell efficiency is to employ one of the MPPT techniques to obtain the maximum probable power from a varying source. Each curve has a unique point named MPP, whereby the module is operated at its maximum efficiency to yield the maximum output power depending on its operating conditions (radiation and temperature). The MPPT method is a technique that constantly tracks the MPP on the characteristic curve of P–V or I–V and to ensure that the PV module can operate at the optimal point where most power is obtained. Different MPPT algorithms have been used previously to achieve that task alongside a DC-DC converter whose duty cycle is varied and is being used on the load side powered by a solar panel (Bratcu et al., 2011; Coelho et al., 2009; Ji et al., 2011; Lee, 2014). For this purpose, there are different methods used to track the MPP. These methods were studied in previous researches. In this chapter, the most prominent MPPT methods are studied as follow:

2.7.1 Perturb and Observe (P&O) Method

The perturbation and observation technique is one of the most well-known algorithms employed to track the MPP. The simplicity and ease of implementation render it an attractive method to use. Figure 2.8 shows the flow chart of P&O algorithm. The idea of algorithm is to continuously perturb the PV terminal voltage and compare the corresponding power with the power from previous perturbation. The movement direction of reference voltage stays the same as long as the output power increases or decreases with the perturbation.

The perturbation made by a moderate increment will result in a change of power. If the power is increased, then the direction of perturbation is correctly moving to the MPP position. However, if power decreased after perturbation, then the direction should be reversed. This process is done through a controller, which alters the voltage value by an arbitrary amount and measures the power; if the value of power is increased, additional modification in the same direction is undertaken until the power reaches its maximum value. If the power value is decreased, the modification will be in the opposite manner until power reaches its maximum value.

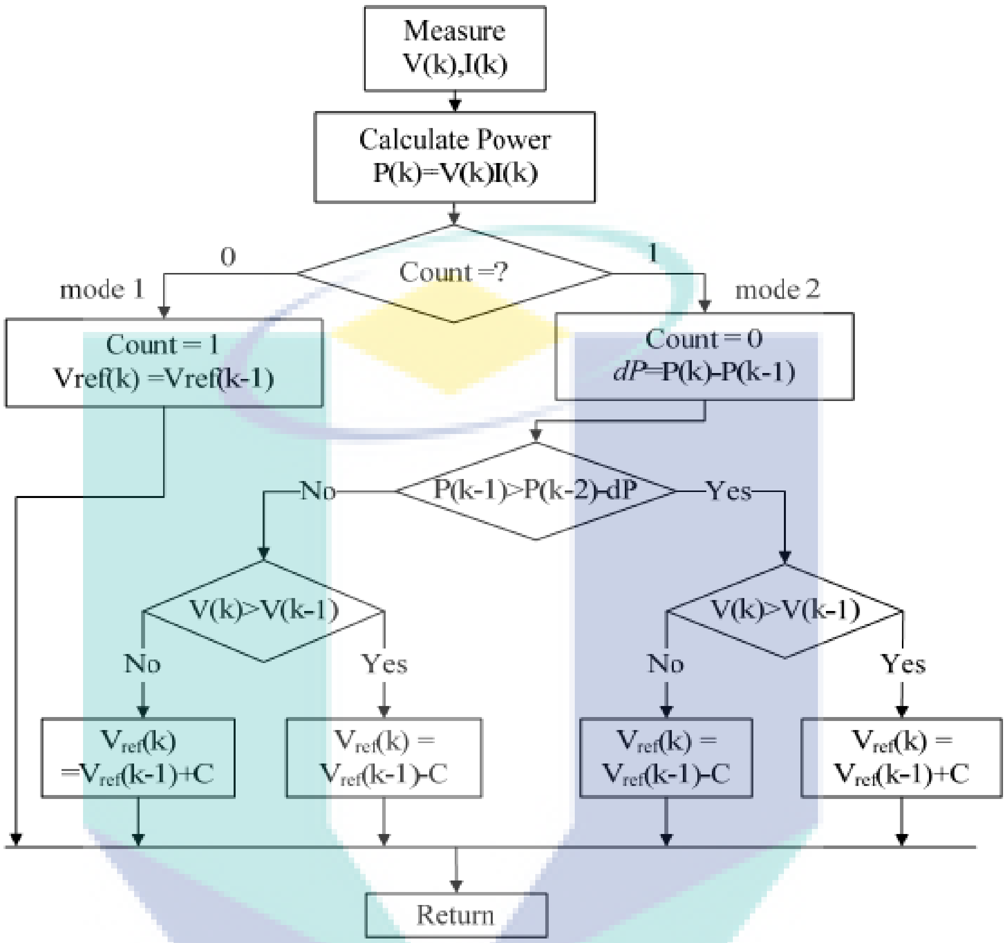

Figure 2.8. Flowchart of P&O

Source (Tafticht et al., 2008)

One of the major drawbacks of this algorithm is the oscillation around the MPP. Once the algorithm reaches a maximum point (local or global), it will keep oscillating back and forth around it, by a value of ΔV. The perturbation size corresponds to the power oscillation around the MPP. The perturbation size also determines the speed of the convergence; larger ΔV will lead to quicker tracking of the MPP. However, it will also lead to a larger oscillation. Each perturbation consumes power and the continuous oscillation around MPP results in a power loss. The P&O algorithm is proven to be an efficient MPPT technique and is widely used because of its simplicity (Abdelsalam et al., 2011; Bianconi et al., 2013; Elgendy et al., 2012; Nedumgatt et al., 2011; Sera et al., 2013). Figure 2.9 describes the tracking operation in detail.

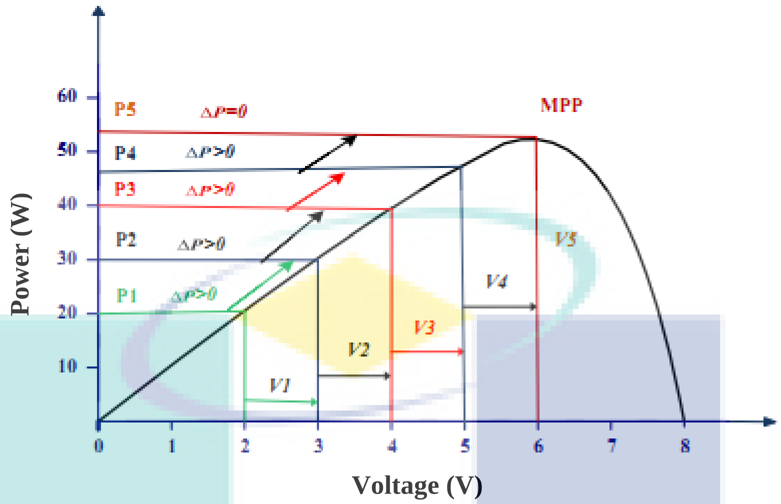

Figure 2.9. P–V Curve for P&O algorithm.

Source (Bhatnagar Nema, 2013)

2.7.2 Incremental Conductance Method

The Incremental Conductance (INC) method can overcome some of the drawbacks of P&O method. It is still a popular method, although it is more complex than the P&O. The MPP is tracked by comparing *dI/dV* by *I/V*. Electrical conductance is reciprocal of electric resistance. The term *dI* is the increment of current while *dV* is the increment of the voltage. The term *I/V* is considered to be the array conductance and *dI/dV* the incremental conductance.

The algorithm computes the incremental conductance and the array conductance. If both values are equal, then the algorithm has reached the MPP, that is both *dV* and *dI* are equal to zero. If the weather condition doesn't fluctuate, then the MPPT keeps working at its MPP. However, in case $dV = 0$ but $dI > 0$, and if the irradiance has increased, it will lead to rise in the MPP voltage value. In this case, it is necessary to increase the value of operating voltage towards the MPP. Nevertheless, if $dV = 0$ and $dI < 0$, and if the irradiance has declined, decreasing the MPP voltage value and necessitating the MPPT to reduce operating voltage value of PV system have to be made. If the value of change in the voltage and current are not equal to zero, then the direction of the change must be in the same direction with the voltage increment which lead to reach the MPP and determined it. The incremental conductance method is widely used by the authors for its accuracy in the normal condition (Lin et al., 2011; Safari Mekhilef, 2011; Sera et al., 2013; Xuesong et al., 2010).

For example, if the operating point of PV module is positioned to the left of MPP on the PV curve, then this implies that the voltage should be increased to grasp the MPP, as presented in Figure 2.10.

The main difference between INC and P&O is that INC does not oscillate around the local maximum. Previous literature proves INC to be a good MPPT algorithm with a slightly enhanced performance compared to P&O.

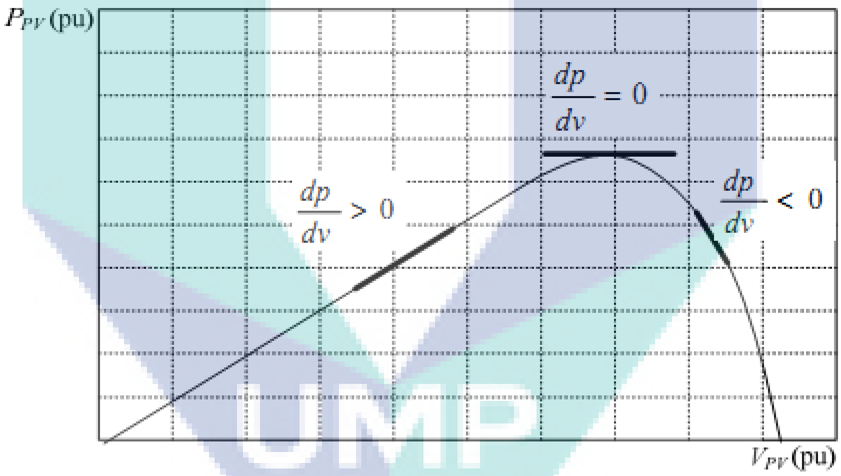

Figure 2.10. Effect of *dp/dv* variation and positioning on the MPPT in the incremental conductance method.

2.7.3 Constant Voltage (CV) Method

In the constant voltage method, the MPP voltage changes moderately with varying solar irradiance. In this method, the ratio of voltage at MPP (V_{MPP}) and open circuit voltage (V_{oc}) are assumed to be approximately constant (Dorofte et al., 2005).

$$\frac{V_{MPP}}{V_{OC}} \cong K\langle 1 \tag{2.6}$$

At first, the solar array is briefly separated with the MPPT and the value of V_{oc} is recorded. After that, the MPPT computes the operating point using the pre-set value of "K" using Eq. (2.6), and adjusts the array voltage till it reaches the V_{MPP}. In general, the ratio is dependent on the solar cell parameters, but a value in the range of 73%-80% is commonly used. The only drawback in this technique is the loss of energy when the load is separated and reconnected to the source.

2.7.4 Look-Up Table Method

As an offline method of tracking MPP, the lookup table method requires a prior knowledge about technical data, material of PV modules, and module characteristic at various weather conditions. These aforementioned information being saved later to use in the tracking process. The PV module output voltage V_{PV} and output current I_{PV} are then detected. Towards tracking MPP, power subsequently undergoes computation process and comparison with those stored values. Then, the operation point acquires shifting to a new MPP. Therefore, a great amount of data is needed to be kept before the MPP is being truly tracked; the system likewise needs a big capacity of memory in order to save the preceding data. The system is able to cope with changes in the weather condition (Tafticht et al., 2008). As a technique for MPP tracking, this method is not very accurate because of its slow speed and its larger requirement in terms of number of sensors.

2.7.5 Parasitic Capacitance (PC) Method

This technique depends on the fact that every solar cell is built with a parasitic capacitance, and this capacitance helps in discovering MPP (Hohm Ropp, 2003). Since the size of parasitic capacitance is very small in each module, it is only employed in systems with few modules in parallel. In this technique, the array conductance is computed by utilising the average ripple in the array power and voltage. After that, the direction of the operating point of MPPT is determined using previously described incremental conductance algorithm. This method is a type of modified incremental conductance technique, and is equally complex.

2.7.6 Ripple Correlation Control (RCC) MPPT

This method utilises ripples in the alteration operation towards achieving the MPP; therefore, the external changes in weather condition are not considered (Bazzi Krein, 2011; Esram et al., 2006; Kimball Krein, 2008). This method, which is referred to as 'Physics-based method' (Bazzi Krein, 2011), is appropriate for an union-stage configuration. Switching the power converters leads to voltage, current, and, therefore, power ripple, which is utilised for tracking MPPT. To track MPP, the time derivatives of the time-varying current and time-varying power (i.e. panel voltage) are controlled in order to set power at MPP to zero.

The high frequency ripples in power and voltage are captured with the use of filters that are then utilised in finding out the dP_{PV}/dV_{PV} (Spiazzi et al., 2009). The dP_{PV}/dV_{PV} variation is later employed to find MPP. Therefore, the fundamental principle of such MPPT algorithm is to employ the voltage and current oscillations that are resulted by instantaneous power pulsations. These oscillations provide information concerning power gradient and also allow to track MPP because the instantaneous power pulsations are at a frequency that is twice as much as the grid frequency. This technique employs the instantaneous power double frequency oscillations as perturbation signals (Spiazzi et al., 2009).

At the point when changes occur in atmospheric condition, the time derivative of current or voltage will be increased. Should power increase, the power time derivative similarly will increase; then, the operating point falls below MPP. Conversely, if the current or voltage heightens and the power will decrease. Then, the power time derivative will become negative, and the operating point drops above MPP. The inverter voltage is controlled towards obtaining the inverter sinusoidal current output in phase with the source voltage's fundamental component. The DC link voltage regulator generates the amplitude of the source current based on the error between panel's reference DC voltage and the DC link voltage. In tracking MPP, the MPPT algorithm alters this reference DC voltage according to the environmental conditions. The RCC thus provides a connection between power’s time derivative and voltage or current’s time derivative. This time derivatives are not zero due to natural ripples that happen amid high frequency conversion; this technique is therefore referred to as ‘ripple correlation’ control (Spiazzi et al., 2009). This method possesses various advantages. The power converter switching speed and the MPP tracking speed can both be very high. This method also has best initialisation time in comparison with INC, P&O, and temperature method (Bazzi Krein, 2014). It is likewise very accurate; despite being difficult to be applied due to electromagnetic interference issues if it is utilised on converter frequency.

2.7.7 Particle Swarm Optimisation (PSO) Based MPPT

This is a method that utilises the Particle Swarm Optimization (PSO) algorithm towards predicting the PV system’s MPP (Ishaque et al., 2012). Since partially shaded I–V curve exhibits multimodal characteristics, PSO methods are envisaged and very effective to track global MPP and distinguish it from the local ones under this condition.

As shown in Figure 2.11, toward the beginning of the advancement, the PSO is utilised for global search. When it touches base at the MPP’s region, the algorithm gets activated to rapidly get the local optimal point. Such a plan prompts an effective enhancement of the local search’s speed. Generally, PSO is more properly utilised for partial shading conditions, as depicted in the Figure 2.11, for both P–V and I–V characteristic curves and has the ability to track MPP. However, it has some oscillation around the MPP at most times.

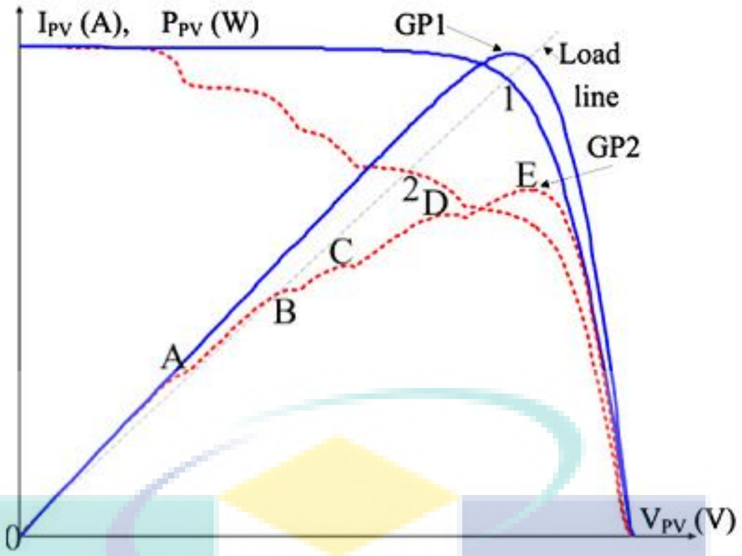

Figure 2.11. P–V and I–V characteristic curves, used to evaluate the PSO MPPT method, the blue colour under normal conditions while the dot ones are under shadow conditions.

Source (Ishaque Salam, 2013)

2.7.8 Ant Colony Optimisation (ACO) Based MPPT

Ant Colony Optimization (ACO) method is supposed to be one of the most effective methods in the operation of tracking MPP from a PV. This is because it combines a positive feedback appliance, distributed calculating, as well as greedy search method. In the process of searching for the optimal solution, it has a sturdy level of ability like, the positive feedback mechanism which guarantees that the ACO is almost capable in perceiving the optimal solution in the early stages. By applying desirous search, adequate results are quickly obtained and efficiency of the output results are improved. Due to aforementioned merits, the problems of tracking MPP in PV arrays could be solved via an adapted ACO-based MPPT (Jiang et al., 2013). They adopted ACO to track the MPP for a PV system operating under shadow condition. The proposed structure is shown in Figure 2.12. It shows that the system which contains two strings of PV modules operate under mismatch condition.

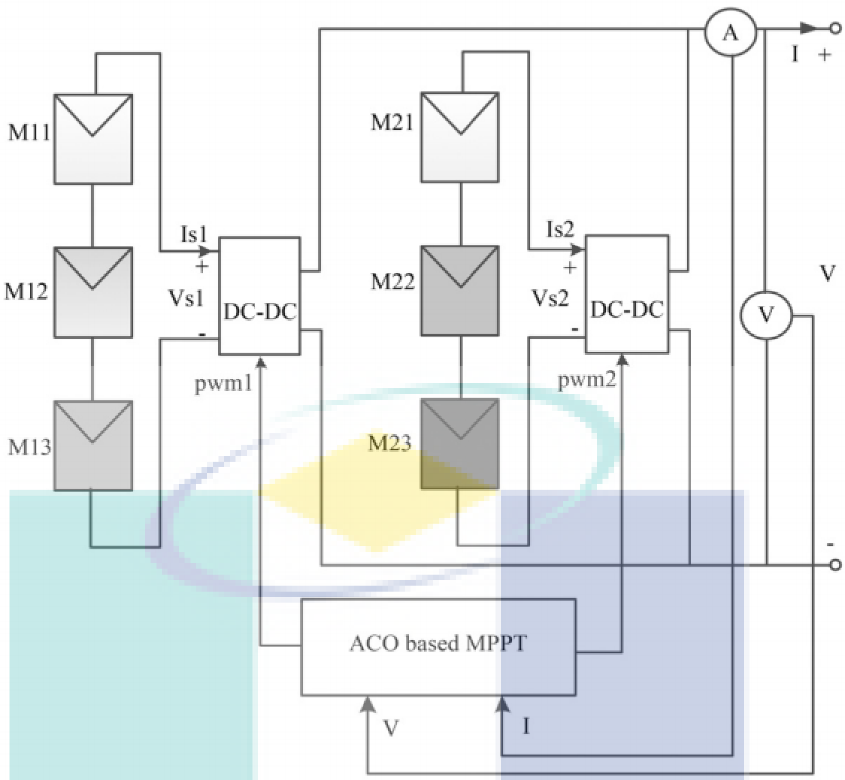

Figure 2.12. Suggested schematic of ACO based MPPT method.

Source (Jiang et al., 2013)

Table 2.2 presents a general comparison between the reviewed MPPT methods in current study to show validity of MPPTs in term of different factors.

To test the ability of the method to track the global point among the local ones, Jiang et al., (2013) selected different three shadow patterns. The results of these three shadow conditions are presented in Figure 2.13.

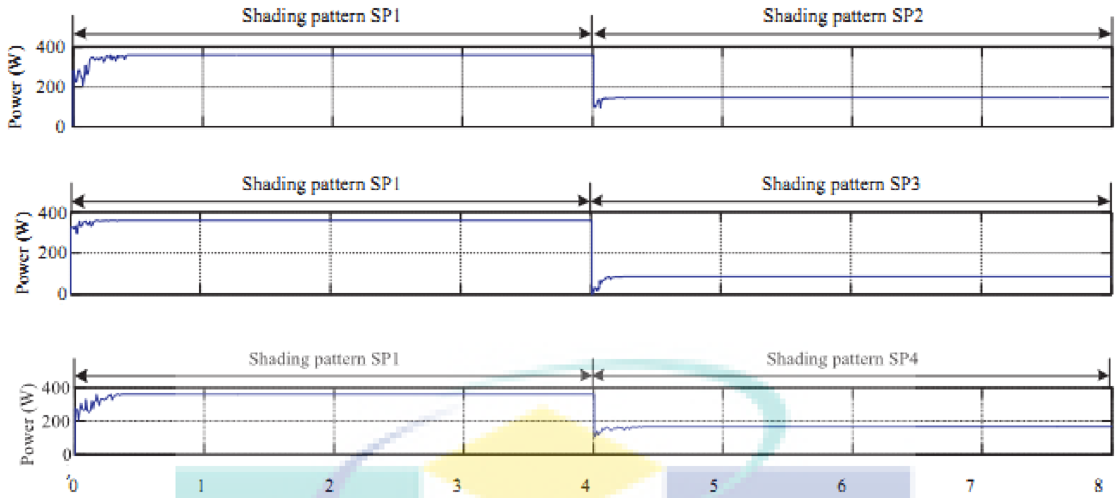

Figure 2.13. Power values after tracking from different the shadow patterns

Source (Jiang et al., 2013)

Table 2.2.
General comparisons between MPPT methods

MPPT technique	Complex ity	Convergence speed	Depending on Prior Knowledge	Memory requireme nt	Accuracy in Shadow condition
P&O	Simple	Slow	No	No	Nominal
INC	Simple	Depends	No	No	Nominal
Constant Voltage	Simple	Fast	No	High	Low
Lookup Table	Simple	Fast	Yes	High	Nominal
Parasitic Capacitance	Simple	Depends	Yes	Low	Low
Ripple Correlation Control	Medium	Fast	No	Low	Low
Fuzzy Logic (FL)	High	Slow	Yes	High	Medium
Neural Network	High	Slow	Yes	High	High
Neuro-fuzzy Logic	High	Slow	Yes	High	High
Particle Swarm ptimization	High	Depend	Yes	Low	High
Ant Colony Optimisation	High	Depend	Yes	Low	High

Outcomes of these three shadow patterns demonstrate that when the shadow condition changes from a uniform condition to a partially shaded condition at 4s (middle of time), the proposed MPPT algorithm can locate the global MPP for new shading pattern. However, some of oscillation patterns appeared after tracking the global MPP.

2.8 Summary

This chapter has presented the relevant literature review of the study. It also reviews the performance of previous developed models of PV cell. The fundamentals of power conversion unit of a PV system is discussed precisely; which is to overview the operation of electron movement and current generation of these PV cells. The available PV modules (single-diode model and double-diode model) models are also reviewed and discussed.

PV solar cell model parameters and its extraction technologies, based on different number of parameters and different models, are also briefly debated including the foremost issues of parameters based on either single-diode model or double-diode model. Meanwhile, the PV cell depends on the number of PV parameters. Therefore, the most important models based on the number of parameters in previous studies have been briefly discussed in this chapter with all available numbers of parameters. The models were based on, five, four, three, two, and one parameter(s) respectively. From the comparison between all dependent number of parameters, five-parameter model is expected to have a better accuracy than the others. In addition to it, based on the literature, the single-diode model is the widely used model, because it is the simplest and also adequately describes the characteristic behaviour of most solar cells. Literature review shows that even the single-diode model with five parameters model has better accuracy than other models, therefore this research will be using the single diode model with five parameters as a basis.

Moreover, a comprehensive literature review on the MPPT methods has been provided. The most conventional and famous methods are considered in this study. However, each method has their distinctive advantages. Most of them are not capable of tracking the real MPP, which is also called the global power point. In addition to that, some of these methods still vibrate around the MPP while some others are very slow and difficult to be used. Therefore, it is necessary to employ the soft-computing methods in the tracking operation, like the AO, GE and PSO and other methods. Even though most of these methods succeed in tracking the MPP, they have their own disadvantages. Like how the PSO method was found to be the most suitable for the MPPT operation, based on this review and previous studies, the suitable optimisation method can be predicted. This current review is useful in terms of PV modelling, development of the MPPT method, and also to solve transient problem around MPP after reaching its best value for a system operating under non-uniform operating conditions.

CHAPTER III

RESEARCH METHODOLOGY

3.1 Introduction

This chapter presents the research methodology of the study. Research framework is presented in order to demonstrate the breadth and depth of whole research work. The mathematical equations of a PV model have been initiated and its electrical parameters were experimentally performed and specified. The electrical characteristics of PV cell model and its parameters are also calculated. Different evaluation criteria have been employed in this chapter to confirm the accuracy of the used model and its parameters. The proposed PV model will be employed in PV system to evaluate the enhancement in MPP. Method of tracking MPP for different shadow conditions are presented in this chapter to show that the proposed method is capable of locating the maximum power accurately. Optimal PID controller have been employed and presented in this chapter to attain steady state condition of the extracted power in order to ensure system reliability. Finally, two different PV technologies have been practically employed in two different PV systems to validate the proposed PV system model based on different evaluation criteria.

3.2 Research Framework

The strategic framework of the present research methodology is illustrated in block diagram in Figure 3.1. The key implements including the PV modelling, develop a new MPPT method, and attaining the steady state condition. The results were clarified via well techniques based on this flowchart. The outcomes of this framework strategy are summarized in the conclusions and recommendations for future studies.

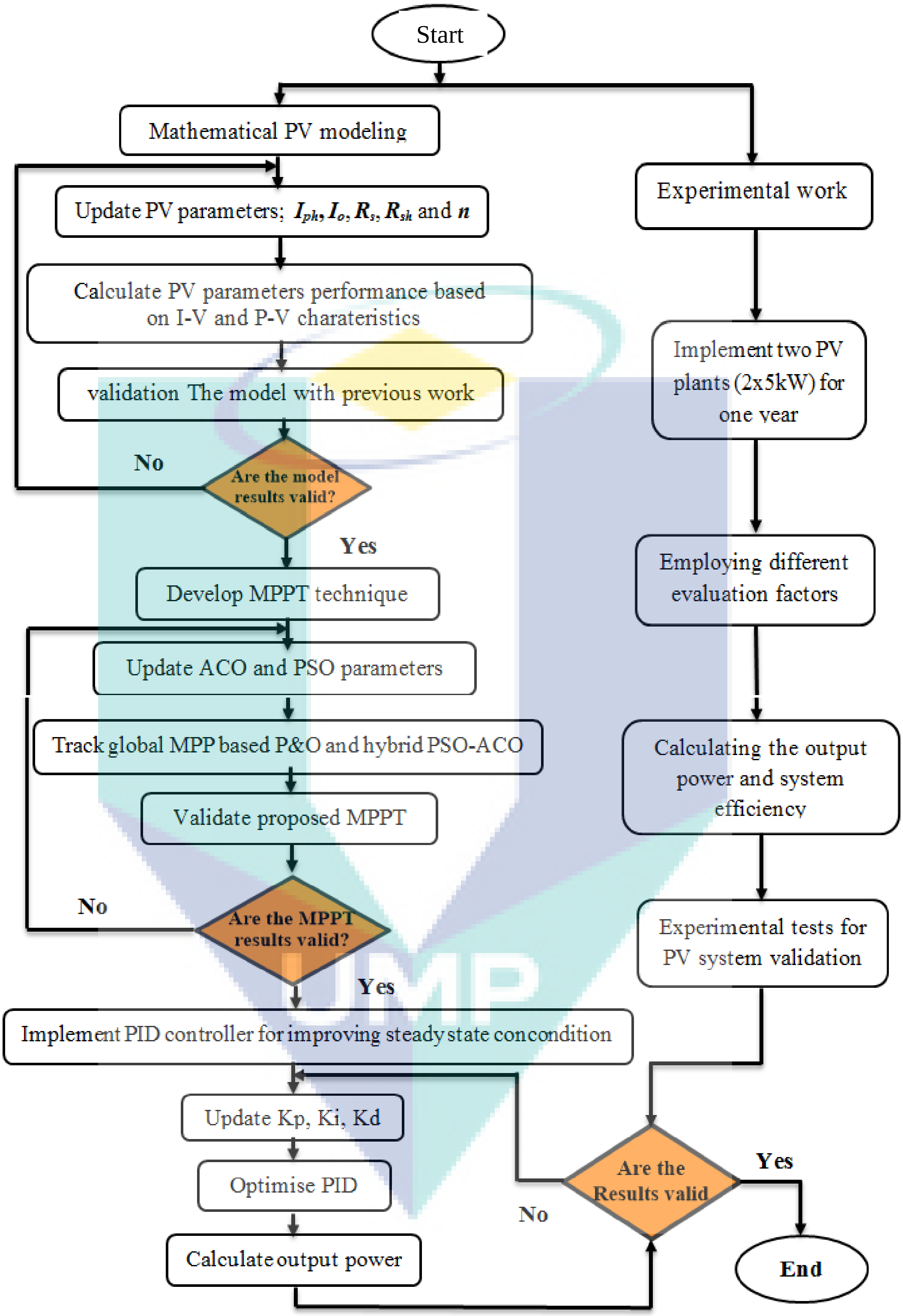

Figure 3.1. Flowchart of research framework

3.3 Proposed Mathematical Model for PV Performance Improvement

In this segment, the methodology of PV system modelling and characterisation is illustrated and demonstrated in detail. Five-parameters model (n, I_{ph}, I_o, R_s, R_{sh}) is employed to characterize the PV array. A precise mathematical model for PV system is developed using real parameters derive from mathematical calculations as the basis.

3.3.1 Proposed PV Array Modelling

In this research, a 5 kW PV system with 23 mono-crystalline PV modules installed in Bangi, Malaysia, is regarded as a case study. The system specifications are shown in Table 3.1.

Table 3.1
Specifications of the implemented PV system.

Parameter	Value and Units
Number of PV modules	23
Maximum Power (P_{MP})	216 Watts
Maximum Voltage (V_{MP})	24.10 Volts
Maximum Current (I_{MP})	8.952 Amps
Open Circuit Voltage (V_{oc})	24.5 Volts
Short Circuit Current (I_{sc})	9.05 Amps

In general, in this research, the PV system is modelled using single diode model as a basis. The general form of this single-diode model is presented in Figure 2.5. Therefore, a solar cell can be modelled by a comparable circuit which contains current source, a diode in the reverse mode and a resistance connected in series, whereby every part of the model is referred to a particular parameter. The cell photo current is denoted by a current source as depicted in the model.

At normal conditions or when there is no sunlight, it will perform like a semiconductor diode in darkness. When that happens, this semiconductor is denoted by a normal diode, where its characteristics (I–V) can be represented by (3.1).

$$I_D = I_o\left(exp^{\frac{V_D}{V_t}} - 1\right) \tag{3.1}$$

And

$$V_t = \frac{q}{nkT} \tag{3.2}$$

Where I is the PV output current, I_{ph} is the photo current, I_o is the diode reverse saturation current, q is the electron charge value which equal to 1.602×10^{-19} °C, T is the temperature of ambient, V_D is the voltage across the diode terminals, k is the Boltzmann constant (1.381×10^{-23} J/K), V is the output voltage, V_D is thermal voltage value, R_s is the series resistance, and n is the ideality diode factor (quality factor or sometimes the emission coefficient).

Whereas, when the solar cell is illuminated, a perfect cell is depicted as a current generator connected in parallel with a diode and its I–V characteristic is illustrated by Queisser, S. (1961) (Shockley Queisser, 1961) with the following equation:

$$I = I_L - I_D - I_{R_{sh}} = I_L - I_o(exp^{\frac{(V+IR_S)}{V_t}} - 1) - \frac{V+IR_S}{R_{sh}} \tag{3.3}$$

The ideality factor (n) usually ranges between 1 and 2 (in some cases, it could be greater than 2), and is dependent on the construction method and semiconductor material. In general, the proposed PV system model is from the five parameters model, particularly I_L, I_o, a, R_s, and R_{sh}. This model could be employed for an individual cell, for a module comprising several cells, or for an array comprising several modules.

However, as finding the accurate value of n is challenging, it is assumed that:

$$C_{coef1} = \frac{q}{nk} \tag{3.4}$$

Then

$$a = \frac{T}{C_{coef1}} \tag{3.5}$$

Usually, the light generation-current (I_{ph}) is relative to the solar irradiation's value and it should be directly dependent on the effective cell temperature (T) (Cotfas et al., 2013). As a result, a new equation is proposed in order to represent the light generation-current as shown in equation (3.6):

$$I_{ph} = \left(C_{coef2} + C_{coef3}T - C_{coef4}\right)G \tag{3.6}$$

In a related literature (Kaushika et al., 2005), researchers proved that the cell temperature (T) is affecting the diode saturation current, I_o in a linear mode.Thus, in this study a new equation to represent I_o is introduced as shown in Eq. (3.7).

$$I_o = C_{coef5}T^3 \exp(-\frac{C_{coef6}}{T}) \tag{3.7}$$

On the other hand, the series resistance (R_s) is mainly depending on the value of effective cell temperature (T) (Shi et al., 2014). Accordingly, a new equation for the series resistance could be defined as:

$$R_S = C_{coef7} - \frac{C_{coef8}}{T} \exp(-\frac{T}{C_{coef9}}) \tag{3.8}$$

Where the value of $C_{coef\,7}$ is presented and called as R_{So} (the reciprocal of the gradient at the open-circuit point), its value can be found from the slope at open-circuit point, or called open circuit voltage (V_{oc}), as follows:

$$R_{So} = -[\frac{dv}{di}]\,|_{Voc} \tag{3.9}$$

Whereas the value of R_{sh} can be found directly from the slope at short-circuit point, which is also called as short circuit current (I_{oc}), as follows:

$$R_{Sh} = R_{Sho} = -[\frac{dv}{di}]\Big|_{Isc} \tag{3.10}$$

Where, R_{Sho} (the reciprocal of the gradient at the short-circuit point), $C_{coef\ 1}$–$C_{coef\ 9}$ are coefficients, G is the value of solar irradiance, and T is the value of the temperature of the cell.

In this study, the attained experimental outcomes have been applied to estimate precise values of the constant coefficients $C_{coef\ 1}$–$C_{coef\ 9}$. These coefficients are obtained via applying curve fitting Matlab tool. Nevertheless, due to the constantly changing climate conditions (irradiance and temperature), the values of the voltage and current are continually registers and saved for every 1 second.

These data include actual values for all parameters a, I_{ph}, I_o, R_s, and $R_{sh\ used}$. The experimental values of these parameters are used to obtain constant coefficient values ($C_{coef\ 1}$–$C_{coef\ 9}$) and then to find the theoretical values for purpose of attaining precise values of constant coefficients ($C_{coef\ 1}$–$C_{coef\ 9}$).

3.3.2 Solar Inverter Modelling

In order to attain an accurate evaluation of PV system performance, the evaluation of model performance of PV module and inverter is vital (Khatib et al., 2013). The performance of PV system is dependent on the converter or inverter performance. Besides that, it also depends on the PV module performance. This part aims to investigate the inverter's characteristics. Sunny Mini Central SMC 5200, as the closest match with practical implementation, is the inverter employed in this research. As a matter of fact, a DC/AC inverter converts DC current originating from PV array to AC current. The proficiency of this energy conversion process is denoted by Eq. (3.11).

$$\eta(t) = (P_{in}(t) - P_{loss}(t))/P_{in}(t) \tag{3.11}$$

Where, P_{in} is the input power coming from the PV array, while P_{loss} is conversion power loss.

Apart from that, generally, the connection between inverter efficiency and PV power is derived to model and characterise inverter, and is represented by the following expression:

$$\eta_{inv} = A\, P_{pv}^{n} + B \quad \text{for} \quad 0 < P_{pv} < \mathrm{N} \tag{3.12}$$

$$\eta_{inv} = AP_{pv} + B \quad \text{for} \quad P_{pv} \geq \mathrm{N} \tag{3.13}$$

Where, P_{pv} is the PV power, while A, B and N are constants. The inverter behaviour (efficiency curve) is different before and after considering N value, since N is a critical value. Inverter efficiency is supposed to be unstable and depends on value of n, when the value of PV power between 0 and N ($0 < P_{pv} < N$). However, for the value of $P_{pv} > N$, the efficiency curve (behaviour of inverter) is linear.

Hence, the technique employed in this research is to model an inverter by taking into account the correlation method between the curve given by the manufacturer and the experimental outcomes. Therefore, this will produce an efficient model, which could be implemented for all types of inverter in any climate condition. In general, these last two equations are applicable to this type of inverter in terms of inverter efficiency. However, it also can be employed to other similar inverters. Hence, in cases of inverter brand selection, the users need to derive new equations to attain an accurate inverter model, based on the inverter type.

3.3.3 Model Evaluation Criteria

A productive assessment between real curves of the PV panels and proposed models are performed in this research. This assessment depends on numerous benchmarks to guarantee the precision of the proposed model with respect to real data. All these criteria indicate that the proposed model has a negligible error factor with respect to PV panel's real data. The assessment taking into account the most prominent factors such as

MAPE, SSE, R-square, SSR, SST is executed in this study. In this study, MAPE is mean absolute percentage errors, SSE is sum of squares due to error, SSR is sum of square due to regression, SST is sum of square due to the total, and R-square is the net of the division of SSR to SST. All factors which are used in this evaluation have corresponding formula as shown below.

$$MAPE = [|\frac{(X_{real} - X_{prop})}{X_{real}}|/n] \times 100\% \tag{3.14}$$

$$SSE = \sum_{i=1}^{n} (X_{real_i} - X_{prop_i})^2 \tag{3.15}$$

$$SSR = \sum_{i=1}^{n} (X_{real_i} - Cel_i)^2 \tag{3.16}$$

$$SST = SSR + SSE \tag{3.17}$$

$$R^2 = SSR/SST \tag{3.18}$$

Where X_{real} is real value, X_{prop} is proposed model value, *Cel* is central horizontal line drawn horizontally from the centre of the prospected curve and *n* is number of testing points.

3.4 Proposed ACO-PSO Algorithm for MPPT Parameter Optimisation

3.4.1 MPPT from Easy to Complicated

An MPPT calculation is vital in PV applications in light of the fact that the MPP of a solar panel shifts with irradiation and temperature. Accordingly, the utilisation of MPPT algorithms is required to acquire maximum power from a solar array. Over the past decades, numerous strategies to discover MPP have been produced and distributed. These procedures vary in its multifaceted nature and in numerous different aspects, for example, required sensors, cost, scope of viability, convergence speed, and correct tracking when irradiation and/or temperature change. Among these techniques, the P&O and the INC algorithms are the most common. These strategies have the benefit of simple usage, however they likewise have a few downsides, such as being inactive when the climate or shadow conditions change.

Therefore, it is necessary to implement an MPPT method that is able to overcome these drawbacks. As mentioned before, in order to construct PV arrays on top of any roof, numerous PV cells are put in series or in parallel, and a bypass diode is connected in parallel with every PV module in order to avoid hot spots being formed when some modules receive less insulation than others. When no partial shading occurs, the P–V characteristic of the PV array presents a single operating point where the power generated is maximised (maximum power point, MPP). In this situation, it is easy to track MPP on that characteristic curve, and there are many techniques that could be implemented to track this point efficiently without any impediments. However, when parts of the PV array are shaded for different reasons (such as neighbouring cells, surrounding buildings, trees, etc.), each PV array presents multiple operating point in the power–voltage (P–V) characteristic whereby some are local maxima and only one of them corresponds to the global MPP. In this situation, the operation of MPP tracking becomes much complicated and requires an accurate and exact method to be employed for the purpose of tracking that particular point.

Contingent upon the arrangement of PV modules and the shading patterns, the magnitude and location of the local and global MPPs would be different. In the past, many MPP tracking methods have been deployed with the objective to operate the PV array at MPP point, and maximise the PV energy production under the persistently changing solar irradiation and temperature conditions. Nevertheless, most of these algorithms developed do not produce maximum productivity due to the fact that they depend on tracking the global MPP by controlling the operating voltage of the PV array load. The subsequent operation point lies on the crossing point of PV array and P–V characteristics. Therefore, they are unable to make sure that it will differentiate between local and global MPPs (Tey Mekhilef, 2014).

In this thesis, a PV array is connected to a DC-DC power converter, controlled by an MPPT algorithm. This technique goes through a few stages. First, the DC-DC converter starts drawing a high amount of power continuously. So, the operating point starts moving toward the MPP where the output power is at its maximum. Therefore, the operating point does not get trapped in the lower output power operating points. Every time there are changes in the shading conditions, it is crucial to continuously update tracking process. Then, the PV array output voltage is regulated to where the operating point reaches the global MPP by controlling the duty cycle of the DC-DC converter. The last phase is the proposed MPPT method where it keeps track of the changes happening between the present and the last global MPP detected.

3.4.2 Tracking the Global MPP

In order to locate the global MPP, it is very important to understand the partial shading phenomenon. As explained above, under partial shading conditions, different local and one global maximum occurs. The first step in the proposed tracking procedure, in this study, is when the DC-DC converter starts to continuously draw higher amount of power so that the operating point starts moving from one local maximum to the others until it reaches the MPP where the output power is at its maximum. This procedure is done until there is no possible increment in the output power. The relationship between the input and output voltage of a boost-type DC-DC converter is (Matsuo et al., 1993):

$$V_o = \left(\frac{V_{in}}{1-D}\right) \tag{3.19}$$

Where V_{in} (in volts) is the DC-DC converter input level, V_o is the DC-DC converter output level, and D is the converter duty cycle ($0 \leq D \leq 1$).

During the process of tracking the global maximum, the PV array output voltage is measured and stored consistently in the microcontroller memory. After the global maximum is detected, the DC-DC converter duty cycle decreases until the PV array output voltage is controlled to the global MPP. Later, the proposed algorithm is employed in order to monitor the fluctuations that might occur to the global MPP.

3.4.3 Proposed ACO-PSO Based MPPT Technique

In this segment, a hybrid ACO-PSO algorithm is proposed for the optimisation of swarming agent on the basis of multicast of routing problems. A brief definition on ACO and PSO is presented at the beginning of this section.

A: ACO Algorithm

Drigo et al., (1996) were the first to introduce the ACO (Ant Colony Optimisation) system which begins with a basic ant system (Drigo et al., 1996). The current study has embraced the ant system mainly because of its clarity. The natural manner of conduct of ants has inspired the objective of this technique, that is to form a coordinated examination of a couple of constructive arithmetic threads involving localised problem information. They are structured in a dynamic way, comprising quality results from a previously performed analysis. The ant system matches each arithmetic resource to an ant from a pretended ant colony. The colony represents a type of oblique, environmentally arbitrated communication whose purpose is to establish the nearest route between the target and the ant nest. This algorithm has demonstrated its strength in terms of providing a prompt universal solution to be way better than alternative heuristic techniques like genetic algorithms and simulated annealing. A specific, highly beneficial trait of the ant algorithms is that it can carry on a computation from where it was left instead of doing it all over again.

The ACO is a combination of positive feedback mechanism, distributed computing, and a greedy search algorithm. It has strong abilities to look for the optimal solution. For instance, the positive feedback mechanism ensures that the ant colony algorithm is able to identify the optimal solution in earlier stage. By using the greedy search, the acceptable solution is quickly found and efficiency of the system is improved. Therefore, the MPPT convergence speed problem in a PV system is solved through modified ACO-based optimisation. ACO-based MPPT is applied in this study to find the shortest path, to increase convergence speed. The equation below describes the ant's behaviour towards finding the shortest path to the global MPP point, denoting the amount of pheromone toward the shortest path.

$$Ph_{xy} = Ph_{xy}(1-\beta) + \sum_i \Delta Ph_{xy}{}^{i} \tag{3.20}$$

Where Ph_{xy} is the amount of pheromone deposited for a state transition xy, β is the pheromone evaporation coefficient, $\Delta Ph_{xy}{}^{i}$ is the amount of pheromone deposited by i_{th} ant.

$$\Delta Ph_{xy}{}^{i} = \begin{cases} K / L_i & \text{if ant } i \text{ uses curve } xy \text{ in its tour} \\ 0 & \text{otherwise} \end{cases}$$

Where L_i is the cost of the i_{th} ant's tour (typically length) and K is a constant. Due to aforementioned merits of using ACO, the problem of slow MPP tracking for PV arrays could be solved via adopting ACO based MPPT (Jiang et al., 2013). The flowchart of ACO method used in this study is shown in Figure 3.2.

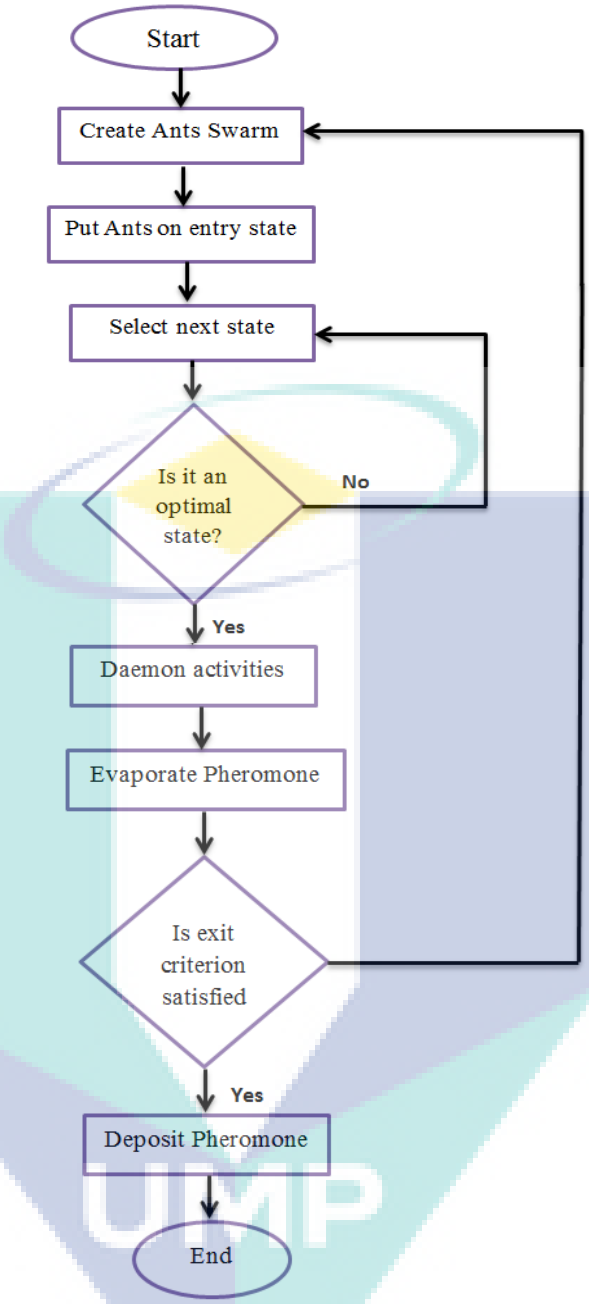

Figure 3.2. Ant Colony Optimisation (ACO) flowchart based MPPT.

B: PSO Algorithm

The Particle Swarm Optimisation (PSO) algorithm relies on population. It uses several possible solutions in order to establish the best one or a combination of solutions to a particular problem. Its objective is to provide the global optimum of the fitness function (the real valued function) ascribed to a particular search space. The characters in the PSO algorithms are referred to as 'particles'. They move around in a space characterised by several dimensions, i.e., the 'belief' space. Since the individuals are memory-based, even when they change their state, they still keep part of the information from their preceding ones. Each particle has its own distinctiveness even though it should not necessarily retain its characteristics when changing states. The influences involved in particle movement are socialist, or the particles' inclination to aim for the best prior position of their neighbouring individual, and individuality, or the particles' targeting their best original state.

The PSO algorithm appoints an assured particle number (N) to reconnoiter the search space D-dimensional of the appointed problem. At every iteration, each particle represents a solution to the problem based on particle's location in the search space X_n. The particles move stochastically by means of velocity vector of V_n, a resultant of three vectors: 1) the best location experienced by the particle (P_{best}); 2) the best location experienced by the entire swarm (G_b); and 3) a portion of itself in the last iteration.

The P_{best} and G_b must be kept up-to-date at each iteration all through the optimisation process. To do this, a fitness function should be defined to identify the location of every particle at each step. The mathematical form of acquiring the velocity and updating the location of each particle is shown in Eqs. (3.21) and (3.22), individually. The equations below are the basis for computing the position and velocity of individuals. They are used to search the global point in current study.

$$V_n^{i+1} = wv_n^i + \frac{c_1 r_1 (P_{best} - X_n^i)}{\Delta t} + \frac{c_2 r_2 (G_{best} - X_n^i)}{\Delta t} \tag{3.21}$$

$$X_n^{i+1} = X_n^i + V_n^i \Delta t \tag{3.22}$$

Where the subscription n represents the number of used particles; i refers to the number of iterations; V^i_n stands for the velocity vector of the n_{th} particle and X^i_n for location vector, at i_{th} iteration. The c_1 and c_2 stand for weight factors with constant value. P_{best} is the best position of the n_{th} particle. G_{best} represents the best position located by the neighbours of the n_{th} particle. r_1 and r_2 are random factors in the [0, 1] interval. Also, Δt is the time step for each iteration. Finally, w stands for the inertia weight, which reduces constantly all through the optimisation process and regulates the scale of particle movements.

Due to the remarkable merits of PSO in approaching and recognising the global point among the local ones, it is appointed to search and track the global MPP point in this study via using Eqs. (3.21) and (3.22). The whole process of searching global point is illustrated in the flowchart in Figure 3.3, below.

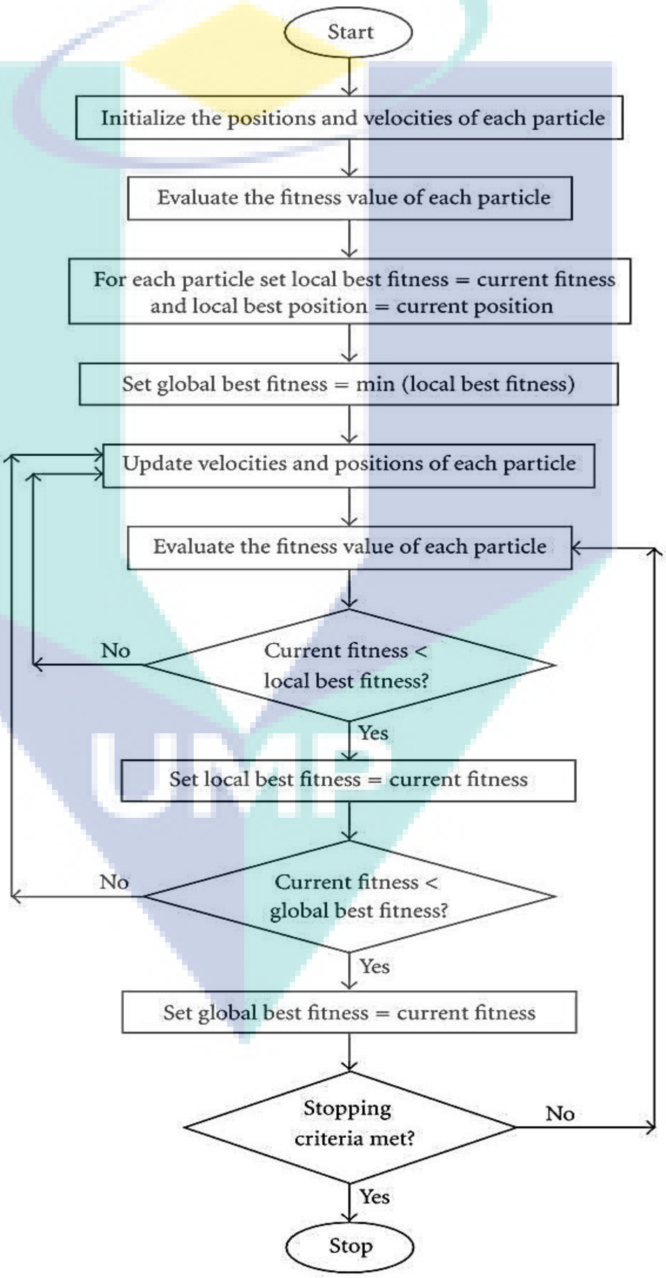

Figure 3.3. Flowchart of PSO based MPPT.

C: Combination of Proposed ACO-PSO based MPPT

The search operation of MPPT within shadow conditions is more difficult, due to multi peaks appearing on the P-V characteristic curve. Different local points and only one global point will be generated on the P-V characteristic curve. A technique of using Perturbation and Observation method (P&O) combined with a Particle Swarm Optimization method (PSO) has shown an efficient result for tracking global MPP and differentiate it from the local ones (Reisi et al., 2013; Suryavanshi et al., 2012). However, it has the disadvantage of long convergence time and failure to track global MPP, especially when the array is exposed to fast changing weather conditions.

Therefore, to overcome these drawbacks, this study proposes a new method of combining the P&O method with a hybrid method of ACO-PSO. This is because the above mentioned merits of PSO in differentiating the global point and tracking it efficiently, the ability of ACO algorithms in adapting to the rapid changes in weather condition and its fast convergence speed (Besheer Adly, 2012; Salam et al., 2013). This will lead to producing an accurate MPPT method with fast convergence speed. In this method, DC/DC converter (boost converter) is used to control the maximum global point via employing the proposed MPPT algorithm, which adjusts the duty cycle of boost converter. The schematic diagram of interleaved proposed MPPT controller is shown in Figure 3.4. In the proposed system, to control the step size, firstly the perturb and observe algorithm are activated. They are used because of the ability to track the first local point and changing the step size of the search in a proper way. In the next step, the calculation process of a hybrid ACO-PSO algorithm is carried out as this can track the global MPP in a very fast convergence speed and efficient mode.

3.4.4 ACO/PSO-based Variable Step P&O MPPT

Temperature and solar irradiance are the specifications which have an effect on the solar cells' I–V characteristic features. Therefore, they can also influence the power produced by the PV array. The working point should be driven to its highest power point if researcher wants to enhance the transfer of energy from the PV array to the load. The MPPT controllers hence force the converter to go through the DC/DC duty cycle change. More often than not, the controller generates a PWM (Pulse Width

Modulation) generator reference voltage in order to bring about the necessary pulses. Although the P&O fixed step method is the preferred technique for the majority of control schemes, oscillation complications are inevitable. In order to fight these complications, a P&O algorithm involving ACO/PSO variable step algorithm is applied. P&O variable step optimisation is possible when the ACO/PSO algorithm tunes the PID controller by picking out the Ki, Kd, and Kp parameters for the PID, which in turn enhances the transfer of power through the DC/DC converter. Figure 3.4 shows the scheme using a structure block.

The P&O method, relying on fixed iteration step size, has proven to boost performance. Nonetheless, the P&O method is not short of disadvantages. The main ones being that when the state is stable, a residue energy is lost due operating point's oscillation around MPP, and while the accuracy is decreased, the step size is increased and the other way around. The current research presents an adjusted MPPT algorithm using a shifting step size in order to compensate for the aforesaid shortcomings.

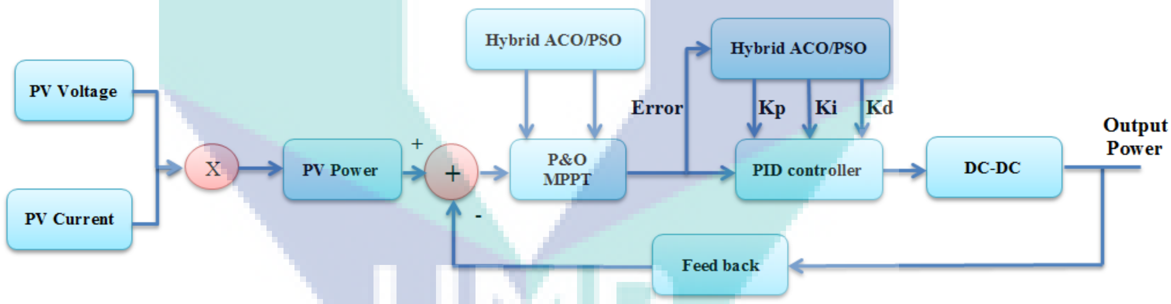

Figure 3.4. Block diagram of proposed ACO-PSO based P&O MPPT and PID controller.

The study presents an upgraded P&O MPPT approach, which applies variable step size and PID controller. It is an essentially alternative ACO/PSO algorithm. A boost converter has been linked to a PV model in order to appraise the efficacy of the approach. The improved algorithm has been scientifically compared to the traditional fixed step size P&O. Several enhancements have been proposed and applied, namely overshot, response time, and ripple or oscillation. Moreover, the strength of the algorithm has been demonstrated via different shadow condition used and implemented in this study. It is proven that the algorithm can track the MPP even when the atmospheric conditions are rapidly changing or when arbitrary values are assigned.

3.4.5 The Boost Converter

The boost converter is connected to the PV array and regulated by a microcontroller based control unit to draw a high amount of power. The input and the output generator is a DC voltage source. The output voltage is constantly smoothed by a capacitor, and the switches are expected to be ideal. The Simulink model of the boost converter is shown in Figure 3.5.

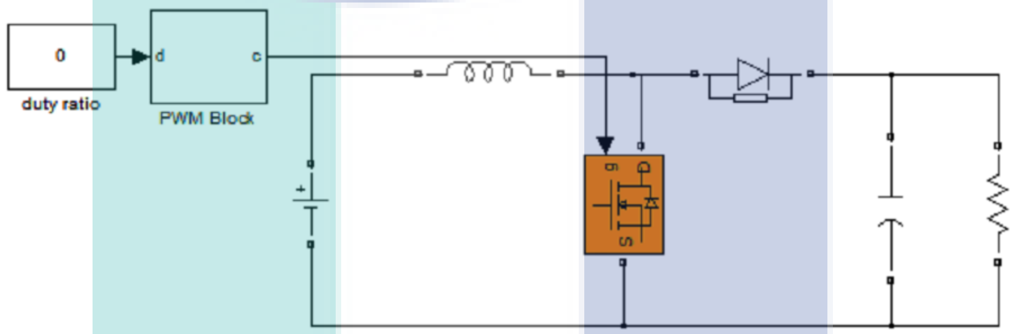

Figure 3.5. Boost converter in Simulink model.

3.5 Proposed PID Controller for Steady State Condition Improvement

In general, an electrical PV systems are exposed to a continuous change in the weather conditions and this causse a disturbance in the output power condition. Under this circumstance, keeping extracted power within the acceptable level of transient or within steady state condition is one of the important tasks for power system control.

The current research has adopted the hybrid ACO-PSO algorithm for achieving the MPP tracking. In addition to that, this ACO-PSO algorithm is also used to optimise a PID controller for the purpose of attaining steady state condition of extracted power in order to achieve the system stability and reliability. The proposed algorithm relies on the combination of ACO-PSO for the forced tuning method, which aims to optimise the power output extracted from a solar panel by the PID framework. The controller framework of standard PID controller is created using dynamic model. It is, however, challenging to reach the targeted performance due to the non-linear nature of DC- DC converter. This is why ACO-PSO optimisation of the control framework is so efficient. Optimum particle strength requires Simulink model designing of boost converter and the programming of a combination technique in order to locate the PID's best control framework.

The current research estimates the best control framework for tuning PID by applying a combination method (ACO-PSO). The ACO-PSO combinative technique is ingrained in the feedback compensation circuit designed, which is assigned in the frequency domain. The method, with the help of Bode plots, implicates the aligning of zeros and poles of the given compensation circuit, in order to discard any unfavorable outcome of the power phase. The configuration of this research proposes the boost converter as the means for transmissioning power to the load from solar PV module. The PV array and the load are mediated by a DC-DC converter. Figure 3.6 shows the whole arrangement as described below:

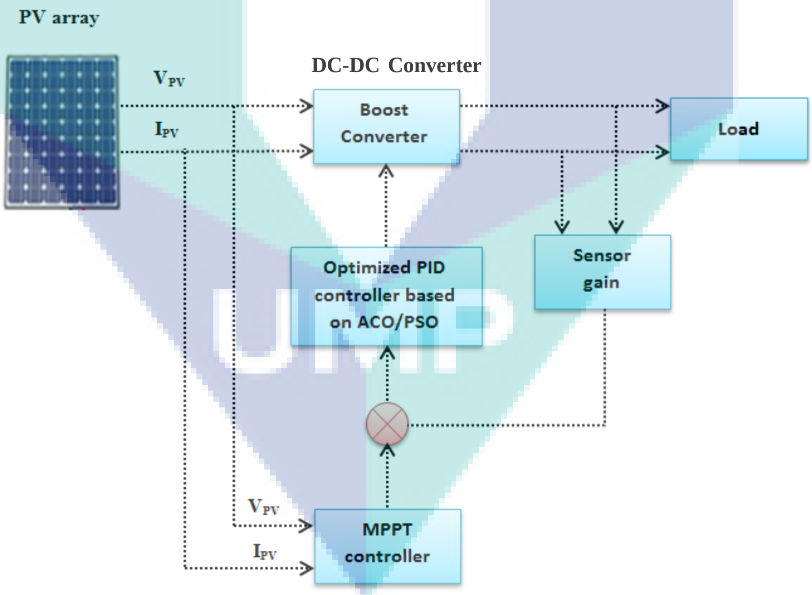

Figure 3.6. PV system with proposed MPPT diagram & optimal PID controller.

As a matter of fact, the performance of any optimisation technique depends on the selected objective function or fitness function. The integral time absolute error (ITAE) helps in shrinking the peak overshoot. Also, the integral time square error (ITSE) decreases the settling time, which cannot be achieved with the integral absolute error (IAE) or the integral square error (ISE) based-tuning (Fang et al., 2011). Consequently, in this research, ITAE and ITSE are used as objective functions or cost functions to improve the PID design process, as shown in Eqs. (3.23) and (3.24).

$$ITAE = \int_0^T t|e(t)|.dt \tag{3.23}$$

$$ITSE = \int_0^T te(t)^2.dt \tag{3.24}$$

As introduced in the beginning of this section, the ACO-PSO algorithm have been used in this study for tuning PID controller.

3.5.1 ACO-PSO-based PID Controller Fulfilment

Figure 3.7 depicts the whole configuration in the form of a block diagram. Whereas *R(s)* stands for the system output, *C(s)* for the system input, and *G(s)* for the reference input to the PID controller. Optimum quality control at particular operating settings is granted by the ACO-PSO application to the PID controller tuning.

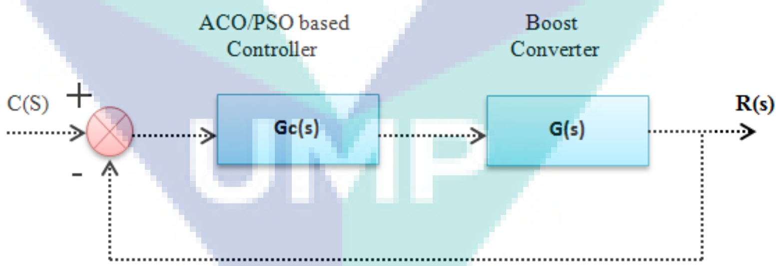

Figure 3.7. Whole system block diagram

By employing the optimal values of the K_P, Ki, and Kd obtained from the (ACO-PSO) optimisation method that attempts finally to produce worthy values for the three PID gain parameters. The method is executed via setting the first values of both I and D gains to zero.

The transfer function of the boost converter is given below (Luo Ye, 2007),

$$\mathrm{G}(S)=\frac{1}{(1-d)(1+S\dfrac{L}{R(1-d)}+S^{2}\dfrac{LC}{(1-d)^{2}})} \tag{3.25}$$

While the transfer function of PID controller is described below,

$$\mathrm{G}_{C}(S)=K_{P}(1+\frac{1}{K_{i}S}+K_{d}S) \tag{3.26}$$

Based on the whole system block diagram as depicted in Figure 3.7, the whole system transfer function can be derived as follow,

$$e(S)=C(S)-R(S) \tag{3.27}$$

$$R(S)=e(S)G_{C}(S)G(S) \tag{3.28}$$

$$R(S)=[C(S)-R(S)]G_{C}(S)G(S)) \tag{3.29}$$

$$R(S)=G_{C}(S)G(S)C(S)-R(S)G_{C}(S)G(S)) \tag{3.30}$$

$$R(S)[1+G_{C}(S)G(S)]=G_{C}(S)G(S)C(S) \tag{3.31}$$

$$\frac{R(S)}{C(S)}=\frac{G_{C}(S)G(S)}{1+G_{C}(S)G(S)} \tag{3.32}$$

After compensating the *G (S)* and G_C *(S)* values, from equations (3.25) and (3.26), in the main block diagram, as shown in Figure 3.8, it will get the equation below.

$$\frac{R(S)}{C(S)}=\frac{K_{P}(1+\dfrac{1}{K_{i}S}+K_{d}S)\dfrac{1}{(1-d)(1+S\dfrac{L}{R(1-d)}+S^{2}\dfrac{LC}{(1-d)^{2}})}}{1+K_{P}(1+\dfrac{1}{K_{i}S}+K_{d}S)\dfrac{1}{(1-d)(1+S\dfrac{L}{R(1-d)}+S^{2}\dfrac{LC}{(1-d)^{2}})}} \tag{3.33}$$

By multiplying the numerator and denominator by S, then will get the global transfer function of whole system becomes as follow,

$$\frac{R(S)}{C(S)} = \frac{K_d S^2 + K_p S + K_i}{\frac{LC}{(1-d)} S^3 + (K_d + \frac{L}{R(1-d)}) S^2 + (K_p + (1-d)) s + K_i} \tag{3.34}$$

Where R is the resistive load value, L and C are the conductance and capacitance belonging to the boost converter, respectively.

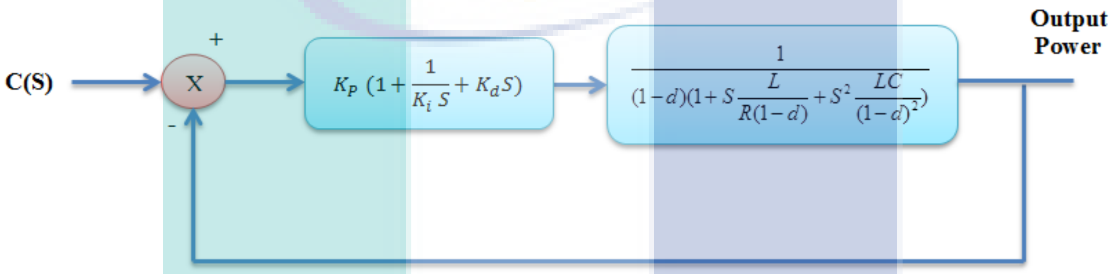

Figure 3.8. Whole system block diagram based on transfer function

3.6. Different Case Studies of Shadow Conditions Affect The P–V and I–V Characteristics

To illustrate the impact of partial shading and the effectiveness of proposed method, four PV arrays are connected in series as shown in Figure 3.9, and combined with a bypass diode connected in parallel with each PV module to protect the solar cells against efficiency degradation and hot-spot failure effects. In order to represent the shadow condition and to prove the reliability of the proposed MPPT method, different three shadow conditions are presented. The four PV modules faced different irradiance values, since the first shadow condition. The sequence of irradiance values are 900 W/m^2, 500 W/m^2, 400 W/m^2, 1000 W/m^2, respectively. The second shadow condition irradiance sequence is 700 W/m^2, 800 W/m^2, 400 W/m^2, 200 W/m^2, and the third condition is 200 W/m^2, 500 W/m^2, 700 W/m^2, 1000 W/m^2, respectively. The proposed algorithm employed and examined these three different shadow conditions. In order to do that, the PV modules have been connected in series, their voltages were added to produce total array voltage, while their current was kept the same. In order to test the functionality of the PV block under partial shading, a feedback is needed for the PV current input. A resistor is placed after the output voltage and a current measurement tool is used to measure the current across varying resistor. The idea is to change the value of resistor and measure the changes happening within the current and the voltage. The power is then calculated and measured by multiplying both sources P=I*V. These processes are represented in Figure 3.9, which illustrates the block diagram of PV modules system containing four PV modules connected in series.

This makes it conceivable to observe and assess the system's response to sudden changes in the operating conditions, for example, variations in irradiance caused by shading.

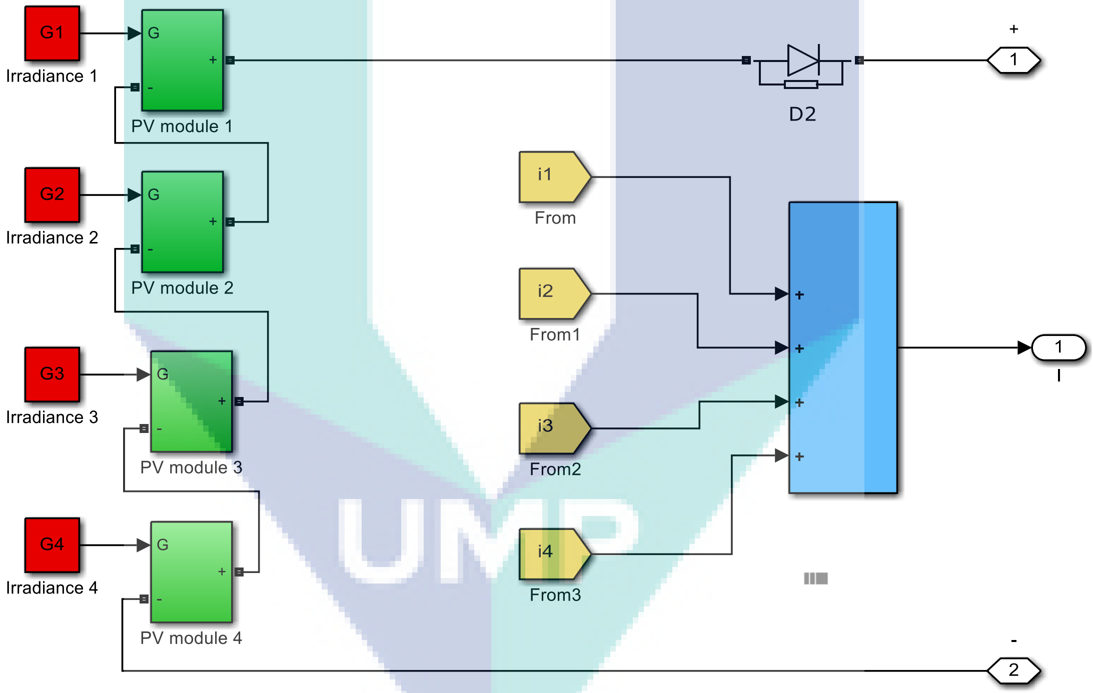

Figure 3.9. Block diagram of a PV array with four PV modules.

3.7 PV System Model Validation

In this part, a validation and real assessment of the used PV system model within a real PV system (consisted of two different PV technologies) data are achieved, including all PV system outputs such as PV array generated power, inverter efficiency and PV module efficiency. Then, these specific dynamic factors are tested in order to figure out the PV system model performance like PV system efficiency and PV system performance. In general, PV efficiency is derived by dividing the PV output power to the PV input power in a specific area within a period of time. Meanwhile, one can express the PV performance by dividing of the PV module efficiency in specific operating conditions to the PV efficiency at reference conditions (η_{ref}) as 17.4 percent (Khatib et al., 2013).

3.7.1 PV System Model Performance

In terms of PV module efficiency, the user of PV system usually gets the result at the ideal conditions to achieve the best outcomes. However, when this condition (I_{max}, V_{max}) is reached, it leads to ensure that the PV array operates at P_{max} as below:

$$P_{max} = I_{max} \cdot V_{max} \tag{3.35}$$

In reality, it is just getting the real values of output voltage and output current for normal condition. In addition to that, the most commonly used factor to relate the PV system performance is the PV system efficiency. Meanwhile, the main part of the PV system is the PV module and therefore its efficiency is playing an important role as compared to the whole system efficiency. This efficiency is mainly dependant on the local temperature and the amount of light from the sun. In other words, PV module efficiency is defined as the ratio of the power output from the module itself to the incident power coming from the sunlight, which is normally depending on the area of module, as shown in the following equation.

$$\eta_{PV} = \frac{E_{PV}}{E_{sun}} = \frac{\sum_{t0}^{t} P(t)}{\sum_{t0}^{t} A_{PV} . G_T(t)} = \frac{\int_{t0}^{t} P(t)dt}{A_{PV} \int_{t0}^{t} G_T(t)dt} \tag{3.36}$$

Where, E_{PV} is the energy output power from a module, E_{sun} is the energy of the sunlight or the incident irradiance in W, A_{PV} is the area of the PV module, and $G(t)$ is the radiation value with the time varying.

A: Potential of Solar Energy in Malaysia

Malaysia, being located at the equatorial zone is ideal for solar energy expansion. Malaysia was one of the top 5 countries in PV system production with energy generation up to 1600 kWh/KWp per year for a rooftop integrated PV systems (Jensen et al., 2006). On a yearly average basis, the day-to-day solar irradiations for Malaysia is ranged from 4.21–5.56 kWh/m^2. Solar energy could be acquired to produce electricity during 12 hours of daylight. Energy generation of about 900–1600 kWh/kWp per year was expected from the solar power installations in Malaysia (Solangi et al., 2011). About 1000–1500 kWh/kWp per year of power was acquired from a plant (Rahim et al.). The solar radiation and temperature values in Bangi, Malaysia are illustrated in Figure 3.10.

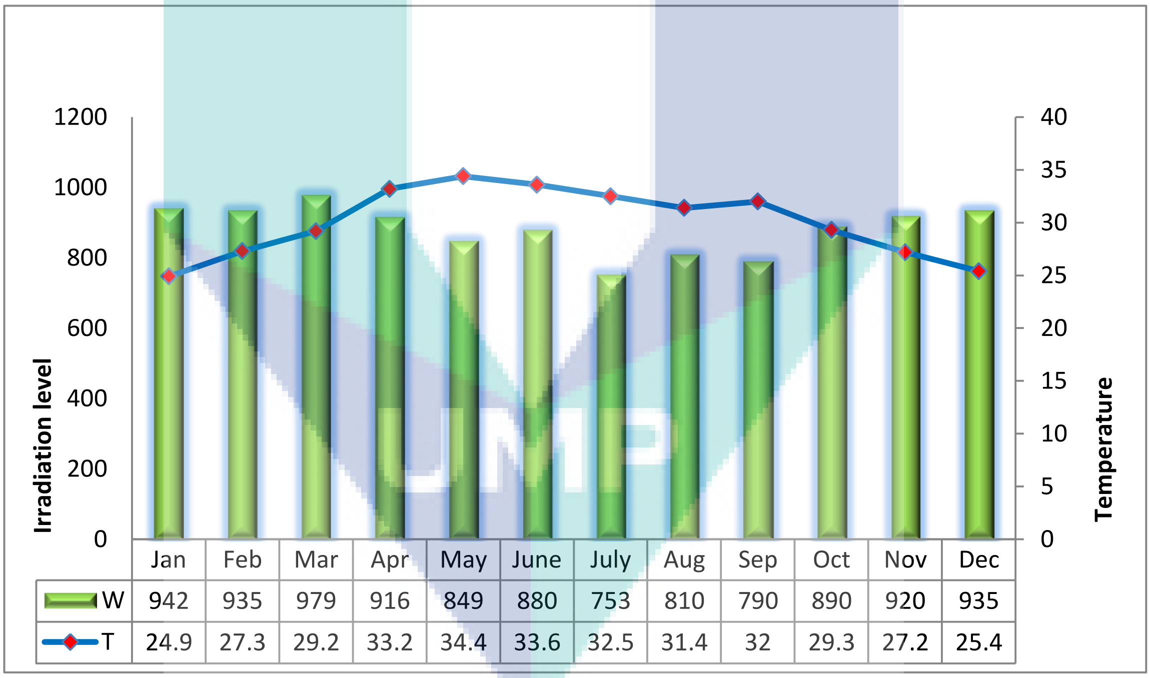

Figure 3.10. Mean monthly solar radiation and temperature for Bangi.

From January to December 2014, the surrounding temperature and hourly direct and diffuse solar radiation (the irradiance incident on the plane-of the array (POA)) were recorded. The Sunny Boy data logger from SMA brand, manufactured in Germany, is the source of data. The system configuration consists of two plants. Each plant is constructed in seven strings where each string consists of six PV modules (series-parallel configuration). To maximise the average power generated, the PV modules are installed at a fixed tilt angle of 17^{o} (optimum tilt angle for Malaysia) towards the true south (Ng et al., 2014).

From January to December 2014, the global and diffuse solar radiation were recorded. During the midday (12–2PM), the solar radiation values were recorded as high. In the early (7AM–9AM) and late (5–7PM) daytime, a small solar radiation value was recorded. In this tropical area, Bangi has a reasonable clear sky for most days (at noon time), as depicted in Figure 3.11. Moreover, direct radiation is acquired almost throughout the day. On an average, solar radiation obtained in Bangi is 4.885 kWh/m2/day. The temperature was recorded during the daytime with a mean value of 30 °C. On the other hand, the temperatures dropped from 24 °C to 35 °C (Johari et al., 2011; Solangi et al., 2011).

B: Evaluation Criteria of The PV System model Performance

An effective evaluation is carried out based on the energy generated, energy efficiency, and performance ratio of the proposed model and compared with other models and results of two real PV plants. This is to validate and assess the reliability of the proposed model in achieving better results based on real results from two distinctive PV innovations (c-Si and CIS) in Bangi city, Malaysia employed in this research and exhibited in Figure 3.12. These two PV power plants were consolidated in parallel to deliver a single point of interconnection with the grid. Numerous technical factors were applied in this study, for example, the daily *E(d)* and monthly *E(m)* generated energy from the PV power system and Performance Ratio *(PR)*.

The Eqs. (3.37) and (3.38) show the daily *E(d)* and monthly *E(m)* energy generated by the PV power system.

$$E(d) = \sum_{h=1}^{h=24} E(h) \tag{3.37}$$

$$E(m) = \sum_{d=1}^{d=n} E(d) \tag{3.38}$$

Where *n* represents the number of days in the month.

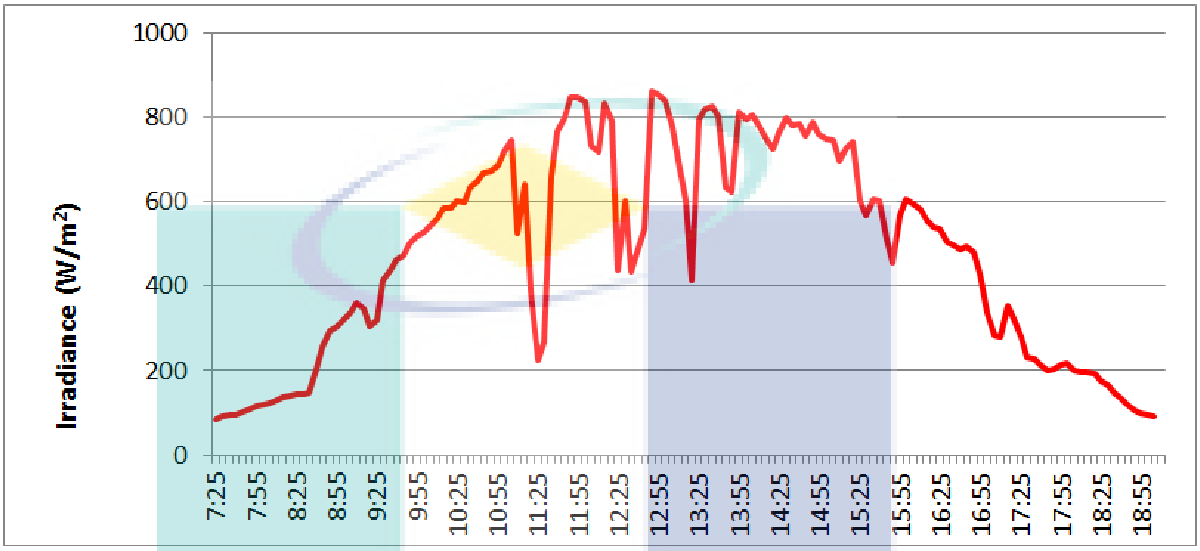

Figure 3.11. Daily irradiance level in Bangi area for January 2014.

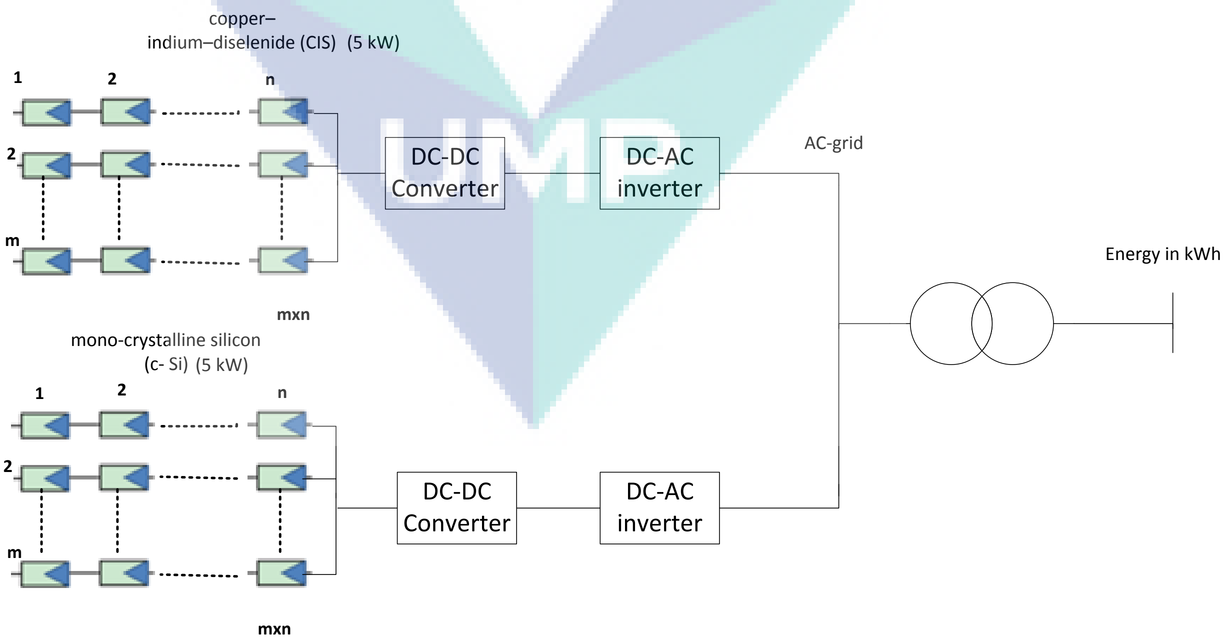

Figure 3.12. Schematic of two 5 kW solar PV plants installed in Bangi, Malaysia.

Where m=7 and n=6, which refer to the number of PV module in the PV plants. The energy produced by solar PV power plant was measured after DC-AC conversion to acquire energy output, instantaneously.

The aggregate weight losses in a PV module normal power output is signified by *PR*, that is dictated by the array temperature and fragmented use of incident solar radiation with the system component inefficiencies or failures. The performance proximity of solar plant to the ideal performance during real operations is given by *PR*. This can be utilised to differentiate the solar power plant regardless of the location, orientation, tilt angle, and their normal rated capacity. A comparison between the solar PV power plant efficiency and the nominal efficiency of PV generator under standard test conditions is executed. Equation (3.39) gives the performance ratio, (Lotsch et al., 2005). Alternatively, it can be expressed as the percent of net ratio of the actual to the theoretical energy outputs of PV array as expressed in Eq. (3.41) (Essah et al., 2015; Kymakis et al., 2009).

$$PR = \frac{E_{AC}}{G\eta_{STC}} \tag{3.39}$$

Hence,

$$\eta_{STC} = \frac{P_{AC(STC)}}{G_{STC} \times A} \tag{3.40}$$

PR can also be expressed by Eq. (3.35).

$$PR = \frac{E_{real}}{E_{ideal}} \tag{3.41}$$

3.8 Summary

The details of the PV modelling methodology, MPPT algorithm implementation and PID controller for steady state condition attaining are presented in this chapter. All available five parameters of PV cell were considered in this study to develop PV model that is able to emulate PV characteristics when operating under different weather conditions. Ant Colony Optimization (ACO) and Particle Swarm Optimisation (PSO) algorithms are combined and employed to develop MPPT method for PV system operating under shadow conditions. Three different case studies have been applied to investigate the ability of the proposed method in locating the global MPP. Moreover, this chapter also presented an optimal PID controller, which is employed to attain the steady state condition for the power output value after tracking it. The results are presented in the following chapter.

CHAPTER IV

RESULTS AND DISCUSSION

4.1 Introduction

This chapter focuses on the results and discussions obtained based on the two dominant fields of solar PV system: (1) modelling and characterisation of solar PV system under different shadow conditions and (2) improving and implementing an algorithm of MPPT to enhance the performance of solar PV system that operates under different shadow conditions. Modelling and characterising solar PV arrays are important tasks in solar PV system. Solar PV system design needs to meet demands by taking applicable restrictions into consideration. These restrictions are mainly the changing and fluctuating surrounding weather conditions (like the irradiance and temperature). Therefore, this chapter essentially presents the results and its discussion for modelling and characterisation of solar PV systems. This model is then used in the proposed MPPT method in different shadow conditions, to evaluate the quality and the reliability of the proposed method as presented and discussed earlier. Finally, the results of the model validation and its performance based on two real PV plants are presented in this chapter.

4.2 Photovoltaic Modelling

In general, the modelling of a PV cell/module includes the computation of the power–voltage (P–V) and current–voltage (I–V) characteristics by utilising a particular model. Nevertheless, it is a complex and difficult assignment to create models that represent numerous irradiance and temperature conditions that can figure out the parameters in a an accurate manner (Ciulla et al., 2014; Keogh et al., 2004). As such, the modelling involves a diversified types of methods used. In addition to that, the accurate measurement of I–V and P–V characteristics are essential in controlling the quality of solar cells and evaluating the performance of PV systems. Nevertheless, such measurement's accuracy is directly linked to the number of DC parameters extracted in that model. Literature studies differ in terms of the utilisation of a number of parameters in building its models. As specified in chapter III, only few studies used the five-parameters model, while others built the PV model based on four-, three-, two-, or even one-parameter model. However, the five-parameters model is the most widely used model and mostly accurate, particularly for outdoor condition tests(Brano et al., 2010; Celik Acikgoz, 2007). Therefore, by considering all available DC parameters, the model should be equipped with better accuracy.

As presented in chapter three, this study is built on the basis of single-diode, five- parameter model. The traditional equation illustrates a simple single-diode model with distinctive I–V characteristics, Eq. (2.3) which was presented in chapter II.

4.2.1 PV Array Modelling and Characterisation

Based on the general definition of PV modelling, the I–V and P–V characteristics of solar cells/modules have the most significance in the PV industry because it precisely reflects the cell/module performance. Nevertheless, it is not an easy way out to get the model parameters from these I–V and P–V curve for PV cells/modules (Chan Phang, 1987; Ortiz-Rivera Peng, 2005). For example, the I–V and P–V characteristics of the one-diode model are affected by the cell temperature and irradiance value apart from the effect of five electric parameters.

In this work, experimental data for a PV system installed under Malaysian climate condition were used to get an accurate value for the constants of $C_{coef\ 1}$ to $C_{coef\ 9}$ (coefficient of the equations of the five-parameter used in this study, presented in chapter III) and then to utilise an accurate global PV model. The values of these constants are presented in table 4.1. The chosen system comprises of 5 kW grid-connected PV systems, which have been investigated through simulation for a period of one month (from 01.05.2014 to 31.05.2014). Its specification are presented in table 3.1. Throughout this period, irradiations, cell temperatures, output current, output voltage and PV output power are recorded every 0.1 seconds. These constant values ($C_{coef\,1}$-$C_{coef\,9}$) are derived from different illumination levels and are based on the tropical weather conditions. These constant coefficients are measured accurately based on experimental results obtained (as presented in table 3.1). The obtained coefficient results are collected from different samples besides the results for optimal value which are used in the model

Table 4.1
$C_{coef\,1}$-$C_{coef\,9}$ coefficient values

Factor	Sample 1	Sample 2	Sample 3	Sample 4	Sample 5	Optimal Value
$C_{coef\,1}$	0.0069	0.0072	0.0060	0.0048	0.0059	0.0062
$C_{coef\,2}$	0.0041	0.0053	0.0052	0.0045	0.0047	0.0048
$C_{coef\,3}$	6.48×10^{-6}	5.38×10^{-6}	7.04×10^{-6}	5.35×10^{-6}	5.17×10^{-6}	6.75×10^{-6}
$C_{coef\,4}$	3.92×10^{-8}	7.08×10^{-8}	3.57×10^{-8}	2.20×10^{-8}	4.23×10^{-8}	3.23×10^{-8}
$C_{coef\,5}$	2.765×10^{-4}	2.93×10^{-4}	2.27×10^{-4}	2.38×10^{-4}	2.96×10^{-4}	2.67×10^{-4}
$C_{coef\,6}$	6366	6372	6318	6372	6413	6399
$C_{coef\,7}$	112	119	122	125	119	117
$C_{coef\,8}$	3425	3481	3495	3482	3552	3502

As mentioned above, this work has focused on all five DC electric parameters a, I_L, I_o, R_s, and Rsh. Other works suggest that (Akkaya Kulaksiz, 2004) the characteristics depend on only two parameters: a and I_{ph}. On the other hand, in another study (Kaushika et al., 2005), the model is dependant only on the equations for I_{ph} and I_o. This research aims to derive new parameters within tropical site (Malaysia as the case study). The derivation of new set of equations based on extracted values are as follow:

$$a = \frac{T_c}{0.0062} \tag{4.2}$$

$$I_L = (0.0048 + 6.745\times10^{-6}\,T - 0.025)G_T \tag{4.3}$$

$$I_o = 2.677\text{E} - 4T^3\exp(-\frac{6399}{T}) \tag{4.4}$$

$$R_S = 4.03 - \frac{117}{G}\exp(-\frac{G}{3502}) \tag{4.5}$$

Figures 4.1 to 4.5 show the parameters (a, I_L, I_o, R_s, and R_{sh}) characterisation results.

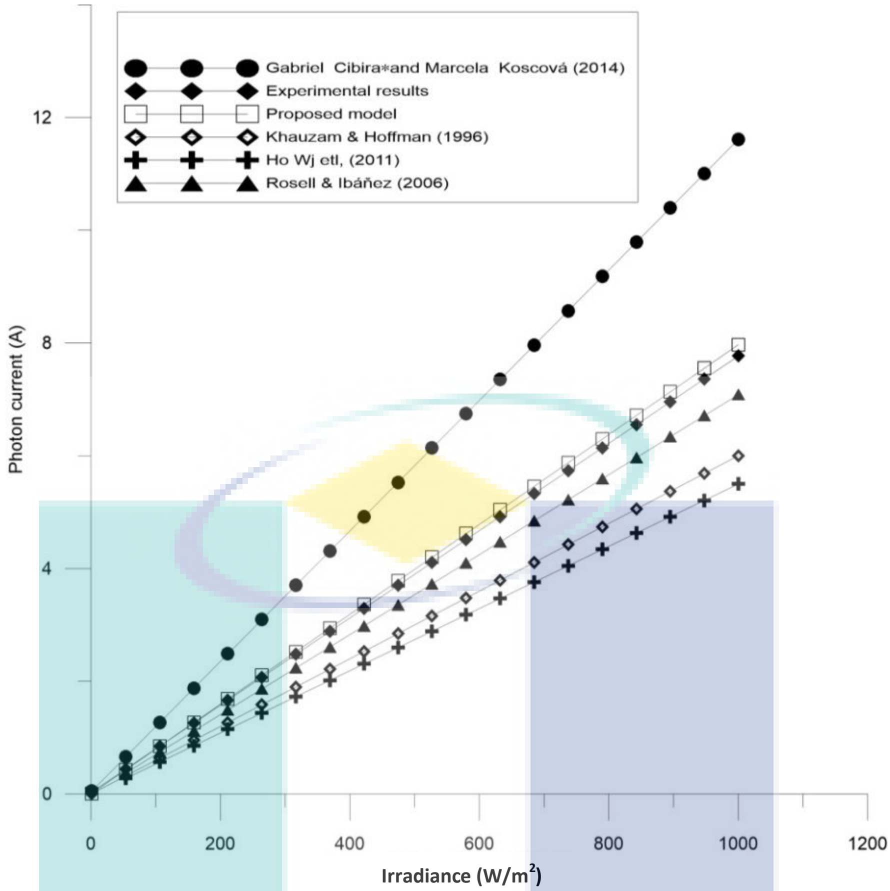

Figure 4.1. Results of the photon current of the proposed model compared with other models from the literature.

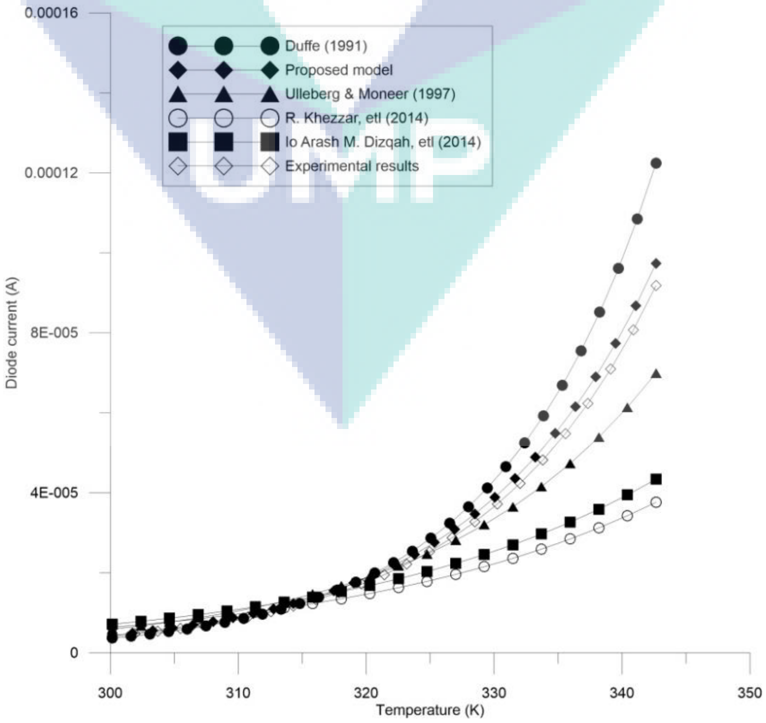

Figure 4.2. Results of the diode current of the proposed model compared with other models from the literature.

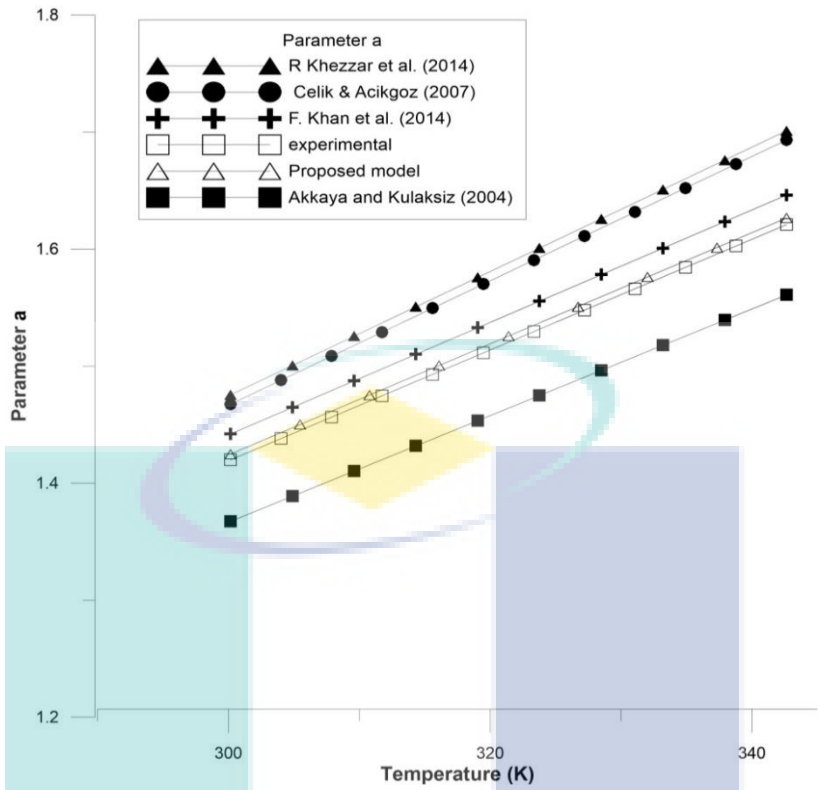

Figure 4.3. Results of parameter *a* of the proposed model compared with other models from the literature.

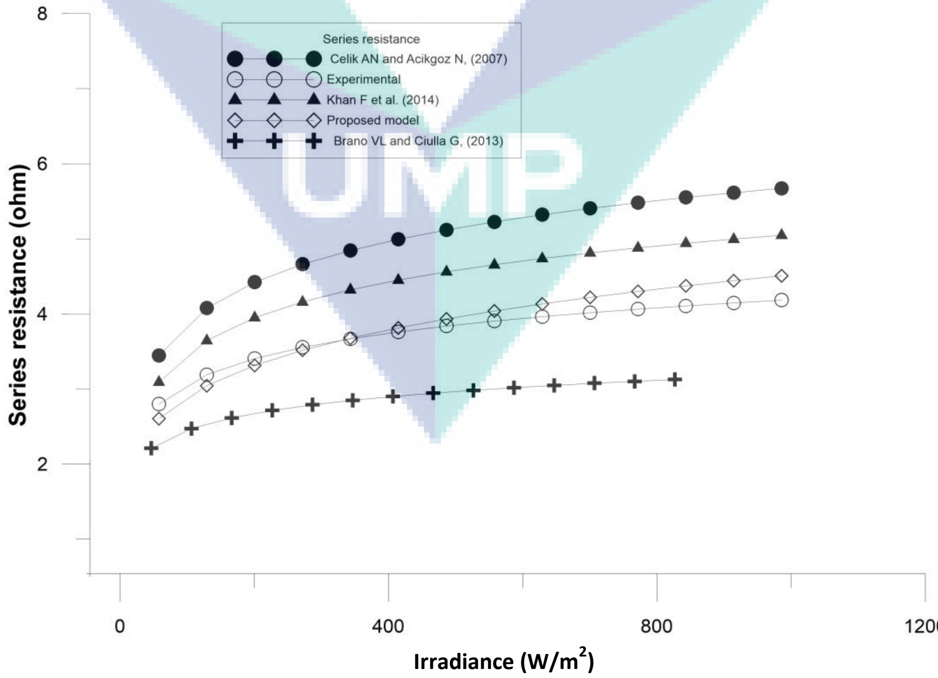

Figure 4.4. Results of the series resistance of the proposed model compared with other models from the literature.

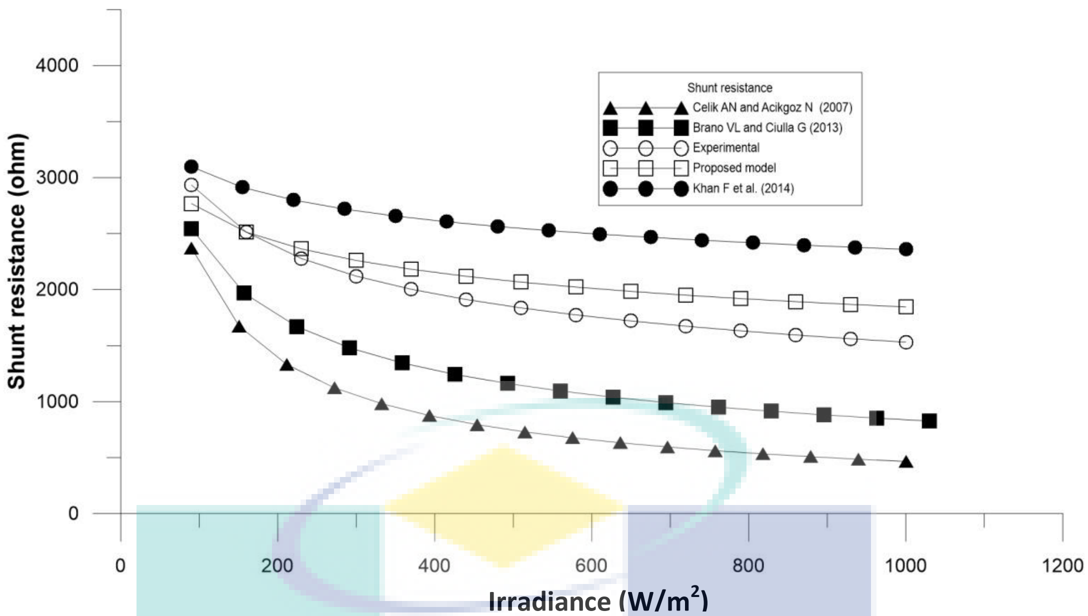

Figure 4.5. Results of the shunt resistance of the proposed model compared with other models from the literature.

Results of the five parameters (I_L, I_o, a, R_s and R_{sh}) are presented in Figures 4.1 to 4.5. Different evaluation criteria were used to validate the results of these parameters for the proposed model, which are then compared with other models from previous studies. The validation of parameters was performed using MAPE, SSE, and R-square. As shown in Table 4.2, the validation was executed using the five parameters (I_L, I_o, a, R_s and R_{sh}) equations, which were calculated from this study and the previously studied models. From Figures 4.1 to 4.5, the equations observed in this research study were found to be in good relation with the experimental data as compared to previously stated models (Brano Ciulla, 2013; Celik Acikgoz, 2007; Cibira Koščová, 2014b; Khan et al., 2014; Khezzar et al., 2014; Khouzam Hoffman, 1996).

In addition to that, as shown in Table 4.2, the computed coefficients are found to be more accurate in comparison with other models. Additionally, the proposed equations in models used for comparison compared contain several constants, which made the models' implementation more difficult. However, the proposed model in this research study comprises of five parameters (I_L, I_o, a, R_s and R_{sh}). This renders the model more accurate. The models used for comparison in this study contain less parameters, affecting the accuracy of these models. For instance, Cai, G. (2013)'s model contains four parameters (Gong Cai, 2013), while Rajasekar et al. (2013) employed three parameters (R_s, R_{sh}, a) (Rajasekar et al., 2013). However, some studies relied on only two parameters. Ortiz-Conde et al. (2006) used the R_s and parameter a (Ortiz-Conde et al., 2006), and El-Dein et al., (2013) used R_s and R_{sh} in those model (El-Dein et al., 2013). Cotfas et al. (2013) took only one parameter, the R_s to validate the model (Cotfas et al., 2013). Therefore, this current study is aimed to formulate new relations, considering the tropical weather conditions which have not been presented before. In general, the purpose of this research is to endorse the precision of the proposed model, on the basis of few benchmarks like mean absolute percentage error (MAPE), R-square, SSE, SSR, and SST as stated before. The results of calculated model parameters evaluation factors are presented in Table 4.2.

The research data for the five parameters (I_L, I_o, a, R_s and R_{sh}) are employed to investigate the accuracy and reliability (via applying evaluation criteria presented in chapter III, 3.3.3) values for coefficients used in this research (C_{coef1} to C_{coef9}) by differentiating them with the theoretical results. However, due to the speedy and persistent climate fluctuation conditions; such as irradiance and temperature, data logging has been accomplished continuously for both current and voltage (every 1 second). The results of of the evaluation criteria of these parameters are presented in Table 4.2.

Table 4.2.
Results of evaluation criteria of the proposed model.

Evaluation Creteria	**Parameter *A***	**Parameter I_o**	**Parameter I_L**	**Parameter R_s**	**Parameter R_{sh}**
MAPE	3.12%	4.9%	2.3%	7.3%	11.3%
SSE	2.198×10^{-16}	2.721×10^{-15}	7.216×10^{-14}	4.374×10^{-12}	4.345×10^{-11}
R-square	0.9998	0.998	0.997	0.995	0.993
SSR	1.0987×10^{-12}	1.3613×10^{-12}	2.39812×10^{-11}	8.473×10^{-10}	9.872×10^{-9}
SST	1.099×10^{-12}	1.364×10^{-12}	2.405×10^{-11}	6.463×10^{-10}	4.324×10^{-9}

4.2.2 Inverter Modelling and Characterisation

The assessment for inverter's efficiency which has been executed through the expected and real results is illustrated in Figures 4.6 and 4.7, and their relationship is represented by the Eqs. (4.6) and (4.7) below.

$$\eta_{inv} = 105.1\, P_{pv}^{0.1456} \quad \text{for} \quad 0 < P_{pv} < 0.517 \tag{4.6}$$

$$\eta_{inv} = 0.6032 P_{pv} + 94.64 \quad \text{for} \quad P_{pv} \geq 0.517 \tag{4.7}$$

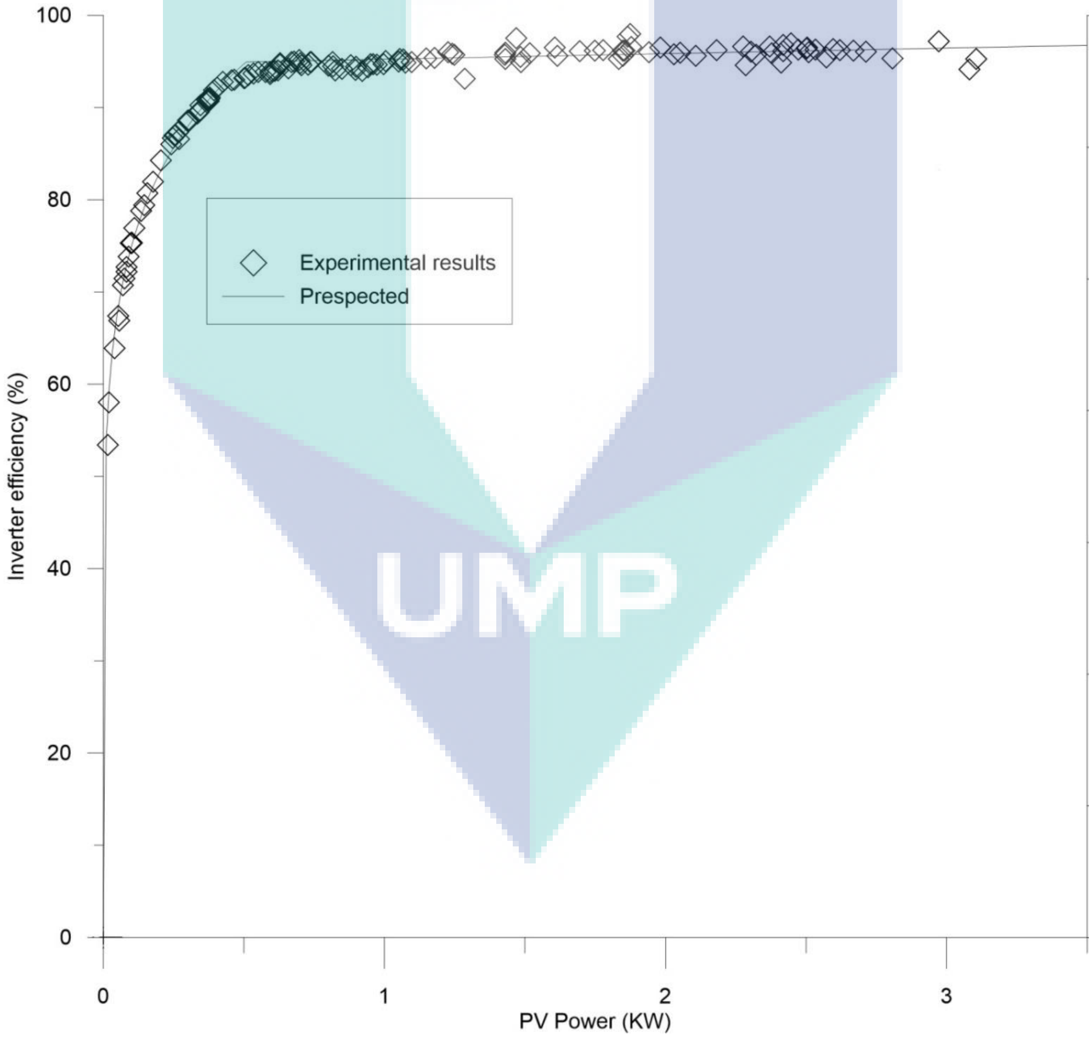

Figure 4.6. Inverter efficiency curves from both experimental and proposed model.

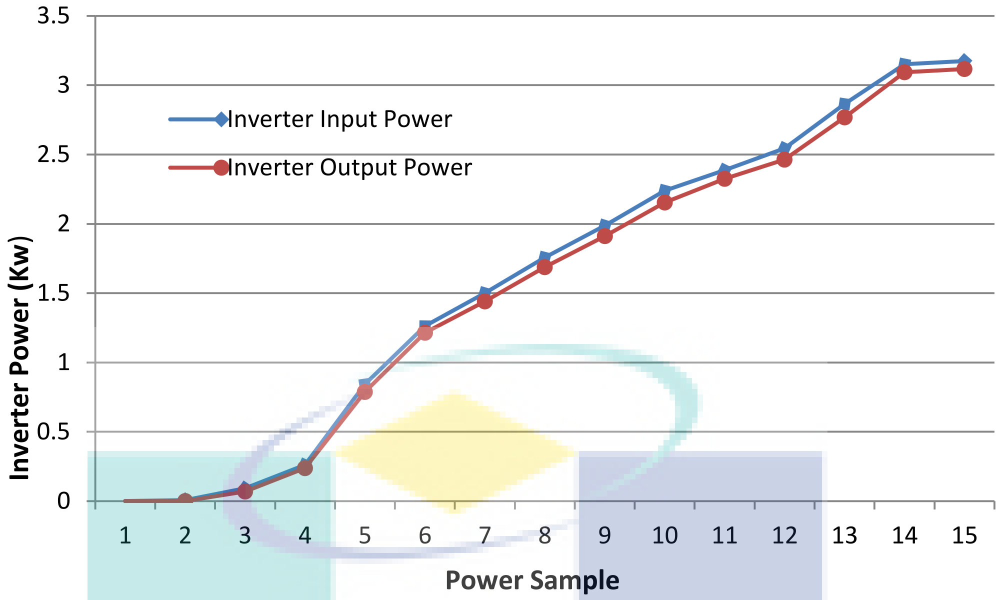

Figure 4.7. Inverter power curves for input and output power values.

Figure 4.6 presents the curves of the inverter efficiency for both the proposed model and real data, depicting that the efficiency of model inverter is fitting the real data provided. Therefore, it could be concluded that the inverter efficiency equations achieve a good level of accuracy (as much as possible), as shown through the difference between input and output power in Figure 4.7. Therefore, Figure 4.7 shows the precision level of the proposed model, proving that the used model depicts good results in term of accuracy, when compared between input and output power of the inverter. As can be seen from Figure 4.7, inverter output power is almost close to inverter input power, and this for all sample power taken. Consequently, based on these results as shown in Figure 4.6, these equations may be considered standard for certain type of inverter, which operates through a system in the same weather conditions.

4.2.3 Model Performance Based on Temperature and Irradiance Effect

The above mentioned model Eqs. (4.1 to 4.5) are used to simulate Kyocera KC175GHT PV module in order to test model performance by fitting the I–V and P–V curve at standard test conditions (E =1000 W/m^2 ; T = 25 °C). In the first step, ambient temperature was kept constant (25 °C) with varied irradiance values and its characteristics were studied, as shown in Figure 4.8 and 4.9. In the second step, the irradiance value was fixed (1000 W/m^2) and the performance was observed with changing temperature values (Kyocera PV module Table 3.1), as shown in Figure 4.10 and 4.11. Furthermore, other models were employed (Brano Ciulla, 2013; Celik Acikgoz, 2007; Khan et al., 2014) from literature, to prove the precision of the proposed model with respect to the real results (experimental). In addition to the effect of irradiance and temperature values, the behaviour of a solar panel for different values of solar parameters on the I–V and P–V were studied and the results obtained were compared with respective models.

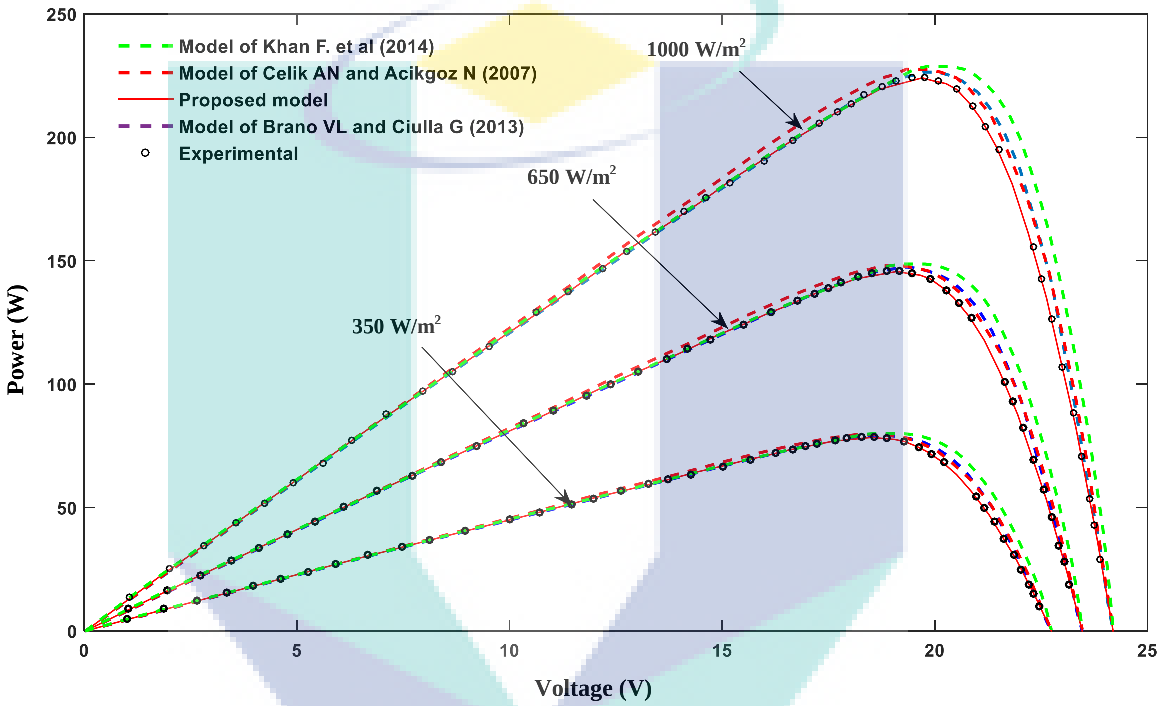

Figure 4.8. Effect of changing irradiance conditions on the P–V characteristic curve, with fixed cell temperature (25 °C)

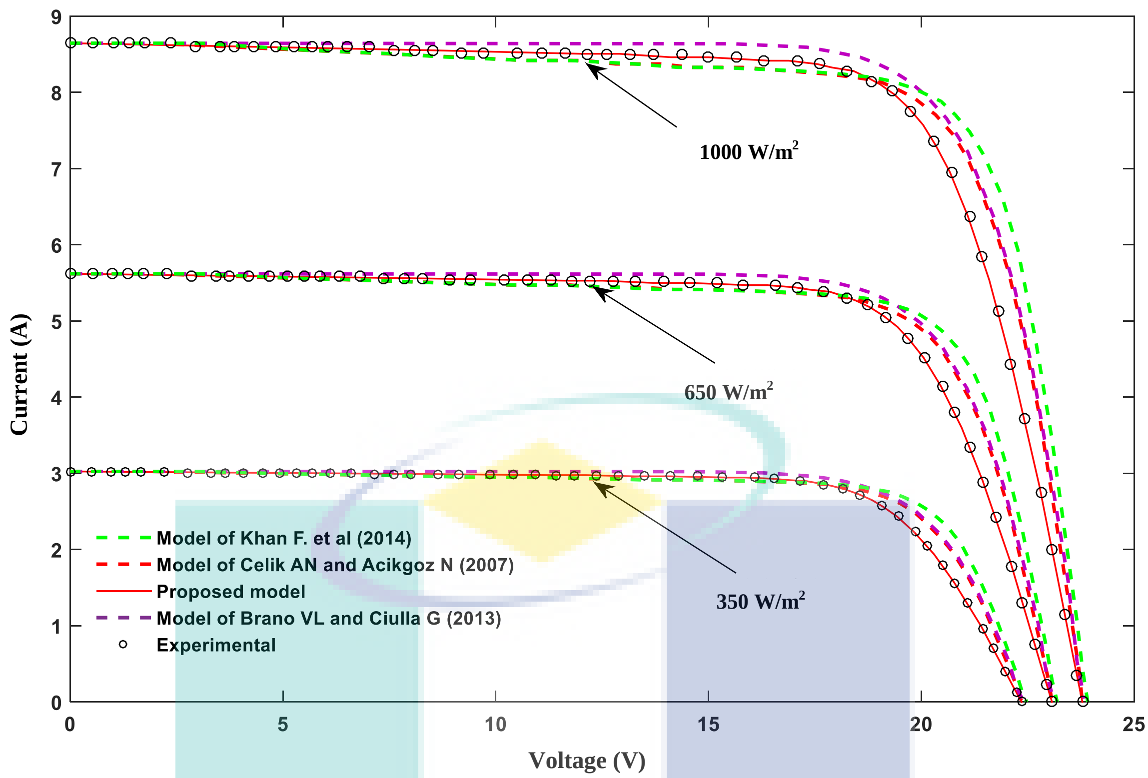

Figure 4.9. Effect of changing irradiance conditions on the I–V characteristic curve, with fixed cell temperature (25 °C)

Figures 4.8 and 4.9 show that the model fits the I–V and P–V curves at different irradiance values at fixed temperature (25 °C). The results evidenced that in both I–V and P–V characteristic curves, the proposed model is making a smooth convergence with experimental results more than the other models (Brano Ciulla, 2013; Celik Acikgoz, 2007; Khan et al., 2014), as presented in table 4.3. In addition to that, from the two Figures (4.8 and 4.9), it is found that all models are affected by the change in irradiance values in equal proportion, except for Ciulla, B. (2013)'s (Brano Ciulla, 2013) model. With reference to Ciulla, B. (2013)'s model (Brano Ciulla, 2013), the MPP decreased more than other models which had more significant decrement in irradiance as compared to MPP. This is due to considering the irradiance value that had affected MPP directly, rather than the open circuit voltage (V_{oc}) and short circuit current (I_{sc}) values. Furthermore, changing the radiation level has the proportional effect on both V_{oc} and I_{sc} values, for all compared models and the proposed model. On the other hand, the impact of changing cell temperature values on the P–V and I–V characteristic curves showed different pattern. The results of changing cell temperature levels by fixing the irradiance (1000 W/m^2) are presented in Figures 4. 10 and 4.11, for P–V and I–V characteristic curves, individually.

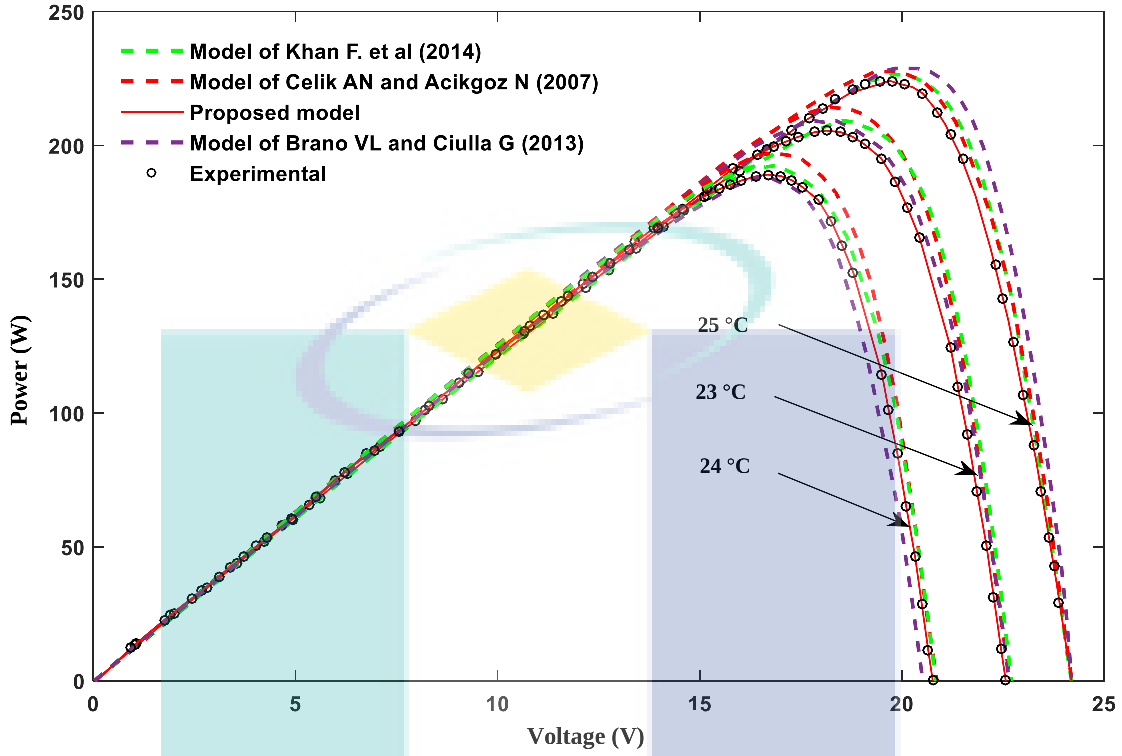

Figure 4.10. Effect of changing cell temperature on P–V characteristic curve, with the fixed irradiance level (1000 W/m^2).

Results of Figures 4.10 and 4.11 showed that the model fits the I–V and P–V curves at various cell temperature and fixed irradiance (W/m^2) values. These results depicted, that in both P–V and I–V characteristic curves, the proposed model is in good agreement with the experimental results, and in fact, even better than the previous models (Ciulla, B., 2013; Acikgoz, C., 2007; Khan et al., 2014) (Brano Ciulla, 2013; Celik Acikgoz, 2007; Khan et al., 2014). Apart from good accuracy, the accuracy of the proposed model's effect within cell temperature as compared to the other models is also presented in Table 4.3. In addition to that, it is observed from Figures (4.10 and 4.11), that all models are affected by changing the cell temperature values in the same proportion, other than Ciulla, B. (2013)'s (Brano Ciulla, 2013) model. In Ciulla, B. (2013)'s model (Brano Ciulla, 2013), the MPP and radiance decreased more than the other models. Ciulla, B. (2013), in his model, proposed that the cell temperature value will have a direct effect on the MPP values, and not on the open circuit voltage (V_{oc}) and short circuit current (I_{sc}) values.

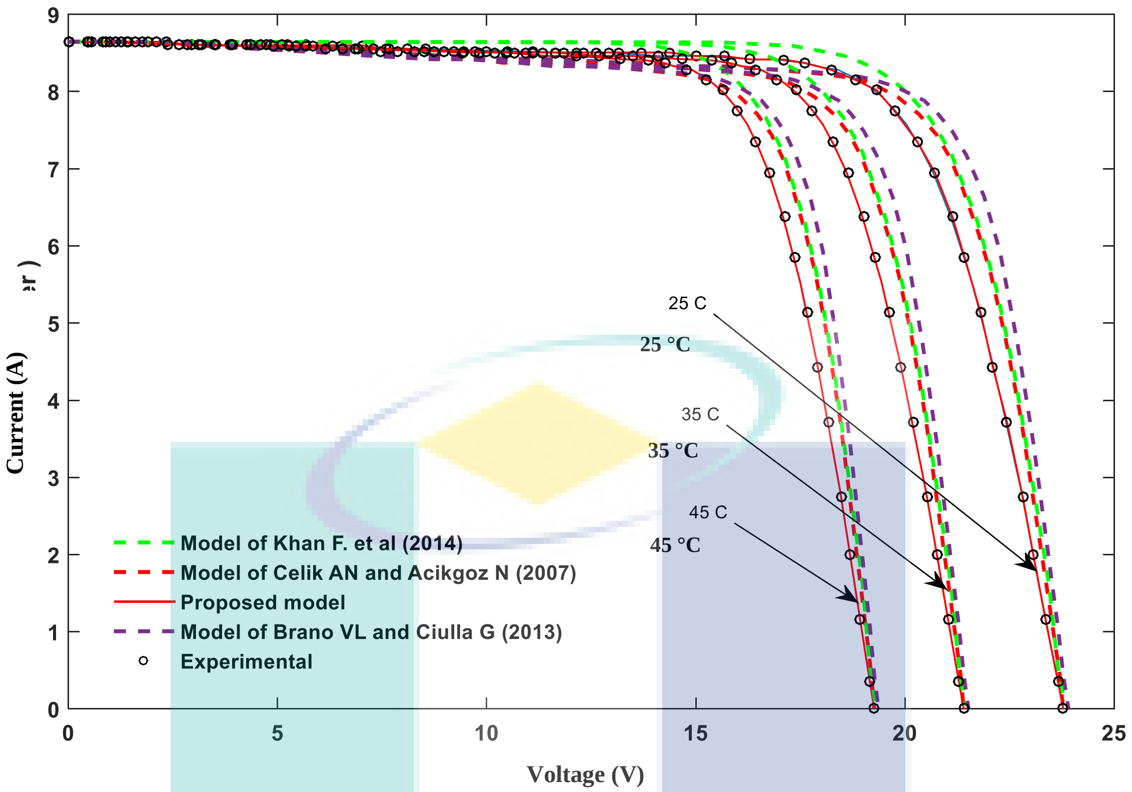

Figure 4.11. Effect of changing cell temperature on I–V characteristic curve, with fixed irradiance level (1000W/m^2).

4.2.4 Model Performance Based on Solar Cell Parameters Effect

The equations of solar cell parameters were applied practically (using Kyocera KC175GHT PV modules) to validate the P–V and I–V characteristics of the proposed PV model, and then simulated in the Matlab environment. The specification of the Kyocera KC175GHT module were summarised previously, in table 3.1. In addition to the effect of cell temperature and solar irradiance level on P–V and I–V characteristics, this part explains the influence of solar cell parameters, on P–V and I–V characteristic curves. The fundamental parameters of interest are the photocurrent, I_{ph}, the ideality factor of diode, a, the reverse diode saturation current, I_o, the series resistance, R_s, and the shunt resistance, R_{sh}. In this section, the influence of these five parameters is deduced and the improvement in the parameters performance during the characterisation (I–V and P–V characteristics) is studied. It is then validated by comparing it with different models at the standard test conditions (G = 1000 W/m^2, T = 25 °C).

A: Effect of Photocurrent, I_{ph}

Initially, all parameters were implemented separately to depict the influence of these parameters on the I–V and P–V characteristic curves, and then on the MPP, simulated separately as presented in Figures 4.12 to 4.19. The first parameter considered was the photocurrent, I_{ph}. The results of this parameter's influence on both I–V and P–V characteristic curves are illustrated in Figures 4.12 and 4.13, individually.

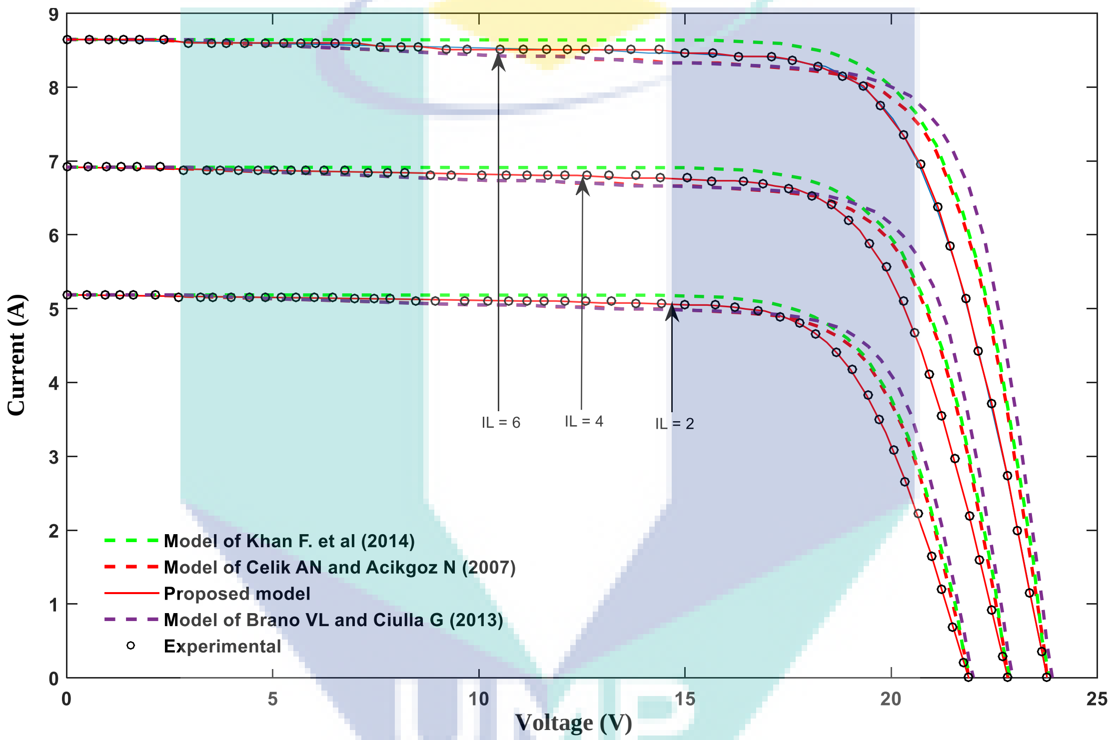

Figure 4.12. Influence of changing increasing I_{ph} on the I–V characteristic curve, at standard test condition (1000 W/m^2, 25 °C)

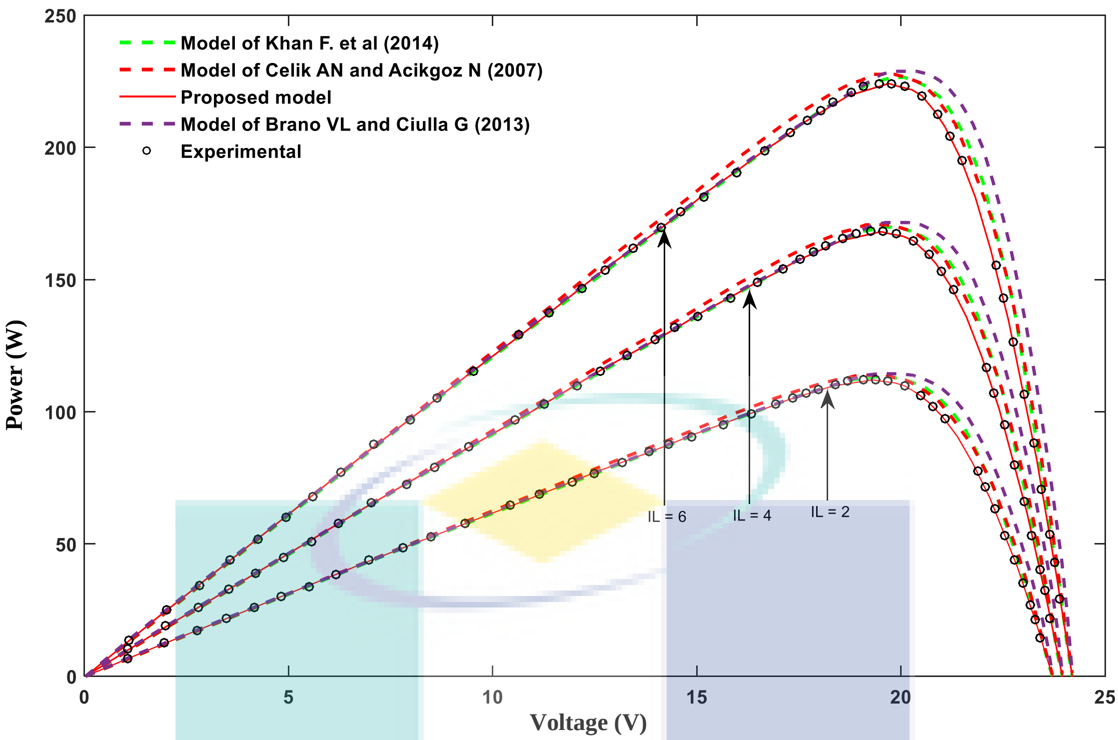

Figure 4.13. Influence of changing increasing I_{ph} on the P–V characteristic curve, at standard test condition (1000 W/m^2, 25 °C)

From Figures 4.12 and 4.13 it can be deduced that the results produced by different models are in concordance with the proposed model and the experimental results of both the I–V and P–V characteristics. However, based on more than one benchmark subjected in this study, the precision of the proposed model fit the experimental results in higher accordance than all the other compared models. These results of accuracy are presented in table 4.3.

In addition to that, an increase in the photocurrent I_{ph}, as shown in Figures 4.12 and 4.13 leads to increment in the MPP in a prominent way. Furthermore, it also affects short circuit current, I_{sc} and open circuit voltage, V_{oc}. This effect is also positive. Hence, an increase in the I_{ph} leads to an increase in both I_{sc} and V_{oc} values. However, the I_{sc}, was found to be more affected than V_{oc} with this increase.

B: Effect of Reverse Diode Saturation Current, I_o

The reverse diode saturation current, I_o is second parameter in consideration for this study. The same conditions of cell temperature and irradiance value (1000 W/m^2, 25 °C) are applied to carry out the influence of I_o on both I–V and P–V characteristic curves. The results of this parameter's effect on I–V and P–V characteristic curves are presented in Figures 4.14 and 4.15, respectively.

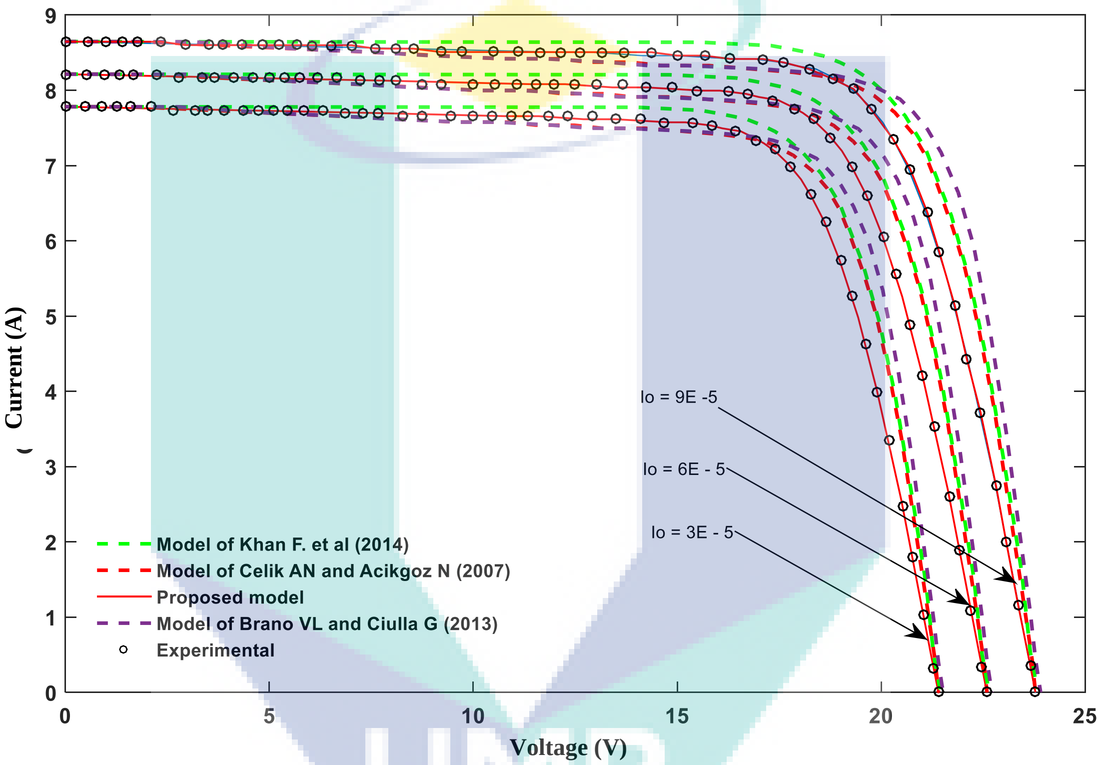

Figure 4.14. Influence of changing reverse diode saturation current, *Io* on the I–V characteristic curve, at standard test condition (1000 W/m^2, 25 °C)

From Figures 4.14 and 4.15, it is evident that the results of the proposed model merit in high convergence fitting as compared to results of other selected models from literature (Brano Ciulla, 2013; Celik Acikgoz, 2007; Khan et al., 2014), and for both I–V and P–V characteristics. Furthermore, based on more than one benchmark subjected in this study, the accuracy of the proposed model is in close matching with experimental results, higher than all other compared models. The accuracy results of these models with the proposed model are shown in table 4.3.

Moreover, these Figures (4.14 and 4.15) deduced that an increase in the reverse diode saturation current, I_o results in an increment in the MPP at an average mode. In addition to that, it also affects the open circuit voltage, V_{oc} and short circuit current, I_{sc}. These effects are also found to be in a positive direction. Furthermore, an increase in the reverse diode saturation current, I_o leads to an increase in both the I_{sc} and V_{oc}. Hence, both I_{sc} and V_{oc} are affected by approximately the same proportion.

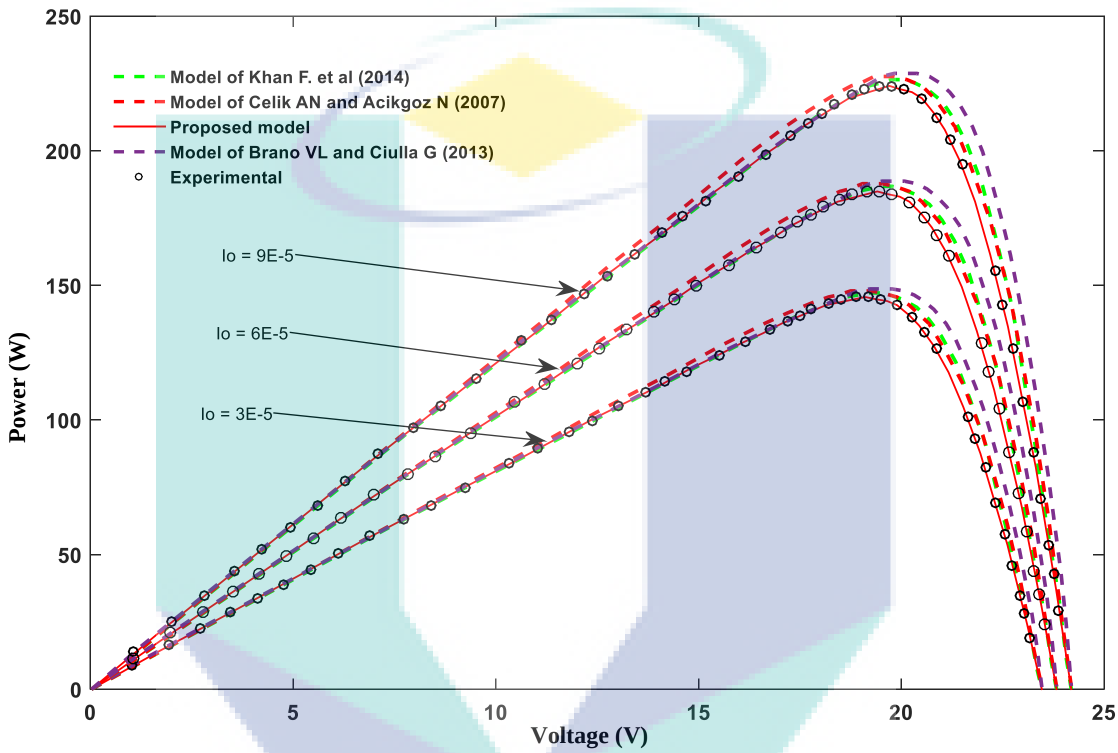

Figure 4.15. Influence of changing reverse diode saturation current, *Io* on the P–V characteristic curve, at standard test condition (1000 W/m^2, 25 °C)

C: Effect of Reverse Diode Ideality Factor, *n*

The ideality factor parameter, *n* depends mainly on cell temperature, rather than irradiance level. Investigation of this parameter's impact on the I–V and P–V characteristic curves with available real results and comparing them with other models (Brano Ciulla, 2013; Celik Acikgoz, 2007; Khan et al., 2014) were carried out in this study. This was accomplished when the cell temperature and irradiance level were kept constant at standard test condition (1000 W/m^2, 25 °C). The results of this parameter's effect on the I–V and P–V characteristic curves are presented in Figures 4.16 and 4.17, respectively.

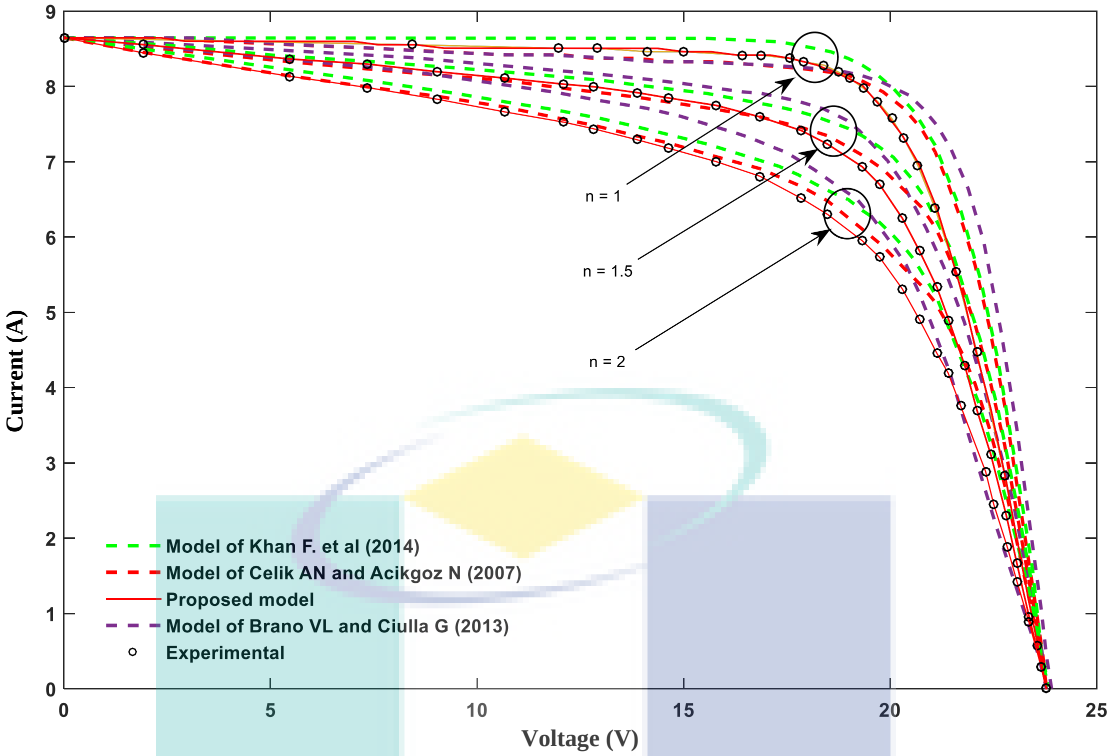

Figure 4.16. Influence of changing diode ideality factor, *n* on the I–V characteristic curve, at standard test condition (1000 W/m^2, 25°C)

The results obtained from Figure 4.16 and 4.17 showed that the change in diode ideality factor, *n* did not affect the values of the open circuit voltage, V_{oc} and short circuit current, I_{sc}. On the other hand, it was observed that the increase in diode ideality factor, *n* leads to a decrement in the value of MPP for both I–V and P–V characteristic curves.

The results of the diode ideality factor's effect on the P–V and I–V characteristic curves were derived by simulation and were compared with the experimental results. In terms of accuracy, the results obtained for different diode ideality factor (2, 1.5, and 1) vary from one model to another, where the Celik AN and Acikgoz N (2007)'s model model is strongly influenced by the variation of *n*. On the other hand, the proposed model showed good performance, regardless of variation in *n* values. However, the rest of the models compared were less affected by changing *n* values.

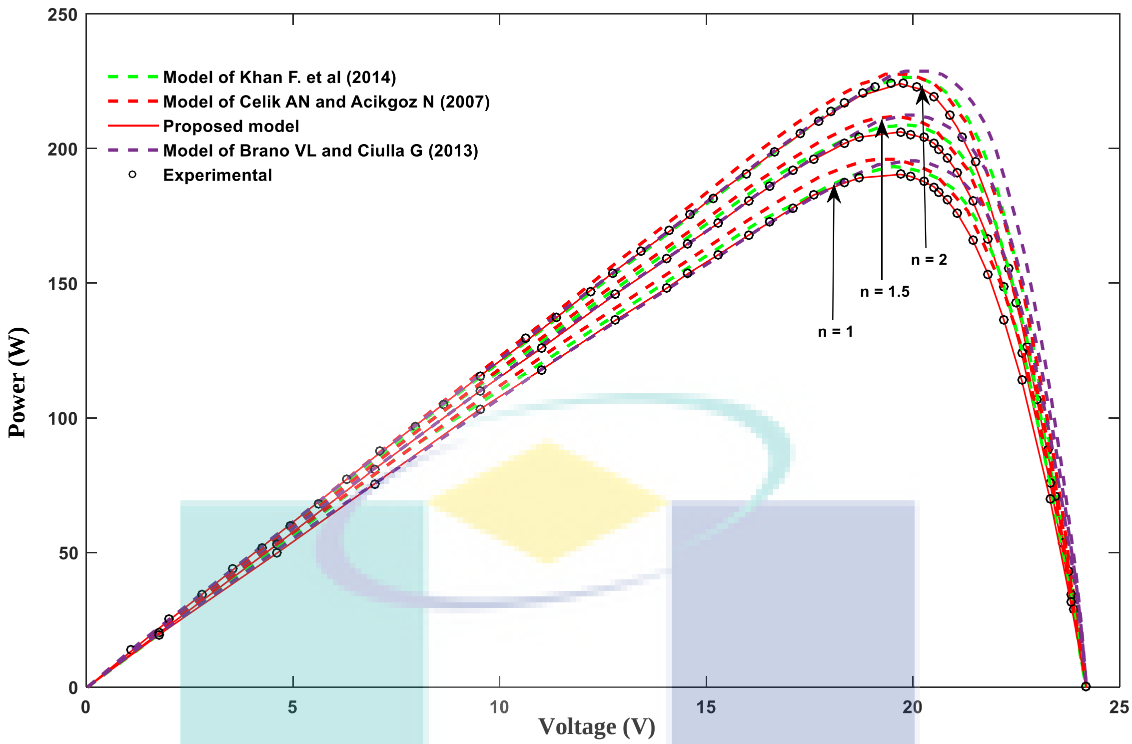

Figure 4.17. Influence of changing diode ideality factor, *n* on the I–V characteristic curve, at standard test condition (1000 W/m^2, 25 °C)

D: Effect of Series Resistance, R_s

The series resistance, R_s, shown in Eq. (4.5), is another important parameter to be considered for ploting the P–V and I–V characteristic curves. It was observed that this parameter is depending on the effective solar irradiance, *G* and the cell temperature, *T*. Since it regulates the location of the MPP, it also regulates the current and voltage at the MPP. Investigation of this parameter's effect on the P–V and I–V characteristic curves are also compared with experimental and other models' (Bruno Ciulla, 2013; Celik Acikgoz, 2007; Khan et al., 2014) results. For the same standard test conditions, the test was conducted by keeping the cell temperature and irradiance level constant (1000 W/m^2, 25 °C) and varying the series resistance value in the range (0.5Ω, 5Ω, and 10Ω), since the average value of R_s is around 5Ω as presented by Khatib et al., (Khatib et al., 2013). The results of this parameter's effect on the P–V and I–V characteristic curves are presented in Figures 4.18 and 4.19, respectively.

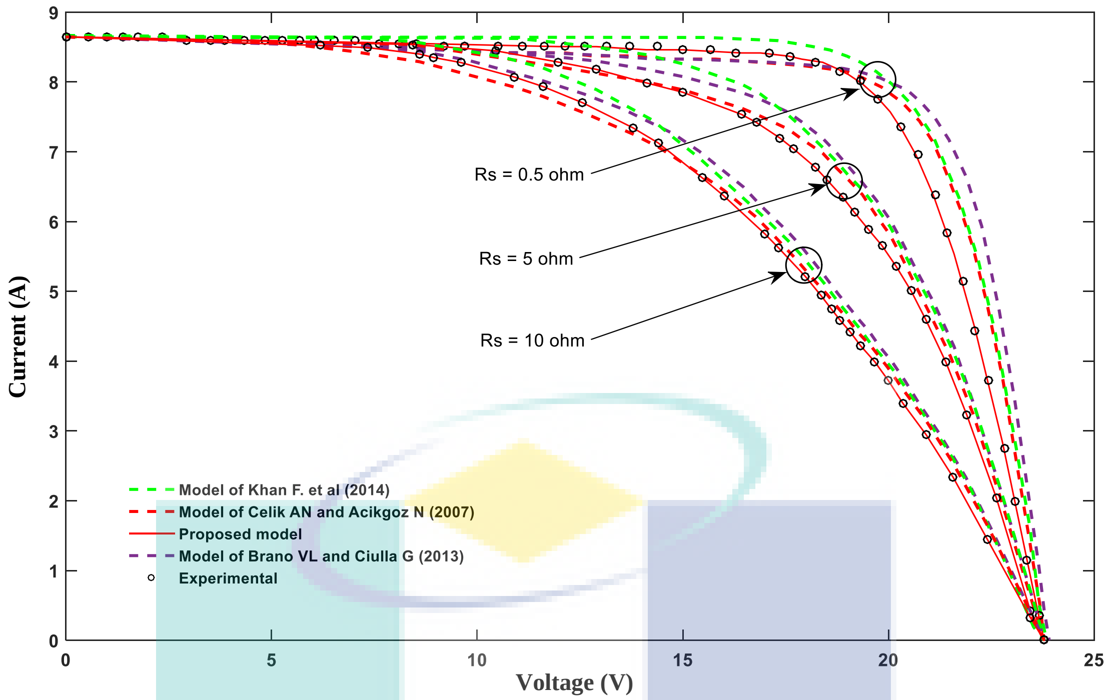

Figure 4.18. Influence of changing series resistance, R_S on the I–V characteristic curve, at standard test condition (1000 W/m^2, 25 °C).

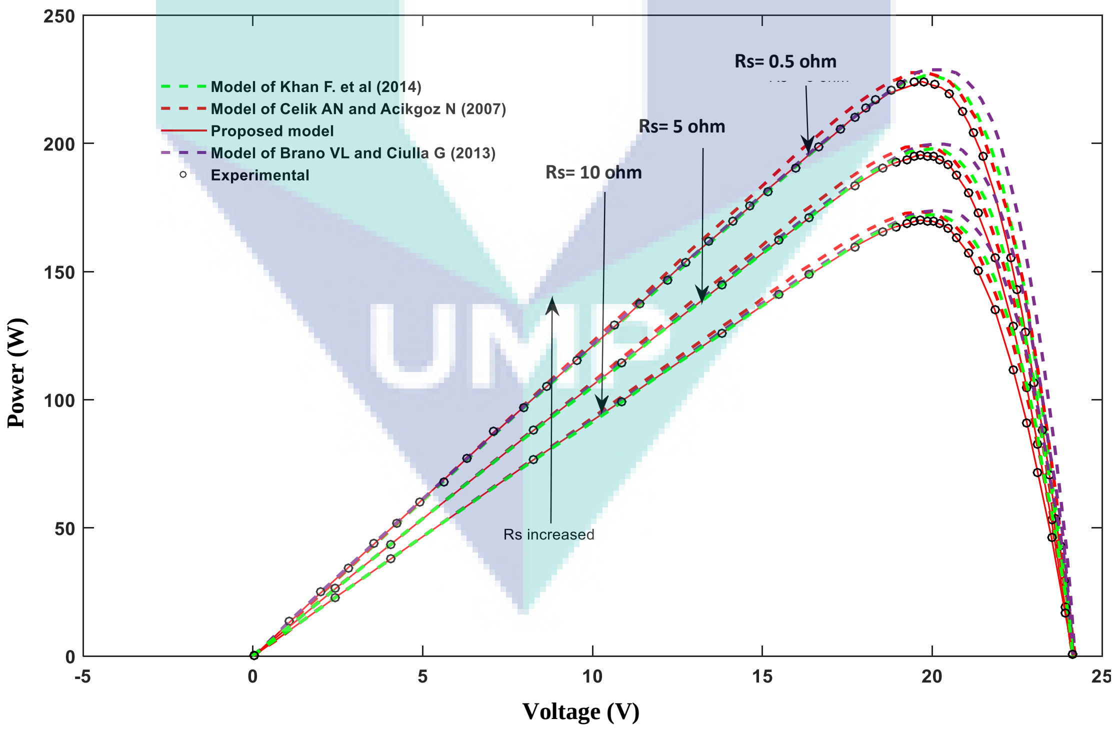

Figure 4.19. Influence of changing series resistance, R_S on the P–V characteristic curve, at standard test condition (1000 W/m^2, 25°C).

As mentioned earlier, Figures 4.18 and 4.19 present the results of the effect of increment in the series resistance, R_s's value on P–V and I–V characteristic curves. These results showed that the increasing R_s values, did not affect the values of the open circuit voltage, V_{oc} and short circuit current, I_{sc}. On the other hand, it was observed that the increasing R_s values tend to decrease the MPP values, and both the I–V and P–V characteristic curves, prominently.

Furthermore, the results of series resistance's effect on I–V and P–V characteristic curves, derived by simulation are compared with the experimental and other models results (Brano Ciulla, 2013; Celik Acikgoz, 2007; Khan et al., 2014) accordingly. Finally, the precision of the results proved that the proposed model exactly fits the experimental results for different series resistance values (5, 3, and 0.5).

E: Effect of Parallel Resistance, R_{sh}

The fifth parameter of interest was the shunt resistance, R_{sh}. For this purpose, the effect of varying parallel resistance, R_{sh} on P–V and I–V characteristic curves of a PV module were considered in this research. However, influence of this parameter is found to be barely noticeable for all MPP, I_{sc}, and V_{oc}.

Table 4.3.
Evaluation of Parameter performance based on accauracy level and models.

Parameter Accuracy Based on Model	Model of F Khan		Model of Brano VL		Model of Celik AN		Proposed model	
	MAPE (%)	R-square	MAPE (%)	R-square	MAPE (%)	R-square	MAPE (%)	R-square
Effect of photocurrent, I_{ph}	4.35 (%)	0.9843	5.18 (%)	0.9885	3.87 (%)	0.9887	0.85 (%)	0.99873
Effect of diode current, I_o	5.34 (%)	0.9823	6.15 (%)	0.9839	4.74 (%)	0.9858	0.94 (%)	80.99842
Effect of diode idealiry factor, n	4.28 (%)	0.9855	4.95 (%)	0.9874	4.27 (%)	0.9865	1.05 (%)	0.998242
Effect of series resistance, R_s	4.11 (%)	0.9865	5.37 (%)	0.9813	4.83 (%)	0.9847	0.35 (%)	0.999432
Effect of shunt resistance, R_{sh}	-----------	---------	-----------	---------	-----------	---------	----------	---------

4.3 MPP Tracking and Steady State Condition Attaining

The MPPT techniques, introduced in chapter II, are important for the success of PV energy extraction through an energy conversion system, since they ensure that most of these methods succeed in tracking and extracting the maximum power. However, each method was used in a certain weather condition for a specific system, but not all available shadow conditions were considered; like shadow conditions with rapid change in the weather conditions. The tracking of MPP is challenging because the characteristics of PV array are nonlinear and change as the irradiance and temperature conditions change. An optimum algorithm should be able to track the MPP quickly as soon as environmental conditions change. The hill climbing algorithm is commonly used in most PV systems because, it is one of the simplest methods and it does not need earlier researches or modelling of PV array characteristics (Abdelsalam et al., 2011; Elgendy et al., 2012). However, it doesn't represent for characteristics' drift as a result of abnormal changes like change in shadow condition or other operating irregularities such as rapid change in radiation or temperature.

Therefore, even though the P&O technique operates well in normal conditions, it displays erratic behaviour in case of rapid change in irradiance and temperature levels which leads to wrong tracking. This led to the development of a new MPPT method, which improves and enhances efficiency of the extracted power within different weather conditions. Consequently, the proposed MPPT based on ACO-PSO and variable step size P&O applied and tested through three different shadow conditions helps in overcoming the effect of these shadow conditions on the extracted power. In all these shadow conditions, the MPPT method and optimal PID controller presented a clear enhancement for all oscillation round MPP, the settling time and the response time.

In this study, the proposed algorithm and controller were tested for all available conditions, such as normal and shadow conditions. A numbers of test sets were done in order to ensure good functionality of the proposed MPPT and PID controller. Firstly, the proposed method applied on the system was operated under normal weather conditions. The results of the output power based on the proposed method were later compared with the frequently used MPPT method (P&O method) and the result is also presented in this chapter. However, in case of shadow conditions, it presents different results, especially for output power which differs depending upon different shadow conditions. It was observed that the MPP was achieved from three different shadow conditions. Later, the graphs of three cases compared with the P&O MPPT technique is also presented.

4.3.1 Operation under Normal Conditions

Under no shadow conditions, the I–V and P–V characteristic curves of the PV system's array are presented in Figures 4.20 and 4.21, which represents the general characteristics of the PV model operating in normal condition. The results of tracking MPP at this operating condition are shown in Figure 4.22, where the MPP is tracked and extracted directly.

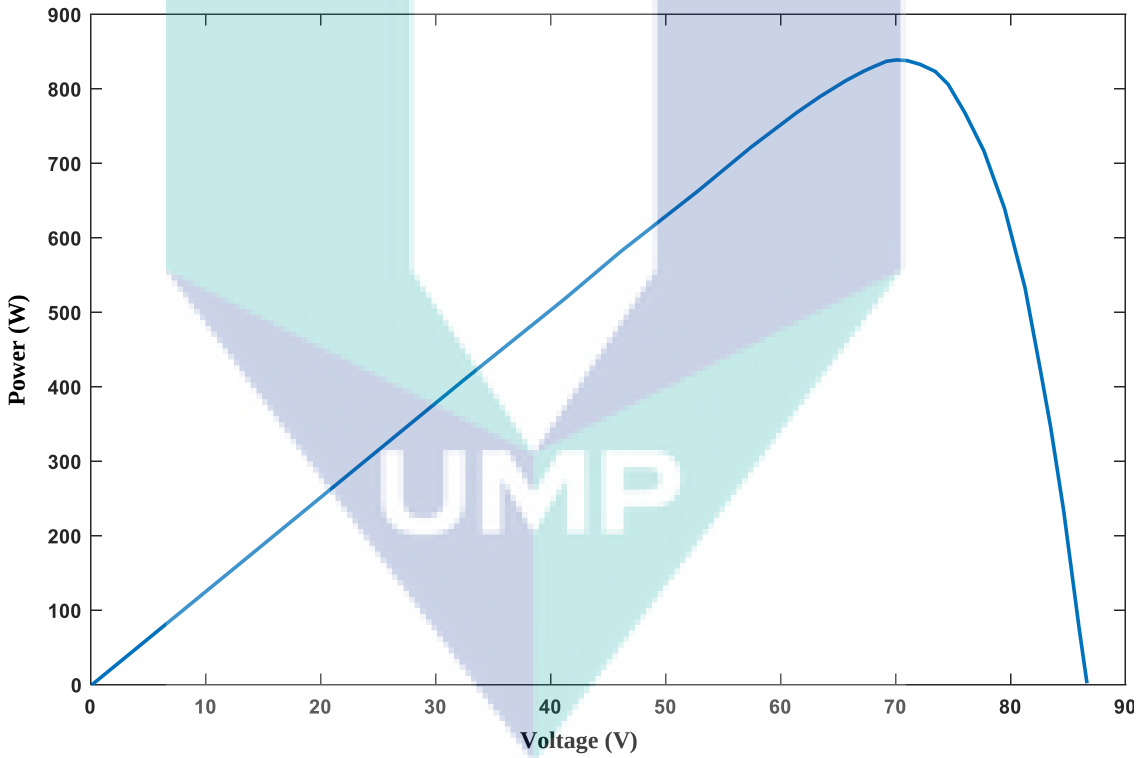

Figure 4.20. P–V characteristics of the PV array operating under normal conditions.

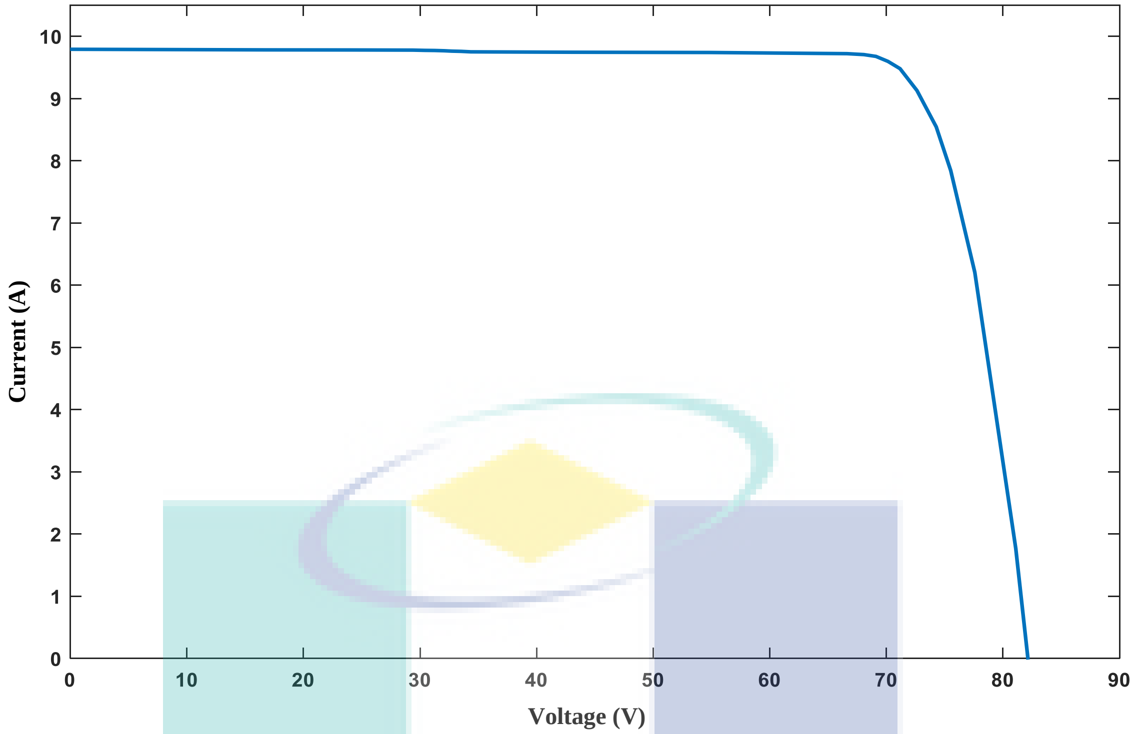

Figure 4.21. I–V characteristics of the PV array operating under normal conditions.

By using the proposed MPPT method, the extracted and output power graph is plotted, as shown in Figure 4.22.

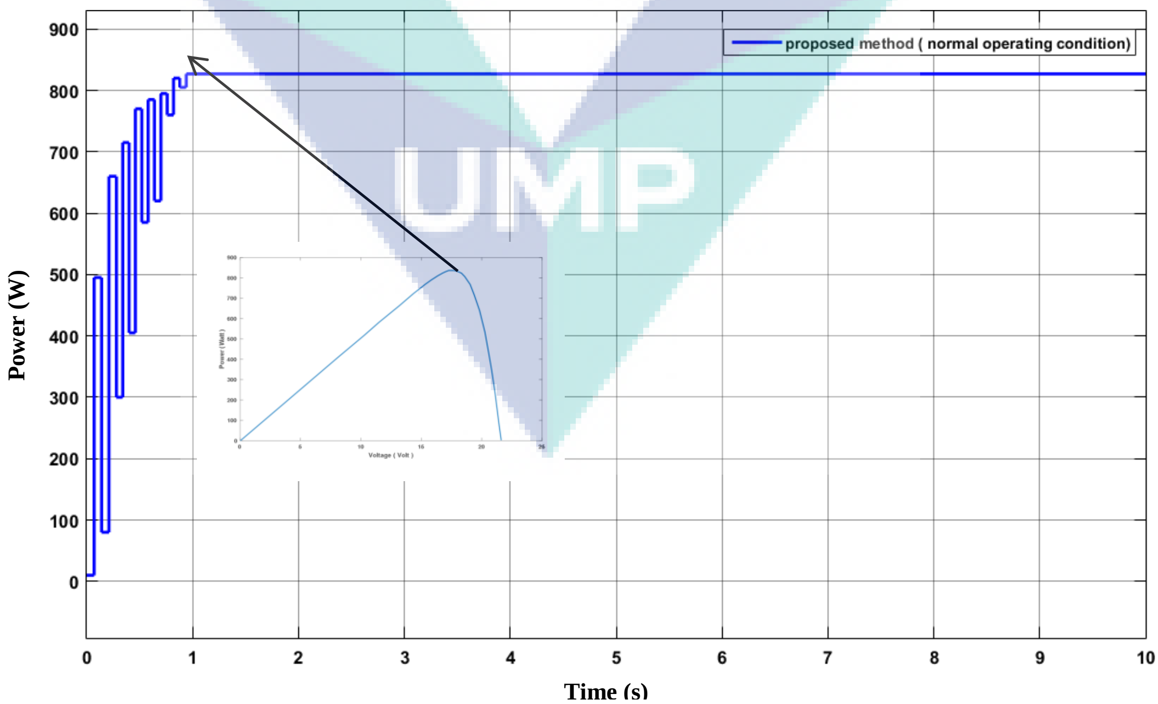

Figure 4.22. Extracted power using the proposed method (ACO-PSO), under normal conditions.

In the event of normal condition (equal distribution of insolation), the process of MPP tracking works directly well without any fluctuation in the power value. In this case, the tracking operation was kept at the value of power of 827 W at time 0.93 s, as shown in Figure 4.22, which is the MPP. The process of MPP tracking was very fast and accurate in the normal operating condition. In addition to this, the settling time of MPP in the proposed method is also very fast (0.93s). Moreover, the more important aspect in the proposed method is the oscillation pattern around MPP, which was free.

4.3.2 Operation under Partial Shadows

Under partial shadowing conditions, there are many MPPT techniques introduced and proposed in the literature. However, each method had its restrictions and limitations. Some methods could track the MPP but it so complicated whereas other methods have an oscillation around the MPP, but failed to track MPP within fast changing weather conditions. This is because when the PV system operates under shadow conditions the I-V and P-V characteristic curves will generate many local maximum points and only one global point. Tracking this MPP global point and distinguishing it among the local ones is a big constraint for most MPPT methods. Also, transient issues of extracting power are added up to the limitations facing tracking operation. Therefore, the proposed method serves to resolve the most important issue; which is to track the MPP. To insure the capability of proposed method to treat the most important issue for any change in weather condition, this study was applied in three different shadow conditions to examine the reliability of method used.

A: First Case Steady

The first applied shadow condition was as in the following sequence; 400 W/m^2; 400 W/m^2; 800 W/m^2; 800 W/m^2, for each PV module and connected in series. The P–V and I–V characteristic curves of the array of the PV system’s array are as presented in Figures 4.23 and 4.24, the output which represents the general characteristics of the PV model operating in the shadow condition. The results of tracking the MPP using the proposed method and the P&O comparison method are presented and plotted in Figures 4.25 and 4.26, which were recorded under two different levels of shadow conditions. The first level is 400 W/m^2 and applied on the 1st and the 2nd PV modules, and the second level is 800 W/m^2 applied on the 3rd and 4th PV modules, when these four PV modules are connected in a series. The second important issue shown in the results is the attainment of steady state condition for the extracted power.

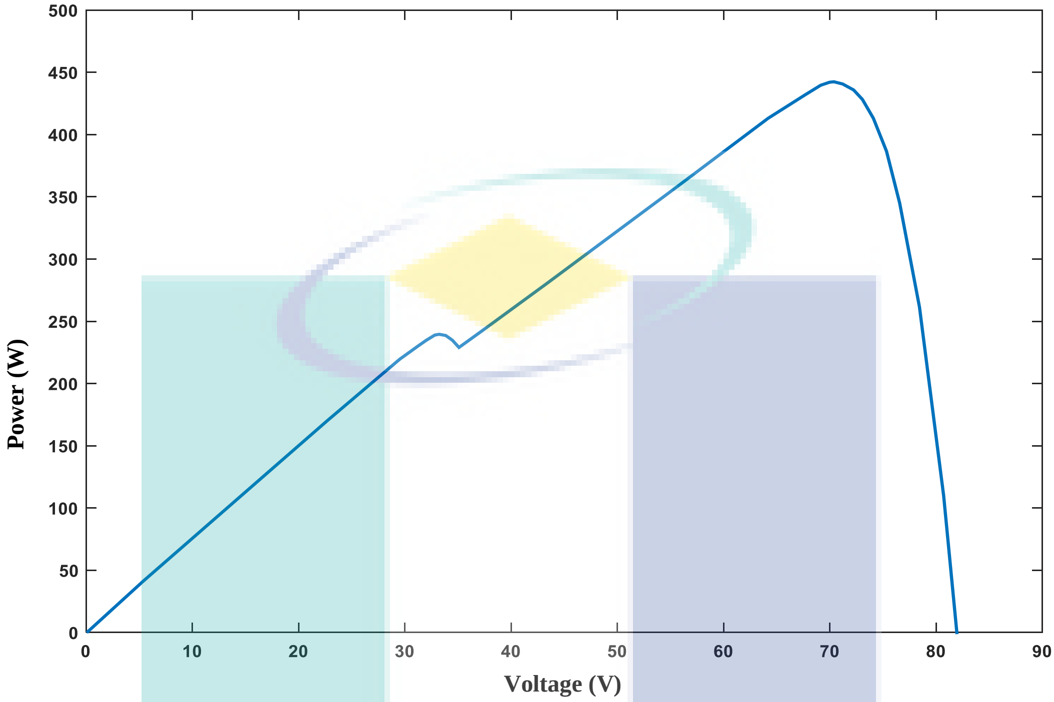

Figure 4.23. P–V characteristics of the PV array operating under shadow conditions, (400 W/m^2; 400 W/m^2; 800 W/m^2; 800 W/m^2).

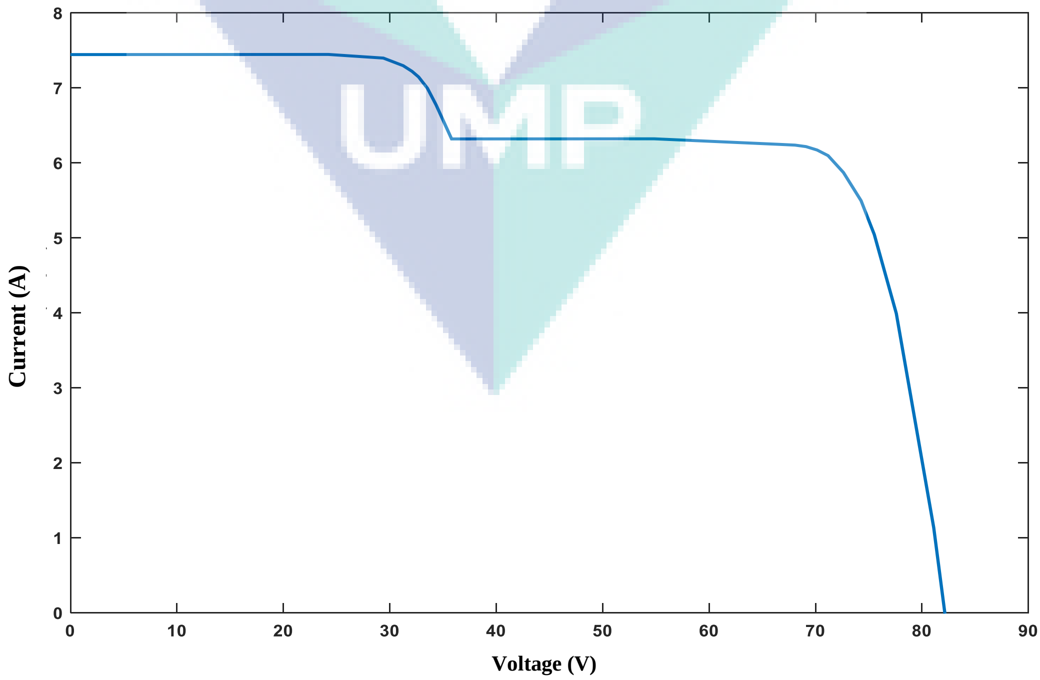

Figure 4.24. I–V characteristics of the PV array operating under shadow conditions, (400 W/m^2; 400 W/m^2; 800 W/m^2; 800 W/m^2).

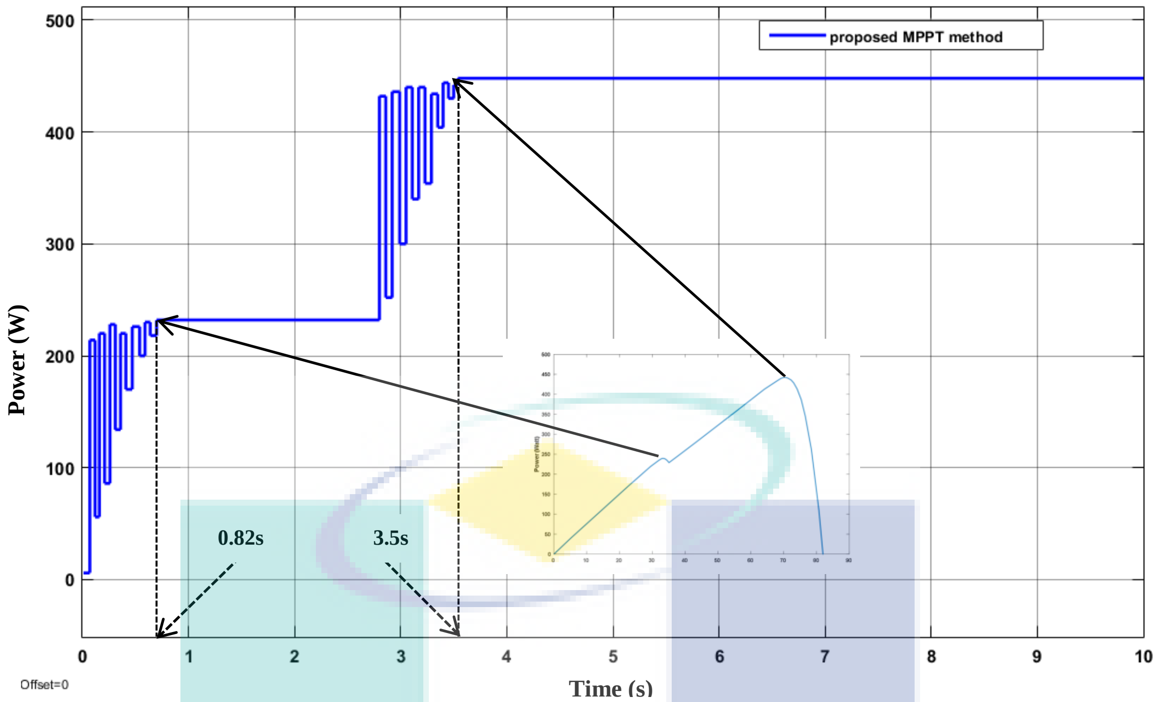

Figure 4.25. Extracted power using the proposed method (ACO-PSO), under shadow conditions (400 W/m^2; 400 W/m^2; 800 W/m^2; 800 W/m^2).

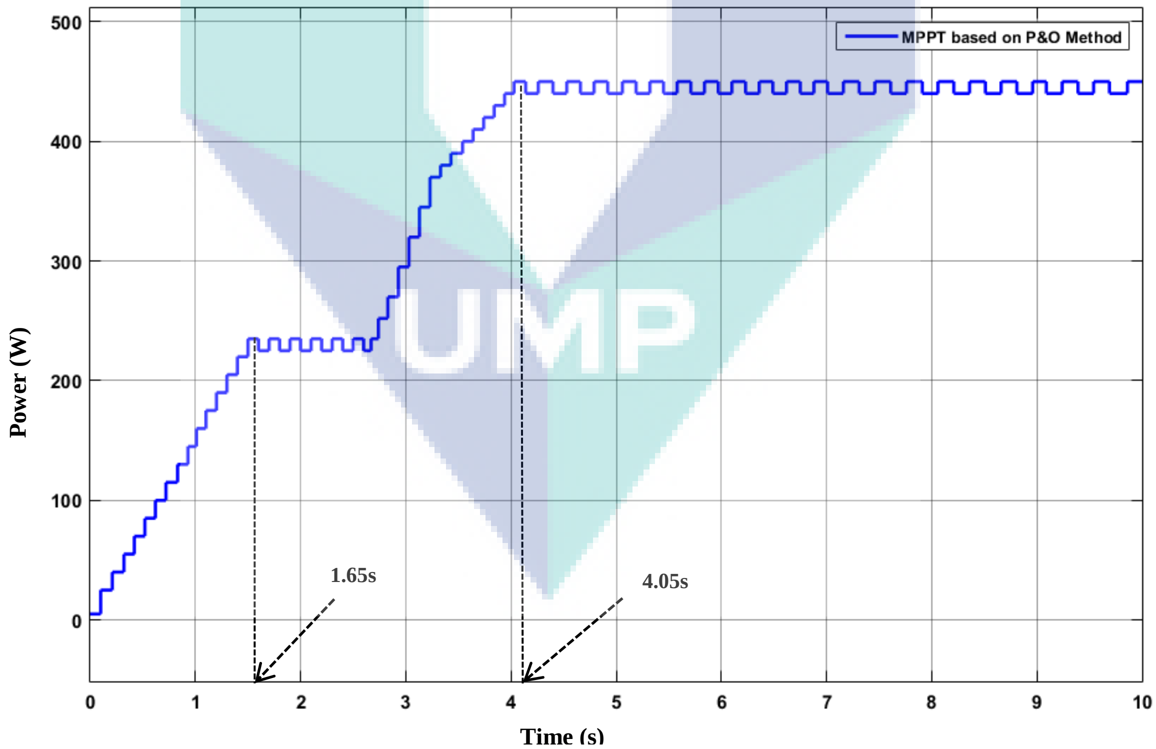

Figure 4.26. Extracted power using the P&O method, under shadow conditions (400 W/m^2; 400 W/m^2; 800 W/m^2; 800 W/m^2).

The effectiveness of the proposed MPPT method was tested and investigated through three different shadow conditions, which represented the most common shadow conditions that could happen on the PV system. Figure 4.25 displays the extracted power’s simulation results through the proposed MPPT technique. Whereas, Figure 4.26 is displaying the extracted power’s simulation results by the P&O comparison method. By using the proposed method, it can be seen that at the thirteenth selection interval, the algorithm tracked the local MPP at a value of 231W and at a time of 0.82 s. The algorithm continued to search until finding the second point which represented the global point. It was tracked accurately at 3.5 s and 447 W. However, in the comparison method (P&O method), the first local point tracked at the eighteenth selection interval with power value ranging from 225 W and 235 W. The global point was tracked at the time of 4.05 s with power value ranging between 443 W and 453 W. From the two Figures (4.25 and 4.26), it can be concluded that in addition to the fast tracking time of the proposed method, it also recorded other advantages in terms of efficiency and time response besides acquiring the steady state condition around MPP value. In the tracking operation of the first shadow condition, settling time of MPP in the proposed method was shorter than the P&O method, which occurred at 3.5 s for global point. However, it took 4.05 s in the P&O method. Furthermore, the other important issue considered in the proposed method is the oscillation pattern around MPP, which was oscillation-free in comparison with the P&O method; ranging from 443 W to 453 W along the time after the global MPP tracking was achieved.

B: Second Case Steady

The second case selected shadow condition as per the following sequence: 600 W/m^2; 1000 W/m^2; 1000 W/m^2; 800 W/m^2 and the shape of P–V and I–V characteristic curves of the PV system’s array are presented in Figures 4.27 and 4.28. The output represents the general characteristics of the PV model operating in shadow condition.

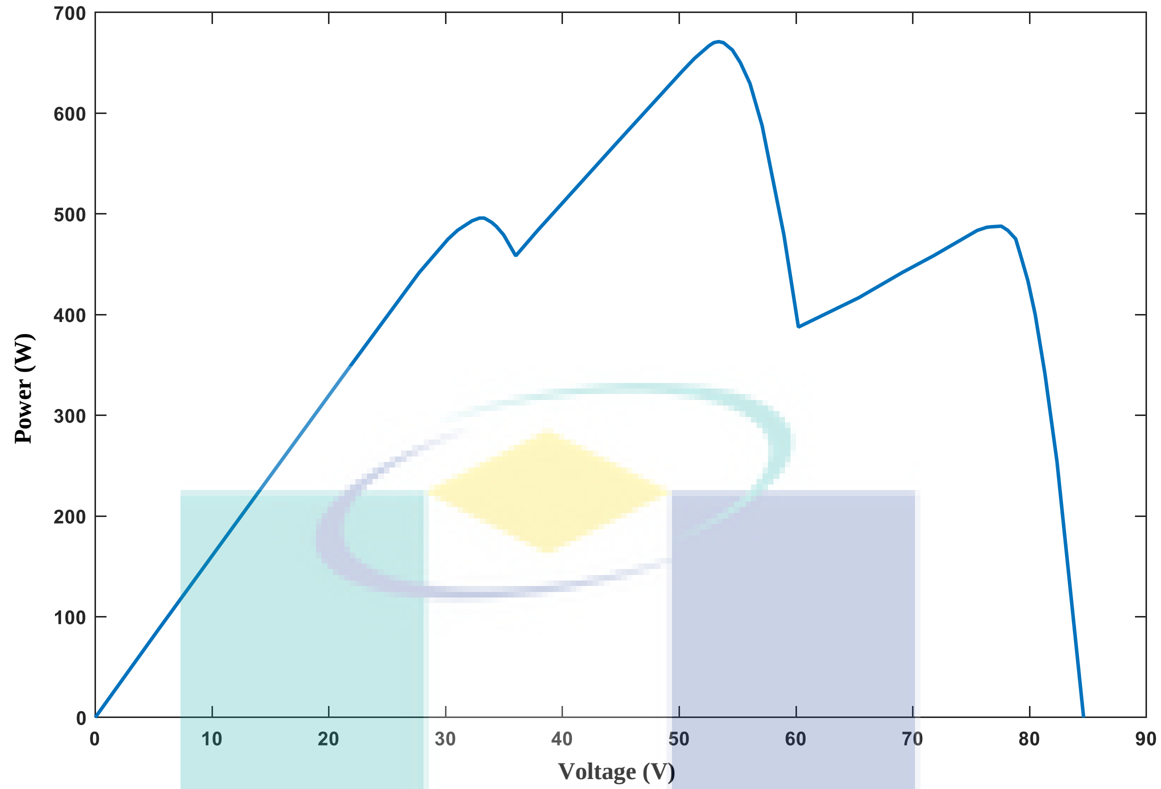

Figure 4.27. P–V characteristics of the PV array operating under shadow conditions, (600 W/m^2; 1000 W/m^2; 1000 W/m^2; 800 W/m^2).

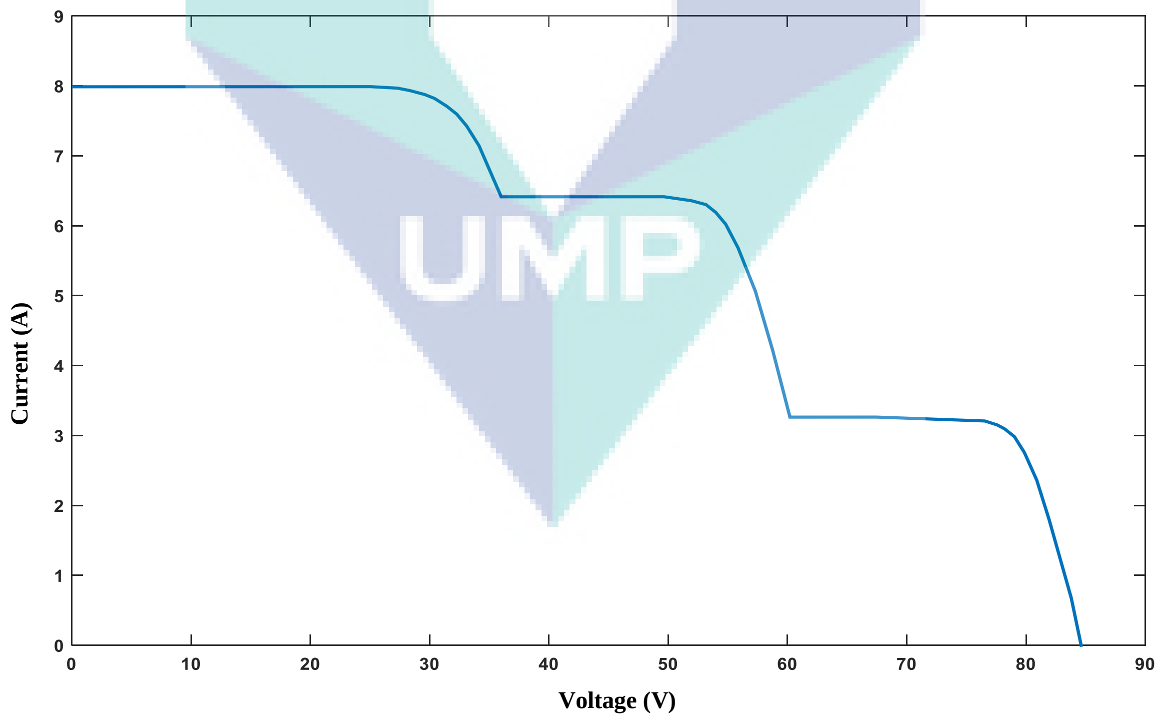

Figure 4.28. I–V characteristics of the PV array operating under shadow conditions, (600 W/m^2; 1000 W/m^2; 1000 W/m^2; 800 W/m^2).

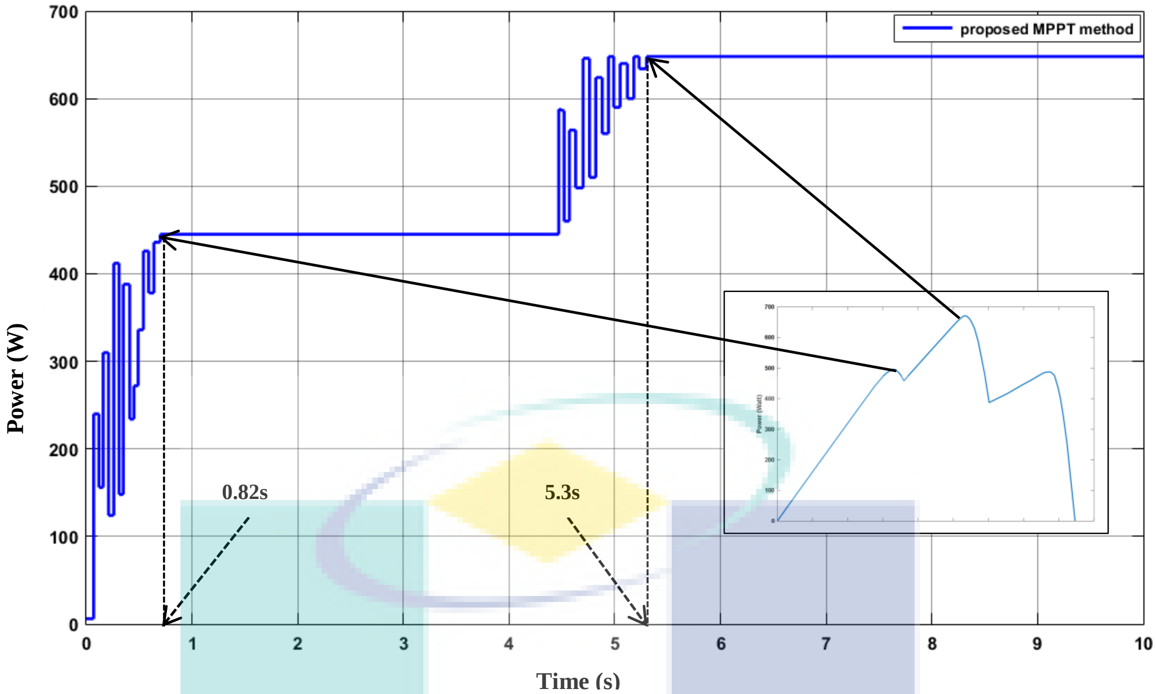

Figure 4.29. Extracted power using the proposed method (ACO-PSO), under shadow conditions (600 W/m^2; 1000 W/m^2; 1000 W/m^2; 800 W/m^2).

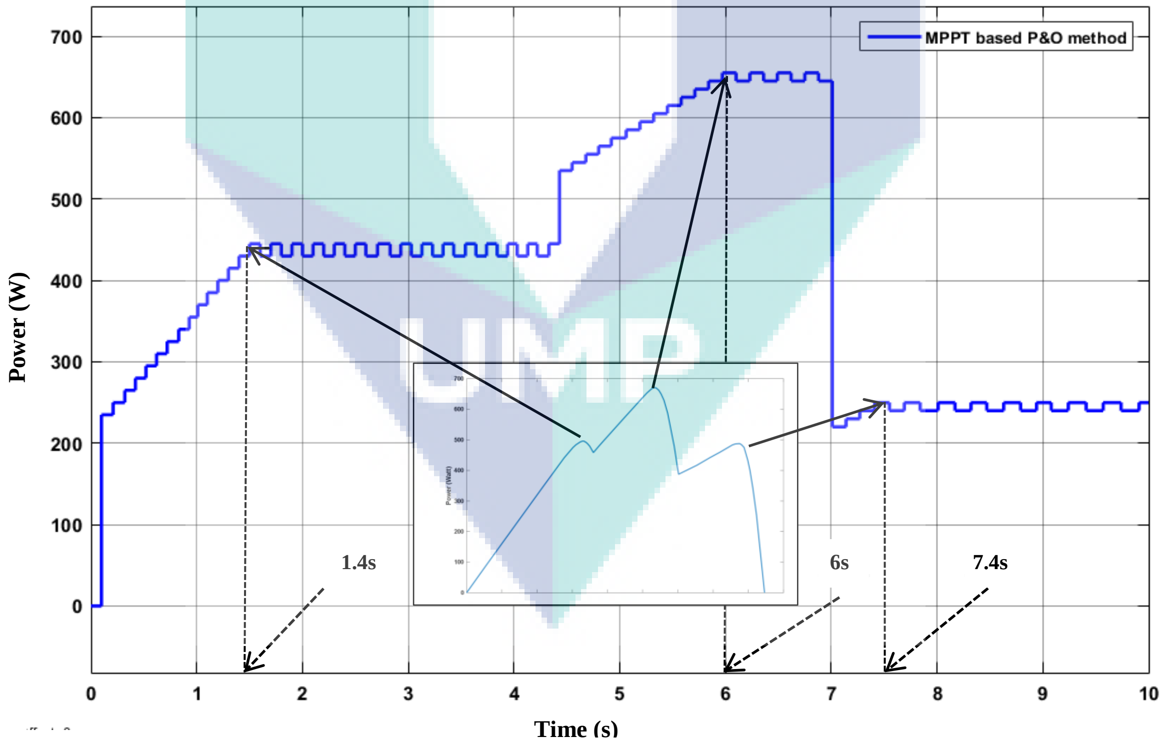

Figure 4.30. Extracted power using P&O method, under shadow conditions (600 W/m^2; 1000 W/m^2; 1000 W/m^2; 800 W/m^2).

The result of tracking MPP in second operating condition, using the proposed method is presented in Figure 4.29 and by using the comparative P&O method presented in Figure 4.30. In this shadow condition, the same way of tracking the first shadow condition was used. However, in this method, two local points and one global point were taken. In the tracking process, it initially tracked the first local point at 0.82 s and 445 W in the proposed method. Afterward, the searching process continued and it tracked the global point at 5.3 s and 648 W. In the second local point, the tracker maintained the same power value of global point, although the change is observed in the power characteristic curve, as shown in Figure 4.27. This change is due to the fact that the proposed method tried to maintain the maximum value of extracted power. However, as shown in Figure 4.30, in the second local MPP, the power extracted in P&O method continued to track the MPP and the value of power plunges very fast. Under this P&O method, the maximum tracked power was at 245 W. However, in the proposed method, it maintained at 648 W.

Another most important comparative point, within the tracking process, is the proposed algorithm, which tracked the first local MPP at the twelfth selection interval of 445 W and 0.82 s. However, in the P&O, it was tracked at power value in the range of 437 W and 447 W and 1.4 s. The tracking process continued searching until it finding the global point at 648 W and 5.3 s. Similarly, in the P&O method, the global point was tracked at 5.88 s with a power value ranging between 640 W and 650 W. In the comparative method, the search continued, resulting in tracking the third MPP point (i.e. the second local point) at 7.4 s with a maximum power value of 245 W. Therefore, the important difference between the proposed method and the P&O method; is that the proposed method was successful in tracking the global point, while P&O failed in tracking it. Contradictorily, the P&O method continued tracking each local point on the power curve, which finally resulted in a decrease in power value at all time values. But, in the proposed method, the focus was on the global point.

C: Third Case Steady

After that, the last shadow condition was considered in this study, as presented in the following sequence: 300 W/m^2; 600 W/m^2; 600 W/m^2; 900 W/m^2. The shape of the P–V and I–V characteristic curves of the whole PV system’s array were as presented in Figures 4.31 and 4.32 respectively, and the output represents the general characteristics of PV model operated in shadow condition. The result of tracking MPP in the current proposed MPPT method was presented in Figure 4.33 and the result of tracking MPP in P&O MPPT method is illustrated in Figure 4.34. In this shadow condition, as shown in Figure 4.33, the power curve has three MPP points, where two of them are local and one is global. Differing from the last two shadow conditions discussed earlier, the MPP value in this shadow condition was tracked three times by the proposed method. In the MPP tracking process, it firstly tracked the first local point at 0.7 s and 147 W. Afterward, the searching process continued and it tracked the second MPP local point at 3.5 s and 372 W. Later, the searching of global MPP continued until tracking and extracting it at 5.2 s and 450 W.

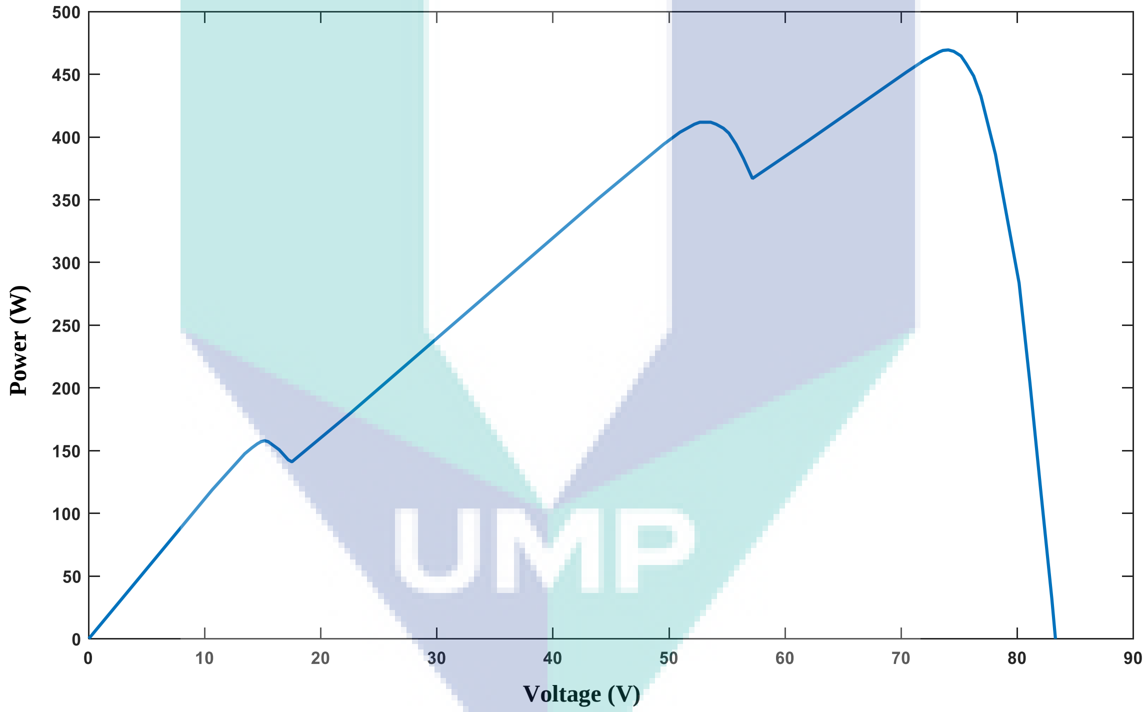

Figure 4.31. P–V characteristics of the PV array operating under shadow conditions, (300 W/m^2; 600 W/m^2; 600 W/m^2; 900 W/m^2).

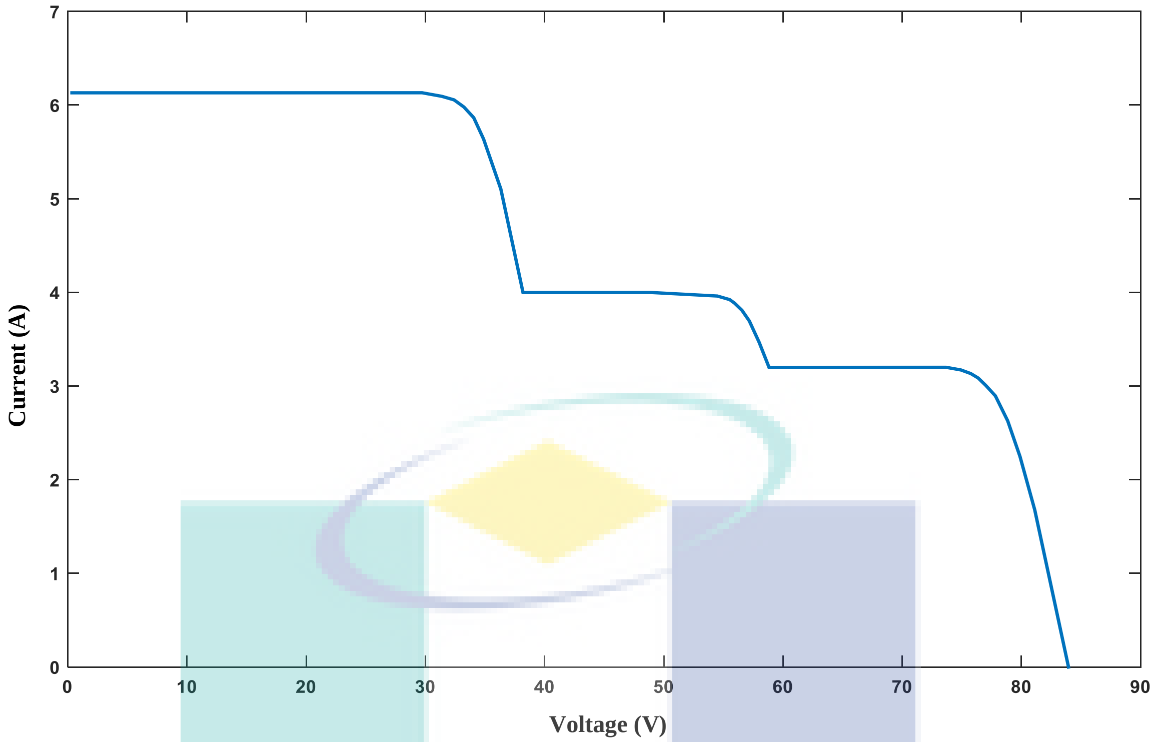

Figure 4.32. I–V characteristics of the PV array operating under shadow conditions, (300 W/m^2; 600 W/m^2; 600 W/m^2; 900 W/m^2).

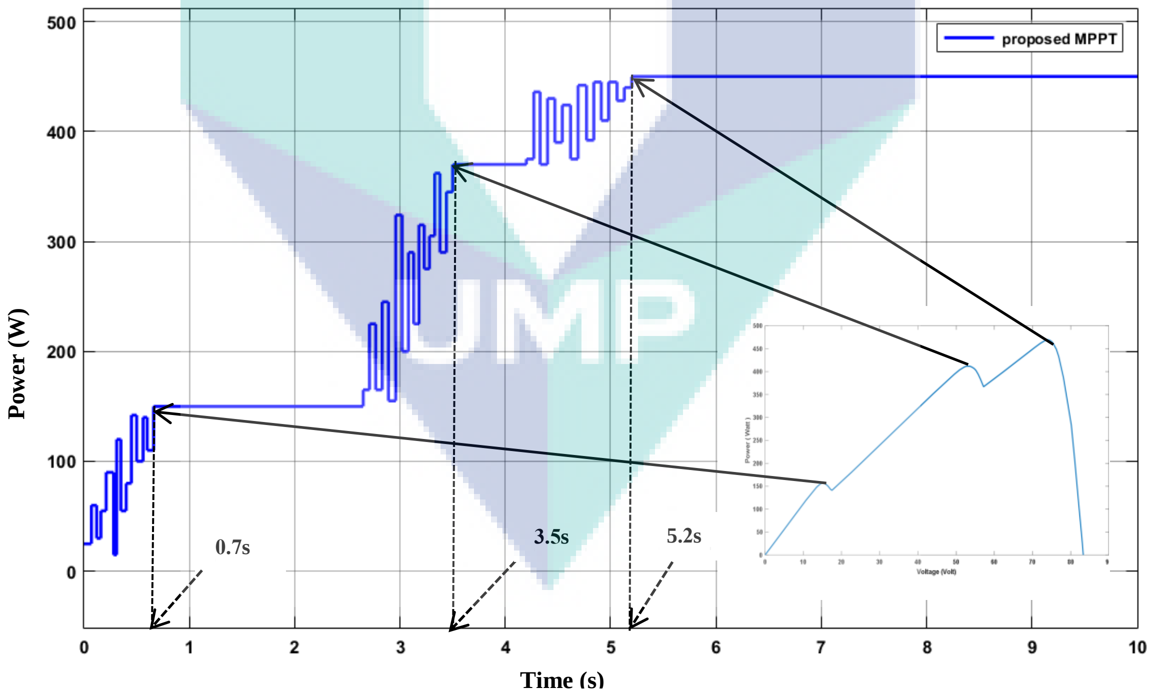

Figure 4.33. Extracted power using the proposed method (ACO-PSO), under shadow conditions (300 W/m^2; 600 W/m^2; 600 W/m^2; 900 W/m^2).

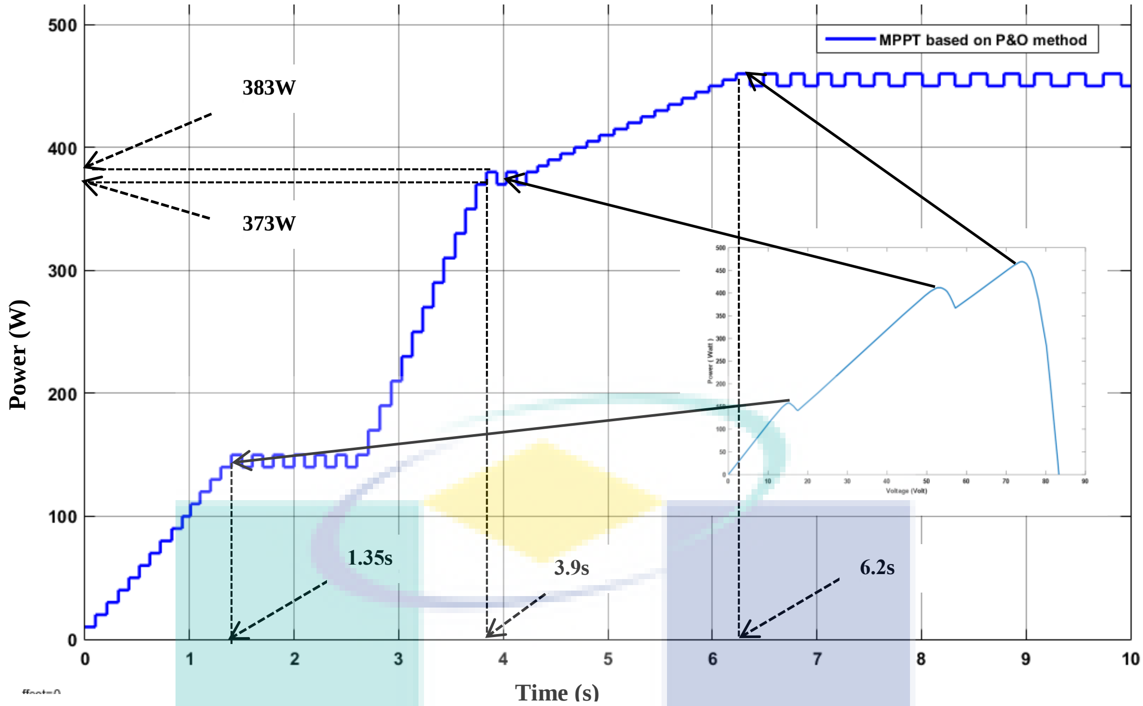

Figure 4.34. Extracted power using the P&O method, under shadow conditions (300 W/m^2; 600 W/m^2; 600 W/m^2; 900 W/m^2).

As a general comparison between the proposed and P&O method during this tracking process, the proposed algorithm tracked the first local MPP at the tenth selection interval at 0.7 s and 147 W, but the compared P&O method MPP tracked it at 1.35 s and power value ranging from 139 W to 149 W. The second local MPP was tracked at the twelfth selection interval, but in the compared P&O method, it was tracked at the sixteenth selection interval at 3.9 s and power value between 373 W and 383 W. The third MPP (global MPP) was tracked at the fourteenth selection interval, but in the compared P&O method, it was tracked at the nineteenth selection interval of 6.2 s and power value ranging from 451 W to 461 W.

Therefore, for all the case studies tested in this study, the MPPT proposed method recorded fast tracking time as compared to the P&O method which was much slower than the proposed method. In addition to that, the proposed method also depicts other benefits in terms of power efficiency and time response, as well the steady state occurring around the MPP values. For this purpose, the tracking operation of the third shadow condition, settling time of MPP in the proposed method was shorter than the one in P&O method occurring at 5.2 s for global point in proposed method, whereas in P&O, it occurred at 5.8 s. Additionally, in the proposed method, the oscillation pattern around MPP was not found, indicating that it had attained the steady state condition. In comparison with P&O method where the oscillation around MPP was present, the third shadow condition was ranging from 451 W to 461 W, along with the time after the global MPP tracking was attained.

4.4 PV System Model Evaluations Based on Two Real PV Plants

Validation of the simulation results is an important part of any numerical investigation. In the proposed study, a real PV system from two different PV technologies was implemented to validate the PV system outcome. From January to December 2014, the monthly average in-plane solar radiation of the PV system was extracted using the weather station at Bangi, Selangor. In March, the monthly average solar radiation's fluctuation was recorded from 753 W/m^2 in July to 979 W/m^2. There was variation in temperature, ranging from 24.9 °C in January and 34.4 °C in May. The irradiance and temperature values were both presented, in chapter III Figure (3.10). Based on the evaluation criteria used in this study and mentioned in chapter III, for the PV system model evaluation, Figure 4.35 and 4.36 show the results of monthly energy generation by using the proposed model, as compared to another related PV model from the literature (Khan et al., 2014; Kimball Krein, 2008; Navabi et al., 2015), and validated against two real power plant (c-Si and CIS power plant) results.

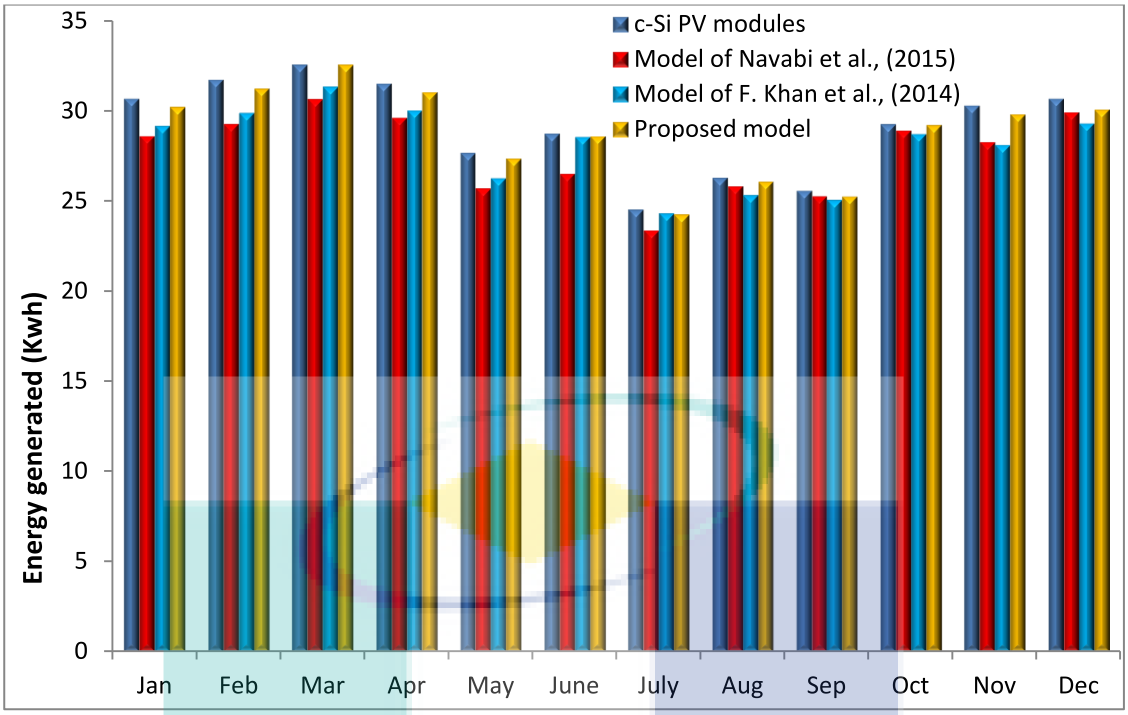

Figure 4.35. Average monthly energy generated (in kWh) from proposed model, compared with other models and validated with real results of c-Si PV modules.

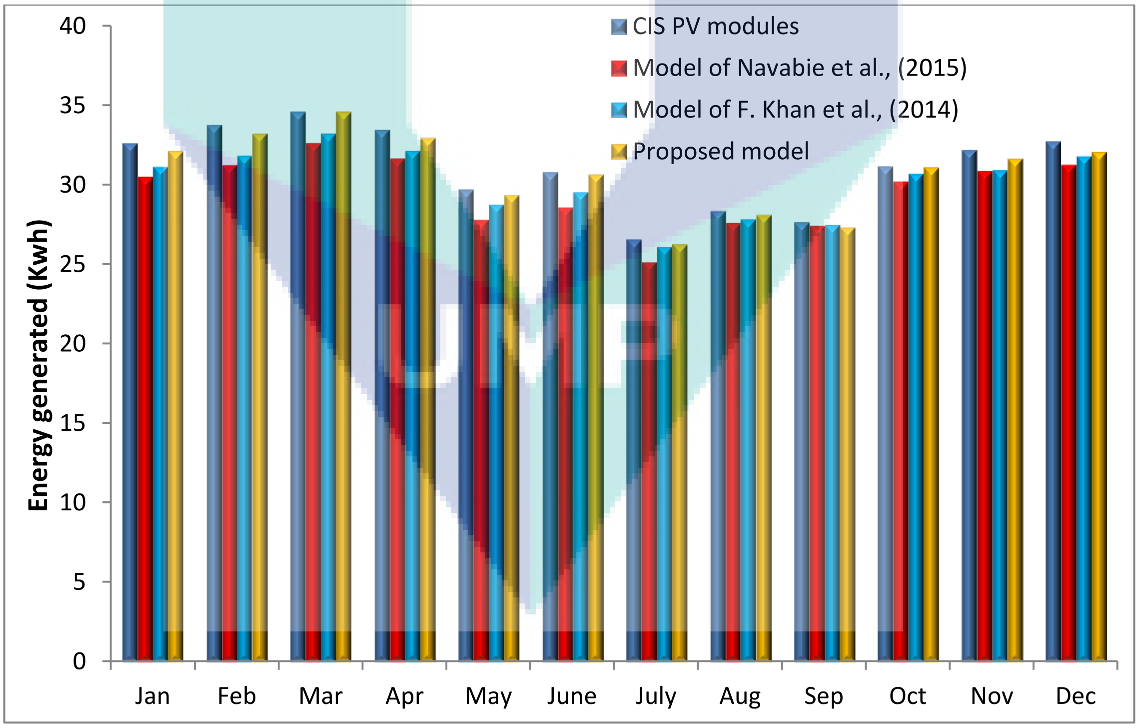

Figure 4.36. Average monthly energy generated (in kWh) from proposed model, compared with other models and validated with real results of CIS PV modules.

Figures 4.35 and 4.36 show the average monthly power generated, based on the proposed model. It is then compared with two PV models and validated against real results from two PV plants (c-Si and CIS power plants). From the results of the generated energy, it can be perceived that the results of the proposed model are almost close to real results achieved by the real PV plants (CIS and c-Si power plants) results. However, in both compared PV models, there were some error in fitting the obtained results with real results. The level of the energy generated was also lower in the models used for comparison than in the proposed model.The level of the energy generated was also lower in the models used for comparison than in the proposed model throughout the study.

The energy generation varied and the changes were recorded from July to March, from 24.53 kWh to the highest value of 32.57 kWh for c-Si PV modules. This result was obtained when the monthly average value was 29.63 kWh with a yearly gross power generation of 355.5667 kWh. The variation in energy generation for CIS PV plant ranged from 26.55 kWh in July to the highest value of 34.615 kWh in March. The monthly average was computed as 31.12 kWh with yearly gross electricity generated per year as 373.39 kWh. In July, the energy generated was low, as depicted in Figures 4.35 and 4.36. In this month, low radiance level with high temperatures and cloudy days resulted in low energy generation.

In addition to that, Figure 4.37 and 4.38 show the recorded results of monthly energy efficiency values of all the proposed model, as compared to other related PV models from literature (Khan et al., 2014; Navabi et al., 2015), and validated with two real PV power plants (c-Si and CIS power plant) results.

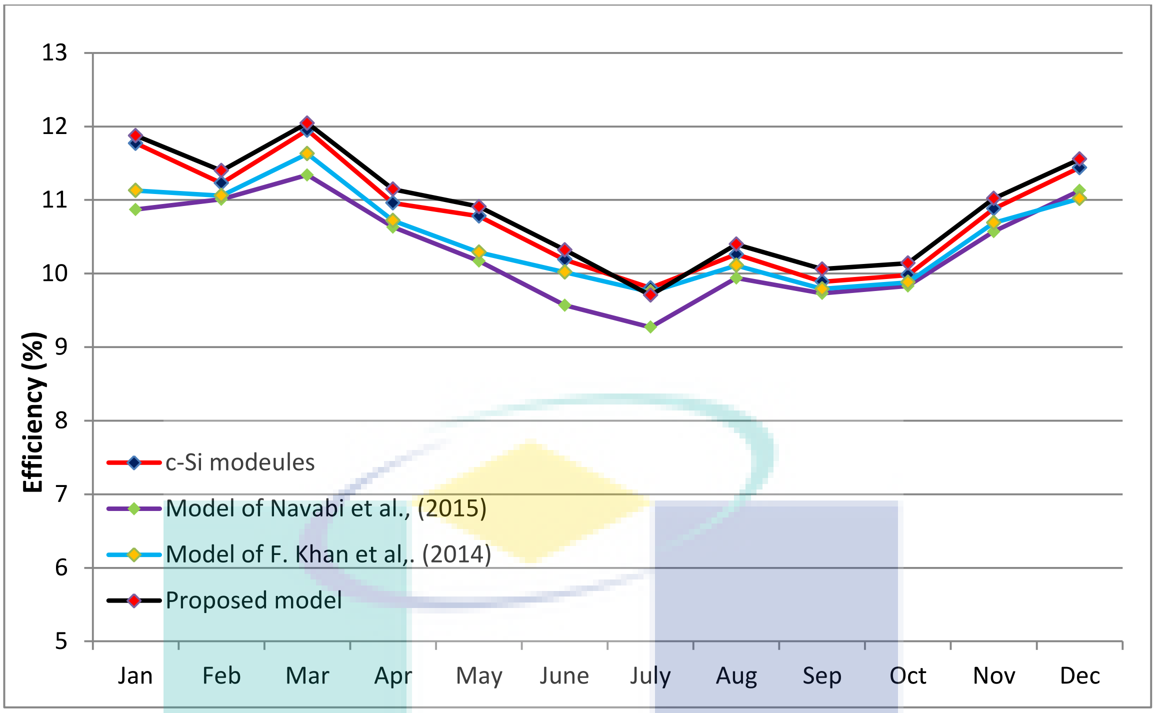

Figure 4.37. Average monthly energy efficiency of proposed model compared with real PV modules efficiency of c-Si and two other models .

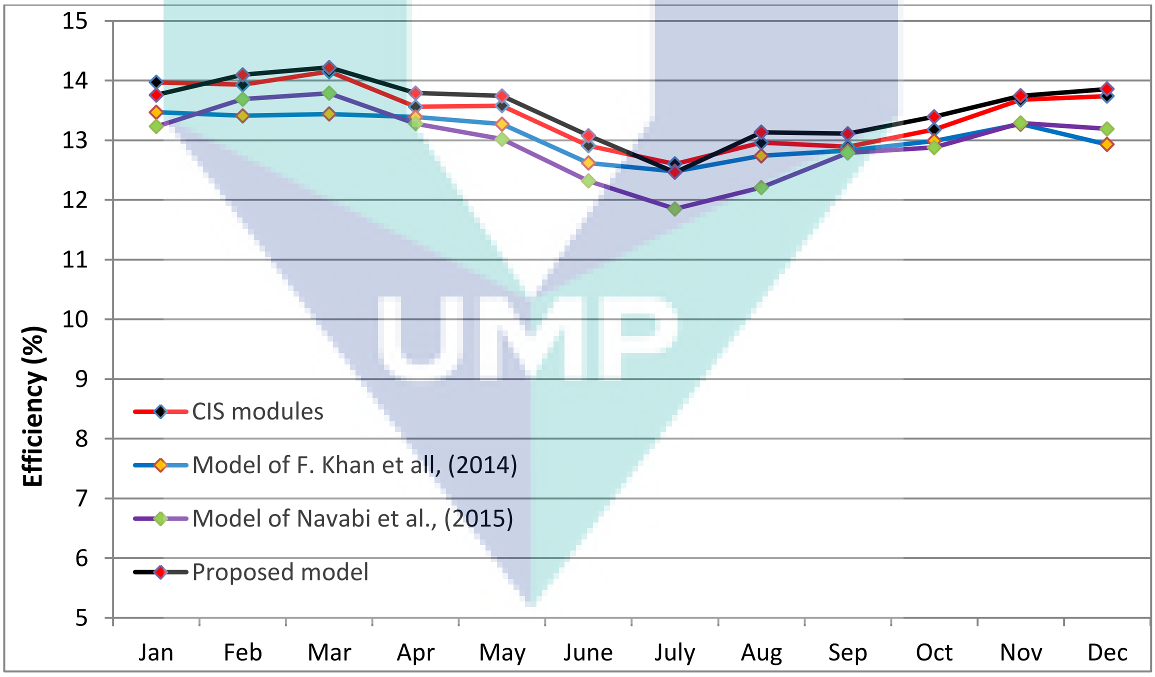

Figure 4.38. Average monthly energy efficiency of proposed model compared with real PV modules efficiency of CIS and two other models.

The results of proposed model's energy efficiency was differentiated with the results of the other two PV models and then validated against the energy efficiency of two real PV technologies (c-Si and CIS), as shown in Figures 4.37 and 4.38 respectively. From these two Figures, it can be concluded that the results of the proposed model fit the real results for both PV plants (c-Si and CIS plants). Nonetheless, both compared PV models exhibited a certain level of error when compared to real results, and had lower energy efficiency level as compared to the on in the proposed model in the testing period. It was also found that the energy efficiency is low in July, for all models (proposed model, two compared models and the two case studies), and this is because of higher module temperature and low irradiation. In addition to that, the efficiency of the proposed model and ral results were affected in similar manner when changing the temperature and irradiance. However, the effects of temperature and irradiance on efficiency from both models used for comparison are different as the effect is greater in F. Khan's model (Khan et al., 2014).

Moreover, the efficiency of CIS PV modules is slightly greater than the c-Si PV modules' efficiency by 23% all through the year, as shown in Figure 4.37 and 4.38. As far as energy generation is concerned, in the rest of the year, both PV plants of equivalent capacity would be operating at high generation level because of high irradiation level.

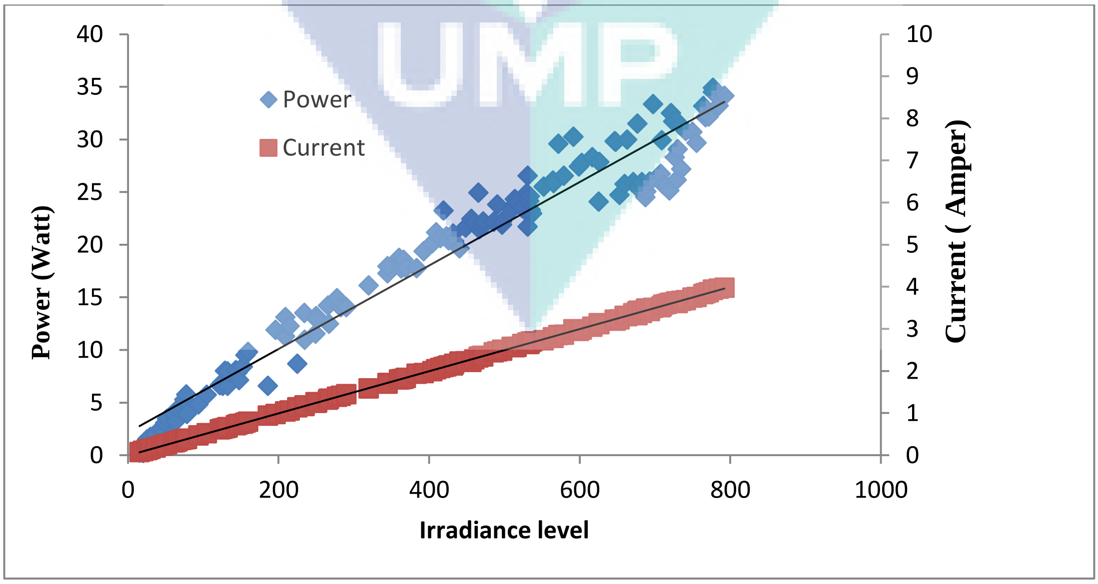

Figure 4.39. Power generated and current values as a function of the irradiance values.

The energy generation is determined by the solar irradiation and ambient temperatures. As depicted in Figure 4.39, when the radiation intensity increases, the output current and power generated from solar PV modules increases. The increment in current is due to increasing number of photons striking the solar PV module. This subsequently results in electron–hole pair generation and then to the higher photocurrent. The module temperature hardly affects the performance of solar PV module. When the decive temperature increases, the short circuit current increases slightly. On the other hand, as the reverse saturation current is exponentially dependant on temperature, the open-circuit voltage drops rapidly. As the temperature rises, the open circuit voltage drops. This relationship between temperature and open circuit voltage was observed through theoretical evaluation. The reduction in the intrinsic semiconductor's band gap is resulted by the rise in temperature. For a given radiance, the photocurrent increases, with the increment of temperature. This happens due to the high injection of electrons from the valence band to the conduction band of a semiconductor material. In general, the outputs and the comparative statistical error analysis confirmed that proposed model results merits over the compared models' results with low error value.

4.5 Evaluation PV System Model Performance Based on Performance Ratio

Another effective and valid factor to evaluate the PV model performance is the performance ratio (*PR*) factor. Based on the evaluation criteria applied in Eqs. (3.26 to 3.28) in chapter III are used to validate the PV system model's performance ratio based on real results from c-Si and CIS PV plants. The results are presented in Figure 4.40 and 4.41, respectively.

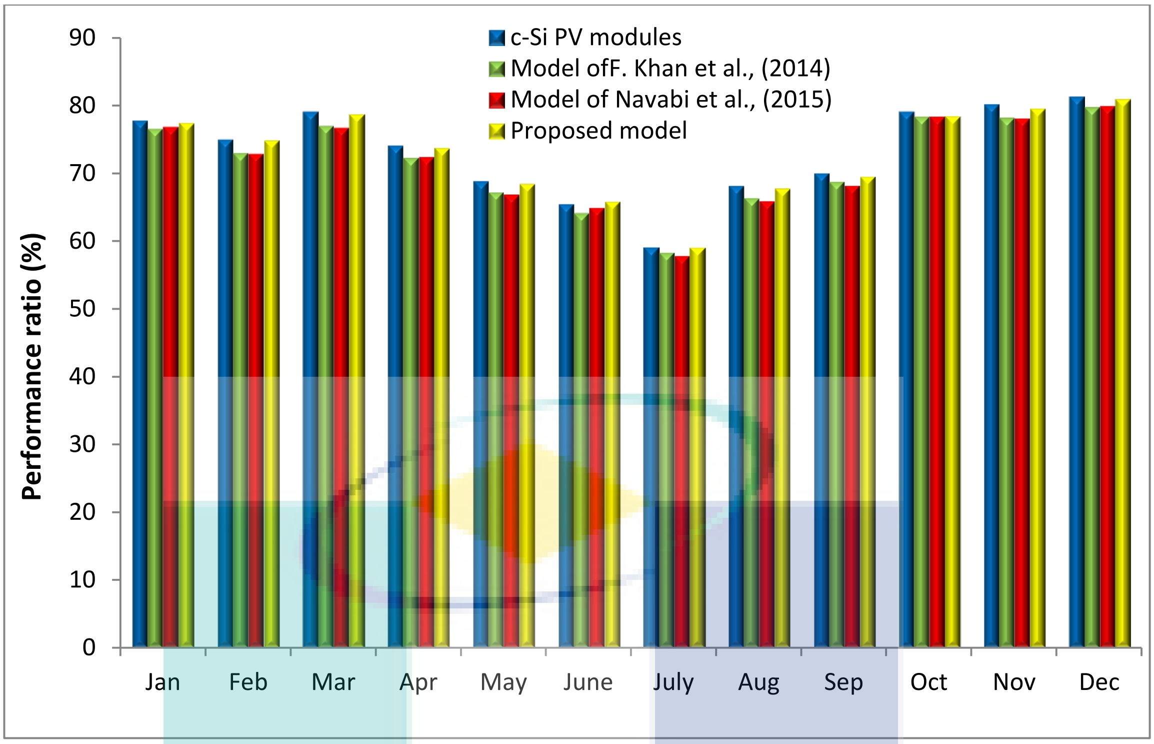

Figure 4.40. Average *PR* of proposed model compared with real PV modules efficiency of c-Si and two other models .

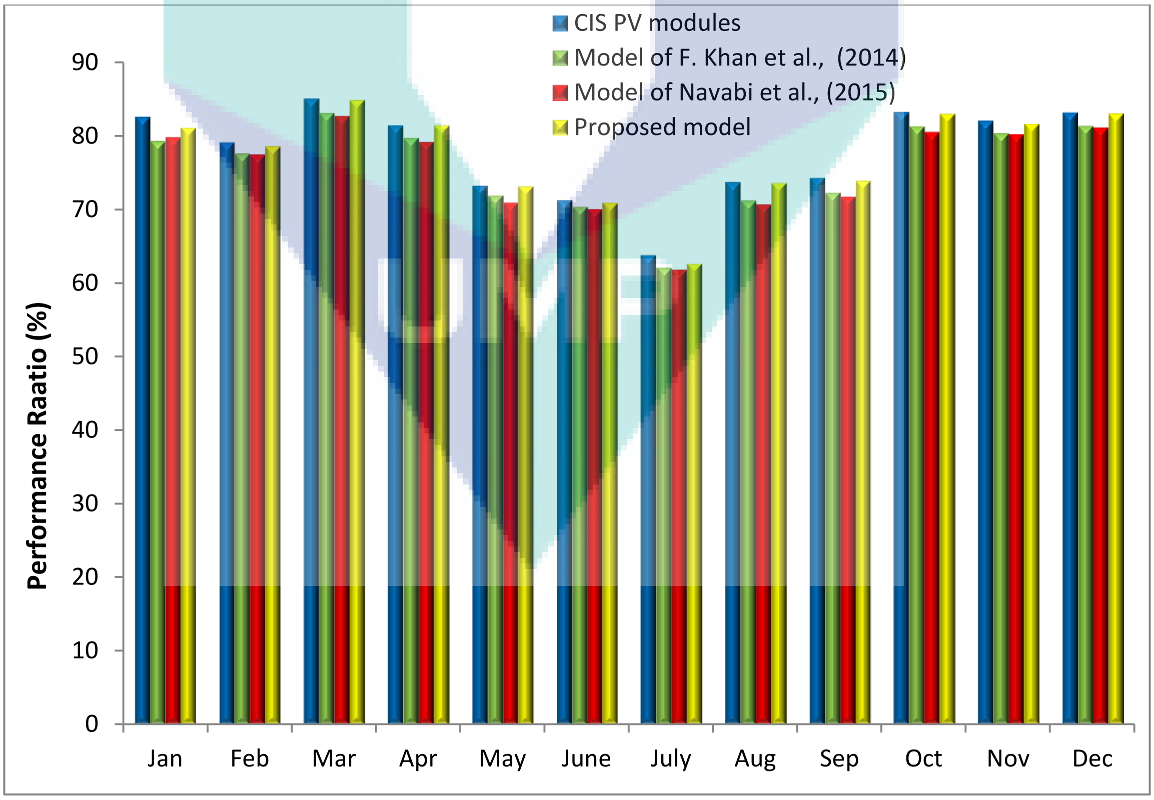

Figure 4.41. Average *PR* of proposed model compared with real PV modules efficiency of CIS and two other models.

Figures 4.40 and 4.41 present brief results of the normalised performance ratio's consequences. Results evidenced that the proposed model nearly fits the real results from both PV plants technologies along the evaluation time. Results of Figure 4.40 shows that the *PR* for proposed model ranged from 59.12 in July to 78.74 in March, while *PR* of model of F. Khan and model of Navabi ranged from 58.35 and 57.79 in July to 77.02 and 76.73 in March, respectively. Whereas, the *PR* of c-Si was between 59.12 in July and 79.14 in March. Results of Figure 4.41 displays that the *PR* for proposed model was lower in July (62.64) and higher (84.87) in March. Whereas, the *PR* of F. Khan's and Navabi's model ranged between 62.1 and 61.8 in July, and 83.1 and 83.67 in March. On the other hand, the *PR* of CIS was between 63.8 in July and 85.13 in March.

The month to month radiation patterns and negative trend of temperature in comparison with Figure 3.10 was outlined in Figure 4.41. Table 4.4 demonstrates the comparison of various existing solar PV power plants from different areas.Hence, the aforementioned results still reflect and assign to the type, connections, site (location), and utilisations of PV system. A brief result is summarised in table 4.4 for the system performance studied for systems implemented in tropical nations as found in literature, apart from the current research analysis. This table focuses on four parameters (as PV efficiency, PV performance, capacity factor, and finally the yield factor) that are regarded as the most effective performance parameters. By referring to table 4.4, the average value of module efficiency is 10.92% and average performance is 74 %. Besides that, the average value of capacity factor is 15.6% in terms of system productivity and the yield factor is found to be 3.8% with an average inverter efficiency of 94.2%. All these results are very similar with the ones found in literatures and used as approach validation in this study.

In current research, it is developed the PV model based on sturdy evidences of real results to get the electrical P-V and I-V characteristics of a PV system. In order to get the most accurate model, comparison with different models will be conducted for future research based on the prolonged data monitoring period (one years).

Table 4.4.
Different PV systems performances installed under different tropical climates.

Author	PV Technology	System Capacity	Locatio	PV eff.	PV Perf.	Cap. Factor	Yield Factor kWh/kWp/d
A. Chimtavee et al. 2012	multi-crystalline	11kWp	Thailand	10.4%	73.4 %	14%	3.84
Gayathri et al.. 2013	monocrystalline silicon	10 kWp	Malaysi	12.2%	64%	21.3%	2.97
Stephen W. et al.. 2012	polycrystalline silicon	142 kWp	Singapor	11.2%	81%	15.7%	3.12
Elieser et al.. 2014	multi-crystalline silicon	5.4 kWp	Indonesia	8%	75.4%	12%	5.15
Masoud et al.. 2015	mono-crystalline silicon	3 kWp	Malaysia	10.1%	77.2%	15.7%	3.8
This study	copper–indium–diselenid	5kWp	Malaysia	13.2%	77.5%	18.9%	3.63
This study	mono-crystalline silicon	5kWp	Malaysia	10.7%	73.5%	18%	3.52

4.6 Summary

The current research shows how to model and characterise PV solar cells, and then how to maximise the extracted power generated from the PV cells and the modules. In addition to that, another concern for this research is to reduce the oscillation that could happen around the extracted MPP, and to validate the proposed PV system model based on performance and the power efficiency with two real PV plants (from two important PV technologies). The results obtained from the experimental data and the simulation study were presented. The experimental data was used to identify the coefficient values of solar cells' five parameters. These five parameters were used to build the PV model mathematically. In addition to that, the proposed model generated was compared with previous models, and the experimental data were employed to calibrate and validate the electrical characteristics of these five parameters. In the same manner, an accurate mathematical PV model had been designed based on theoretical and experimental calculations. Furthermore, an improved MPPT method was established to enhance the MPP extracted from the PV system. Another objective of the study is to improve the steady state case of the MPP and the settling time apart from improving the power generation efficiency. Additionally, the evaluation of proposed PV system model based on two real PV plants and previously studied models was conducted by calculating the energy generation, its efficiency, and the actual performance.

CHAPTER V

CONCLUSIONS AND RECOMMENDATION

5.1 Introduction

Economic demand for renewable energies is resulting in the widespread of solar power generation; this is due to the fact that the solar power is one of the most popular renewable energy sources Solar power source has numerous advantages, such as generation of electricity at the load point, power loss reduction and more reliable electrical system. Therefore, it is essential to understand the significant issues, directly related and affecting the efficiency of power generation from solar source.

The presented research is a detailed model which might play as the base and the origin for any further advancement in the respective field. In addition, for energy utilisation in a more efficient way, the MPPT method has been always a key to enhance the energy generation performance area. Due to the above mentioned facts, the presented thesis is focussed on the development of a reliable PV model, emulation and implementation system with a novel MPPT method, and to attain the steady state condition for system reliability. In this research thesis, the main issues are related to the research and development of a reliable and accurate PV model based on real data. The reliability and accuracy of the proposed model elucidated through the characterisation of the model parameters and improving the performance of these PV cell parameters. Moreover, to efficiently harvest the maximum power available from PV system, an improved MPPT method is proposed. To minimize the oscillation around the maximum power point an optimal PID controller has been employed. Finally, to validate the proposed model two real PV plants used and related models from previous works are considered for comparative study.

5.2 Summary of Findings and Contributions

In this thesis, an accurate and reliable single diode model for the PV cell and module has been developed and applied under the shadow weather conditions. The proposed model considered a numerical approach which is based on solving a system of non-linear equations derived from the current–voltage characteristic equations. These equations expressed all the available five PV solar cell parameters which are the photocurrent, I_{ph}, the reverse diode saturation current, I_o, the ideality factor of diode, n, the series resistance, R_s, and the shunt resistance, R_{sh}. In addition, the used model expressed explicitly both of the current–voltage and power–voltage characteristics within different temperature and irradiance levels. These characteristics have been tested and found fit the characteristics of experimental data (real data), later were compared with other models of the same level and the number of dependent parameters. The results of fitting of these parameters characteristics with the real ones are found to be in a reasonable and high accuracy, as compared to the other models used before in the literature.

Moreover, performance of these five solar cell parameters (I_{ph}, I_o, n, R_s, R_{sh}) are also observed to be improved in the proposed model by fitting characteristics with the real data, and compared with other models of the previous studies. Firstly, the photocurrent, I_{ph} effect on both of I–V and P–V characteristic curves has been tested and compared with other models. The results showed an increase in the I_{ph}, which leads to increase the maximum power point in a prominent way, besides to its effect on the short circuit current, I_{sc} and open circuit voltage, V_{oc}. This effect was also found to be in a positive direction, since when the I_{ph} has been increased lead to increase both of the I_{sc} and V_{oc}. The results of the reverse diode saturation current, I_o, effect on the I–V and P–V characteristics deduced that the increase in the I_o leads to increase the maximum power point in an average mode, in addition to that it has affected the short circuit current, I_{sc} and open circuit voltage, V_{oc} as well. This effect is also in a positive mode with an equal weight. Further, the results of the effect of the ideality factor of the diode, n showed that the changing of the diode ideality factor, n did not affect the values of the short circuit current I_{sc} and open circuit voltage V_{oc}. On the other hand, it was found that the increase in n value led to decrease the value of the maximum power point for both of the I–V and P–V characteristic curves. However, the results of increase in the series resistance, R_s showed a decrease in the value of the maximum power point, notably, and for both of the I–V and P–V characteristic curves. The results showed that the increase of the R_s does not affect the values of the short circuit current I_{sc} and open circuit voltage V_{oc}. Finally, the effect of the shunt resistance, R_{sh} was also studied. However, the influence of this parameter found to be barely noticeable for all of the maximum power point, I_{sc}, and V_{oc}.

In this study, an improved MPPT algorithm using hybrid ACO-PSO algorithm has been implemented by referring to the output of the mechanisms of the conventional P&O algorithm and nonlinear characteristics of photovoltaic as an input to the PID controller. The strategy is to create variable and adaptive perturbation intensities for accelerating the MPPT velocity and improving the MPPT efficiency was validated by the most famous and used P&O MPPT method. To improve the overall performance of the PV system, an optimised PID controller has been implemented for the purpose of oscillation filtering and noise suppression as taken in this design, as well as the time response and settling time. In addition, the proposed method has been used to track the maximum global power point under shadow conditions. For this purpose, three different shadow conditions were tested as a case study to test the ability and accuracy of the proposed method. The results of tracking MPP by the proposed MPPT technique showed that the improved method tracked the MPP for all the tested cases with a reasonable accuracy in a very short settling time as compared to the P&O method. It was found that the extracted power had no oscillation around the MPP, when comparing with the P&O method with a noticeable oscillation around the MPP which resulted in decreasing the efficiency of the extracted power from the PV system.

Furthermore, two 5 kWp PV systems with two different PV technologies (mono-crystalline silicon (c-Si) and copper–indium–diselenide (CIS)) were installed in the same area (Bangi, Selangore) and investigated the PV model performance based on energy generation. The fluctuations in temperature and radiation were observed in both the power plants. Different evaluation criteria were used to analyse the system performance; including energy generated, energy efficiency, and performance ratio. The recordings were noted down under the actual climatic conditions for one entire year. Variations in the energy generation of c-Si were as low as 24.53 kWh in July to the highest value of 32.57 kWh in March. The energy generation for CIS power plant ranged from 26.55 kWh in July to 34.615 kWh in March. The monthly average energy generation recorded was 31.12 kWh for CIS power plant, while 29.63 kWh for c-Si power plant. The gross yearly generated electricity recorded was observed 373.39 kWh from CIS and 355.5667 kWh from c-Si PV plant.

5.3 Recommendations for Future Work

Future studies should focus on further investigation of the accomplishments of the present study by conducting the following:

I. Extension to more realistic scenarios, in modelling the example system, certain weather conditions (tropical weather conditions), as assumptions were made. The extended model could be considered for a more realistic data set, like a different data from different locations on the Earth's surface, like a desert or varied seasons area, besides to the tropical area taken as a reference in the current study.

II. A more in depth study of the performance of model parameters and its effect on the I–V and P–V characteristic curves is advised, recommended to take the effect of changing the weather conditions (irradiance and temperature) beside the change in the values of these solar cell parameters at the same time, which could increase the focus on the effect of these parameters and its performance in a short time.

III. Study the effectiveness of the proposed MPPT technique with different cases and PV systems, like PV grid connected and variable load.

IV. Study on the performance of the whole PV system based on varied weather conditions, like the desert area or area with variable seasons.

REFERENCES

Abdelsalam, A.K., Massoud, A.M., Ahmed, S., and Enjeti, P., (2011). High-performance adaptive perturb and observe MPPT technique for photovoltaic-based microgrids. *Power Electronics, IEEE Transactions on, 26*(4), 1010-1021.

Aberle, A., Wenham, S., & Green, M., 1993. *A new method for accurate measurements of the lumped series resistance of solar cells.* Paper presented at the Photovoltaic Specialists Conference, (1993)., Conference Record of the Twenty Third IEEE.

Ahmed, K,(1994). Renewable energy technologies. *A Review of the Status and Costs of.*

Akbaba, M., and Alattawi, M.A., (1995). A new model for I–V characteristic of solar cell generators and its applications. *Solar energy materials and solar cells, 37*(2), 123-132.

Akkaya, R., and Kulaksiz, A., (2004). A microcontroller-based stand-alone photovoltaic power system for residential appliances. *Applied Energy, 78*(4), 419-431.

Amin, N., Lung, C.W., and Sopian, K., (2009). A practical field study of various solar cells on their performance in Malaysia. *Renewable Energy, 34*(8), 1939-1946.

Araujo, G.L., and Sanchez, E., (1982). A new method for experimental determination of the series resistance of a solar cell. *Electron Devices, IEEE Transactions on, 29*(10), 1511-1513.

Arcipiani, B., (1985). Generalization of the area method for the determination of the parameters of a non-ideal solar cell. *Revue de physique appliquée, 20*(5), 269-272.

Bazzi, A.M., and Krein, P.T., (2011). Concerning “Maximum Power Point Tracking for photovoltaic optimization using ripple-based Extremum Seeking Control”. *Power Electronics, IEEE Transactions on, 26*(6), 1611-1612.

Bazzi, A.M., and Krein, P.T., (2014). Ripple correlation control: an extremum seeking control perspective for real-time optimization. *Power Electronics, IEEE Transactions on, 29*(2), 988-995.

Besheer, A., and Adly, M., (2012). *Ant colony system based PI maximum power point tracking for stand alone photovoltaic system.* Paper presented at the Industrial Technology (ICIT), 2012 IEEE International Conference on.

Bhatnagar, P., and Nema, R., (2013). Maximum power point tracking control techniques: State-of-the-art in photovoltaic applications. *Renewable and Sustainable Energy Reviews, 23*, 224-241.

Bianconi, E., Calvente, J., Giral, R., Mamarelis, E., Petrone, G., Ramos-Paja, C.A., . . . Vitelli, M., (2013). Perturb and observe MPPT algorithm with a current controller based on the sliding mode. *International Journal of Electrical Power and Energy Systems*, *44*(1), 346-356.

Bowden, S., and Rohatgi, A., (2001). Rapid and accurate determination of series resistance and fill factor losses in industrial silicon solar cells.

Brano, V.L., and Ciulla, G., (2013). An efficient analytical approach for obtaining a five parameters model of photovoltaic modules using only reference data. *Applied Energy*, *111*, 894-903.

Brano, V.L., Orioli, A., Ciulla, G., and Di Gangi, A., (2010). An improved five-parameter model for photovoltaic modules. *Solar Energy Materials and Solar Cells*, *94*(8), 1358-1370.

Bratcu, A.I., Munteanu, I., Bacha, S., Picault, D., and Raison, B., (2011). Cascaded dc–dc converter photovoltaic systems: Power optimization issues. *Industrial Electronics, IEEE Transactions on*, *58*(2), 403-411.

Bube, R., (2012). *Fundamentals of solar cells: photovoltaic solar energy conversion*: Elsevier.

Celik, A.N., and Acikgoz, N., (2007). Modelling and experimental verification of the operating current of mono-crystalline photovoltaic modules using four-and five-parameter models. *Applied energy*, *84*(1), 1-15.

Chan, D., Phillips, J., and Phang, J., (1986). A comparative study of extraction methods for solar cell model parameters. *Solid-State Electronics*, *29*(3), 329-337.

Chan, D.S., and Phang, J.C., (1987). Analytical methods for the extraction of solar-cell single-and double-diode model parameters from IV characteristics. *IEEE Transactions on Electron Devices*, 286-293.

Chegaar, M., Azzouzi, G., and Mialhe, P., (2006). Simple parameter extraction method for illuminated solar cells. *Solid-State Electronics*, *50*(7), 1234-1237.

Cibira, G., and Koščová, M., (2014a). Photovoltaic module parameters acquisition model. *Applied Surface Science*.

Cibira, G., and Koščová, M., (2014b). Photovoltaic module parameters acquisition model. *Applied Surface Science*, *312*, 74-80.

Ciulla, G., Brano, V.L., Di Dio, V., and Cipriani, G., (2014). A comparison of different one-diode models for the representation of I–V characteristic of a PV cell. *Renewable and Sustainable Energy Reviews*, *32*, 684-696.

Coelho, R.F., Concer, F., and Martins, D.C., (2009). *A study of the basic DC-DC converters applied in maximum power point tracking.* Paper presented at the Power Electronics Conference, 2009. COBEP'09. Brazilian.

Cotfas, D., Cotfas, P., and Kaplanis, S., (2013). Methods to determine the dc parameters of solar cells: A critical review. *Renewable and Sustainable Energy Reviews, 28*, 588-596.

Cotfas, D., Cotfas, P., Kaplanis, S., and Ursutiu, D., (2008). Results on series and shunt resistances in a c-Si PV cell. Comparison using existing methods and a new one. *Journal of optoelectronics and advanced materials, 10*(11), 3124-3130.

De Blas, M., Torres, J., Prieto, E., and Garcıa, A., (2002). Selecting a suitable model for characterizing photovoltaic devices. *Renewable energy, 25*(3), 371-380.

De Brito, M.A.G., Galotto Jr, L., Sampaio, L.P., de Azevedo e Melo, G., and Canesin, C.A., (2013). Evaluation of the main MPPT techniques for photovoltaic applications. *Industrial Electronics, IEEE Transactions on, 60*(3), 1156-1167.

Dizqah, A.M., Maheri, A., and Busawon, K., (2014). An accurate method for the PV model identification based on a genetic algorithm and the interior-point method. *Renewable Energy, 72*, 212-222.

Dorofte, C., Borup, U., and Blaabjerg, F., (2005). *A combined two-method MPPT control scheme for grid-connected photovoltaic systems.* Paper presented at the Power electronics and applications, 2005 European conference on.

Drigo, M., Maniezzo, V., and Colorni, A., (1996). The ant system: optimization by a colony of cooperation agents. *IEEE Transactions of Systems, Man, and Cybernetics*(Part B), 29-41.

Duffie, J.A., (2006). William A. Beckman Solar Engineering of Thermal Processes: JOHN WILEY and SONS, INC. NY.

El-Adawi, M., and Al-Nuaim, I., (2001). A method to determine the solar cell series resistance from a single I–V. Characteristic curve considering its shunt resistance—new approach. *Vacuum, 64*(1), 33-36.

El-Dein, M.S., Kazerani, M., and Salama, M., (2013). Optimal photovoltaic array reconfiguration to reduce partial shading losses. *Sustainable Energy, IEEE Transactions on, 4*(1), 145-153.

Elgendy, M., Zahawi, B., and Atkinson, D.J., (2012). Assessment of perturb and observe MPPT algorithm implementation techniques for PV pumping applications. *Sustainable Energy, IEEE Transactions on, 3*(1), 21-33.

Esram, T., Kimball, J.W., Krein, P.T., Chapman, P.L., and Midya, P., (2006). Dynamic maximum power point tracking of photovoltaic arrays using ripple correlation control. *Power Electronics, IEEE Transactions on, 21*(5), 1282-1291.

Essah, E.A., Arguelles, A.R., and Glover, N., (2015). Assessing the performance of a building integrated BP c-Si PV system. *Renewable Energy, 73*, 36-45.

Fang, H., Chen, L., and Shen, Z., (2011). Application of an improved PSO algorithm to optimal tuning of PID gains for water turbine governor. *Energy Conversion and Management, 52*(4), 1763-1770.

Garrido-Alzar, C., (1997). Algorithm for extraction of solar cell parameters from I–V curve using double exponential model. *Renewable Energy, 10*(2), 125-128.

Gong, W., and Cai, Z., (2013). Parameter extraction of solar cell models using repaired adaptive differential evolution. *Solar Energy, 94*, 209-220.

Grätzel, M., (2005). Solar energy conversion by dye-sensitized photovoltaic cells. *Inorganic chemistry, 44*(20), 6841-6851.

Haouari-Merbah, M., Belhamel, M., Tobias, I., and Ruiz, J., (2005). Extraction and analysis of solar cell parameters from the illuminated current–voltage curve. *Solar Energy Materials and Solar Cells, 87*(1), 225-233.

Hohm, D., and Ropp, M.E., (2003). Comparative study of maximum power point tracking algorithms. *Progress in photovoltaics: Research and Applications, 11*(1), 47-62.

Humada, A.M., Hojabri, M., Mekhilef, S., and Hamada, H.M., (2016). Solar cell parameters extraction based on single and double-diode models: A review. *Renewable and Sustainable Energy Reviews, 56*, 494-509.

Ishaque, K., and Salam, Z., (2011a). A comprehensive MATLAB Simulink PV system simulator with partial shading capability based on two-diode model. *Solar Energy, 85*(9), 2217-2227.

Ishaque, K., and Salam, Z., (2011b). An improved modeling method to determine the model parameters of photovoltaic (PV) modules using differential evolution (DE). *Solar Energy, 85*(9), 2349-2359.

Ishaque, K., and Salam, Z., (2013). A review of maximum power point tracking techniques of PV system for uniform insolation and partial shading condition. *Renewable and Sustainable Energy Reviews, 19*, 475-488.

Ishaque, K., Salam, Z., Amjad, M., and Mekhilef, S., (2012). An improved Particle Swarm Optimization (PSO)–based MPPT for PV with reduced steady-state oscillation. *Power Electronics, IEEE Transactions on, 27*(8), 3627-3638.

Ismail, M., Moghavvemi, M., and Mahlia, T., (2013a). Characterization of PV panel and global optimization of its model parameters using genetic algorithm. *Energy Conversion and Management, 73*, 10-25.

Ismail, M., Moghavvemi, M., and Mahlia, T., (2013b). Design of an optimized photovoltaic and microturbine hybrid power system for a remote small community: case study of Palestine. *Energy Conversion and Management, 75*, 271-281.

Jensen, H., Lalchand, G., and Mak, G., (2006). Compared assessment of selected environmental indicators of photovoltaic electricity in selected OECD cities and Malaysia cities. *Malaysia: Pusat Tenaga Malaysia*.

Ji, Y.-H., Jung, D.-Y., Kim, J.-G., Kim, J.-H., Lee, T.-W., and Won, C.-Y., (2011). A real maximum power point tracking method for mismatching compensation in PV array under partially shaded conditions. *Power Electronics, IEEE Transactions on, 26*(4), 1001-1009.

Jia, Q., Anderson, W.A., Liu, E., and Zhang, S., (1988). A novel approach for evaluating the series resistance of solar cells. *Solar Cells, 25*(3), 311-318.

Jiang, L.L., Maskell, D.L., and Patra, J.C., (2013). A novel ant colony optimization-based maximum power point tracking for photovoltaic systems under partially shaded conditions. *Energy and Buildings, 58*, 227-236.

Jiang, Y., Qahouq, J., and Orabi, M., (2011). *Matlab/Pspice hybrid simulation modeling of solar PV cell/module.* Paper presented at the Applied Power Electronics Conference and Exposition (APEC), 2011 Twenty-Sixth Annual IEEE.

Johari, A., Hafshar, S.S., Ramli, M., and Hashim, H., (2011). *Potential use of solar photovoltaic in Peninsular Malaysia.* Paper presented at the Clean Energy and Technology (CET), 2011 IEEE First Conference on.

Kadri, R., Andrei, H., Gaubert, J.-P., Ivanovici, T., Champenois, G., and Andrei, P., (2012). Modeling of the photovoltaic cell circuit parameters for optimum connection model and real-time emulator with partial shadow conditions. *Energy, 42*(1), 57-67.

Kaminski, A., Marchand, J., and Laugier, A., (1999). I–V methods to extract junction parameters with special emphasis on low series resistance. *Solid-State Electronics, 43*(4), 741-745.

Kaushika, N., Gautam, N.K., and Kaushik, K., (2005). Simulation model for sizing of stand-alone solar PV system with interconnected array. *Solar Energy Materials and Solar Cells, 85*(4), 499-519.

Keogh, W.M., Blakers, A.W., and Cuevas, A., (2004). Constant voltage I–V curve flash tester for solar cells. *Solar Energy Materials and Solar Cells, 81*(2), 183-196.

Khan, B., (2006). *Non-conventional energy resources*: Tata McGraw-Hill Education.

Khan, F., Baek, S.-H., and Kim, J.H., (2014). Intensity dependency of photovoltaic cell parameters under high illumination conditions: An analysis. *Applied Energy, 133*, 356-362.

Khan, F., Singh, S., and Husain, M., (2010). Effect of illumination intensity on cell parameters of a silicon solar cell. *Solar Energy Materials and Solar Cells, 94*(9), 1473-1476.

Khatib, T., Sopian, K., and Kazem, H.A., (2013). Actual performance and characteristic of a grid connected photovoltaic power system in the tropics: A short term evaluation. *Energy Conversion and Management, 71*, 115-119.

Khezzar, R., Zereg, M., and Khezzar, A., (2014). Modeling improvement of the four parameter model for photovoltaic modules. *Solar Energy, 110*, 452-462.

Khouzam, K., and Hoffman, K., (1996). Real-time simulation of photovoltaic modules. *Solar Energy, 56*(6), 521-526.

Kim, W., and Choi, W., (2010). A novel parameter extraction method for the one-diode solar cell model. *Solar Energy, 84*(6), 1008-1019.

Kimball, J.W., and Krein, P.T., (2008). Discrete-time ripple correlation control for maximum power point tracking. *Power Electronics, IEEE Transactions on, 23*(5), 2353-2362.

Kiran, E., and İnan, D., (1999). Technical note An approximation to solar cell equation for determination of solar cell parameters. *Renewable energy, 17*(2), 235-241.

Kou, Q., Klein, S., and Beckman, W., (1998). A method for estimating the long-term performance of direct-coupled PV pumping systems. *Solar Energy, 64*(1), 33-40.

Kymakis, E., Kalykakis, S., and Papazoglou, T.M., (2009). Performance analysis of a grid connected photovoltaic park on the island of Crete. *Energy Conversion and Management, 50*(3), 433-438.

Lal, M., and Singh, S., (2007). A new method of determination of series and shunt resistances of silicon solar cells. *Solar Energy Materials and Solar Cells, 91*(2), 137-142.

Lasdon, L.S., Waren, A.D., Jain, A., and Ratner, M., (1978). Design and testing of a generalized reduced gradient code for nonlinear programming. *ACM Transactions on Mathematical Software (TOMS), 4*(1), 34-50.

Laudani, A., and Fulginei, F.R., (2014). Comments on "An efficient analytical approach for obtaining a five parameters model of photovoltaic modules using only reference data"(Appl. Energy 111 (2013) 894–903). *Applied Energy*.

Lee, K.S., (2014). Maximum power point tracking method: Google Patents.

Leyva, R., Alonso, C., Queinnec, I., Cid-Pastor, A., Lagrange, D., and Martinez-Salamero, L., (2006). MPPT of photovoltaic systems using extremum-seeking control. *Aerospace and Electronic Systems, IEEE Transactions on, 42*(1), 249-258.

Lin, C.-H., Huang, C.-H., Du, Y.-C., and Chen, J.-L., (2011). Maximum photovoltaic power tracking for the PV array using the fractional-order incremental conductance method. *Applied Energy, 88*(12), 4840-4847.

Lotsch, H., Goetzberger, A., and U. Hoffmann, V., (2005). Efficiency and Performance of PV Systems. *Photovoltaic Solar Energy Generation*, 147-161.

Luo, F.L., and Ye, H., (2007). Small signal analysis of energy factor and mathematical modeling for power dc–dc converters. *Power Electronics, IEEE Transactions on, 22*(1), 69-79.

Macabebe, E.Q.B., Sheppard, C.J., and van Dyk, E.E., (2011). Parameter extraction from I–V characteristics of PV devices. *Solar Energy, 85*(1), 12-18.

Matsuo, H., Shigemizu, T., Kurokawa, F., and Watanabe, N., (1993). *Characteristics of the multiple-input DC-DC converter*. Paper presented at the Power Electronics Specialists Conference, 1993. PESC'93 Record., 24th Annual IEEE.

McEvoy, A., Markvart, T., Castañer, L., Markvart, T., and Castaner, L., (2003). *Practical handbook of photovoltaics: fundamentals and applications*: Elsevier.

Navabi, R., Abedi, S., Hosseinian, S.H., and Pal, R., (2015). On the fast convergence modeling and accurate calculation of PV output energy for operation and planning studies. *Energy Conversion and Management, 89*, 497-506.

Nedumgatt, J.J., Jayakrishnan, K., Umashankar, S., Vijayakumar, D., and Kothari, D., (2011). *Perturb and observe MPPT algorithm for solar PV systems-modeling and simulation*. Paper presented at the India Conference (INDICON), 2011 Annual IEEE.

Ng, K.M., Adam, N.M., Inayatullah, O., and Kadir, M.Z.A.A., (2014). Assessment of solar radiation on diversely oriented surfaces and optimum tilts for solar absorbers in Malaysian tropical latitude. *International Journal of Energy and Environmental Engineering, 5*(1), 1-13.

Nguyen, D.D., and Lehman, B., (2006). *Modeling and simulation of solar PV arrays under changing illumination conditions*. Paper presented at the Computers in Power Electronics, 2006. COMPEL'06. IEEE Workshops on.

Orioli, A., and Di Gangi, A., (2013). A procedure to calculate the five-parameter model of crystalline silicon photovoltaic modules on the basis of the tabular performance data. *Applied Energy, 102*, 1160-1177.

Ortiz-Conde, A., Sánchez, F.J.G., and Muci, J., (2006). New method to extract the model parameters of solar cells from the explicit analytic solutions of their illuminated I–V characteristics. *Solar Energy Materials and Solar Cells, 90*(3), 352-361.

Ortiz-Rivera, E., and Peng, F.Z., (2005). *Analytical model for a photovoltaic module using the electrical characteristics provided by the manufacturer data sheet*. Paper presented at the Power Electronics Specialists Conference, 2005. PESC'05. IEEE 36th.

Ouennoughi, Z., and Chegaar, M., (1999). A simpler method for extracting solar cell parameters using the conductance method. *Solid-State Electronics*, *43*(11), 1985-1988.

Patel, M.R., (2005). *Wind and solar power systems: design, analysis, and operation*: CRC press.

Polman, A., Van Sark, W., Sinke, W., and Saris, F., (1986). A new method for the evaluation of solar cell parameters. *Solar cells, 17*(2), 241-251.

Rajasekar, N., Krishna Kumar, N., and Venugopalan, R., (2013). Bacterial Foraging Algorithm based solar PV parameter estimation. *Solar Energy, 97*, 255-265.

Reisi, A.R., Moradi, M.H., and Jamasb, S., (2013). Classification and comparison of maximum power point tracking techniques for photovoltaic system: A review. *Renewable and Sustainable Energy Reviews, 19*, 433-443.

Rosell, J., and Ibanez, M., (2006). Modelling power output in photovoltaic modules for outdoor operating conditions. *Energy Conversion and Management, 47*(15), 2424-2430.

Safari, A., and Mekhilef, S., (2011). Simulation and hardware implementation of incremental conductance MPPT with direct control method using cuk converter. *Industrial Electronics, IEEE Transactions on, 58*(4), 1154-1161.

Salam, Z., Ahmed, J., and Merugu, B.S., (2013). The application of soft computing methods for MPPT of PV system: A technological and status review. *Applied Energy, 107*, 135-148.

Sera, D., Mathe, L., Kerekes, T., Spataru, S.V., and Teodorescu, R., (2013). On the perturb-and-observe and incremental conductance MPPT methods for PV systems. *Photovoltaics, IEEE Journal of, 3*(3), 1070-1078.

Shi, J., Dong, J., Lv, S., Xu, Y., Zhu, L., Xiao, J., . . . Luo, Y., (2014). Hole-conductor-free perovskite organic lead iodide heterojunction thin-film solar cells: High efficiency and junction property. *Applied Physics Letters, 104*(6), 063901.

Shockley, W., 1953. Electrons and holes in semiconductors.

Shockley, W., and Queisser, H.J., (1961). Detailed balance limit of efficiency of p-n junction solar cells. *Journal of applied physics, 32*(3), 510-519.

Solangi, K., Islam, M., Saidur, R., Rahim, N., and Fayaz, H., (2011). A review on global solar energy policy. *Renewable and sustainable energy reviews, 15*(4), 2149-2163.

Spiazzi, G., Buso, S., and Mattavelli, P., (2009). *Analysis of MPPT algorithms for photovoltaic panels based on ripple correlation techniques in presence of parasitic components.* Paper presented at the Power Electronics Conference, 2009. COBEP'09. Brazilian.

Suryavanshi, R., Joshi, D.R., and Jangamshetti, S.H., (2012). *PSO and PandO based MPPT technique for SPV panel under varying atmospheric conditions.* Paper presented at the Power, Signals, Controls and Computation (EPSCICON), 2012 International Conference on.

Tafticht, T., Agbossou, K., Doumbia, M., and Chériti, A., (2008). An improved maximum power point tracking method for photovoltaic systems. *Renewable energy, 33*(7), 1508-1516.

Tang, J., and Sargent, E.H., (2011). Infrared colloidal quantum dots for photovoltaics: fundamentals and recent progress. *Advanced materials, 23*(1), 12-29.

Tey, K.S., and Mekhilef, S., (2014). Modified incremental conductance MPPT algorithm to mitigate inaccurate responses under fast-changing solar irradiation level. *Solar Energy, 101*, 333-342.

Tivanov, M., Patryn, A., Drozdov, N., Fedotov, A., and Mazanik, A., (2005). Determination of solar cell parameters from its current–voltage and spectral characteristics. *Solar energy materials and solar cells, 87*(1), 457-465.

Villalva, M.G., and Gazoli, J.R., (2009). Comprehensive approach to modeling and simulation of photovoltaic arrays. *Power Electronics, IEEE Transactions on, 24*(5), 1198-1208.

Wolf, M., and Rauschenbach, H., (1963). Series resistance effects on solar cell measurements. *Advanced energy conversion, 3*(2), 455-479.

Xuesong, Z., Daichun, S., Youjie, M., and Deshu, C., (2010). *The simulation and design for MPPT of PV system Based on Incremental Conductance Method.* Paper presented at the information engineering (ICIE), 2010 WASE international conference on.

APPENDIX A

$$I(G^{\nabla},T)=\alpha_G I_L(T)-I_o(G^{\nabla},\mathrm{T})[\exp[(G^{\nabla}\{\mathrm{V}+\mathrm{KI(T - T_{STC})}\}+\mathrm{IR_{RS}})/G^{\nabla}\mathrm{nT}]-1]$$
$$-(\frac{G^{\nabla}\{\mathrm{V}+\mathrm{KI(T - T_{STC})}\}+\mathrm{IR_{RS}}}{\mathrm{R_{sh}}}) \qquad \text{(A.1)}$$

Where,

$$K=\frac{V_{mp}-V^{*}{}_{mp}}{I^{*}{}_{mp}(T^{*}\text{-}T_{STC})} \qquad \text{(A.2)}$$

Where V^*_{mp} and I^*_{mp} are the coordinates of the maximum power point at $T=T^*$ issued by the manufacturer, and *vamp* is the voltage corresponding to the maximum power point calculated by Eq. (A.5), with K fixed at 0. In addition, the quantity $G^{\nabla}=G/G_{STC}$ represents the ratio of the generic solar irradiance to the solar irradiance at STC, while K is the thermal correction factor similar to the curve correction factor defined by the IEC 891. Hence, the parameters can be evaluated according to the following equation,

$$I_{ph}(T)=I_{ph,STC}+\mu_{Isc}(T-T_{STC}) \qquad \text{(A.3)}$$

Clearly, $G^{\nabla}=1$, $T=25C^{\circ}$ at STC, and Eq. (A.1) will be equivalent to the conventional five parameters in Eq. (A.3).

$$I_{ph,STC}=I_{SC,STC} \quad \text{and} \quad R_{sh}=R_{sh0} \qquad \text{(A.4)}$$

Then, under the common conditions that have been extensively fulfilled, R_s, R_{sh}, and n can be found by applying Eq. (A.5)

$$R_s\langle\langle R_{sho}\,\frac{I_{o,STC}}{nT_{STC}}\exp(I_{SC,STC}R_S/nT_{STC}\langle\langle\frac{1}{R_{sho}} \qquad \text{(A.5)}$$

Another noteworthy observation is with regard to the current I_o (G, T), whose value for the irradiance and temperature individually can be calculated by means of the following equation:

$$I_o(G^{\nabla},T) = \exp[\frac{(G^{\nabla}-0.2)}{(1-0.2)}\ln\frac{I_o(1,T)}{I_o(0.2,T)} + \ln I_o(0.2,T)] \qquad \text{(A.6)}$$

$$R_{so} = -(\frac{dV}{dI})_{V=V_{OC}} \qquad \text{(A.7)}$$

$$R_{sho} = -(\frac{dV}{dI})_{I=I_{SC}} \qquad \text{(A.8)}$$

Where R_{so} is the reciprocal of the gradient at the open-circuit point, while R_{sho} is the reciprocal of the gradient at the short-circuit point.

$$I_L = I_{SC}(1+\frac{R_S}{R_{sh}}) + I_o(\exp[\frac{I_{SC}R_S}{mV_t}]-1) \qquad \text{(A.9)}$$

$$I_o = (I_{SC} - \frac{V_{OC}}{R_{sh}})\exp[-\frac{V_{OC}}{mV_t}] \qquad \text{(A.10)}$$

$$R_S = R_{SO} - (\frac{mV_t}{I_o}(\exp[-\frac{V_{OC}}{mV_t}] \qquad \text{(A.11)}$$

$$R_{Sh} = R_{Sho} \qquad \text{(A.12)}$$

$$m = \frac{V_{mp} + I_{mp}R_{so} - V_{OC}}{V_t\{\ln(I_{SC} - \frac{V_{mp}}{R_{sh}} - I_{mp}) - \ln(I_{SC} - \frac{V_{OC}}{R_{sh}}) + (\frac{I_{mp}}{I_{SC} - \frac{V_{OC}}{R_{sh}}})\}} \qquad \text{(A.13)}$$

Where the values of I_{sc} and V_{oc} at a temperature and solar irradiance level besides the reference values can be calculated as follows:

$$I_{SC} = I_{SC,STC} G^{\nabla} + \mu_{I_{SC}} (T - T_{STC}) \tag{A.14}$$

$$V_{OC} = V_{OC,STC} + mV_t \ln G^{\nabla} + \mu_{V_{OC}} (T - T_{STC}) \tag{A.15}$$

$$n = -(\frac{A}{V_t (B + C)}) \tag{A.16}$$

where A, B and C can be derived as follows:

$$A = V_m + R_{So} I_m - V_{OC} \tag{A.17}$$

$$B = \ln(I_{SC} - \frac{V_m}{R_{sh}} - I_m) - \ln(I_{SC} - \frac{V_{OC}}{R_{sh}}) \tag{A.18}$$

$$C = \frac{I_m}{(I_{SC} - \frac{V_{OC}}{R_{sh}})} \tag{A.19}$$

$$I_o = (I_{SC} - \frac{V_{OC}}{R_{sh}}) \exp(-\frac{V_{OC}}{nV_T}) \tag{A.20}$$

$$R_S = R_{So} - \frac{nV_t}{I_o} \exp(-\frac{V_{OC}}{nV_T}) \tag{A.21}$$

$$I_{ph} = I_{SC} (1 + \frac{R_S}{R_{sh}}) + I_o (\exp(\frac{I_{SC} R_S}{nV_T}) - 1) \tag{A.22}$$

$$f_{n1} : I_L + [1 - \exp(\frac{I_{SC} R_S}{nT})] I_o - \frac{I_{SC} R_S}{R_{sh}} - I_{SC} = 0 \tag{A.23}$$

$$f_{n2}: I_L + [1 - \exp(\frac{V_{OC}}{nT})]I_o - \frac{V_{OC}}{R_{sh}} = 0 \quad \text{(A.24)}$$

$$f_{n3}: I_L + [1 - \exp(\frac{I_{mpp}R_S + V_{mpp}}{nT})]I_o - \frac{I_{mpp}R_S + V_{mpp}}{R_{sh}} - I_{mpp} = 0 \quad \text{(A.25)}$$

$$f_{n4}: \frac{-nT - [\exp(\frac{I_{mpp}R_S + V_{mpp}}{nT})]I_o R_{sh}}{nT.(R_S + R_{sh}) + [\exp(\frac{I_{mpp}R_S + V_{mpp}}{nT})]I_o R_{sh}.R_S} + \frac{I_{mpp}}{V_{mpp}} = 0 \quad \text{(A.26)}$$

$$f_{n5}: \frac{V_{mpp}.nT[I_o R_{sh} + I_L R_{sh} - 2V_{mpp} + [\exp(\frac{I_{mpp}V_{mpp}R_S + V^2{}_{mpp}}{V_{mpp}nT})]I_o R_{sh}[I_{mpp}V_{mpp}.R_S - V_{mpp}(nT + V_{mpp})}{V_{mpp}\{I_o.R_S.R_{sh}.[\exp(\frac{I_{mpp}V_{mpp}R_S + V^2{}_{mpp}}{V_{mpp}nT})] + nT(R_{sh} + R_S)\}} = 0$$

(A.27)

$$\begin{cases} f_{n1} = 0 \\ f_{n2} = 0 \\ f_{n3} = 0 \\ f_{n4} = 0 \\ f_{n5} = 0 \end{cases} \quad \text{(A.28)}$$

$$I = I_{SC} - G_{sh}^f V - a_3 h^f(I,V) \quad \text{(A.29)}$$

$$V = V_{OC} - IR_S^s - b_3 h^s(I,V) \quad \text{(A.30)}$$

$$I_{ph,STC} = I_{SC,STC} \quad \text{(A.31)}$$

$$n_{STC} = \frac{\mu_{V_{OC}} T_{STC} - V_{OC,STC} + E_q N_S}{\frac{\mu_{I_{,SC}} T_{STC}}{I_{L,STC}} - 3} \quad \text{(A.32)}$$

$$R_{S,STC}=\frac{n_{STC}.\ln(1-\frac{I_{mp,STC}}{I_{L,STC}})-V_{mpp,STC}+V_{OC,STC}}{I_{mpp,STC}} \tag{A.33}$$

$$I_{o,STC}=\frac{I_{L,STC}}{\exp(\frac{V_{OC,STC}}{n_{,STC}})-1} \tag{A.34}$$

$$I_L=G^{\nabla}[I_{L,STC}+\mu_{I_{,SC}}(T-T_{STC}) \tag{A.35}$$

$$I_o=I_{o,STC}(T^{\nabla})^3\exp[\frac{E_qN_s}{n})(1-\frac{1}{T^{\nabla}}) \tag{A.36}$$

$$R_S=R_{S,STC} \tag{A.37}$$

$$n=n_{STC}T^{\nabla} \tag{A.38}$$

where $T^{\nabla}=T/T_{STC}$.

$$R_S=\frac{1}{2}\{[(a-b)^2+\frac{2p}{I_{SC}}(a-b)+(\frac{V_{OC}}{I_{SC}})^2]^{\frac{1}{2}}+(a+b)+\frac{V_{OC}}{I_{SC}}\} \tag{A.39}$$

$$R_{sh}=\frac{V_{OC}}{\frac{nV_T}{b+R_S}-\frac{nV_T}{a+R_S}+I_{SC}} \tag{A.40}$$

$$I_o=\frac{I_{SC}}{\lambda}-\frac{V_{OC}}{\lambda R_{sh}}\text{, where } \lambda=\exp\frac{V_{OC}}{nV_T}-1 \tag{A.41}$$

$$n=\frac{(V_m-I_mR_S)(I_{SC}+I_o-I_m-V_m/R_{sh})}{V_T(I_m-V_m/R_{sh})} \tag{A.42}$$

$$R_{sh} = R_{sho} = -(\frac{dV}{dI})_{I=I_{SC}} \tag{A.43}$$

$$P(V) = V - V_a \ln(I_{ph} - I) \tag{A.44}$$

Where V_a denotes a random value of the voltage. By using Eq. (2.3) minus the last term and by replacing V with I, Eq. (A.44) then becomes

$$F(I) = aI + b\ln(I_{ph} - I) + c_o \tag{A.45}$$

$$\text{where } a = -R_S, b = nV_T \text{ and } c = -nV_T I_o \tag{A.46}$$

$$R_{sh} = R_{SC} \tag{A.47}$$

$$R_S = R_{OC} - \frac{(V_m + R_{OC} I_m - V_{OC})}{I_m + [\ln(I_{SC} - I_m) - \ln(I_{SC})].I_{SC}} \tag{A.48}$$

$$n = \frac{(V_m + R_{OC} I_m - V_{OC})}{[\ln(I_{SC} - I_m) - \ln(I_{SC})].V_T} \tag{A.49}$$

$$I_o = \frac{nV_T}{(R_{OC} - R_S)} \exp(-\frac{V_{OC}}{nV_T}) \tag{A.50}$$

Where R_{sc} and R_{oc} are the inverse of the gradients [(dJ/dV)-1] under the short circuit ($V = 0$, $I = -I_{sc}$) and the open circuit ($V = V_{oc}$, $I = 0$) conditions, respectively, while V_m is the voltage and I_m is the current density at the maximum power point.

$$y = \frac{1}{n_d V_T}(-R_S + X), y = \frac{\ln(I/I_1)}{I - I_1}, X = \frac{V - V_1}{I - I_1} \tag{A.51}$$

Where (V_1, I_1) represents a point on the first section of the I–V characteristic of the solar cell.

$$I = I_{or}(\exp[\frac{V_D}{n_r V_T}]) \tag{A.52}$$

$$R_{sh} = [(\frac{dI}{dV})_{I=I_{SC}} - \frac{I_{or}}{n_r V_T}]^{-1} \tag{A.53}$$

Where V_T represents the thermal voltage, (V_T= kT/q), V_D is the diode voltage.

$$I = \frac{nV_T}{R_S} LambertW\{\frac{R_S}{nV_T}(I_{SC} - \frac{V_{OC}}{R_S + R_{sh}})\exp(\frac{-V_{OC}}{nV_T}).\exp\frac{1}{nV_T}(R_S I_{SC} + \frac{R_{sh}V}{R_S + R_{sh}})\}$$
$$+\frac{V}{R_S} - I_{SC} - \frac{R_{sh}V}{R_S(R_S + R_{sh})} \tag{A.54}$$

$$-\frac{dV}{dI} = \frac{nV_T}{I_{SC} - I - [V - R_S(I_{SC} - I) - n} \tag{A.55}$$

$$I_o = [I_{SC} - \frac{nV_{OC} - I_{SC}R_S}{R_{Sh}}]\exp(-\frac{V_{OC}}{nV_T}) \tag{A.56}$$

$$I_{ph} = \frac{V_{OC}}{R_{Sh}} + I_o[\exp(\frac{V_{OC}}{nV_T}) - 1] \tag{A.57}$$

$$V = V_{OC} - IR_S + mV_T \ln[\frac{I_{SC} - I}{I_{SC}} + \exp\frac{I_{SC}R_S - V_{OC}}{nV_T}] \tag{A.58}$$

$$A = (I_{ph} + I_o)(V_{OC} - rI_{SC})r + I_{SC}(1 + gr)(\frac{rI_{SC}}{2} - V_T n) + V_{OC}g(V_T n - \frac{V_{OC}}{2}) \tag{A.59}$$

Where r denotes the R_s and g the R_{sh}. By taking into account the generally accepted approximations of $gr \ll 1$, $I_o < I_{ph}$ and $I_{sc}\ EI_{ph}$ (Khan et al., 2010), Eq. (A.60) becomes;

$$y=\frac{I_{SC}}{2V_{OC}}r+\frac{1}{V_{OC}}V_T n+\frac{V_{OC}}{2I_{SC}}g-\frac{1}{I_{SC}}V_T gn, y=\frac{I_{SC}V_{OC}-A}{I_{SC}V_{OC}} \tag{A.60}$$

$$I=I_L-I_o[\exp(\frac{\mathrm{qV_D}}{\mathrm{nkT}})-1] \tag{A.61}$$

$$n=\frac{T}{K_1} \tag{A.62}$$

Where K_1 denotes the coefficient in this equation.

$$K_1=\frac{q}{nk} \tag{A.63}$$

$$I_L=(K_2+K_3.T)G \tag{A.64}$$

$$I_o=K_4.T.\exp(-\frac{K}{T}) \tag{A.65}$$

$$n=\frac{V_{OC}}{V_T[\ln\{I_{or}+I_{ph}-I_{od}(\exp(\frac{V_{OC}}{V_T}-1))-\frac{V_{OC}}{R_{sh}}\}-\ln I_{or}]} \tag{A.66}$$

$$I_5=I_{ph}-I_{od}[\exp(\frac{\mathrm{V}_5+I_5R_S}{\mathrm{V_T}})-1]-I_{or}[\exp(\frac{\mathrm{V}_5+I_5R_S}{\mathrm{V_t m_t}})-1]-\frac{\mathrm{V}_5+I_5R_S}{\mathrm{R_{sh}}} \tag{A.67}$$

$$R_S=\frac{\mathrm{V_{OC,0,1}}-\mathrm{V}_{m,1}}{\mathrm{I_{SC,1}}-\mathrm{I_{SC,0,1}}} \tag{A.68}$$

$$n=\frac{V_{OC,1}-V_{OC,0,1}1}{\ln(I_{SC,1}/I_{SC,0,1})V_T} \tag{A.69}$$

$$R_{sh}\to\infty, I_{SC}\approx I_{ph},\ \exp(\frac{V_{OC}}{nV_T})\rangle\rangle 1 \tag{A.70}$$

$$\ln(I_{SC}-\frac{V_{OC}}{R_{sh}})=\ln I_o+\frac{V_{OC}}{nV_T} \tag{A.71}$$

$$I_o R_{sh} \exp(\frac{V+IR_S}{nV_T}) \rangle\rangle V\ ,\ \frac{R_S I_i}{R_{sh}} \langle I_{SC} + I_o - I_{i,} i = 1{,}2\ ,\ I_{SC} \rangle\rangle I_o\ ,\ I_{SC} \rangle\rangle I_{ph} \tag{A.72}$$

$$R_{SC} = \frac{nV_T}{I_1 - I_2} \ln \frac{I_{SC} - I_2}{I_{SC} - I_1} - \frac{V_2 - V_1}{I_2 - I_1} \tag{A.73}$$

$$\frac{R_{sh} + R_S}{R_{sh}(I_{SC} - I_1) - R_S I_1} = \frac{V_1 - R_S}{nV_T I_1} \tag{A.74}$$

$$I = I_o [\exp(\frac{V_1 - R_S}{nV_T})] \tag{A.75}$$

$$y = nV_T + R_S X\ ,\quad X = \frac{I + I_1}{2}\ ,\quad y = \frac{1}{I - I_1} \int_{V1}^{V} I dV \tag{A.76}$$

$$R_S = \frac{(V_m(1/V_T)(I_{SC} - I_m)\{V_{OC} + V_T \ln[1 - (I_m / I_{SC})]\} - I_m}{(I_m(1/V_T)(I_{SC} - I_m)\{V_{OC} + V_T \ln[1 - (I_m / I_{SC})]\} + I_m} \tag{A.77}$$

$$n = (V_m + I_m R_S) / \{V_{OC} + V_T \ln[(I_m / I_{SC}) / I_{SC}]\} \tag{A.78}$$

$$R_S = \frac{1}{\lambda} \frac{1}{(I_2 - I_1)} = \ln [\frac{I_{ph} - I_2}{I_{ph} - I_1}] - \frac{V_2 - V_1}{I_2 - I_1} \tag{A.79}$$

$$R_S = \frac{\Delta V}{I_m} = \frac{V_{dark,m} - V_m}{I_m} \tag{A.80}$$

$$R_S = \frac{V_{dark,m} - V_m - (I_{SC} - I_m) R_{S,dark}}{I_m} \tag{A.81}$$

$$R_S = \frac{V_{SC} - V_{OC}}{I_{SC}} \tag{A.82}$$

$$R_S = \frac{\Delta V}{I_m} = \frac{V_{ideal} - V_m}{I_m} \tag{2.83}$$

$$R_S = 2\left(\frac{V_{OC}}{I_{SC}} - \frac{A}{I_{SC}^2} - \frac{V_T}{I_{SC}}\right) \tag{A.84}$$

$$R_S = -\left(\left(\frac{\partial I}{\partial V}\right)_{V=V_{OC}}\right)^{-1} - \left(\frac{I_{ph}}{nV_T}\right)^{-1} \tag{A.85}$$

APPENDIX B

Experimental Setup of Data Collection

Figure B.1. Two PV plants (C-Si) and (Cis) installed in Bangi, Malaysia.

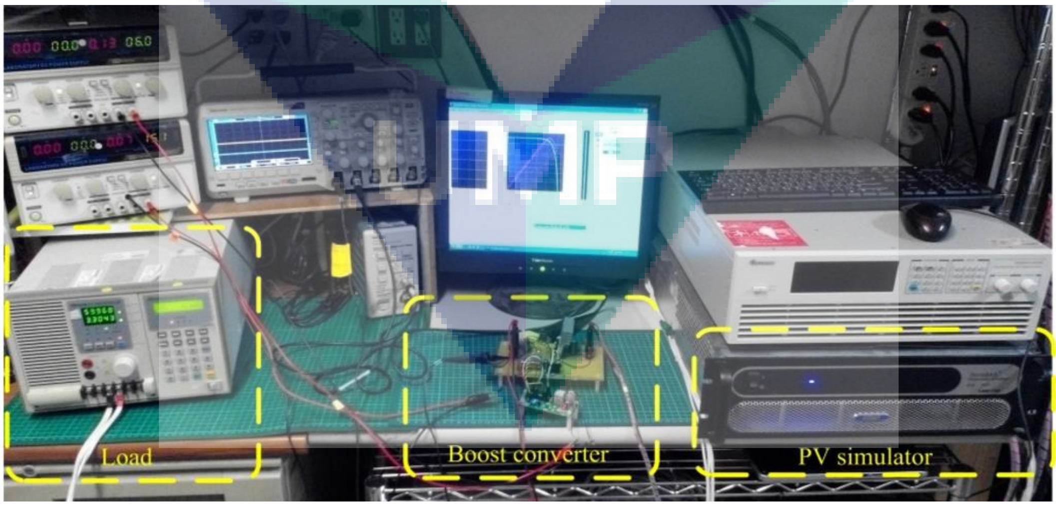

Figure B.2. Experimental setup of PV system data collection

APPENDIX C

EXPERIMENTAL DATA OF PV CHARACTERISTICS

The main PV model parameters were derived based on real data for a PV system installed for a whole year (1.1.2014 to 31.12.2015). Due to the huge a mount of these data, in this study just attached a sample for the first ten days from May 2014. The table below illustrate these dependent sample data. Each date smple taken an average of five minuite time.

Date	PYRANOMETER W/m^2	PVTemp °C	Amb.Temp. °C	Iac A	Vac V	Ipv A	Vpv V
5/1/2014 7:15:00	25.08	28.30	24.81	0.000	0.00	0.000	0
5/1/2014 7:20:00	25.08	28.28	24.75	0.000	0.00	0.000	0
5/1/2014 7:25:00	25.08	28.17	24.84	0.035	0.02	0.055	0.024
5/1/2014 7:30:00	23.82	28.18	24.89	0.120	0.15	0.175	0.163
5/1/2014 7:35:00	25.08	28.19	24.93	0.201	0.17	0.266	0.187
5/1/2014 7:40:00	25.08	28.33	25.16	0.266	0.32	0.334	0.35
5/1/2014 7:45:00	26.17	28.47	25.36	0.298	0.56	0.354	0.612
5/1/2014 7:50:00	31.35	28.68	25.45	0.379	0.81	0.433	0.875
5/1/2014 7:55:00	31.05	28.80	25.48	0.404	1.05	0.444	1.137
5/1/2014 8:00:00	33.10	28.88	25.57	0.518	1.29	0.553	1.4
5/1/2014 8:05:00	43.89	29.14	25.85	0.613	1.53	0.627	1.663
5/1/2014 8:10:00	49.01	29.45	26.18	0.794	1.77	0.783	1.925
5/1/2014 8:15:00	50.15	29.79	26.49	0.984	2.01	0.941	2.188
5/1/2014 8:20:00	54.33	30.29	26.82	1.158	2.25	1.098	2.45
5/1/2014 8:25:00	68.96	30.85	27.10	1.279	2.50	1.228	2.713
5/1/2014 8:30:00	75.23	31.45	27.71	1.368	2.74	1.302	2.976
5/1/2014 8:35:00	91.95	31.79	27.86	1.405	2.98	1.353	3.238
5/1/2014 8:40:00	100.31	32.20	28.05	1.491	3.22	1.431	3.501
5/1/2014 8:45:00	118.84	33.22	28.44	1.809	3.46	1.615	3.763
5/1/2014 8:50:00	149.46	35.53	28.50	1.501	3.56	1.355	3.867
5/1/2014 8:55:00	147.04	36.22	28.67	1.346	3.65	1.249	3.97
5/1/2014 9:00:00	125.39	35.28	28.58	1.322	3.75	1.293	4.073
5/1/2014 9:05:00	139.43	34.97	28.96	1.607	3.84	1.481	4.176
5/1/2014 9:10:00	145.45	35.30	30.11	1.674	3.94	1.515	4.28
5/1/2014 9:15:00	145.90	35.45	29.93	1.951	4.03	1.742	4.383
5/1/2014 9:20:00	142.83	36.58	29.73	2.127	4.13	1.889	4.486
5/1/2014 9:25:00	121.97	37.90	30.34	1.513	4.22	1.431	4.589
5/1/2014 9:30:00	200.62	39.49	31.15	2.475	4.32	2.319	4.693
5/1/2014 9:35:00	221.51	41.92	32.67	2.857	4.41	2.595	4.796
5/1/2014 9:40:00	224.69	43.78	33.28	3.155	4.51	2.862	4.899
5/1/2014 9:45:00	218.73	45.14	33.20	3.013	4.60	2.726	5.002
5/1/2014 9:50:00	185.35	44.46	32.03	2.544	4.70	2.319	5.106

5/1/2014 9:55:00	156.43	43.51	31.70	2.338	4.79	2.146	5.209
5/1/2014 10:00:00	150.46	43.43	31.99	2.304	4.89	2.113	5.312
5/1/2014 10:05:00	176.68	43.42	31.87	2.592	4.98	2.389	5.415
5/1/2014 10:10:00	176.59	43.88	31.95	2.636	5.08	2.467	5.519
5/1/2014 10:15:00	189.12	43.90	31.77	2.873	5.17	2.635	5.622
5/1/2014 10:20:00	187.42	43.55	32.02	2.920	5.27	2.729	5.725
5/1/2014 10:25:00	180.99	43.52	32.28	2.945	5.36	2.687	5.828
5/1/2014 10:30:00	202.62	44.12	32.80	3.307	5.46	2.987	5.932
5/1/2014 10:35:00	219.43	44.54	32.60	3.520	5.55	3.142	6.035
5/1/2014 10:40:00	226.83	44.84	33.32	3.772	5.65	3.373	6.138
5/1/2014 10:45:00	243.46	46.03	33.86	3.977	5.74	3.570	6.241
5/1/2014 10:50:00	277.10	46.71	33.73	4.358	5.84	4.057	6.345
5/1/2014 10:55:00	242.79	47.31	34.01	3.925	5.93	3.683	6.448
5/1/2014 11:00:00	223.60	47.80	33.41	3.620	6.03	3.324	6.551
5/1/2014 11:05:00	225.69	47.85	33.83	3.785	6.12	3.409	6.654
5/1/2014 11:10:00	227.88	48.15	34.83	3.863	6.22	3.498	6.758
5/1/2014 11:15:00	232.53	48.17	34.48	3.881	6.31	3.577	6.861
5/1/2014 11:20:00	250.77	47.93	34.80	4.100	6.41	3.730	6.964
5/1/2014 11:25:00	269.25	47.54	35.55	4.192	6.50	3.780	7.067
5/1/2014 11:30:00	268.22	48.22	35.67	4.008	6.60	3.641	7.171
5/1/2014 11:35:00	376.16	48.50	35.45	5.394	6.69	4.911	7.274
5/1/2014 11:40:00	304.20	46.88	35.87	4.370	6.79	4.140	7.377
5/1/2014 11:45:00	304.20	47.50	35.73	4.435	6.88	4.198	7.48
5/1/2014 11:50:00	274.71	47.33	35.34	4.113	6.98	3.843	7.584
5/1/2014 11:55:00	291.37	48.36	35.30	4.483	7.07	4.180	7.687
5/1/2014 12:00:00	323.72	47.59	34.81	4.704	7.17	4.334	7.79
5/1/2014 12:05:00	303.02	47.62	34.30	4.514	7.26	4.216	7.893
5/1/2014 12:10:00	327.26	48.09	34.45	4.808	7.36	4.481	7.997
5/1/2014 12:15:00	385.56	49.19	36.53	5.164	7.45	4.659	8.1
5/1/2014 12:20:00	430.49	51.02	36.15	5.521	7.55	5.138	8.203
5/1/2014 12:25:00	196.44	46.28	33.68	2.879	7.64	2.743	8.307
5/1/2014 12:30:00	275.85	44.01	33.88	3.632	7.74	3.447	8.41
5/1/2014 12:35:00	341.05	44.33	35.57	4.847	7.83	4.496	8.513
5/1/2014 12:40:00	398.23	44.39	35.67	5.333	7.93	5.134	8.616
5/1/2014 12:45:00	598.43	44.60	37.85	7.018	7.97	6.789	8.667
5/1/2014 12:50:00	550.44	46.54	36.73	6.308	8.02	6.095	8.719
5/1/2014 12:55:00	517.22	46.13	37.11	5.913	8.07	5.631	8.77
5/1/2014 13:00:00	526.62	48.15	36.87	5.445	8.12	5.227	8.821
5/1/2014 13:05:00	505.72	48.21	36.19	5.316	8.16	5.100	8.872
5/1/2014 13:10:00	549.42	47.56	36.47	5.955	8.21	5.793	8.924
5/1/2014 13:15:00	422.89	49.07	37.22	4.832	8.26	4.677	8.975
5/1/2014 13:20:00	337.50	49.14	35.57	4.481	8.30	4.366	9.026
5/1/2014 13:25:00	280.03	49.47	36.07	4.033	8.35	3.900	9.077
5/1/2014 13:30:00	274.76	49.38	36.08	4.132	8.40	3.933	9.128
5/1/2014 13:35:00	299.61	49.29	36.37	4.319	8.45	4.089	9.18
5/1/2014 13:40:00	275.85	48.70	35.28	4.253	8.49	4.040	9.231
5/1/2014 13:45:00	275.85	46.54	35.71	4.151	8.54	3.910	9.282
5/1/2014 13:50:00	295.70	44.11	35.13	4.303	8.59	4.028	9.333
5/1/2014 13:55:00	275.85	43.43	35.11	4.242	8.63	3.973	9.385
5/1/2014 14:00:00	287.25	41.82	34.63	4.428	8.68	4.168	9.436
5/1/2014 14:05:00	279.27	40.74	33.87	4.362	8.73	4.057	9.487
5/1/2014 14:10:00	286.11	40.40	34.69	4.340	8.77	4.031	9.538
5/1/2014 14:15:00	327.20	42.31	36.67	4.449	8.82	4.193	9.589
5/1/2014 14:20:00	330.36	43.05	36.49	4.656	8.87	4.384	9.641

5/1/2014 14:25:00	515.13	45.11	37.44	6.534	8.92	6.340	9.692
5/1/2014 14:30:00	396.68	45.69	37.49	5.157	8.96	4.830	9.743
5/1/2014 14:35:00	380.12	45.83	36.37	5.298	9.01	4.921	9.794
5/1/2014 14:40:00	435.72	44.21	35.58	5.703	9.06	5.336	9.846
5/1/2014 14:45:00	408.76	44.87	37.29	5.323	9.11	5.108	9.897
5/1/2014 14:50:00	285.40	46.21	37.52	3.980	9.15	3.866	9.948
5/1/2014 14:55:00	261.03	44.09	35.33	3.871	9.20	3.717	9.999
5/1/2014 15:00:00	241.65	44.02	34.88	3.600	9.25	3.439	10.05
5/1/2014 15:05:00	256.74	41.88	34.07	3.880	9.29	3.693	10.102
5/1/2014 15:10:00	304.06	40.18	34.19	4.642	9.34	4.298	10.153
5/1/2014 15:15:00	267.07	40.90	35.87	4.216	9.39	3.942	10.204
5/1/2014 15:20:00	258.09	42.44	34.96	4.092	9.43	3.787	10.255
5/1/2014 15:25:00	276.94	44.08	35.22	4.291	9.48	3.934	10.307
5/1/2014 15:30:00	308.56	44.71	35.74	4.800	9.53	4.332	10.358
5/1/2014 15:35:00	268.22	46.12	35.98	4.127	9.58	3.749	10.409
5/1/2014 15:40:00	255.55	45.08	35.20	4.086	9.62	3.838	10.46
5/1/2014 15:45:00	269.31	41.78	34.77	4.271	9.67	3.920	10.511
5/1/2014 15:50:00	294.33	43.28	36.01	4.591	9.72	4.232	10.563
5/1/2014 15:55:00	279.12	44.77	36.73	4.276	9.76	3.914	10.614
5/1/2014 16:00:00	298.54	45.13	36.22	4.544	9.81	4.212	10.665
5/1/2014 16:05:00	328.09	45.75	37.65	4.891	9.86	4.664	10.716
5/1/2014 16:10:00	330.56	42.72	35.07	4.875	9.91	4.542	10.767
5/1/2014 16:15:00	410.35	44.00	37.37	5.584	9.95	5.281	10.819
5/1/2014 16:20:00	378.34	44.77	37.50	4.963	10.00	4.621	10.87
5/1/2014 16:25:00	323.36	44.92	35.86	4.700	10.05	4.485	10.921
5/1/2014 16:30:00	283.83	43.08	34.97	4.154	10.09	3.895	10.972
5/1/2014 16:35:00	255.79	41.18	34.03	3.810	10.14	3.635	11.024
5/1/2014 16:40:00	284.21	40.10	34.05	3.867	10.19	3.663	11.075
5/1/2014 16:45:00	196.26	39.69	33.61	2.937	10.24	2.733	11.126
5/1/2014 16:50:00	163.00	39.70	33.48	2.598	10.28	2.416	11.177
5/1/2014 16:55:00	149.27	39.99	33.24	2.402	10.33	2.269	11.228
5/1/2014 17:00:00	132.23	39.06	32.67	2.132	10.38	2.014	11.28
5/1/2014 17:05:00	122.11	38.78	32.53	1.913	10.42	1.844	11.331
5/1/2014 17:10:00	123.30	39.05	32.50	1.858	10.47	1.779	11.382
5/1/2014 17:15:00	117.41	37.91	31.90	1.770	10.52	1.691	11.433
5/1/2014 17:20:00	112.25	38.07	32.46	1.738	10.57	1.670	11.485
5/1/2014 17:25:00	119.42	38.49	32.80	1.733	10.61	1.606	11.536
5/1/2014 17:30:00	121.43	38.28	32.25	1.735	10.66	1.616	11.587
5/1/2014 17:35:00	115.35	37.67	31.88	1.672	10.71	1.555	11.638
5/1/2014 17:40:00	102.49	37.60	32.25	1.593	10.75	1.533	11.689
5/1/2014 17:45:00	94.34	37.77	32.36	1.408	10.80	1.366	11.741
5/1/2014 17:50:00	76.32	37.33	31.28	1.171	10.85	1.178	11.792
5/1/2014 17:55:00	75.23	37.02	31.33	0.984	10.90	1.015	11.843
5/1/2014 18:00:00	65.20	36.83	31.94	0.856	10.94	0.923	11.894
5/1/2014 18:05:00	56.75	36.99	31.61	0.777	10.99	0.844	11.946
5/1/2014 18:10:00	50.15	37.04	31.51	0.699	11.04	0.767	11.997
5/1/2014 18:15:00	50.15	36.75	31.90	0.578	11.08	0.617	12.048
5/1/2014 18:20:00	50.15	36.40	31.55	0.586	11.13	0.611	12.099
5/1/2014 18:25:00	51.29	36.21	31.50	0.631	11.18	0.652	12.15
5/1/2014 18:30:00	50.15	35.89	31.25	0.605	11.23	0.631	12.202
5/1/2014 18:35:00	50.15	35.64	30.92	0.528	11.27	0.561	12.253
5/1/2014 18:40:00	50.15	35.54	30.57	0.444	11.32	0.486	12.304
5/1/2014 18:45:00	42.27	35.50	30.39	0.300	11.37	0.352	12.355
5/1/2014 18:50:00	28.84	35.37	30.21	0.185	11.41	0.241	12.407

5/1/2014 18:55:00	25.08	35.30	30.04	0.081	11.46	0.119	12.458
5/1/2014 19:00:00	24.43	35.10	29.87	0.018	11.51	0.029	12.509
5/1/2014 19:05:00	25.08	34.82	29.51	0.000	11.56	0.000	12.56
5/1/2014 19:10:00	25.08	34.52	29.46	0.000	11.60	0.000	12.611
5/1/2014 19:15:00	22.37	34.18	29.35	0.000	11.65	0.000	12.663
5/2/2014 7:15:00	23.82	28.23	24.90	0.000	11.70	0.000	12.714
5/2/2014 7:20:00	25.08	28.20	24.95	0.000	11.74	0.000	12.765
5/2/2014 7:25:00	23.88	28.17	24.95	0.031	11.79	0.048	12.816
5/2/2014 7:30:00	25.08	28.05	24.91	0.075	11.84	0.116	12.867
5/2/2014 7:35:00	25.08	28.04	24.95	0.149	11.89	0.206	12.919
5/2/2014 7:40:00	25.08	28.23	25.06	0.214	11.93	0.282	12.97
5/2/2014 7:45:00	25.08	28.35	25.31	0.259	11.98	0.326	13.021
5/2/2014 7:50:00	25.08	28.47	25.47	0.276	12.03	0.335	13.072
5/2/2014 7:55:00	25.08	28.60	25.57	0.323	12.07	0.374	13.124
5/2/2014 8:00:00	31.62	28.69	25.81	0.449	12.12	0.496	13.175
5/2/2014 8:05:00	38.28	28.84	25.98	0.546	12.17	0.579	13.226
5/2/2014 8:10:00	44.93	29.18	26.16	0.651	12.21	0.659	13.277
5/2/2014 8:15:00	50.15	29.46	26.33	0.670	12.26	0.667	13.328
5/2/2014 8:20:00	50.15	29.76	26.50	0.846	12.31	0.833	13.38
5/2/2014 8:25:00	50.15	30.08	26.64	0.937	12.36	0.941	13.431
5/2/2014 8:30:00	52.33	30.40	27.09	0.997	12.40	1.017	13.482
5/2/2014 8:35:00	67.60	30.71	27.59	1.096	12.45	1.066	13.533
5/2/2014 8:40:00	75.23	30.84	28.19	1.256	12.50	1.221	13.585
5/2/2014 8:45:00	91.59	31.24	28.37	1.322	12.55	1.265	13.636
5/2/2014 8:50:00	107.47	32.06	29.07	1.519	12.59	1.402	13.687
5/2/2014 8:55:00	126.48	32.57	29.55	1.755	12.64	1.599	13.738
5/2/2014 9:00:00	148.07	33.53	30.12	1.816	12.69	1.635	13.789
5/2/2014 9:05:00	93.47	34.13	29.88	0.939	12.73	0.914	13.841
5/2/2014 9:10:00	104.49	33.78	29.14	1.317	12.78	1.268	13.892
5/2/2014 9:15:00	142.10	33.01	28.56	1.928	12.83	1.784	13.943
5/2/2014 9:20:00	193.30	32.17	27.44	2.561	12.87	2.299	13.994
5/2/2014 9:25:00	246.41	33.64	28.21	3.055	12.92	2.797	14.046
5/2/2014 9:30:00	196.86	35.09	28.84	2.710	12.97	2.388	14.097
5/2/2014 9:35:00	172.12	35.19	29.05	2.612	13.02	2.289	14.148
5/2/2014 9:40:00	167.91	34.62	28.77	2.807	13.06	2.476	14.199
5/2/2014 9:45:00	203.40	35.10	29.18	3.282	13.11	2.864	14.25
5/2/2014 9:50:00	213.16	35.99	29.97	3.274	13.16	2.909	14.302
5/2/2014 9:55:00	198.23	37.38	30.60	2.759	13.20	2.439	14.353
5/2/2014 10:00:00	153.60	35.69	28.50	2.616	13.25	2.284	14.404
5/2/2014 10:05:00	170.32	35.18	29.82	2.811	13.30	2.473	14.455
5/2/2014 10:10:00	165.73	34.71	28.97	2.778	13.35	2.479	14.507
5/2/2014 10:15:00	168.70	34.72	29.23	2.868	13.39	2.516	14.558
5/2/2014 10:20:00	153.25	34.60	29.33	2.703	13.44	2.373	14.609
5/2/2014 10:25:00	165.51	34.27	28.84	2.769	13.49	2.413	14.66
5/2/2014 10:30:00	175.54	34.28	29.58	2.948	13.53	2.609	14.711
5/2/2014 10:35:00	183.17	34.86	29.08	3.158	13.58	2.774	14.763
5/2/2014 10:40:00	207.93	35.25	29.51	3.469	13.63	3.032	14.814
5/2/2014 10:45:00	298.84	36.42	31.25	4.259	13.68	3.619	14.865
5/2/2014 10:50:00	326.00	37.72	31.52	4.290	13.72	3.782	14.916
5/2/2014 10:55:00	423.04	42.08	34.20	5.660	13.77	5.171	14.967
5/2/2014 11:00:00	252.78	44.01	33.29	3.783	13.82	3.623	15.019
5/2/2014 11:05:00	225.69	43.56	32.27	3.460	13.86	3.238	15.07
5/2/2014 11:10:00	258.40	43.02	32.49	3.865	13.91	3.581	15.121
5/2/2014 11:15:00	260.32	43.94	32.38	3.864	13.96	3.583	15.172

5/2/2014 11:20:00	369.32	44.68	33.54	5.039	14.01	4.535	15.224
5/2/2014 11:25:00	307.89	43.52	32.57	4.500	14.05	4.113	15.275
5/2/2014 11:30:00	283.48	43.77	32.48	4.297	14.10	3.925	15.326
5/2/2014 11:35:00	251.91	43.71	32.94	4.015	14.15	3.649	15.377
5/2/2014 11:40:00	303.21	43.70	33.61	4.463	14.19	4.092	15.428
5/2/2014 11:45:00	438.31	43.93	33.63	5.704	14.24	5.181	15.48
5/2/2014 11:50:00	317.23	43.60	33.37	4.457	14.29	4.064	15.531
5/2/2014 11:55:00	416.28	43.06	33.28	5.671	14.34	5.288	15.582
5/2/2014 12:00:00	436.12	45.83	35.65	5.454	14.38	5.228	15.633
5/2/2014 12:05:00	512.45	44.87	34.15	6.005	14.43	5.583	15.685
5/2/2014 12:10:00	662.46	46.18	35.15	7.438	14.48	7.273	15.736
5/2/2014 12:15:00	586.53	46.09	35.18	7.037	14.52	6.862	15.787
5/2/2014 12:20:00	659.93	48.84	36.30	7.501	14.57	7.322	15.838
5/2/2014 12:25:00	628.02	49.36	35.89	7.209	14.62	7.062	15.889
5/2/2014 12:30:00	596.28	48.78	35.17	7.000	14.67	6.836	15.941
5/2/2014 12:35:00	588.27	47.77	35.56	6.828	14.71	6.657	15.992
5/2/2014 12:40:00	660.37	46.89	34.99	7.489	14.76	7.337	16.043
5/2/2014 12:45:00	672.52	50.00	36.95	7.338	14.81	7.195	16.094
5/2/2014 12:50:00	628.12	52.24	37.73	7.115	14.85	6.957	16.146
5/2/2014 12:55:00	597.67	52.46	36.87	6.648	14.90	6.435	16.197
5/2/2014 13:00:00	588.27	48.20	34.45	6.508	14.95	6.322	16.248
5/2/2014 13:05:00	393.71	45.06	33.61	5.083	15.00	4.901	16.299
5/2/2014 13:10:00	444.37	43.55	34.00	5.403	15.04	5.126	16.35
5/2/2014 13:15:00	585.89	43.40	34.12	6.740	15.09	6.540	16.402
5/2/2014 13:20:00	621.70	45.45	35.23	6.563	15.14	6.384	16.453
5/2/2014 13:25:00	653.33	45.32	35.36	6.906	15.18	6.705	16.504
5/2/2014 13:30:00	696.46	47.28	36.35	7.052	15.14	6.861	16.453
5/2/2014 13:35:00	719.71	47.40	35.03	7.119	15.09	6.963	16.402
5/2/2014 13:40:00	689.02	48.24	35.81	6.617	15.04	6.491	16.35
5/2/2014 13:45:00	667.27	49.53	37.30	6.122	15.00	6.015	16.299
5/2/2014 13:50:00	653.05	51.52	37.70	5.863	14.95	5.772	16.248
5/2/2014 13:55:00	552.79	53.55	37.58	5.117	14.90	5.021	16.197
5/2/2014 14:00:00	588.72	54.41	35.54	5.818	14.85	5.691	16.146
5/2/2014 14:05:00	478.75	51.85	36.32	5.077	14.81	4.924	16.094
5/2/2014 14:10:00	388.10	48.93	35.49	4.244	14.76	4.162	16.043
5/2/2014 14:15:00	194.92	42.43	33.25	2.878	14.71	2.784	15.992
5/2/2014 14:20:00	447.21	43.82	35.78	4.900	14.67	4.607	15.941
5/2/2014 14:25:00	527.76	45.99	36.92	5.696	14.62	5.434	15.889
5/2/2014 14:30:00	505.56	46.36	36.61	5.585	14.57	5.366	15.838
5/2/2014 14:35:00	395.54	45.62	35.20	4.997	14.52	4.853	15.787
5/2/2014 14:40:00	199.48	42.74	33.44	3.055	14.48	3.003	15.736
5/2/2014 14:45:00	571.76	42.15	36.24	6.304	14.43	5.944	15.685
5/2/2014 14:50:00	366.75	44.29	37.00	3.697	14.38	3.609	15.633
5/2/2014 14:55:00	227.88	43.27	35.07	3.101	14.34	2.995	15.582
5/2/2014 15:00:00	211.52	42.30	34.50	2.941	14.29	2.779	15.531
5/2/2014 15:05:00	315.26	41.29	35.36	4.422	14.24	4.104	15.48
5/2/2014 15:10:00	358.71	42.77	35.86	3.782	14.19	3.534	15.428
5/2/2014 15:15:00	186.69	41.52	34.37	2.583	14.15	2.485	15.377
5/2/2014 15:20:00	185.09	40.67	34.02	3.180	14.10	3.023	15.326
5/2/2014 15:25:00	422.73	40.87	35.79	4.705	14.05	4.447	15.275
5/2/2014 15:30:00	312.96	42.21	36.16	3.895	14.01	3.709	15.224
5/2/2014 15:35:00	421.95	43.15	37.10	4.933	13.96	4.751	15.172
5/2/2014 15:40:00	420.61	43.09	36.28	4.958	13.91	4.825	15.121
5/2/2014 15:45:00	416.50	45.09	37.82	4.816	13.86	4.575	15.07

5/2/2014 15:50:00	373.65	46.57	37.46	4.413	13.82	4.273	15.019
5/2/2014 15:55:00	349.99	47.62	38.07	3.949	13.77	3.802	14.967
5/2/2014 16:00:00	348.99	47.79	37.21	3.972	13.72	3.825	14.916
5/2/2014 16:05:00	329.76	46.77	37.83	3.817	13.68	3.642	14.865
5/2/2014 16:10:00	324.96	47.29	37.63	3.780	13.63	3.686	14.814
5/2/2014 16:15:00	305.29	47.65	37.64	3.664	13.58	3.548	14.763
5/2/2014 16:20:00	287.73	48.07	36.78	3.406	13.53	3.284	14.711
5/2/2014 16:25:00	269.58	46.19	36.21	3.237	13.49	3.125	14.66
5/2/2014 16:30:00	211.23	44.32	35.90	2.614	13.44	2.497	14.609
5/2/2014 16:35:00	230.06	44.89	37.03	2.865	13.39	2.698	14.558
5/2/2014 16:40:00	212.02	43.40	36.96	2.426	13.35	2.283	14.507
5/2/2014 16:45:00	200.62	44.03	36.27	2.315	13.30	2.244	14.455
5/2/2014 16:50:00	175.54	44.05	35.66	1.969	13.25	1.868	14.404
5/2/2014 16:55:00	143.86	44.42	35.85	1.857	13.20	1.783	14.353
5/2/2014 17:00:00	125.39	44.01	34.91	1.650	13.16	1.639	14.302
5/2/2014 17:05:00	98.22	42.74	34.80	1.252	13.11	1.271	14.25
5/2/2014 17:10:00	77.41	42.94	35.23	1.037	12.91	1.078	14.037
5/2/2014 17:15:00	79.41	42.67	35.02	1.028	12.72	1.085	13.823
5/2/2014 17:20:00	81.77	42.23	34.76	1.096	12.52	1.147	13.609
5/2/2014 17:25:00	85.79	41.79	34.35	1.168	12.32	1.219	13.395
5/2/2014 17:30:00	78.37	41.67	34.42	1.198	12.13	1.234	13.181
5/2/2014 17:35:00	77.41	41.34	34.13	1.139	11.93	1.156	12.967
5/2/2014 17:40:00	75.23	41.05	34.00	1.086	11.73	1.098	12.754
5/2/2014 17:45:00	75.23	40.79	33.83	1.095	11.54	1.120	12.54
5/2/2014 17:50:00	75.23	40.28	33.59	1.028	11.34	1.062	12.326
5/2/2014 17:55:00	75.23	39.89	33.43	0.949	11.14	1.008	12.112
5/2/2014 18:00:00	68.96	39.66	33.03	0.887	10.80	0.952	11.736
5/2/2014 18:05:00	62.69	39.24	33.14	0.812	10.45	0.885	11.359
5/2/2014 18:10:00	53.43	38.86	33.24	0.719	10.10	0.797	10.983
5/2/2014 18:15:00	51.24	38.47	32.79	0.591	9.76	0.657	10.607
5/2/2014 18:20:00	49.01	38.08	32.30	0.539	9.11	0.577	9.905
5/2/2014 18:25:00	50.15	37.72	31.89	0.375	8.47	0.407	9.203
5/2/2014 18:30:00	50.15	37.51	31.97	0.430	7.82	0.482	8.502
5/2/2014 18:35:00	47.29	37.19	32.10	0.358	7.18	0.409	7.8
5/2/2014 18:40:00	42.49	36.83	31.90	0.335	6.53	0.400	7.098
5/2/2014 18:45:00	37.26	36.43	31.67	0.267	5.89	0.330	6.397
5/2/2014 18:50:00	28.66	35.97	30.81	0.213	5.24	0.280	5.695
5/2/2014 18:55:00	25.74	35.55	30.25	0.149	4.59	0.209	4.993
5/2/2014 19:00:00	25.08	35.27	30.05	0.066	0.15	0.101	0.163
5/2/2014 19:05:00	25.08	34.96	29.75	0.006	0.00	0.009	0
5/2/2014 19:10:00	24.40	34.52	29.49	0.000	0.00	0.000	0
5/2/2014 19:15:00	24.40	34.04	29.22	0.000	0.00	0.000	0
5/2/2014 19:20:00	25.08	33.71	29.13	0.000	0.00	0.000	0
5/3/2014 7:15:00	23.99	27.37	24.61	0.000	0.00	0.000	0
5/3/2014 7:20:00	25.08	27.37	24.70	0.000	0.00	0.000	0
5/3/2014 7:25:00	25.08	27.57	24.90	0.051	0.01	0.082	0.016
5/3/2014 7:30:00	25.08	27.66	24.90	0.100	0.07	0.147	0.081
5/3/2014 7:35:00	25.08	27.99	24.99	0.168	0.12	0.234	0.133
5/3/2014 7:40:00	25.08	28.08	25.10	0.228	0.17	0.299	0.184
5/3/2014 7:45:00	25.08	28.10	25.20	0.260	3.91	0.317	4.249
5/3/2014 7:50:00	25.08	28.33	25.58	0.362	5.41	0.426	5.875
5/3/2014 7:55:00	30.09	28.60	25.77	0.382	6.30	0.424	6.85
5/3/2014 8:00:00	26.27	28.76	25.90	0.479	7.13	0.518	7.745
5/3/2014 8:05:00	38.35	28.91	26.15	0.546	7.95	0.562	8.639

5/3/2014 8:10:00	40.12	29.27	26.24	0.614	9.59	0.624	10.428
5/3/2014 8:15:00	46.39	29.60	26.55	0.567	9.67	0.564	10.509
5/3/2014 8:20:00	50.15	29.93	26.99	0.738	9.74	0.730	10.59
5/3/2014 8:25:00	50.15	30.23	27.42	0.875	11.31	0.864	12.298
5/3/2014 8:30:00	50.15	30.56	27.54	0.930	11.46	0.932	12.46
5/3/2014 8:35:00	54.11	30.91	27.97	0.968	11.61	0.955	12.623
5/3/2014 8:40:00	60.71	31.18	28.26	1.015	11.76	1.007	12.785
5/3/2014 8:45:00	92.79	32.48	28.39	1.556	11.91	1.454	12.948
5/3/2014 8:50:00	121.97	34.59	28.53	1.503	12.06	1.378	13.111
5/3/2014 8:55:00	154.05	34.40	29.08	1.837	12.21	1.636	13.273
5/3/2014 9:00:00	134.50	34.40	29.25	1.585	12.36	1.437	13.436
5/3/2014 9:05:00	126.48	34.41	29.43	1.536	12.51	1.405	13.598
5/3/2014 9:10:00	164.39	34.71	30.24	2.010	12.66	1.792	13.761
5/3/2014 9:15:00	165.99	35.22	29.86	2.126	12.51	1.888	13.598
5/3/2014 9:20:00	157.00	35.51	30.30	1.874	12.36	1.671	13.436
5/3/2014 9:25:00	165.99	35.98	30.58	2.077	12.21	1.902	13.273
5/3/2014 9:30:00	212.56	38.17	31.44	2.987	12.06	2.744	13.111
5/3/2014 9:35:00	125.39	38.25	31.53	1.927	12.06	1.792	13.111
5/3/2014 9:40:00	123.21	38.09	31.20	1.782	12.06	1.678	13.111
5/3/2014 9:45:00	146.50	38.39	30.66	2.233	12.06	2.087	13.111
5/3/2014 9:50:00	177.93	39.38	31.66	2.735	12.06	2.485	13.111
5/3/2014 9:55:00	228.08	40.67	31.98	3.170	12.06	2.899	13.111
5/3/2014 10:00:00	326.00	43.53	33.82	3.897	12.06	3.488	13.111
5/3/2014 10:05:00	329.96	46.26	33.47	3.857	12.06	3.451	13.111
5/3/2014 10:10:00	314.12	48.22	34.04	3.670	12.06	3.317	13.111
5/3/2014 10:15:00	359.44	49.35	33.25	3.882	12.06	3.573	13.111
5/3/2014 10:20:00	376.16	51.04	33.69	4.042	12.06	3.712	13.111
5/3/2014 10:25:00	383.00	52.52	35.22	4.094	12.06	3.854	13.111
5/3/2014 10:30:00	424.03	53.84	36.72	4.501	12.06	4.238	13.111
5/3/2014 10:35:00	407.50	54.74	36.46	4.324	12.06	4.165	13.111
5/3/2014 10:40:00	430.87	55.94	34.38	4.549	12.06	4.292	13.111
5/3/2014 10:45:00	388.70	56.97	35.07	4.215	12.06	3.922	13.111
5/3/2014 10:50:00	412.38	57.47	36.18	4.366	12.06	4.162	13.111
5/3/2014 10:55:00	408.76	58.57	37.53	4.495	12.06	4.334	13.111
5/3/2014 11:00:00	406.93	59.22	37.81	4.569	12.06	4.454	13.111
5/3/2014 11:05:00	421.30	59.10	37.57	4.711	12.06	4.563	13.111
5/3/2014 11:10:00	429.89	58.60	36.86	5.019	12.06	4.868	13.111
5/3/2014 11:15:00	430.87	59.57	38.22	5.151	12.06	4.985	13.111
5/3/2014 11:20:00	445.69	55.44	36.90	5.216	12.06	5.111	13.111
5/3/2014 11:25:00	423.53	54.78	37.02	4.925	12.06	4.817	13.111
5/3/2014 11:30:00	499.26	57.71	37.76	5.989	12.06	5.823	13.111
5/3/2014 11:35:00	505.30	58.72	38.42	5.861	12.06	5.763	13.111
5/3/2014 11:40:00	487.21	60.14	37.30	5.549	12.06	5.463	13.111
5/3/2014 11:45:00	349.89	60.06	36.03	4.022	19.15	3.964	20.813
5/3/2014 11:50:00	450.07	59.38	36.77	5.672	19.60	5.454	21.301
5/3/2014 11:55:00	443.47	59.02	38.02	5.266	19.75	5.051	21.463
5/3/2014 12:00:00	256.34	58.21	36.06	3.661	19.52	3.582	21.22
5/3/2014 12:05:00	439.90	57.62	36.54	5.043	19.75	4.833	21.463
5/3/2014 12:10:00	293.01	57.56	37.46	4.514	19.37	4.430	21.057
5/3/2014 12:15:00	191.59	54.36	36.68	2.946	19.52	2.911	21.22
5/3/2014 12:20:00	403.51	54.46	37.64	5.256	20.05	4.998	21.789
5/3/2014 12:25:00	420.04	55.27	37.87	5.025	19.90	4.828	21.626
5/3/2014 12:30:00	242.41	56.29	37.54	3.393	20.34	3.215	22.114
5/3/2014 12:35:00	209.86	54.41	35.48	3.078	19.52	3.045	21.22

5/3/2014 12:40:00	353.59	51.58	35.70	4.784	20.12	4.555	21.87
5/3/2014 12:45:00	426.31	52.35	37.02	5.569	19.75	5.376	21.463
5/3/2014 12:50:00	457.09	53.70	36.66	5.283	19.37	5.131	21.057
5/3/2014 12:55:00	553.79	55.78	39.05	6.439	19.22	6.303	20.894
5/3/2014 13:00:00	416.28	57.22	38.29	5.039	19.60	4.857	21.301
5/3/2014 13:05:00	306.83	55.99	36.64	4.593	19.67	4.409	21.382
5/3/2014 13:10:00	431.09	55.51	37.49	5.279	19.60	5.083	21.301
5/3/2014 13:15:00	347.66	55.40	37.65	4.597	19.52	4.438	21.22
5/3/2014 13:20:00	255.55	54.61	35.57	3.426	19.97	3.266	21.707
5/3/2014 13:25:00	423.53	53.02	35.97	4.414	20.19	4.138	21.951
5/3/2014 13:30:00	261.03	51.94	36.59	3.749	20.27	3.524	22.033
5/3/2014 13:35:00	200.62	51.38	35.29	3.128	20.57	2.905	22.358
5/3/2014 13:40:00	142.10	46.00	32.56	2.216	20.87	2.063	22.683
5/3/2014 13:45:00	139.72	43.22	32.12	2.203	20.57	2.082	22.358
5/3/2014 13:50:00	351.08	42.32	32.76	4.025	21.54	3.538	23.415
5/3/2014 13:55:00	582.75	43.68	34.60	6.856	21.02	6.147	22.846
5/3/2014 14:00:00	452.53	45.22	34.87	5.654	20.27	5.237	22.033
5/3/2014 14:05:00	485.87	45.97	34.63	5.882	20.49	5.413	22.276
5/3/2014 14:10:00	531.64	46.19	34.49	6.594	19.90	6.225	21.626
5/3/2014 14:15:00	580.54	47.62	34.73	6.827	19.67	6.503	21.382
5/3/2014 14:20:00	340.33	47.43	35.34	4.842	19.90	4.564	21.626
5/3/2014 14:25:00	248.49	46.37	33.68	3.846	19.97	3.629	21.707
5/3/2014 14:30:00	360.89	45.69	34.66	4.903	19.67	4.666	21.382
5/3/2014 14:35:00	567.66	45.28	37.17	6.806	19.75	6.401	21.463
5/3/2014 14:40:00	495.97	47.98	36.81	5.775	19.22	5.579	20.894
5/3/2014 14:45:00	224.37	47.47	34.64	3.334	19.67	3.181	21.382
5/3/2014 14:50:00	218.86	45.96	34.62	3.424	20.19	3.179	21.951
5/3/2014 14:55:00	210.02	45.60	35.07	3.314	20.57	3.025	22.358
5/3/2014 15:00:00	302.12	46.76	35.27	4.572	20.42	4.183	22.195
5/3/2014 15:05:00	508.71	47.13	37.57	6.641	20.34	6.047	22.114
5/3/2014 15:10:00	505.13	48.38	37.52	6.451	19.67	6.139	21.382
5/3/2014 15:15:00	469.30	49.13	36.67	5.952	19.67	5.686	21.382
5/3/2014 15:20:00	256.15	50.22	36.09	3.743	19.37	3.677	21.057
5/3/2014 15:25:00	236.44	48.89	34.24	3.586	19.60	3.470	21.301
5/3/2014 15:30:00	255.55	46.92	33.53	3.762	19.37	3.676	21.057
5/3/2014 15:35:00	243.61	45.44	33.06	3.616	20.27	3.384	22.033
5/3/2014 15:40:00	248.49	43.85	33.11	3.729	20.34	3.474	22.114
5/3/2014 15:45:00	258.69	44.17	33.21	3.985	20.64	3.649	22.439
5/3/2014 15:50:00	241.37	44.57	33.40	3.640	20.79	3.332	22.602
5/3/2014 15:55:00	322.42	44.30	35.38	4.355	20.05	4.111	21.789
5/3/2014 16:00:00	314.06	44.92	35.37	4.301	20.19	4.022	21.951
5/3/2014 16:05:00	315.26	45.16	35.03	4.179	20.27	3.888	22.033
5/3/2014 16:10:00	305.70	45.68	35.20	4.019	20.19	3.774	21.951
5/3/2014 16:15:00	318.48	43.90	35.12	3.977	19.97	3.762	21.707
5/3/2014 16:20:00	296.15	42.91	35.27	3.709	19.75	3.562	21.463
5/3/2014 16:25:00	309.29	41.64	34.68	3.802	20.19	3.561	21.951
5/3/2014 16:30:00	293.76	39.92	34.62	3.607	20.34	3.366	22.114
5/3/2014 16:35:00	297.34	40.51	35.52	3.691	20.64	3.401	22.439
5/3/2014 16:40:00	278.24	41.02	35.46	3.377	20.49	3.144	22.276
5/3/2014 16:45:00	240.74	42.46	35.83	2.900	20.19	2.754	21.951
5/3/2014 16:50:00	207.78	41.19	34.73	2.609	20.05	2.516	21.789
5/3/2014 16:55:00	198.95	39.63	33.62	2.460	20.87	2.284	22.683
5/3/2014 17:00:00	165.51	38.77	33.99	2.235	20.57	2.127	22.358
5/3/2014 17:05:00	142.54	39.38	34.63	1.870	20.05	1.842	21.789

5/3/2014 17:10:00	161.86	38.69	33.34	2.051	20.87	1.934	22.683
5/3/2014 17:15:00	113.51	37.74	32.19	1.573	20.79	1.513	22.602
5/3/2014 17:20:00	126.53	37.51	32.45	1.851	21.47	1.716	23.333
5/3/2014 17:25:00	124.25	37.37	32.57	2.042	20.72	1.943	22.52
5/3/2014 17:30:00	112.85	37.13	32.66	1.981	21.24	1.825	23.089
5/3/2014 17:35:00	102.82	36.90	32.10	1.435	21.24	1.351	23.089
5/3/2014 17:40:00	57.79	36.76	31.67	0.739	21.17	0.748	23.008
5/3/2014 17:45:00	50.15	36.59	31.21	0.478	21.24	0.510	23.089
5/3/2014 17:50:00	48.90	36.05	31.19	0.415	20.27	0.473	22.033
5/3/2014 17:55:00	42.18	35.45	30.40	0.332	19.90	0.399	21.626
5/3/2014 18:00:00	26.27	35.23	30.25	0.175	19.75	0.233	21.463
5/3/2014 18:05:00	25.08	34.97	30.16	0.035	19.22	0.056	20.894
5/3/2014 18:10:00	25.08	35.17	29.84	0.001	19.45	0.001	21.138
5/3/2014 18:15:00	25.08	34.94	29.18	0.000	11.52	0.000	12.52
5/3/2014 18:35:00	25.08	30.12	24.41	0.000	18.10	0.000	19.675
5/3/2014 18:40:00	25.08	29.16	24.47	0.000	20.12	0.000	21.87
5/3/2014 18:45:00	24.34	29.01	24.90	0.000	21.02	0.000	22.846
5/3/2014 18:50:00	25.08	28.80	25.77	0.000	21.69	0.000	23.577
5/3/2014 18:55:00	25.08	28.80	26.04	0.000	22.07	0.000	23.984
5/3/2014 19:00:00	24.32	28.80	25.92	0.000	21.17	0.000	23.008
5/3/2014 19:05:00	25.08	28.75	25.40	0.000	20.27	0.000	22.033
5/3/2014 19:10:00	25.08	28.72	25.88	0.000	19.22	0.000	20.894
5/3/2014 19:15:00	22.65	28.65	26.02	0.000	17.05	0.000	18.537
5/3/2014 19:20:00	25.08	28.62	25.92	0.000	12.64	0.000	13.74
5/4/2014 7:15:00	25.08	27.60	24.20	0.000	17.88	0.000	19.431
5/4/2014 7:20:00	25.08	27.49	24.20	0.000	19.75	0.000	21.463
5/4/2014 7:25:00	25.08	27.60	24.40	0.002	21.32	0.005	23.171
5/4/2014 7:30:00	25.08	27.79	24.61	0.067	19.30	0.104	20.976
5/4/2014 7:35:00	25.08	27.83	24.61	0.106	19.90	0.150	21.626
5/4/2014 7:40:00	25.08	27.93	24.68	0.163	19.37	0.225	21.057
5/4/2014 7:45:00	26.17	27.93	24.65	0.219	19.75	0.283	21.463
5/4/2014 7:50:00	25.08	27.86	24.72	0.272	20.05	0.334	21.789
5/4/2014 7:55:00	26.47	27.94	24.85	0.346	20.05	0.409	21.789
5/4/2014 8:15:00	50.15	28.80	25.70	0.377	24.68	0.368	26.829
5/4/2014 8:20:00	49.54	28.95	25.91	0.809	21.69	0.785	23.577
5/4/2014 8:25:00	50.15	29.31	26.12	0.940	21.39	0.908	23.252
5/4/2014 8:30:00	54.44	29.66	26.22	1.130	21.09	1.088	22.927
5/4/2014 8:35:00	73.35	30.11	26.50	1.394	21.99	1.267	23.902
5/4/2014 8:40:00	75.23	30.60	26.53	1.314	22.36	1.183	24.309
5/4/2014 8:45:00	82.30	30.66	26.80	1.316	21.84	1.211	23.74
5/4/2014 8:50:00	96.64	30.86	26.98	1.345	21.77	1.236	23.659
5/4/2014 8:55:00	102.88	31.54	27.26	1.464	21.54	1.351	23.415
5/4/2014 9:00:00	106.58	32.13	27.35	1.501	20.79	1.427	22.602
5/4/2014 9:05:00	127.96	32.51	27.51	1.801	21.54	1.639	23.415
5/4/2014 9:10:00	133.34	32.88	27.82	1.854	21.69	1.673	23.577
5/4/2014 9:15:00	149.82	33.18	28.15	2.073	21.54	1.865	23.415
5/4/2014 9:20:00	151.09	33.32	28.23	2.010	21.92	1.786	23.821
5/4/2014 9:25:00	172.48	33.99	28.43	2.193	22.21	1.912	24.146
5/4/2014 9:30:00	194.83	34.64	28.79	2.508	22.14	2.182	24.065
5/4/2014 9:35:00	212.53	36.34	30.41	2.833	22.36	2.424	24.309
5/4/2014 9:40:00	198.78	37.40	30.14	2.961	21.92	2.584	23.821
5/4/2014 9:45:00	214.12	38.52	30.61	3.175	21.92	2.766	23.821
5/4/2014 9:50:00	229.98	39.75	31.21	3.342	21.69	2.929	23.577
5/4/2014 9:55:00	250.14	40.26	32.07	3.426	21.77	2.992	23.659

5/4/2014 10:00:00	273.97	41.64	32.60	3.612	21.62	3.173	23.496
5/4/2014 10:05:00	297.16	43.71	33.20	3.760	21.32	3.343	23.171
5/4/2014 10:10:00	324.75	44.88	33.63	3.942	21.24	3.514	23.089
5/4/2014 10:15:00	317.85	47.06	33.00	3.935	20.94	3.549	22.764
5/4/2014 10:20:00	333.53	48.30	32.96	4.061	20.57	3.727	22.358
5/4/2014 10:25:00	354.84	49.65	33.84	4.164	20.57	3.814	22.358
5/4/2014 10:30:00	367.16	51.32	34.47	4.284	20.49	3.935	22.276
5/4/2014 10:35:00	378.73	49.25	34.17	4.336	20.12	4.055	21.87
5/4/2014 10:40:00	369.26	50.15	33.67	4.342	20.05	4.086	21.789
5/4/2014 10:45:00	383.68	51.54	34.45	4.757	20.19	4.425	21.951
5/4/2014 10:50:00	410.64	52.92	35.78	5.160	20.19	4.795	21.951
5/4/2014 10:55:00	368.63	53.21	34.26	4.640	20.72	4.203	22.52
5/4/2014 11:00:00	421.92	53.47	36.58	5.090	19.82	4.827	21.545
5/4/2014 11:05:00	452.67	52.74	35.79	5.510	19.97	5.169	21.707
5/4/2014 11:10:00	385.94	52.19	35.61	4.614	19.37	4.469	21.057
5/4/2014 11:15:00	144.19	54.31	33.11	2.122	19.52	2.098	21.22
5/4/2014 11:20:00	268.13	52.89	33.44	3.481	19.37	3.398	21.057
5/4/2014 11:25:00	436.97	53.45	35.57	5.242	19.60	5.022	21.301
5/4/2014 11:30:00	446.37	53.51	35.77	5.128	19.97	4.823	21.707
5/4/2014 11:35:00	458.91	55.14	35.53	5.231	19.30	5.089	20.976
5/4/2014 11:40:00	488.38	57.31	36.38	5.500	19.37	5.327	21.057
5/4/2014 11:45:00	152.91	56.88	33.18	2.241	19.07	2.252	20.732
5/4/2014 11:50:00	130.40	52.85	32.08	1.947	19.22	1.963	20.894
5/4/2014 11:55:00	130.40	50.46	32.19	2.009	19.60	1.978	21.301
5/4/2014 12:00:00	465.81	49.86	34.57	5.442	19.90	5.128	21.626
5/4/2014 12:05:00	551.70	52.84	36.14	6.069	19.75	5.751	21.463
5/4/2014 12:10:00	554.14	55.33	36.34	6.101	19.15	5.963	20.813
5/4/2014 12:15:00	545.27	57.10	36.46	6.199	19.15	6.066	20.813
5/4/2014 12:20:00	422.03	59.17	36.23	4.880	19.97	4.593	21.707
5/4/2014 12:25:00	371.77	57.91	35.82	4.437	20.05	4.166	21.789
5/4/2014 12:30:00	394.80	55.47	35.15	4.892	19.37	4.750	21.057
5/4/2014 12:35:00	391.20	56.04	34.88	4.810	19.45	4.635	21.138
5/4/2014 12:40:00	489.97	56.86	35.68	5.544	19.45	5.336	21.138
5/4/2014 12:45:00	309.28	57.06	35.54	3.916	19.37	3.816	21.057
5/4/2014 12:50:00	532.13	56.52	36.58	6.039	19.15	5.902	20.813
5/4/2014 12:55:00	427.60	56.48	36.76	4.770	19.15	4.679	20.813
5/4/2014 13:00:00	166.98	55.74	34.17	2.470	19.97	2.364	21.707
5/4/2014 13:05:00	433.83	52.41	34.28	5.179	20.27	4.798	22.033
5/4/2014 13:10:00	383.87	53.11	36.08	4.400	20.05	4.124	21.789
5/4/2014 13:15:00	601.22	52.99	36.60	6.331	19.60	6.060	21.301
5/4/2014 13:20:00	276.48	54.87	35.43	3.577	19.15	3.524	20.813
5/4/2014 13:25:00	236.98	53.09	34.80	3.025	19.60	2.933	21.301
5/4/2014 13:30:00	185.19	52.68	34.23	2.702	20.12	2.561	21.87
5/4/2014 13:35:00	181.18	53.26	34.13	2.693	20.27	2.533	22.033
5/4/2014 13:40:00	182.44	52.26	34.65	2.480	20.42	2.327	22.195
5/4/2014 13:45:00	129.15	51.20	34.33	2.004	20.05	1.936	21.789
5/4/2014 13:50:00	432.58	50.90	35.36	5.010	20.34	4.625	22.114
5/4/2014 13:55:00	311.58	51.67	36.78	3.701	19.82	3.524	21.545
5/4/2014 14:00:00	422.55	52.22	36.38	4.789	21.02	4.285	22.846
5/4/2014 14:05:00	525.37	53.49	37.58	5.379	19.90	5.069	21.626
5/4/2014 14:10:00	196.23	53.51	35.59	2.737	19.22	2.715	20.894
5/4/2014 14:15:00	497.15	53.13	37.18	5.598	19.75	5.312	21.463
5/4/2014 14:20:00	357.98	54.52	37.32	4.139	19.30	4.031	20.976
5/4/2014 14:25:00	186.47	54.68	36.41	2.714	19.45	2.654	21.138

5/4/2014 14:30:00	228.20	53.16	35.58	3.166	19.97	3.012	21.707
5/4/2014 14:35:00	376.16	51.37	36.16	4.321	20.94	4.098	22.764
5/4/2014 14:40:00	487.48	51.45	37.01	4.488	22.36	3.976	24.309
5/4/2014 14:45:00	287.13	51.73	36.40	3.358	19.75	3.210	21.463
5/4/2014 14:50:00	323.43	50.45	35.52	4.023	19.30	3.928	20.976
5/4/2014 14:55:00	262.39	50.77	36.40	2.999	19.37	2.948	21.057
5/4/2014 15:00:00	99.05	50.07	34.24	1.380	19.37	1.412	21.057
5/4/2014 15:05:00	286.51	47.83	35.02	3.642	19.82	3.458	21.545
5/4/2014 15:10:00	220.05	47.69	35.56	2.950	19.67	2.850	21.382
5/4/2014 15:15:00	297.79	47.99	35.92	3.853	20.19	3.608	21.951
5/4/2014 15:20:00	260.18	48.49	36.78	3.236	19.45	3.148	21.138
5/4/2014 15:25:00	131.66	48.88	35.26	1.941	19.90	1.890	21.626
5/4/2014 15:30:00	327.84	48.61	36.59	2.414	24.31	2.055	26.423
5/4/2014 15:35:00	401.23	46.95	36.80	4.860	20.64	4.436	22.439
5/4/2014 15:40:00	384.72	46.39	36.89	4.609	19.60	4.421	21.301
5/4/2014 15:45:00	152.34	46.89	35.22	2.044	19.67	2.008	21.382
5/4/2014 15:50:00	305.31	46.44	35.35	3.984	19.97	3.751	21.707
5/4/2014 15:55:00	362.36	45.88	36.28	4.493	20.27	4.168	22.033
5/4/2014 16:00:00	241.99	45.80	35.56	2.816	19.45	2.755	21.138
5/4/2014 16:05:00	146.07	45.91	34.70	1.976	19.07	1.999	20.732
5/4/2014 16:10:00	99.70	45.46	33.98	1.486	19.22	1.520	20.894
5/4/2014 16:40:00	75.23	42.50	33.77	0.320	24.91	0.303	27.073
5/4/2014 16:45:00	133.54	42.33	33.88	1.725	19.97	1.700	21.707
5/4/2014 16:50:00	244.50	42.39	35.48	2.922	20.79	2.677	22.602
5/4/2014 16:55:00	224.41	42.71	36.02	2.631	20.64	2.445	22.439
5/4/2014 17:00:00	174.93	43.04	36.83	2.173	20.87	2.015	22.683
5/4/2014 17:05:00	176.79	43.10	35.96	2.202	20.27	2.100	22.033
5/4/2014 17:10:00	159.87	42.66	35.10	2.071	20.64	1.952	22.439
5/4/2014 17:15:00	163.97	42.80	35.24	2.096	20.42	1.991	22.195
5/4/2014 17:20:00	97.80	40.74	34.44	1.285	20.49	1.255	22.276
5/4/2014 17:25:00	93.88	40.46	34.11	1.238	20.87	1.197	22.683
5/4/2014 17:30:00	90.28	39.16	33.19	1.189	20.42	1.178	22.195
5/4/2014 17:35:00	87.14	38.91	33.81	1.260	19.82	1.272	21.545
5/4/2014 17:40:00	99.05	39.51	34.53	1.401	20.79	1.342	22.602
5/4/2014 17:45:00	96.55	39.08	34.57	1.378	21.92	1.258	23.821
5/4/2014 17:50:00	84.01	38.70	34.60	1.323	21.62	1.227	23.496
5/4/2014 17:55:00	83.59	38.58	34.37	1.271	21.24	1.202	23.089
5/4/2014 18:00:00	75.84	38.20	34.44	1.195	21.17	1.140	23.008
5/4/2014 18:05:00	75.23	37.97	34.00	1.042	20.42	1.044	22.195
5/4/2014 18:10:00	74.01	37.90	33.55	0.934	20.42	0.945	22.195
5/4/2014 18:15:00	70.73	37.65	33.02	0.876	19.75	0.922	21.463
5/4/2014 18:20:00	59.94	37.82	33.09	0.786	19.37	0.851	21.057
5/4/2014 18:25:00	58.51	37.79	32.52	0.716	19.37	0.784	21.057
5/4/2014 18:30:00	53.92	37.56	32.48	0.610	20.34	0.656	22.114
5/4/2014 18:35:00	50.15	37.23	32.31	0.531	20.72	0.568	22.52
5/4/2014 18:40:00	50.15	36.91	32.16	0.448	20.72	0.492	22.52
5/4/2014 18:45:00	50.15	36.65	32.06	0.403	20.27	0.457	22.033
5/4/2014 18:50:00	49.51	36.46	31.95	0.313	20.34	0.369	22.114
5/4/2014 18:55:00	37.62	36.14	31.61	0.237	19.90	0.296	21.626
5/4/2014 19:00:00	28.14	35.76	31.29	0.171	19.75	0.227	21.463
5/4/2014 19:05:00	25.08	35.41	31.05	0.107	19.15	0.155	20.813
5/4/2014 19:10:00	25.08	35.01	30.64	0.024	19.22	0.038	20.894
5/4/2014 19:15:00	25.08	34.56	30.16	0.000	19.37	0.000	21.057
5/4/2014 19:20:00	21.32	34.13	29.71	0.000	14.73	0.000	16.016

5/4/2014 19:25:00	25.08	33.84	29.50	0.000	8.98	0.000	9.756
5/5/2014 7:20:00	25.08	27.51	24.34	0.000	21.24	0.000	23.089
5/5/2014 7:25:00	25.08	27.42	24.41	0.022	20.34	0.037	22.114
5/5/2014 7:30:00	25.08	27.44	24.56	0.071	19.30	0.110	20.976
5/5/2014 7:35:00	25.08	27.44	24.65	0.120	19.45	0.172	21.138
5/5/2014 7:40:00	25.08	27.56	24.73	0.184	19.37	0.248	21.057
5/5/2014 7:45:00	25.08	27.70	24.91	0.246	19.82	0.306	21.545
5/5/2014 7:50:00	25.70	27.81	24.94	0.317	19.90	0.377	21.626
5/5/2014 7:55:00	25.70	27.83	25.13	0.352	20.49	0.404	22.276
5/5/2014 8:00:00	29.97	28.09	25.39	0.406	20.64	0.456	22.439
5/5/2014 8:05:00	31.51	28.34	25.48	0.440	21.02	0.482	22.846
5/5/2014 8:10:00	32.42	28.62	25.59	0.496	21.09	0.530	22.927
5/5/2014 8:15:00	33.85	28.83	25.81	0.513	21.47	0.537	23.333
5/5/2014 8:20:00	41.80	29.01	26.08	0.600	21.54	0.610	23.415
5/5/2014 8:25:00	49.53	29.20	26.10	0.665	21.84	0.660	23.74
5/5/2014 8:30:00	48.90	29.49	26.17	0.724	21.99	0.705	23.902
5/5/2014 8:35:00	50.15	29.76	26.47	0.816	22.07	0.780	23.984
5/5/2014 8:40:00	58.93	30.43	26.62	1.133	22.59	1.023	24.553
5/5/2014 8:45:00	102.82	32.29	26.97	1.704	23.04	1.462	25.041
5/5/2014 8:50:00	172.41	35.31	27.53	1.730	23.19	1.473	25.203
5/5/2014 8:55:00	200.62	37.49	28.12	1.299	23.04	1.138	25.041
5/5/2014 9:00:00	182.44	38.08	28.09	1.140	22.14	1.048	24.065
5/5/2014 9:05:00	132.28	36.46	27.92	1.168	22.29	1.062	24.228
5/5/2014 9:10:00	115.98	35.37	28.44	1.337	21.99	1.216	23.902
5/5/2014 9:15:00	125.39	35.51	29.04	1.735	22.51	1.514	24.472
5/5/2014 9:20:00	159.24	36.73	29.33	2.859	21.69	2.516	23.577
5/5/2014 9:25:00	202.50	39.41	29.88	2.333	22.36	2.011	24.309
5/5/2014 9:30:00	196.86	39.24	30.88	2.599	21.77	2.284	23.659
5/5/2014 9:35:00	226.95	40.65	32.40	3.208	21.84	2.803	23.74
5/5/2014 9:40:00	230.08	42.64	33.54	3.216	21.99	2.795	23.902
5/5/2014 9:45:00	164.26	41.68	31.78	2.314	21.39	2.097	23.252
5/5/2014 9:50:00	288.69	43.27	33.97	3.600	21.92	3.136	23.821
5/5/2014 9:55:00	300.30	45.29	34.37	3.508	21.32	3.145	23.171
5/5/2014 10:00:00	324.12	47.35	35.24	3.676	20.42	3.415	22.195
5/5/2014 10:05:00	335.41	49.26	34.92	3.902	21.17	3.495	23.008
5/5/2014 10:10:00	342.93	50.71	35.72	3.885	20.79	3.535	22.602
5/5/2014 10:15:00	347.12	50.39	35.32	4.080	20.42	3.783	22.195
5/5/2014 10:20:00	383.05	50.94	35.66	4.334	20.05	4.083	21.789
5/5/2014 10:25:00	351.08	52.69	35.40	4.137	19.97	3.902	21.707
5/5/2014 10:30:00	435.72	54.21	35.63	5.006	19.90	4.711	21.626
5/5/2014 10:35:00	344.01	55.51	34.90	4.504	20.12	4.207	21.87
5/5/2014 10:40:00	246.38	54.08	34.23	3.068	21.17	2.754	23.008
5/5/2014 10:45:00	114.10	52.23	32.35	1.531	20.87	1.444	22.683
5/5/2014 10:50:00	83.79	49.37	31.40	1.169	19.97	1.175	21.707
5/5/2014 10:55:00	99.68	47.29	31.63	1.465	20.05	1.448	21.789
5/5/2014 11:00:00	233.84	45.88	32.99	2.895	19.45	2.847	21.138
5/5/2014 11:05:00	425.67	47.19	34.97	4.874	20.27	4.522	22.033
5/5/2014 11:10:00	429.37	48.54	35.91	4.925	19.97	4.645	21.707
5/5/2014 11:15:00	426.94	51.01	36.90	4.947	19.97	4.661	21.707
5/5/2014 11:20:00	421.30	51.81	35.08	5.135	19.52	4.937	21.22
5/5/2014 11:25:00	455.78	51.44	35.56	5.310	19.52	5.094	21.22
5/5/2014 11:30:00	432.74	52.24	35.85	4.990	19.67	4.771	21.382
5/5/2014 11:35:00	452.64	52.43	36.08	5.245	19.60	5.019	21.301
5/5/2014 11:40:00	388.70	53.91	36.20	4.726	19.37	4.591	21.057

5/5/2014 11:45:00	320.22	53.85	35.09	4.125	19.97	3.887	21.707
5/5/2014 11:50:00	462.67	53.73	35.87	5.513	19.52	5.290	21.22
5/5/2014 11:55:00	447.00	53.49	35.32	5.230	19.22	5.108	20.894
5/5/2014 12:00:00	476.47	52.43	36.44	5.673	19.52	5.446	21.22
5/5/2014 12:05:00	399.98	53.52	35.96	4.822	19.52	4.633	21.22
5/5/2014 12:10:00	228.20	52.25	34.60	3.244	19.52	3.156	21.22
5/5/2014 12:15:00	395.59	48.30	34.72	4.948	19.60	4.740	21.301
5/5/2014 12:20:00	377.41	47.84	35.33	4.413	19.67	4.231	21.382
5/5/2014 12:25:00	274.59	47.83	34.42	3.719	19.60	3.602	21.301
5/5/2014 12:30:00	260.18	46.76	34.98	3.401	19.82	3.267	21.545
5/5/2014 12:35:00	363.94	44.06	34.59	4.693	19.90	4.448	21.626
5/5/2014 12:40:00	418.79	45.97	36.00	5.213	19.97	4.903	21.707
5/5/2014 12:45:00	438.53	48.73	36.94	5.329	19.97	5.007	21.707
5/5/2014 12:50:00	410.01	49.83	35.85	4.941	20.19	4.613	21.951
5/5/2014 12:55:00	414.74	49.63	35.03	5.094	20.57	4.664	22.358
5/5/2014 13:00:00	452.00	49.33	35.63	5.458	20.19	5.085	21.951
5/5/2014 13:05:00	327.32	49.12	35.85	4.237	19.37	4.119	21.057
5/5/2014 13:10:00	350.47	48.81	35.67	4.709	19.90	4.441	21.626
5/5/2014 13:15:00	391.83	46.26	35.83	4.884	20.12	4.586	21.87
5/5/2014 13:20:00	392.46	48.46	35.56	5.052	19.82	4.801	21.545
5/5/2014 13:25:00	352.33	49.55	35.88	4.599	19.52	4.423	21.22
5/5/2014 13:30:00	332.43	50.17	35.58	4.408	19.75	4.210	21.463
5/5/2014 13:35:00	176.79	50.30	35.49	2.726	19.97	2.611	21.707
5/5/2014 13:40:00	232.59	49.43	35.63	3.393	20.05	3.200	21.789
5/5/2014 13:45:00	212.83	48.52	36.27	2.998	20.49	2.783	22.276
5/5/2014 13:50:00	179.21	44.76	34.89	2.901	20.19	2.737	21.951
5/5/2014 13:55:00	206.40	45.32	34.91	3.343	20.72	3.068	22.52
5/5/2014 14:00:00	307.65	46.31	35.08	4.317	20.64	3.936	22.439
5/5/2014 14:05:00	329.22	46.13	35.54	4.303	19.67	4.104	21.382
5/5/2014 14:10:00	304.69	46.65	35.56	4.159	19.82	3.944	21.545
5/5/2014 14:15:00	238.86	46.55	35.18	3.627	20.57	3.321	22.358
5/5/2014 14:20:00	219.91	46.81	35.26	3.521	20.49	3.247	22.276
5/5/2014 14:25:00	325.38	47.52	35.17	4.723	20.12	4.404	21.87
5/5/2014 14:30:00	358.80	48.51	36.26	5.019	20.19	4.654	21.951
5/5/2014 14:35:00	337.58	48.50	35.96	4.739	19.90	4.478	21.626
5/5/2014 14:40:00	220.80	47.83	35.85	3.181	19.67	3.067	21.382
5/5/2014 14:45:00	178.76	44.06	34.19	2.875	19.97	2.734	21.707
5/5/2014 14:50:00	285.25	41.97	34.47	4.293	20.57	3.931	22.358
5/5/2014 14:55:00	309.50	42.57	35.24	4.448	20.27	4.136	22.033
5/5/2014 15:00:00	317.85	42.71	35.44	4.284	20.64	3.900	22.439
5/5/2014 15:05:00	208.98	41.81	34.19	2.999	20.34	2.802	22.114
5/5/2014 15:10:00	187.77	40.11	33.80	2.875	21.09	2.593	22.927
5/5/2014 15:15:00	191.21	41.02	34.39	2.958	20.64	2.730	22.439
5/5/2014 15:20:00	199.36	42.14	35.05	3.180	20.87	2.895	22.683
5/5/2014 15:25:00	236.35	42.39	35.06	3.587	20.94	3.248	22.764
5/5/2014 15:30:00	226.32	42.73	35.01	3.513	21.24	3.132	23.089
5/5/2014 15:35:00	282.28	42.73	35.37	4.183	21.17	3.716	23.008
5/5/2014 15:40:00	274.01	42.10	35.18	4.117	20.64	3.759	22.439
5/5/2014 15:45:00	275.85	43.33	35.47	4.084	20.72	3.728	22.52
5/5/2014 15:50:00	274.59	43.29	35.41	4.103	20.34	3.810	22.114
5/5/2014 15:55:00	271.46	41.76	34.58	4.137	20.64	3.791	22.439
5/5/2014 16:00:00	260.18	42.40	35.58	3.902	20.72	3.567	22.52
5/5/2014 16:05:00	218.97	42.07	34.93	3.401	20.64	3.128	22.439
5/5/2014 16:10:00	211.28	40.60	34.33	3.356	20.87	3.060	22.683

5/5/2014 16:15:00	230.20	40.47	34.35	3.561	20.94	3.227	22.764
5/5/2014 16:20:00	211.02	41.45	34.57	3.233	20.34	3.020	22.114
5/5/2014 16:25:00	218.17	39.96	33.85	3.339	20.94	3.035	22.764
5/5/2014 16:30:00	210.91	39.15	33.71	3.278	20.94	2.977	22.764
5/5/2014 16:35:00	200.62	38.82	33.47	3.113	21.17	2.802	23.008
5/5/2014 16:40:00	192.47	39.64	34.59	2.933	21.24	2.645	23.089
5/5/2014 16:45:00	176.17	40.91	34.83	2.787	20.87	2.563	22.683
5/5/2014 16:50:00	174.91	41.10	34.10	2.646	21.02	2.428	22.846
5/5/2014 16:55:00	173.03	42.14	34.49	2.517	20.57	2.364	22.358
5/5/2014 17:00:00	167.39	42.39	34.13	2.498	20.72	2.329	22.52
5/5/2014 17:05:00	159.87	42.47	34.37	2.441	21.09	2.238	22.927
5/5/2014 17:10:00	151.09	42.62	34.65	2.364	20.87	2.193	22.683
5/5/2014 17:15:00	150.46	42.12	34.46	2.268	21.02	2.091	22.846
5/5/2014 17:20:00	149.21	40.83	34.04	2.194	21.17	2.014	23.008
5/5/2014 17:25:00	141.06	40.58	34.63	2.097	20.79	1.966	22.602
5/5/2014 17:30:00	125.39	41.29	33.87	1.926	20.79	1.815	22.602
5/5/2014 17:35:00	122.17	41.47	33.48	1.792	20.19	1.740	21.951
5/5/2014 17:40:00	110.97	41.44	33.16	1.671	19.90	1.649	21.626
5/5/2014 17:45:00	102.76	41.56	33.26	1.563	20.34	1.520	22.114
5/5/2014 17:50:00	100.31	41.39	33.48	1.462	20.49	1.420	22.276
5/5/2014 17:55:00	100.31	41.46	33.33	1.361	20.19	1.350	21.951
5/5/2014 18:00:00	90.28	41.09	32.76	1.257	20.19	1.255	21.951
5/5/2014 18:05:00	75.86	40.71	32.69	1.153	19.90	1.173	21.626
5/5/2014 18:10:00	75.23	40.60	32.74	1.053	19.97	1.078	21.707
5/5/2014 18:15:00	75.23	40.45	32.98	0.961	19.67	1.006	21.382
5/5/2014 18:20:00	74.01	40.28	32.78	0.883	19.82	0.925	21.545
5/5/2014 18:25:00	64.94	39.74	32.47	0.800	19.75	0.852	21.463
5/5/2014 18:30:00	58.30	39.57	32.34	0.717	19.67	0.774	21.382
5/5/2014 18:35:00	52.04	39.39	32.13	0.591	20.34	0.638	22.114
5/5/2014 18:40:00	50.15	38.67	31.98	0.508	20.79	0.544	22.602
5/5/2014 18:45:00	49.51	37.93	31.74	0.416	20.79	0.458	22.602
5/5/2014 18:50:00	47.71	37.77	31.32	0.346	20.12	0.404	21.87
5/5/2014 18:55:00	33.23	37.43	31.11	0.245	20.05	0.305	21.789
5/5/2014 19:00:00	25.08	36.92	30.89	0.163	19.37	0.224	21.057
5/5/2014 19:05:00	25.08	36.34	30.78	0.076	19.30	0.114	20.976
5/5/2014 19:10:00	25.08	35.88	30.29	0.017	19.07	0.028	20.732
5/5/2014 19:15:00	25.08	35.48	29.76	0.000	19.37	0.000	21.057
5/5/2014 19:20:00	23.85	34.99	29.68	0.000	15.03	0.000	16.341
5/5/2014 19:25:00	22.51	34.41	29.49	0.000	11.67	0.000	12.683
5/5/2014 19:30:00	23.60	34.05	29.15	0.000	13.91	0.000	15.122
5/6/2014 7:20:00	25.08	27.99	25.10	0.063	19.07	0.098	20.732
5/6/2014 7:25:00	25.08	28.17	25.14	0.089	19.15	0.133	20.813
5/6/2014 7:30:00	25.08	28.19	25.22	0.130	18.85	0.187	20.488
5/6/2014 7:35:00	25.08	28.30	25.34	0.181	18.85	0.248	20.488
5/6/2014 7:40:00	25.08	28.47	25.53	0.213	19.67	0.274	21.382
5/6/2014 7:45:00	26.96	28.72	25.55	0.286	19.52	0.356	21.22
5/6/2014 7:50:00	26.96	28.80	25.90	0.354	20.34	0.411	22.114
5/6/2014 7:55:00	31.97	28.97	26.07	0.467	20.27	0.521	22.033
5/6/2014 8:00:00	39.50	29.29	26.19	0.545	21.47	0.563	23.333
5/6/2014 8:05:00	47.65	29.59	26.39	0.678	21.39	0.679	23.252
5/6/2014 8:10:00	50.15	29.87	26.61	0.734	22.07	0.713	23.984
5/6/2014 8:15:00	50.15	30.20	26.92	0.878	20.94	0.874	22.764
5/6/2014 8:20:00	50.15	30.48	27.05	0.950	20.19	0.968	21.951
5/6/2014 8:25:00	53.37	30.79	27.25	1.021	20.34	1.029	22.114

5/6/2014 8:30:00	72.17	31.01	27.45	1.108	20.72	1.091	22.52
5/6/2014 8:35:00	76.49	31.26	27.82	1.219	20.64	1.190	22.439
5/6/2014 8:40:00	90.90	31.72	28.32	1.312	21.47	1.225	23.333
5/6/2014 8:45:00	100.95	32.21	28.60	1.401	21.99	1.275	23.902
5/6/2014 8:50:00	105.20	32.67	28.85	1.485	22.14	1.333	24.065
5/6/2014 8:55:00	102.29	32.83	28.50	1.336	21.54	1.238	23.415
5/6/2014 9:00:00	100.31	33.01	28.45	1.244	21.24	1.172	23.089
5/6/2014 9:05:00	100.31	33.20	28.95	1.225	21.32	1.147	23.171
5/6/2014 9:10:00	114.10	33.30	29.19	1.488	21.77	1.352	23.659
5/6/2014 9:15:00	144.82	33.66	29.86	1.960	21.32	1.794	23.171
5/6/2014 9:20:00	161.75	34.11	29.26	2.094	21.62	1.897	23.496
5/6/2014 9:25:00	172.41	34.81	30.24	2.180	21.92	1.944	23.821
5/6/2014 9:30:00	167.39	35.56	30.37	2.234	21.84	1.990	23.74
5/6/2014 9:35:00	171.04	36.47	30.62	2.471	21.99	2.179	23.902
5/6/2014 9:40:00	150.46	37.12	31.19	2.347	21.54	2.115	23.415
5/6/2014 9:45:00	160.75	37.77	31.66	2.562	21.62	2.293	23.496
5/6/2014 9:50:00	156.58	38.47	31.12	2.619	21.47	2.357	23.333
5/6/2014 9:55:00	169.11	39.39	31.46	2.729	21.54	2.444	23.415
5/6/2014 10:00:00	178.67	40.08	30.94	2.961	20.87	2.721	22.683
5/6/2014 10:05:00	207.05	41.07	31.93	3.123	20.94	2.858	22.764
5/6/2014 10:10:00	148.63	41.76	31.10	2.342	21.02	2.158	22.846
5/6/2014 10:15:00	174.29	41.85	31.80	2.725	21.02	2.492	22.846
5/6/2014 10:20:00	181.18	42.58	32.28	2.794	20.87	2.566	22.683
5/6/2014 10:25:00	258.49	43.33	33.48	3.560	20.27	3.339	22.033
5/6/2014 10:30:00	231.81	45.02	34.11	3.474	20.05	3.288	21.789
5/6/2014 10:35:00	280.99	45.23	33.02	4.024	21.02	3.614	22.846
5/6/2014 10:40:00	324.17	46.35	35.34	4.234	20.79	3.870	22.602
5/6/2014 10:45:00	217.34	45.67	33.57	3.042	20.79	2.800	22.602
5/6/2014 10:50:00	212.53	44.80	33.17	3.137	20.94	2.863	22.764
5/6/2014 10:55:00	224.44	43.89	33.53	3.441	20.79	3.161	22.602
5/6/2014 11:00:00	314.43	44.88	35.08	4.658	20.57	4.289	22.358
5/6/2014 11:05:00	353.65	47.71	36.53	5.018	20.72	4.588	22.52
5/6/2014 11:10:00	435.49	48.91	37.22	5.947	20.12	5.585	21.87
5/6/2014 11:15:00	471.97	51.21	38.75	6.250	20.42	5.779	22.195
5/6/2014 11:20:00	450.10	51.40	37.39	5.993	20.12	5.628	21.87
5/6/2014 11:25:00	231.34	51.75	35.84	3.350	20.12	3.174	21.87
5/6/2014 11:30:00	240.37	51.26	35.66	3.585	20.05	3.419	21.789
5/6/2014 11:35:00	230.20	51.94	35.67	3.247	20.57	3.025	22.358
5/6/2014 11:40:00	191.21	51.48	36.23	2.742	20.42	2.589	22.195
5/6/2014 11:45:00	134.16	49.73	35.33	1.883	20.34	1.818	22.114
5/6/2014 11:50:00	75.86	47.72	33.94	0.978	20.05	1.010	21.789
5/6/2014 11:55:00	76.49	44.76	33.54	1.013	19.45	1.071	21.138
5/6/2014 12:00:00	55.94	44.18	33.07	0.822	19.37	0.892	21.057
5/6/2014 12:05:00	64.57	42.93	32.33	0.908	20.19	0.941	21.951
5/6/2014 12:10:00	73.98	40.93	31.76	1.188	20.87	1.165	22.683
5/6/2014 12:15:00	77.74	39.90	31.89	1.321	20.87	1.281	22.683
5/6/2014 12:20:00	75.23	39.04	32.20	1.131	20.57	1.128	22.358
5/6/2014 12:25:00	74.60	38.48	31.83	1.087	20.57	1.088	22.358
5/6/2014 12:30:00	44.37	37.82	31.09	0.473	20.57	0.518	22.358
5/6/2014 12:35:00	25.70	36.14	29.35	0.098	20.64	0.135	22.439
5/6/2014 12:40:00	25.08	33.68	26.64	0.035	19.37	0.056	21.057
5/6/2014 12:45:00	25.08	30.28	25.28	0.062	19.22	0.097	20.894
5/6/2014 12:50:00	25.08	29.57	25.05	0.063	19.52	0.097	21.22
5/6/2014 12:55:00	25.08	29.34	24.89	0.047	19.45	0.074	21.138

5/6/2014 13:00:00	25.08	29.25	24.71	0.160	19.52	0.217	21.22
5/6/2014 13:05:00	30.09	29.09	24.71	0.288	19.45	0.361	21.138
5/6/2014 13:10:00	38.87	29.08	24.86	0.416	20.57	0.469	22.358
5/6/2014 13:15:00	48.90	29.32	25.16	0.576	20.57	0.620	22.358
5/6/2014 13:20:00	53.92	29.38	25.48	0.711	21.39	0.721	23.252
5/6/2014 13:25:00	85.26	29.31	25.67	1.371	20.34	1.366	22.114
5/6/2014 13:30:00	149.21	29.96	26.05	2.431	20.79	2.275	22.602
5/6/2014 13:35:00	258.29	30.88	26.86	3.976	22.21	3.445	24.146
5/6/2014 13:40:00	399.35	31.89	27.56	6.045	22.44	5.130	24.39
5/6/2014 13:45:00	571.13	33.40	30.49	7.703	22.29	6.576	24.228
5/6/2014 13:50:00	450.17	34.11	32.07	6.457	22.29	5.539	24.228
5/6/2014 13:55:00	597.46	34.59	33.63	7.787	21.09	7.016	22.927
5/6/2014 14:00:00	565.15	36.22	33.93	7.487	20.34	6.965	22.114
5/6/2014 14:05:00	433.38	37.52	34.35	5.838	20.05	5.512	21.789
5/6/2014 14:10:00	401.23	39.04	33.18	5.591	20.27	5.239	22.033
5/6/2014 14:15:00	313.14	40.69	33.11	4.571	20.72	4.214	22.52
5/6/2014 14:20:00	378.25	42.63	34.49	5.083	21.09	4.590	22.927
5/6/2014 14:25:00	389.71	41.04	32.96	5.244	20.34	4.887	22.114
5/6/2014 14:30:00	330.33	38.94	32.09	4.756	20.79	4.355	22.602
5/6/2014 14:35:00	231.77	39.08	32.04	3.433	20.79	3.166	22.602
5/6/2014 14:40:00	224.98	38.55	31.15	3.330	20.79	3.076	22.602
5/6/2014 14:45:00	224.08	38.32	31.14	3.212	20.64	2.992	22.439
5/6/2014 14:50:00	260.48	39.60	30.90	3.733	20.64	3.462	22.439
5/6/2014 14:55:00	187.45	38.85	31.56	2.950	20.94	2.727	22.764
5/6/2014 15:00:00	166.37	37.59	32.61	2.647	22.07	2.337	23.984
5/6/2014 15:05:00	153.03	37.20	32.80	2.540	21.99	2.254	23.902
5/6/2014 15:10:00	170.04	37.36	32.53	2.601	21.09	2.397	22.927
5/6/2014 15:15:00	166.76	37.47	32.38	2.611	21.47	2.370	23.333
5/6/2014 15:20:00	174.29	38.30	33.39	2.703	20.94	2.498	22.764
5/6/2014 15:25:00	189.10	38.86	33.05	2.874	21.02	2.647	22.846
5/6/2014 15:30:00	236.70	39.66	33.69	3.443	21.77	3.038	23.659
5/6/2014 15:35:00	276.48	40.01	34.71	3.933	21.17	3.550	23.008
5/6/2014 15:40:00	224.44	41.25	34.69	3.430	20.87	3.152	22.683
5/6/2014 15:45:00	224.44	41.96	34.78	3.376	20.94	3.085	22.764
5/6/2014 15:50:00	285.63	42.29	34.83	4.347	21.17	3.908	23.008
5/6/2014 15:55:00	304.78	43.36	35.58	4.394	20.72	4.040	22.52
5/6/2014 16:00:00	298.48	44.34	35.69	4.061	21.02	3.694	22.846
5/6/2014 16:05:00	255.27	44.89	35.99	3.487	20.72	3.224	22.52
5/6/2014 16:10:00	260.80	45.90	35.95	3.612	20.57	3.354	22.358
5/6/2014 16:15:00	338.54	44.17	34.39	4.408	19.75	4.241	21.463
5/6/2014 16:20:00	305.82	42.37	35.04	3.999	19.97	3.813	21.707
5/6/2014 16:25:00	327.93	42.70	35.35	4.317	20.49	4.007	22.276
5/6/2014 16:30:00	376.16	42.69	34.16	5.085	20.64	4.677	22.439
5/6/2014 16:35:00	382.10	44.09	35.81	5.153	20.19	4.829	21.951
5/6/2014 16:40:00	368.01	43.78	35.99	4.840	20.27	4.530	22.033
5/6/2014 16:45:00	340.15	43.97	36.11	4.417	20.49	4.106	22.276
5/6/2014 16:50:00	320.50	43.29	35.74	4.240	20.12	4.026	21.87
5/6/2014 16:55:00	310.33	43.69	36.21	4.017	20.19	3.797	21.951
5/6/2014 17:00:00	205.12	41.67	33.19	2.887	19.97	2.795	21.707
5/6/2014 17:05:00	226.32	41.21	34.74	3.156	20.34	3.003	22.114
5/6/2014 17:10:00	204.38	42.65	35.67	2.884	20.42	2.731	22.195
5/6/2014 17:15:00	180.56	43.28	34.97	2.575	20.49	2.443	22.276
5/6/2014 17:20:00	182.44	43.85	34.66	2.616	21.09	2.419	22.927
5/6/2014 17:25:00	174.91	44.09	35.44	2.464	20.72	2.323	22.52

5/6/2014 17:30:00	159.24	42.67	34.15	2.642	20.87	2.448	22.683
5/6/2014 17:35:00	137.62	42.85	35.21	2.374	20.57	2.231	22.358
5/6/2014 17:40:00	128.52	42.80	35.13	2.351	21.77	2.087	23.659
5/6/2014 17:45:00	136.32	42.26	34.48	2.366	21.69	2.107	23.577
5/6/2014 17:50:00	138.23	40.57	33.63	2.402	21.99	2.108	23.902
5/6/2014 17:55:00	144.19	41.02	34.86	2.323	21.62	2.083	23.496
5/6/2014 18:00:00	130.40	40.12	33.51	2.290	21.77	2.041	23.659
5/6/2014 18:05:00	123.51	40.82	35.79	2.108	21.47	1.918	23.333
5/6/2014 18:10:00	102.14	40.02	34.45	1.733	21.02	1.619	22.846
5/6/2014 18:15:00	82.13	39.50	32.99	1.231	20.79	1.192	22.602
5/6/2014 18:20:00	75.23	39.04	33.18	1.011	19.97	1.037	21.707
5/6/2014 18:25:00	77.11	38.66	33.09	0.875	19.15	0.945	20.813
5/6/2014 18:30:00	60.71	38.28	33.03	0.669	19.15	0.746	20.813
5/6/2014 18:35:00	49.53	37.76	32.40	0.497	19.15	0.576	20.813
5/6/2014 18:40:00	37.92	37.33	31.62	0.305	19.75	0.372	21.463
5/6/2014 18:45:00	33.85	36.51	31.25	0.215	19.60	0.278	21.301
5/6/2014 18:50:00	30.86	36.01	31.04	0.208	19.37	0.274	21.057
5/6/2014 18:55:00	28.84	35.63	31.13	0.207	19.15	0.276	20.813
5/6/2014 19:00:00	25.70	35.44	30.91	0.161	19.22	0.222	20.894
5/6/2014 19:05:00	25.70	34.85	29.99	0.114	19.00	0.167	20.65
5/6/2014 19:10:00	25.08	34.35	29.76	0.034	19.07	0.053	20.732
5/6/2014 19:15:00	25.08	33.87	29.28	0.000	19.30	0.000	20.976
5/6/2014 19:20:00	23.10	33.50	29.22	0.000	14.29	0.000	15.528
5/7/2014 7:10:00	25.08	27.24	24.22	0.000	18.40	0.000	20
5/7/2014 7:15:00	25.08	27.32	24.46	0.000	21.39	0.000	23.252
5/7/2014 7:20:00	25.08	27.34	24.56	0.057	19.22	0.090	20.894
5/7/2014 7:25:00	25.08	27.49	24.61	0.131	19.15	0.187	20.813
5/7/2014 7:30:00	25.08	27.63	24.67	0.202	19.45	0.266	21.138
5/7/2014 7:35:00	25.08	27.89	24.95	0.278	19.30	0.350	20.976
5/7/2014 7:40:00	26.91	27.95	25.18	0.331	20.34	0.387	22.114
5/7/2014 7:45:00	29.04	28.13	25.36	0.420	20.27	0.473	22.033
5/7/2014 7:50:00	34.48	28.37	25.59	0.483	21.24	0.513	23.089
5/7/2014 7:55:00	36.99	28.67	25.94	0.599	21.24	0.617	23.089
5/7/2014 8:00:00	43.43	28.89	26.17	0.633	21.84	0.630	23.74
5/7/2014 8:05:00	47.02	29.20	26.20	0.654	21.84	0.650	23.74
5/7/2014 8:10:00	42.00	29.47	26.26	0.605	21.99	0.607	23.902
5/7/2014 8:15:00	46.39	29.70	26.47	0.647	21.69	0.647	23.577
5/7/2014 8:20:00	50.15	29.94	26.64	0.674	21.84	0.667	23.74
5/7/2014 8:25:00	50.15	30.14	26.87	0.737	21.62	0.727	23.496
5/7/2014 8:30:00	50.15	30.38	27.09	0.741	21.99	0.720	23.902
5/7/2014 8:35:00	55.17	30.53	26.97	0.899	20.79	0.893	22.602
5/7/2014 8:40:00	67.71	31.31	27.33	1.096	20.94	1.056	22.764
5/7/2014 8:45:00	109.71	33.16	27.83	1.394	21.02	1.321	22.846
5/7/2014 8:50:00	177.42	35.92	28.22	1.334	22.21	1.212	24.146
5/7/2014 8:55:00	171.15	37.57	28.30	1.269	22.14	1.159	24.065
5/7/2014 9:00:00	147.96	37.13	28.67	1.213	21.54	1.140	23.415
5/7/2014 9:05:00	106.58	35.77	29.58	1.244	21.39	1.173	23.252
5/7/2014 9:10:00	126.01	35.76	29.41	1.414	21.69	1.299	23.577
5/7/2014 9:15:00	117.24	35.76	30.17	1.947	21.77	1.757	23.659
5/7/2014 9:20:00	180.56	37.57	30.18	2.603	21.17	2.362	23.008
5/7/2014 9:25:00	244.50	41.18	30.38	2.764	21.84	2.425	23.74
5/7/2014 9:30:00	226.32	43.39	32.02	2.899	21.17	2.609	23.008
5/7/2014 9:35:00	225.69	45.14	34.05	2.989	21.09	2.702	22.927
5/7/2014 9:40:00	236.63	46.63	34.34	3.092	20.79	2.826	22.602

5/7/2014 9:45:00	251.38	48.24	34.76	3.131	20.72	2.866	22.52
5/7/2014 9:50:00	272.09	49.51	35.07	3.230	20.57	2.969	22.358
5/7/2014 9:55:00	299.67	49.64	36.20	3.368	20.57	3.092	22.358
5/7/2014 10:00:00	317.85	51.24	36.07	3.471	20.57	3.181	22.358
5/7/2014 10:05:00	336.29	52.55	35.91	3.587	20.34	3.321	22.114
5/7/2014 10:10:00	362.99	53.31	36.96	3.692	20.57	3.363	22.358
5/7/2014 10:15:00	376.16	50.91	35.91	3.813	20.27	3.527	22.033
5/7/2014 10:20:00	401.23	49.17	35.89	3.874	19.82	3.679	21.545
5/7/2014 10:25:00	401.23	50.97	35.93	3.975	19.60	3.836	21.301
5/7/2014 10:30:00	405.00	52.22	36.85	4.064	19.67	3.901	21.382
5/7/2014 10:35:00	401.23	53.26	37.19	4.131	20.05	3.884	21.789
5/7/2014 10:40:00	406.88	54.60	37.48	4.233	19.75	4.037	21.463
5/7/2014 10:45:00	406.38	53.68	36.75	4.349	19.30	4.239	20.976
5/7/2014 10:50:00	406.88	52.42	37.32	4.442	19.30	4.325	20.976
5/7/2014 10:55:00	413.45	53.09	37.53	4.524	19.67	4.333	21.382
5/7/2014 11:00:00	417.53	53.75	36.83	4.607	19.37	4.473	21.057
5/7/2014 11:05:00	446.89	52.93	36.00	4.729	19.52	4.552	21.22
5/7/2014 11:10:00	448.94	50.84	37.00	4.761	19.22	4.654	20.894
5/7/2014 11:15:00	450.75	52.99	38.73	4.828	19.45	4.659	21.138
5/7/2014 11:20:00	351.71	55.22	38.06	4.029	19.52	3.888	21.22
5/7/2014 11:25:00	207.51	53.60	36.57	2.834	19.67	2.750	21.382
5/7/2014 11:30:00	242.82	51.53	36.17	3.370	19.75	3.226	21.463
5/7/2014 11:35:00	282.74	48.41	35.23	3.817	19.90	3.622	21.626
5/7/2014 11:40:00	403.16	48.03	36.30	4.920	20.57	4.489	22.358
5/7/2014 11:45:00	441.98	50.51	37.23	5.110	19.82	4.856	21.545
5/7/2014 11:50:00	480.85	49.34	36.68	5.508	19.45	5.321	21.138
5/7/2014 11:55:00	468.32	49.35	36.80	5.429	19.37	5.280	21.057
5/7/2014 12:00:00	450.14	51.59	38.22	5.325	19.37	5.212	21.057
5/7/2014 12:05:00	536.65	52.72	39.66	5.901	19.52	5.746	21.22
5/7/2014 12:10:00	501.54	53.13	38.50	5.622	19.52	5.467	21.22
5/7/2014 12:15:00	285.25	52.94	36.92	3.576	19.30	3.552	20.976
5/7/2014 12:20:00	206.26	50.52	35.98	2.910	19.82	2.836	21.545
5/7/2014 12:25:00	188.38	45.47	34.38	2.666	20.12	2.567	21.87
5/7/2014 12:30:00	127.89	41.60	33.71	2.034	19.97	1.997	21.707
5/7/2014 12:35:00	352.33	41.86	35.03	4.566	20.57	4.241	22.358
5/7/2014 12:40:00	515.96	43.59	36.97	6.081	19.75	5.853	21.463
5/7/2014 12:45:00	487.75	45.95	37.34	5.585	19.82	5.349	21.545
5/7/2014 12:50:00	414.69	47.52	37.29	4.890	19.60	4.758	21.301
5/7/2014 12:55:00	502.80	47.09	36.47	5.580	20.12	5.266	21.87
5/7/2014 13:00:00	503.42	47.08	37.33	5.279	19.45	5.163	21.138
5/7/2014 13:05:00	580.54	49.34	39.24	5.831	19.30	5.726	20.976
5/7/2014 13:10:00	615.02	51.13	37.81	6.015	19.30	5.900	20.976
5/7/2014 13:15:00	581.28	48.97	36.57	5.647	19.30	5.521	20.976
5/7/2014 13:20:00	617.75	47.74	37.30	5.968	19.37	5.817	21.057
5/7/2014 13:25:00	614.39	45.67	36.99	5.890	19.37	5.749	21.057
5/7/2014 13:30:00	596.21	44.99	36.56	5.750	19.37	5.617	21.057
5/7/2014 13:35:00	618.15	46.12	37.92	5.931	19.30	5.797	20.976
5/7/2014 13:40:00	438.85	49.43	38.62	4.535	19.37	4.439	21.057
5/7/2014 13:45:00	232.59	50.35	37.15	3.330	19.45	3.259	21.138
5/7/2014 13:50:00	352.92	50.38	36.63	4.354	19.97	4.133	21.707
5/7/2014 13:55:00	548.56	48.10	37.32	5.541	20.57	5.080	22.358
5/7/2014 14:00:00	515.34	48.84	38.46	5.349	19.75	5.099	21.463
5/7/2014 14:05:00	561.10	51.59	38.71	5.885	19.52	5.663	21.22
5/7/2014 14:10:00	557.34	51.85	38.06	5.744	19.90	5.423	21.626

5/7/2014 14:15:00	353.59	51.17	36.91	4.115	19.60	3.975	21.301
5/7/2014 14:20:00	470.20	50.17	37.60	5.314	19.97	4.976	21.707
5/7/2014 14:25:00	474.59	50.52	37.62	5.306	19.52	5.088	21.22
5/7/2014 14:30:00	464.25	48.32	37.07	5.199	19.30	5.039	20.976
5/7/2014 14:35:00	488.38	44.81	35.75	5.386	19.90	5.078	21.626
5/7/2014 14:40:00	509.69	42.24	35.41	5.606	19.37	5.432	21.057
5/7/2014 14:45:00	490.26	43.63	37.74	5.359	19.67	5.127	21.382
5/7/2014 14:50:00	417.75	46.22	37.65	4.762	19.45	4.612	21.138
5/7/2014 14:55:00	381.80	45.55	38.10	4.414	19.67	4.243	21.382
5/7/2014 15:00:00	355.47	45.60	37.26	4.141	19.45	4.037	21.138
5/7/2014 15:05:00	301.54	45.00	36.21	3.486	19.52	3.401	21.22
5/7/2014 15:10:00	375.53	42.56	35.50	4.312	19.67	4.153	21.382
5/7/2014 15:15:00	432.58	42.01	36.09	4.906	19.60	4.729	21.301
5/7/2014 15:20:00	419.58	42.18	36.55	4.865	19.60	4.692	21.301
5/7/2014 15:25:00	257.67	42.81	36.09	3.142	20.05	2.986	21.789
5/7/2014 15:30:00	376.78	42.42	35.88	4.573	20.27	4.259	22.033
5/7/2014 15:35:00	304.06	40.96	35.15	3.762	20.87	3.427	22.683
5/7/2014 15:40:00	352.96	41.62	36.61	4.329	20.34	4.033	22.114
5/7/2014 15:45:00	212.19	41.08	35.14	2.811	19.90	2.698	21.626
5/7/2014 15:50:00	152.30	41.74	34.97	2.322	20.05	2.233	21.789
5/7/2014 15:55:00	141.46	41.61	34.52	2.104	20.19	2.022	21.951
5/7/2014 16:00:00	97.25	40.69	34.18	1.410	20.19	1.389	21.951
5/7/2014 16:05:00	84.88	41.48	34.39	1.215	20.12	1.218	21.87
5/7/2014 16:10:00	108.87	41.09	34.34	1.563	20.34	1.515	22.114
5/7/2014 16:15:00	107.65	40.25	34.19	1.615	20.94	1.521	22.764
5/7/2014 16:20:00	112.85	40.35	33.72	1.799	20.79	1.692	22.602
5/7/2014 16:25:00	140.43	40.03	34.19	2.093	20.64	1.966	22.439
5/7/2014 16:30:00	100.31	40.27	34.06	1.526	20.12	1.499	21.87
5/7/2014 16:35:00	124.77	40.33	34.51	1.917	20.42	1.823	22.195
5/7/2014 16:40:00	146.70	39.90	34.68	2.297	20.79	2.142	22.602
5/7/2014 16:45:00	163.00	40.52	34.70	2.386	20.49	2.262	22.276
5/7/2014 16:50:00	183.69	40.92	35.77	2.475	19.75	2.422	21.463
5/7/2014 16:55:00	140.43	40.00	34.17	2.097	19.90	2.055	21.626
5/7/2014 17:00:00	237.32	40.16	35.49	3.101	20.72	2.875	22.52
5/7/2014 17:05:00	187.45	40.19	35.99	2.151	21.92	1.909	23.821
5/7/2014 17:10:00	66.67	39.42	33.62	0.622	21.99	0.620	23.902
5/7/2014 17:15:00	70.22	38.89	33.38	0.712	21.92	0.697	23.821
5/7/2014 17:20:00	63.32	39.11	33.33	0.746	21.69	0.734	23.577
5/7/2014 17:25:00	75.86	38.55	33.00	1.028	21.47	0.993	23.333
5/7/2014 17:30:00	82.13	38.38	33.13	1.050	21.24	1.022	23.089
5/7/2014 17:35:00	49.53	38.67	33.26	0.551	21.24	0.579	23.089
5/7/2014 17:40:00	72.72	38.67	33.37	0.867	21.02	0.870	22.846
5/7/2014 17:45:00	49.54	38.73	33.51	0.441	20.87	0.485	22.683
5/7/2014 17:50:00	33.85	38.39	33.28	0.223	20.64	0.276	22.439
5/7/2014 17:55:00	34.48	38.12	32.94	0.181	19.52	0.243	21.22
5/7/2014 18:00:00	26.33	37.73	32.61	0.138	19.52	0.192	21.22
5/7/2014 18:05:00	28.84	37.29	32.14	0.176	19.15	0.242	20.813
5/7/2014 18:10:00	31.35	36.81	32.01	0.216	19.30	0.285	20.976
5/7/2014 18:15:00	33.23	36.56	32.03	0.223	19.45	0.290	21.138
5/7/2014 18:20:00	29.97	36.39	31.96	0.213	19.67	0.276	21.382
5/7/2014 18:25:00	50.15	36.12	32.18	0.546	19.67	0.611	21.382
5/7/2014 18:30:00	69.59	36.22	32.68	0.814	19.97	0.857	21.707
5/7/2014 18:35:00	65.83	36.22	32.60	0.751	20.05	0.796	21.789
5/7/2014 18:40:00	50.77	36.30	32.47	0.601	20.12	0.654	21.87

5/7/2014 18:45:00	50.15	36.28	32.08	0.454	20.72	0.501	22.52
5/7/2014 18:50:00	49.53	36.27	32.29	0.365	20.72	0.416	22.52
5/7/2014 18:55:00	39.50	36.11	32.42	0.262	20.27	0.320	22.033
5/7/2014 19:00:00	27.58	35.83	31.97	0.197	19.75	0.257	21.463
5/7/2014 19:05:00	27.58	35.48	31.66	0.117	19.52	0.167	21.22
5/7/2014 19:10:00	25.08	35.19	31.67	0.048	19.15	0.075	20.813
5/7/2014 19:15:00	25.08	34.94	31.25	0.000	19.00	0.000	20.65
5/7/2014 19:20:00	25.08	34.50	30.69	0.000	13.84	0.000	15.041
5/5/2014 7:10:00	23.91	27.31	24.27	0.000	17.95	0.000	19.512
5/5/2014 7:15:00	24.45	27.45	24.55	0.000	20.19	0.000	21.951
5/5/2014 7:20:00	25.08	27.65	24.70	0.000	21.69	0.000	23.577
5/5/2014 7:25:00	25.08	27.63	24.77	0.027	19.15	0.045	20.813
5/5/2014 7:30:00	25.08	27.59	24.64	0.086	19.00	0.130	20.65
5/5/2014 7:35:00	25.72	27.54	24.99	0.116	19.07	0.166	20.732
5/5/2014 7:40:00	25.08	27.61	25.19	0.156	19.00	0.218	20.65
5/5/2014 7:45:00	25.08	27.89	25.38	0.194	19.52	0.255	21.22
5/5/2014 7:50:00	25.08	28.17	25.48	0.254	19.45	0.322	21.138
5/5/2014 7:55:00	25.08	28.29	25.70	0.328	20.34	0.383	22.114
5/5/2014 8:00:00	25.70	28.42	25.83	0.391	20.42	0.445	22.195
5/5/2014 8:05:00	26.96	28.55	25.98	0.407	21.02	0.452	22.846
5/5/2014 8:10:00	34.48	28.73	26.16	0.512	20.94	0.548	22.764
5/5/2014 8:15:00	40.75	28.92	26.37	0.538	21.39	0.563	23.252
5/5/2014 8:20:00	46.48	29.22	26.44	0.649	21.24	0.665	23.089
5/5/2014 8:25:00	49.54	29.59	26.54	0.785	21.77	0.774	23.659
5/5/2014 8:30:00	50.15	29.92	26.96	0.898	21.39	0.878	23.252
5/5/2014 8:35:00	50.15	30.21	27.18	0.848	20.94	0.850	22.764
5/5/2014 8:40:00	63.61	30.72	27.35	1.156	21.24	1.107	23.089
5/5/2014 8:45:00	89.65	32.24	27.77	1.453	21.02	1.381	22.846
5/5/2014 8:50:00	146.07	34.06	28.08	1.570	21.17	1.469	23.008
5/5/2014 8:55:00	173.03	36.23	28.32	1.838	21.92	1.659	23.821
5/5/2014 9:00:00	167.39	36.22	28.51	1.794	21.32	1.663	23.171
5/5/2014 9:05:00	137.92	34.95	28.82	1.673	21.09	1.575	22.927
5/5/2014 9:10:00	149.21	34.89	29.07	1.891	21.92	1.705	23.821
5/5/2014 9:15:00	165.51	35.31	29.45	2.453	22.66	2.112	24.634
5/5/2014 9:20:00	201.28	37.00	29.54	2.608	21.69	2.331	23.577
5/5/2014 9:25:00	178.67	37.83	30.05	2.195	21.47	1.996	23.333
5/5/2014 9:30:00	197.75	39.38	30.99	2.854	21.69	2.540	23.577
5/5/2014 9:35:00	194.83	40.04	32.29	2.849	22.29	2.479	24.228
5/5/2014 9:40:00	228.75	41.07	32.92	3.410	22.07	2.968	23.984
5/5/2014 9:45:00	136.96	41.69	32.45	2.088	21.99	1.856	23.902
5/5/2014 9:50:00	94.04	40.94	31.33	1.306	22.29	1.182	24.228
5/5/2014 9:55:00	228.27	40.47	31.59	2.845	21.92	2.499	23.821
5/5/2014 10:00:00	296.97	41.79	32.93	3.389	21.54	3.006	23.415
5/5/2014 10:05:00	340.44	43.80	33.18	3.891	21.47	3.455	23.333
5/5/2014 10:10:00	398.10	45.07	33.71	4.366	20.87	3.961	22.683
5/5/2014 10:15:00	396.62	44.76	34.06	4.381	20.57	4.036	22.358
5/5/2014 10:20:00	413.77	43.77	33.80	4.652	20.12	4.384	21.87
5/5/2014 10:25:00	387.38	46.26	35.17	4.369	19.52	4.251	21.22
5/5/2014 10:30:00	399.98	46.40	34.69	4.454	19.52	4.319	21.22
5/5/2014 10:35:00	467.69	48.07	36.04	5.008	19.52	4.839	21.22
5/5/2014 10:40:00	435.72	45.62	33.82	5.067	19.45	4.933	21.138
5/5/2014 10:45:00	318.93	42.02	33.35	4.050	20.27	3.783	22.033
5/5/2014 10:50:00	401.85	43.39	35.39	4.864	19.67	4.659	21.382
5/5/2014 10:55:00	188.40	46.67	35.44	2.541	19.37	2.519	21.057

5/5/2014 11:00:00	78.37	45.23	32.27	1.027	19.37	1.080	21.057
5/5/2014 11:05:00	294.66	42.98	32.86	3.649	19.52	3.514	21.22
5/5/2014 11:10:00	478.97	42.77	35.81	5.659	20.12	5.280	21.87
5/5/2014 11:15:00	535.86	45.31	35.81	6.666	19.60	6.379	21.301
5/5/2014 11:20:00	173.97	41.52	32.33	2.285	19.15	2.296	20.813
5/5/2014 11:25:00	96.55	39.35	31.58	1.419	19.30	1.458	20.976
5/5/2014 11:30:00	104.07	39.41	32.07	1.487	19.67	1.495	21.382
5/5/2014 11:35:00	475.84	40.44	35.41	5.711	20.34	5.270	22.114
5/5/2014 11:40:00	552.46	42.72	35.64	6.400	20.57	5.837	22.358
5/5/2014 11:45:00	352.96	44.74	34.93	4.482	20.05	4.207	21.789
5/5/2014 11:50:00	317.64	41.71	33.74	3.823	19.15	3.782	20.813
5/5/2014 11:55:00	112.22	42.69	33.07	1.621	19.30	1.650	20.976
5/5/2014 12:00:00	413.77	41.13	33.56	4.739	19.90	4.516	21.626
5/5/2014 12:05:00	567.37	42.25	34.90	6.141	19.67	5.893	21.382
5/5/2014 12:10:00	472.42	43.68	35.62	5.416	20.05	5.104	21.789
5/5/2014 12:15:00	426.31	45.17	36.63	4.958	20.79	4.527	22.602
5/5/2014 12:20:00	315.35	43.19	33.83	3.964	20.49	3.718	22.276
5/5/2014 12:25:00	557.34	43.26	35.86	6.394	19.60	6.170	21.301
5/5/2014 12:30:00	579.91	46.41	36.52	6.711	19.60	6.482	21.301
5/5/2014 12:35:00	162.08	44.94	34.52	2.111	19.30	2.131	20.976
5/5/2014 12:40:00	122.15	44.31	33.96	1.790	19.82	1.777	21.545
5/5/2014 12:45:00	248.89	42.20	33.75	3.320	19.97	3.196	21.707
5/5/2014 12:50:00	507.81	42.90	35.55	5.995	20.27	5.614	22.033
5/5/2014 12:55:00	536.02	43.96	36.04	6.163	19.67	5.927	21.382
5/5/2014 13:00:00	573.10	42.63	35.33	6.469	19.52	6.264	21.22
5/5/2014 13:05:00	386.19	45.49	36.85	4.657	19.37	4.562	21.057
5/5/2014 13:10:00	348.73	44.13	35.31	4.223	20.05	4.022	21.789
5/5/2014 13:15:00	439.81	44.57	36.28	5.257	19.67	5.059	21.382
5/5/2014 13:20:00	488.70	46.70	35.96	5.950	19.45	5.785	21.138
5/5/2014 13:25:00	205.63	47.00	35.16	2.837	19.52	2.788	21.22
5/5/2014 13:30:00	138.23	43.18	33.53	2.146	19.45	2.143	21.138
5/5/2014 13:35:00	384.31	40.85	33.53	5.014	20.05	4.712	21.789
5/5/2014 13:40:00	311.90	41.72	34.80	4.034	20.27	3.781	22.033
5/5/2014 13:45:00	598.79	41.76	36.03	6.748	20.19	6.277	21.951
5/5/2014 13:50:00	581.79	44.59	37.87	6.366	19.52	6.129	21.22
5/5/2014 13:55:00	384.31	46.20	37.53	4.511	19.75	4.319	21.463
5/5/2014 14:00:00	351.08	45.07	36.00	4.562	19.37	4.455	21.057
5/5/2014 14:05:00	468.94	44.35	35.61	5.357	19.97	5.035	21.707
5/5/2014 14:10:00	489.79	42.14	35.02	5.341	20.27	4.950	22.033
5/5/2014 14:15:00	495.90	44.19	36.66	5.427	19.52	5.211	21.22
5/5/2014 14:20:00	451.39	44.34	35.89	5.294	19.67	5.052	21.382
5/5/2014 14:25:00	396.22	43.27	35.68	4.345	19.82	4.139	21.545
5/5/2014 14:30:00	132.28	42.76	34.61	1.959	20.27	1.873	22.033
5/5/2014 14:35:00	351.71	42.16	34.81	4.355	20.64	3.951	22.439
5/5/2014 14:40:00	521.13	41.51	36.22	5.710	20.42	5.245	22.195
5/5/2014 14:45:00	514.71	43.33	37.39	5.552	19.97	5.198	21.707
5/5/2014 14:50:00	483.36	44.57	37.21	5.257	19.45	5.064	21.138
5/5/2014 14:55:00	502.15	46.97	37.14	5.323	19.22	5.199	20.894
5/5/2014 15:00:00	502.17	48.26	37.86	5.270	19.37	5.112	21.057
5/5/2014 15:05:00	500.92	48.32	39.21	5.349	19.15	5.250	20.813
5/5/2014 15:10:00	489.41	48.22	38.39	5.289	19.15	5.180	20.813
5/5/2014 15:15:00	463.61	45.59	37.45	5.183	19.60	4.968	21.301
5/5/2014 15:20:00	437.32	44.14	36.50	5.072	19.37	4.919	21.057
5/5/2014 15:25:00	300.30	42.22	34.83	3.796	20.12	3.561	21.87

5/5/2014 15:30:00	364.25	41.15	35.14	4.324	19.90	4.089	21.626
5/5/2014 15:35:00	291.52	42.95	36.15	3.777	20.64	3.443	22.439
5/5/2014 15:40:00	311.11	44.14	37.88	3.738	20.34	3.467	22.114
5/5/2014 15:45:00	196.66	43.79	35.86	2.834	20.27	2.661	22.033
5/5/2014 15:50:00	188.44	43.71	35.75	2.724	20.05	2.589	21.789
5/5/2014 15:55:00	172.08	41.90	34.44	2.733	20.42	2.555	22.195
5/5/2014 16:00:00	159.08	42.16	34.70	2.501	20.34	2.348	22.114
5/5/2014 16:05:00	202.83	41.01	34.72	3.241	21.02	2.934	22.846
5/5/2014 16:10:00	236.94	41.15	35.78	3.557	21.02	3.207	22.846
5/5/2014 16:15:00	363.62	41.04	36.63	4.901	20.94	4.395	22.764
5/5/2014 16:20:00	289.17	41.67	37.08	3.727	20.72	3.403	22.52
5/5/2014 16:25:00	286.49	41.04	36.58	3.509	19.75	3.358	21.463
5/5/2014 16:30:00	268.57	42.25	36.93	3.284	19.22	3.229	20.894
5/5/2014 16:35:00	253.64	40.90	35.59	3.111	19.60	3.022	21.301
5/5/2014 16:40:00	273.06	40.96	37.41	3.218	19.60	3.124	21.301
5/5/2014 16:45:00	221.65	42.92	37.54	2.694	20.05	2.574	21.789
5/5/2014 16:50:00	249.20	41.65	35.81	2.846	20.34	2.680	22.114
5/5/2014 16:55:00	224.91	40.23	35.34	2.651	20.72	2.458	22.52
5/5/2014 17:00:00	210.65	41.35	36.35	2.411	19.97	2.329	21.707
5/5/2014 17:05:00	195.92	40.51	35.24	2.290	19.67	2.255	21.382
5/5/2014 17:10:00	206.64	39.94	35.62	2.344	20.49	2.215	22.276
5/5/2014 17:15:00	154.15	39.17	34.56	1.897	20.27	1.843	22.033
5/5/2014 17:20:00	144.56	39.44	34.78	1.757	20.34	1.707	22.114
5/5/2014 17:25:00	154.64	39.69	36.11	1.801	20.12	1.765	21.87
5/5/2014 17:30:00	107.68	39.18	35.18	1.411	19.45	1.454	21.138
5/5/2014 17:35:00	84.55	39.30	35.64	1.680	20.42	1.637	22.195
5/5/2014 17:40:00	75.23	39.66	35.72	0.970	21.09	0.961	22.927
5/5/2014 17:45:00	78.47	39.43	34.95	1.246	21.32	1.195	23.171
5/5/2014 17:50:00	76.66	39.53	34.99	1.256	22.14	1.163	24.065
5/5/2014 17:55:00	75.23	39.47	35.53	1.179	21.99	1.104	23.902
5/5/2014 18:00:00	75.23	39.43	36.13	1.139	22.07	1.059	23.984
5/5/2014 18:05:00	73.66	39.21	35.92	1.098	20.94	1.076	22.764
5/5/2014 18:10:00	68.59	39.30	35.61	1.004	20.34	1.021	22.114
5/5/2014 18:15:00	58.27	38.99	34.71	0.915	19.82	0.964	21.545
5/5/2014 18:20:00	55.32	38.43	34.87	0.793	19.75	0.851	21.463
5/5/2014 18:25:00	75.23	38.15	35.13	0.692	19.75	0.756	21.463
5/5/2014 18:30:00	65.92	37.89	34.91	0.552	20.42	0.603	22.195
5/5/2014 18:35:00	49.37	37.78	34.68	0.452	20.72	0.499	22.52
5/5/2014 18:40:00	48.63	37.54	34.11	0.381	20.19	0.437	21.951
5/5/2014 18:45:00	42.78	37.34	33.91	0.303	19.90	0.364	21.626
5/5/2014 18:50:00	33.44	36.95	33.89	0.236	19.60	0.300	21.301
5/5/2014 18:55:00	26.55	36.44	32.72	0.170	19.15	0.232	20.813
5/5/2014 19:00:00	25.81	36.06	32.31	0.105	19.00	0.154	20.65
5/5/2014 19:05:00	25.79	35.64	31.47	0.023	19.67	0.037	21.382
5/5/2014 19:10:00	24.34	35.24	31.84	0.000	19.00	0.000	20.65
5/5/2014 19:15:00	22.04	34.77	31.55	0.000	16.31	0.000	17.724
5/5/2014 19:20:00	22.29	34.37	31.13	0.000	12.04	0.000	13.089
5/9/2014 7:15:00	24.45	27.61	24.56	0.000	19.82	0.000	21.545
5/9/2014 7:20:00	25.08	27.59	24.61	0.017	20.87	0.027	22.683
5/9/2014 7:25:00	25.08	27.83	24.75	0.096	19.15	0.142	20.813
5/9/2014 7:30:00	25.08	28.04	25.05	0.179	19.37	0.242	21.057
5/9/2014 7:35:00	25.79	28.31	25.19	0.287	19.30	0.359	20.976
5/9/2014 7:40:00	26.64	28.40	25.42	0.373	20.12	0.433	21.87
5/9/2014 7:45:00	28.88	28.58	25.49	0.441	20.94	0.478	22.764

5/9/2014 7:50:00	31.55	28.78	25.64	0.509	21.09	0.534	22.927
5/9/2014 7:55:00	40.51	28.90	25.82	0.594	21.39	0.606	23.252
5/9/2014 8:00:00	47.94	29.19	26.02	0.742	21.54	0.731	23.415
5/9/2014 8:05:00	50.15	29.49	26.08	0.883	21.32	0.859	23.171
5/9/2014 8:10:00	50.15	29.73	26.13	0.965	20.94	0.945	22.764
5/9/2014 8:15:00	50.85	29.94	26.42	1.023	21.02	0.994	22.846
5/9/2014 8:20:00	60.19	30.31	26.66	1.095	20.87	1.067	22.683
5/9/2014 8:25:00	74.23	30.74	27.36	1.242	21.02	1.184	22.846
5/9/2014 8:30:00	88.81	31.08	27.82	1.367	21.39	1.272	23.252
5/9/2014 8:35:00	100.31	31.64	28.23	1.516	21.17	1.403	23.008
5/9/2014 8:40:00	114.54	32.32	28.07	1.620	21.54	1.494	23.415
5/9/2014 8:45:00	132.55	33.19	28.24	1.795	21.24	1.665	23.089
5/9/2014 8:50:00	148.94	34.11	28.58	1.814	21.54	1.657	23.415
5/9/2014 8:55:00	147.57	34.75	28.99	1.840	21.99	1.645	23.902
5/9/2014 9:00:00	153.50	35.14	29.36	1.860	21.54	1.694	23.415
5/9/2014 9:05:00	150.46	34.94	29.42	1.837	21.24	1.699	23.089
5/9/2014 9:10:00	150.46	35.14	29.42	1.917	21.47	1.748	23.333
5/9/2014 9:15:00	174.78	35.53	29.81	2.281	21.77	2.032	23.659
5/9/2014 9:20:00	183.14	36.88	30.15	2.538	21.77	2.247	23.659
5/9/2014 9:25:00	184.22	38.36	30.33	2.659	21.62	2.371	23.496
5/9/2014 9:30:00	176.26	39.29	30.94	2.575	21.92	2.276	23.821
5/9/2014 9:35:00	162.62	38.96	30.69	2.337	21.77	2.090	23.659
5/9/2014 9:40:00	170.22	38.72	31.06	2.454	21.24	2.238	23.089
5/9/2014 9:45:00	192.00	39.35	31.63	2.767	21.24	2.505	23.089
5/9/2014 9:50:00	197.03	40.21	32.02	2.831	21.24	2.572	23.089
5/9/2014 9:55:00	191.59	40.66	31.65	2.793	20.87	2.581	22.683
5/9/2014 10:00:00	245.45	41.58	32.27	3.376	20.42	3.169	22.195
5/9/2014 10:05:00	253.72	43.19	32.43	3.443	20.87	3.165	22.683
5/9/2014 10:10:00	255.47	44.01	32.80	3.468	21.54	3.084	23.415
5/9/2014 10:15:00	242.68	44.75	33.25	3.363	20.94	3.075	22.764
5/9/2014 10:20:00	274.18	45.39	33.24	3.751	20.57	3.468	22.358
5/9/2014 10:25:00	300.93	46.76	33.75	4.070	20.79	3.715	22.602
5/9/2014 10:30:00	316.88	47.67	34.47	4.191	20.27	3.900	22.033
5/9/2014 10:35:00	318.48	47.39	34.24	4.204	20.79	3.815	22.602
5/9/2014 10:40:00	289.53	47.18	33.90	3.806	20.87	3.457	22.683
5/9/2014 10:45:00	306.25	45.14	33.43	4.030	20.34	3.745	22.114
5/9/2014 10:50:00	318.40	45.14	34.28	4.238	20.87	3.840	22.683
5/9/2014 10:55:00	348.99	47.88	35.39	4.740	20.42	4.379	22.195
5/9/2014 11:00:00	342.72	49.56	35.76	4.456	20.12	4.165	21.87
5/9/2014 11:05:00	374.68	48.41	35.25	4.813	20.19	4.462	21.951
5/9/2014 11:10:00	357.72	44.97	33.99	4.677	19.82	4.424	21.545
5/9/2014 11:15:00	315.49	44.94	34.46	4.139	20.42	3.837	22.195
5/9/2014 11:20:00	315.97	46.35	35.44	4.233	20.27	3.978	22.033
5/9/2014 11:25:00	364.08	49.20	36.34	4.683	19.90	4.492	21.626
5/9/2014 11:30:00	360.79	48.57	36.06	4.589	19.60	4.466	21.301
5/9/2014 11:35:00	345.23	48.97	36.48	4.133	20.64	3.830	22.439
5/9/2014 11:40:00	322.20	47.99	35.11	4.517	20.34	4.233	22.114
5/9/2014 11:45:00	424.10	46.89	35.89	5.196	20.42	4.830	22.195
5/9/2014 11:50:00	421.89	47.96	36.75	5.126	19.67	4.952	21.382
5/9/2014 11:55:00	500.54	49.01	35.94	5.636	19.97	5.374	21.707
5/9/2014 12:00:00	550.96	48.87	36.02	5.903	19.67	5.721	21.382
5/9/2014 12:05:00	557.97	46.05	35.26	5.710	19.60	5.562	21.301
5/9/2014 12:10:00	562.67	46.61	36.81	5.699	19.52	5.584	21.22
5/9/2014 12:15:00	557.78	48.50	37.26	5.738	19.52	5.583	21.22

5/9/2014 12:20:00	594.48	48.39	36.56	6.464	19.30	6.309	20.976
5/9/2014 12:25:00	313.46	47.48	34.82	3.437	19.30	3.395	20.976
5/9/2014 12:30:00	490.22	47.12	35.77	5.236	19.30	5.118	20.976
5/9/2014 12:35:00	563.45	45.46	34.99	6.030	19.30	5.886	20.976
5/9/2014 12:40:00	477.27	47.79	35.94	5.281	19.30	5.163	20.976
5/9/2014 12:45:00	494.70	47.92	35.07	5.677	19.30	5.543	20.976
5/9/2014 12:50:00	481.32	43.81	34.53	5.505	19.97	5.202	21.707
5/9/2014 12:55:00	273.67	42.68	34.43	3.772	19.22	3.717	20.894
5/9/2014 13:00:00	420.99	42.66	34.64	4.888	19.45	4.736	21.138
5/9/2014 13:05:00	534.46	43.47	35.77	5.620	19.22	5.481	20.894
5/9/2014 13:10:00	613.61	43.14	35.23	6.352	19.30	6.175	20.976
5/9/2014 13:15:00	606.71	46.45	37.32	6.025	19.15	5.904	20.813
5/9/2014 13:20:00	576.01	50.76	38.75	5.655	19.52	5.437	21.22
5/9/2014 13:25:00	307.68	50.37	36.24	3.365	19.15	3.339	20.813
5/9/2014 13:30:00	522.70	45.64	35.87	5.850	19.52	5.608	21.22
5/9/2014 13:35:00	278.89	45.75	36.21	3.190	19.75	3.061	21.463
5/9/2014 13:40:00	414.91	43.64	35.03	4.832	19.22	4.724	20.894
5/9/2014 13:45:00	539.56	44.56	36.21	5.566	19.30	5.391	20.976
5/9/2014 13:50:00	654.36	47.23	37.38	6.487	19.22	6.274	20.894
5/9/2014 13:55:00	623.35	49.47	38.10	6.254	19.15	6.104	20.813
5/9/2014 14:00:00	576.77	48.23	36.73	5.883	19.22	5.723	20.894
5/9/2014 14:05:00	778.91	46.41	36.47	5.607	19.07	5.500	20.732
5/9/2014 14:10:00	383.21	44.90	34.98	2.677	19.30	2.649	20.976
5/9/2014 14:15:00	644.17	44.26	35.67	6.311	19.52	6.031	21.22
5/9/2014 14:20:00	540.37	44.85	36.48	5.331	19.07	5.230	20.732
5/9/2014 14:25:00	568.42	43.80	36.14	5.526	19.15	5.405	20.813
5/9/2014 14:30:00	539.16	43.51	35.98	5.443	19.22	5.320	20.894
5/9/2014 14:35:00	529.96	43.58	35.83	5.598	19.60	5.359	21.301
5/9/2014 14:40:00	588.24	43.12	36.06	6.037	19.22	5.889	20.894
5/9/2014 14:45:00	656.57	42.82	36.43	7.041	19.37	6.800	21.057
5/9/2014 14:50:00	415.34	44.68	36.83	4.775	19.60	4.593	21.301
5/9/2014 14:55:00	441.17	42.94	35.15	5.218	19.15	5.120	20.813
5/9/2014 15:00:00	341.49	43.16	35.92	4.212	19.45	4.094	21.138
5/9/2014 15:05:00	332.08	43.30	36.02	4.114	19.97	3.885	21.707
5/9/2014 15:10:00	256.85	43.21	35.74	3.106	20.34	2.914	22.114
5/9/2014 15:15:00	273.57	43.49	36.09	3.396	20.19	3.195	21.951
5/9/2014 15:20:00	490.48	42.66	36.99	5.330	19.45	5.170	21.138
5/9/2014 15:25:00	469.44	44.02	37.06	5.117	20.34	4.715	22.114
5/9/2014 15:30:00	515.98	43.99	37.15	5.933	20.12	5.535	21.87
5/9/2014 15:35:00	484.07	43.39	36.75	5.703	19.45	5.500	21.138
5/9/2014 15:40:00	408.52	45.12	37.43	5.295	19.90	4.993	21.626
5/9/2014 15:45:00	292.84	45.55	37.22	4.035	19.75	3.863	21.463
5/9/2014 15:50:00	273.50	45.97	36.61	3.789	20.49	3.495	22.276
5/9/2014 15:55:00	337.65	45.12	36.24	4.606	19.90	4.355	21.626
5/9/2014 16:00:00	417.46	43.63	37.48	5.331	19.52	5.129	21.22
5/9/2014 16:05:00	423.27	46.83	38.38	5.109	19.75	4.852	21.463
5/9/2014 16:10:00	304.27	48.05	38.26	3.789	19.37	3.697	21.057
5/9/2014 16:15:00	203.66	43.89	35.23	2.827	19.37	2.785	21.057
5/9/2014 16:20:00	159.87	43.96	35.42	2.351	19.97	2.270	21.707
5/9/2014 16:25:00	161.07	43.42	35.48	2.288	20.49	2.158	22.276
5/9/2014 16:30:00	202.83	41.86	35.18	2.741	19.90	2.637	21.626
5/9/2014 16:35:00	267.76	42.41	36.81	3.265	20.05	3.088	21.789
5/9/2014 16:40:00	339.33	42.85	38.75	3.688	20.19	3.461	21.951
5/9/2014 16:45:00	222.01	42.88	37.21	2.355	19.52	2.328	21.22

5/9/2014 16:50:00	309.29	43.31	37.53	3.151	19.97	3.015	21.707
5/9/2014 16:55:00	312.50	42.15	37.27	3.033	19.75	2.947	21.463
5/9/2014 17:00:00	271.93	41.83	36.61	2.743	19.22	2.708	20.894
5/9/2014 17:05:00	271.29	40.97	35.80	2.796	20.42	2.607	22.195
5/9/2014 17:10:00	275.85	41.04	37.13	2.969	20.87	2.708	22.683
5/9/2014 17:15:00	257.94	42.41	38.09	2.957	20.27	2.776	22.033
5/9/2014 17:20:00	251.56	41.92	37.78	2.821	20.49	2.633	22.276
5/9/2014 17:25:00	228.59	42.02	37.55	2.530	20.12	2.411	21.87
5/9/2014 17:30:00	182.18	40.54	35.93	2.143	19.90	2.080	21.626
5/9/2014 17:35:00	124.58	41.10	36.43	1.930	19.90	1.891	21.626
5/9/2014 17:40:00	101.12	41.02	35.88	1.637	20.12	1.611	21.87
5/9/2014 17:45:00	100.31	41.09	36.80	1.565	19.37	1.605	21.057
5/9/2014 17:50:00	100.31	40.67	35.72	1.434	19.45	1.473	21.138
5/9/2014 17:55:00	100.31	40.02	34.88	1.386	19.82	1.401	21.545
5/9/2014 18:00:00	92.20	39.86	34.63	1.321	19.67	1.340	21.382
5/9/2014 18:05:00	75.97	39.19	34.09	1.193	19.60	1.217	21.301
5/9/2014 18:10:00	76.04	38.76	34.43	1.168	19.82	1.188	21.545
5/9/2014 18:15:00	74.45	38.77	34.92	1.027	19.45	1.079	21.138
5/9/2014 18:20:00	73.71	38.73	34.77	0.922	19.22	0.991	20.894
5/9/2014 18:25:00	78.27	38.46	34.78	0.904	19.45	0.965	21.138
5/9/2014 18:30:00	70.07	38.26	34.44	0.755	20.19	0.794	21.951
5/9/2014 18:35:00	56.05	38.24	34.21	0.672	20.27	0.715	22.033
5/9/2014 18:40:00	51.67	38.19	33.97	0.543	20.72	0.581	22.52
5/9/2014 18:45:00	50.96	37.81	33.76	0.437	20.79	0.481	22.602
5/9/2014 18:50:00	46.67	37.63	33.56	0.356	20.42	0.411	22.195
5/9/2014 18:55:00	40.28	37.22	32.67	0.288	19.97	0.350	21.707
5/9/2014 19:00:00	33.93	36.79	31.94	0.207	19.75	0.267	21.463
5/9/2014 19:05:00	27.50	36.31	31.41	0.115	19.30	0.164	20.976
5/9/2014 19:10:00	25.08	35.83	30.98	0.013	19.60	0.020	21.301
5/9/2014 19:15:00	24.32	35.30	30.78	0.000	18.77	0.000	20.407
5/9/2014 19:20:00	24.27	34.72	30.18	0.000	13.46	0.000	14.634
5/10/2014 7:20:00	24.36	29.28	25.99	0.000	20.05	0.000	21.789
5/10/2014 7:25:00	25.08	29.33	25.99	0.020	20.64	0.033	22.439
5/10/2014 7:30:00	25.08	29.40	26.20	0.092	19.00	0.137	20.65
5/10/2014 7:35:00	25.08	29.47	26.26	0.128	19.07	0.184	20.732
5/10/2014 7:40:00	25.08	29.56	26.41	0.181	18.92	0.246	20.569
5/10/2014 7:45:00	25.81	29.76	26.56	0.220	19.45	0.285	21.138
5/10/2014 7:50:00	25.08	29.85	26.47	0.270	19.90	0.329	21.626
5/10/2014 7:55:00	25.08	29.98	26.73	0.286	20.34	0.340	22.114
5/10/2014 8:00:00	25.84	30.13	26.82	0.352	20.34	0.405	22.114
5/10/2014 8:05:00	29.00	30.27	26.87	0.451	20.42	0.499	22.195
5/10/2014 8:10:00	31.72	30.45	26.94	0.499	21.09	0.536	22.927
5/10/2014 8:15:00	40.75	30.67	27.25	0.612	21.17	0.633	23.008
5/10/2014 8:20:00	48.72	30.91	27.73	0.787	21.62	0.771	23.496
5/10/2014 8:25:00	50.15	31.13	28.40	1.008	20.87	0.994	22.683
5/10/2014 8:30:00	59.86	31.52	28.99	1.224	20.94	1.179	22.764
5/10/2014 8:35:00	74.42	32.02	29.24	1.371	20.87	1.315	22.683
5/10/2014 8:40:00	84.35	32.55	29.25	1.495	21.02	1.413	22.846
5/10/2014 8:45:00	99.52	33.22	29.25	1.587	21.54	1.457	23.415
5/10/2014 8:50:00	121.80	33.90	29.98	1.663	21.32	1.540	23.171
5/10/2014 8:55:00	126.25	34.53	30.49	1.645	20.57	1.582	22.358
5/10/2014 9:00:00	125.39	35.27	30.86	1.608	20.79	1.532	22.602
5/10/2014 9:05:00	125.39	35.43	30.76	1.629	21.09	1.530	22.927
5/10/2014 9:10:00	127.67	35.65	30.87	1.728	21.92	1.559	23.821

5/10/2014 9:15:00	161.86	36.46	31.08	2.119	22.07	1.870	23.984
5/10/2014 9:20:00	174.76	37.14	31.60	2.266	21.02	2.086	22.846
5/10/2014 9:25:00	179.55	37.58	31.91	2.341	21.32	2.128	23.171
5/10/2014 9:30:00	194.35	37.90	32.17	2.599	21.47	2.333	23.333
5/10/2014 9:35:00	198.19	39.74	32.85	2.787	21.84	2.449	23.74
5/10/2014 9:40:00	192.02	40.71	32.75	2.835	20.72	2.620	22.52
5/10/2014 9:45:00	177.16	40.96	32.42	2.719	20.87	2.509	22.683
5/10/2014 9:50:00	220.21	41.40	32.96	3.250	21.17	2.947	23.008
5/10/2014 9:55:00	178.33	42.51	33.01	2.781	21.24	2.529	23.089
5/10/2014 10:00:00	300.17	42.96	33.99	3.989	20.79	3.655	22.602
5/10/2014 10:05:00	305.78	45.92	35.85	4.036	20.64	3.728	22.439
5/10/2014 10:10:00	405.56	47.87	36.48	4.727	20.27	4.427	22.033
5/10/2014 10:15:00	368.78	48.99	34.97	4.139	20.05	3.914	21.789
5/10/2014 10:20:00	359.17	49.45	35.69	4.195	20.27	3.916	22.033
5/10/2014 10:25:00	397.78	49.31	36.69	4.281	20.49	3.959	22.276
5/10/2014 10:30:00	341.96	46.65	34.15	3.739	20.49	3.465	22.276
5/10/2014 10:35:00	317.89	42.40	32.81	3.608	20.87	3.285	22.683
5/10/2014 10:40:00	385.35	42.75	34.36	4.523	20.57	4.155	22.358
5/10/2014 10:45:00	323.79	43.13	34.05	4.087	19.97	3.877	21.707
5/10/2014 10:50:00	197.61	45.24	34.99	2.630	19.90	2.532	21.626
5/10/2014 10:55:00	284.88	46.20	34.57	3.871	20.27	3.627	22.033
5/10/2014 11:00:00	359.70	47.49	35.46	4.873	20.42	4.517	22.195
5/10/2014 11:05:00	343.20	48.20	36.15	4.590	20.49	4.226	22.276
5/10/2014 11:10:00	378.44	49.80	37.42	5.038	19.60	4.841	21.301
5/10/2014 11:15:00	348.73	50.69	36.83	4.656	19.45	4.523	21.138
5/10/2014 11:20:00	320.52	52.05	36.14	4.429	19.30	4.330	20.976
5/10/2014 11:25:00	244.27	52.52	36.35	3.589	19.67	3.460	21.382
5/10/2014 11:30:00	288.39	51.83	34.74	4.128	20.05	3.881	21.789
5/10/2014 11:35:00	238.59	48.20	34.46	3.593	20.12	3.382	21.87
5/10/2014 11:40:00	422.39	46.84	35.67	5.705	20.64	5.206	22.439
5/10/2014 11:45:00	434.93	47.68	36.39	5.666	20.05	5.309	21.789
5/10/2014 11:50:00	358.68	48.60	35.90	4.735	20.05	4.472	21.789
5/10/2014 11:55:00	167.48	48.68	34.26	2.437	20.27	2.320	22.033
5/10/2014 12:00:00	181.81	47.64	34.59	2.978	19.90	2.835	21.626
5/10/2014 12:05:00	282.32	48.11	36.00	4.217	19.82	3.995	21.545
5/10/2014 12:10:00	336.19	47.11	35.64	4.780	19.30	4.636	20.976
5/10/2014 12:15:00	332.69	44.48	35.47	4.960	20.05	4.646	21.789
5/10/2014 12:20:00	281.75	43.40	34.36	4.287	20.34	3.952	22.114
5/10/2014 12:25:00	276.78	44.33	35.71	3.969	19.97	3.738	21.707
5/10/2014 12:30:00	218.32	45.72	35.45	3.489	19.82	3.325	21.545
5/10/2014 12:35:00	356.57	45.58	36.21	5.063	19.67	4.822	21.382
5/10/2014 12:40:00	398.19	47.88	38.10	5.625	20.42	5.162	22.195
5/10/2014 12:45:00	292.81	48.61	37.29	4.480	20.05	4.211	21.789
5/10/2014 12:50:00	341.49	47.35	35.96	4.938	19.90	4.671	21.626
5/10/2014 12:55:00	437.89	46.48	36.34	6.017	20.42	5.520	22.195
5/10/2014 13:00:00	378.67	48.34	36.24	5.250	19.82	4.983	21.545
5/10/2014 13:05:00	353.29	49.91	36.83	4.868	19.45	4.712	21.138
5/10/2014 13:10:00	224.30	46.94	34.96	3.396	19.90	3.242	21.626
5/10/2014 13:15:00	328.43	45.39	35.82	4.746	19.90	4.481	21.626
5/10/2014 13:20:00	481.03	45.41	36.57	6.148	20.34	5.663	22.114
5/10/2014 13:25:00	419.81	46.58	35.80	5.441	19.45	5.250	21.138
5/10/2014 13:30:00	462.71	44.22	35.29	5.626	19.30	5.466	20.976
5/10/2014 13:35:00	530.42	46.04	37.09	6.230	19.30	6.043	20.976
5/10/2014 13:40:00	412.63	46.18	35.98	5.215	19.67	4.985	21.382

5/10/2014 13:45:00	308.53	47.12	34.80	4.127	19.45	4.004	21.138
5/10/2014 13:50:00	329.04	47.11	36.02	4.539	20.12	4.265	21.87
5/10/2014 13:55:00	495.76	47.05	37.37	5.992	19.45	5.766	21.138
5/10/2014 14:00:00	490.57	47.93	37.54	5.734	19.60	5.483	21.301
5/10/2014 14:05:00	431.47	49.30	36.44	5.134	19.52	4.941	21.22
5/10/2014 14:10:00	433.00	49.43	37.10	5.253	19.90	4.963	21.626
5/10/2014 14:15:00	519.78	50.29	37.96	6.056	19.22	5.872	20.894
5/10/2014 14:20:00	404.24	52.14	37.62	4.888	19.37	4.719	21.057
5/10/2014 14:25:00	143.71	51.85	36.23	1.982	19.22	1.994	20.894
5/10/2014 14:30:00	127.67	50.35	35.57	2.125	19.45	2.092	21.138
5/10/2014 14:35:00	415.44	48.01	36.31	5.895	20.27	5.417	22.033
5/10/2014 14:40:00	423.36	46.74	37.42	5.215	20.19	4.804	21.951
5/10/2014 14:45:00	154.89	48.56	35.81	2.072	19.97	2.009	21.707
5/10/2014 14:50:00	88.15	46.55	34.42	1.366	19.67	1.379	21.382
5/10/2014 14:55:00	142.10	43.12	33.46	2.377	20.27	2.256	22.033
5/10/2014 15:00:00	395.16	43.45	35.89	5.013	20.57	4.601	22.358
5/10/2014 15:05:00	486.34	44.35	37.54	5.615	20.42	5.171	22.195
5/10/2014 15:10:00	498.59	43.91	36.28	5.680	19.82	5.373	21.545
5/10/2014 15:15:00	492.64	43.71	36.32	5.617	19.45	5.414	21.138
5/10/2014 15:20:00	360.67	45.64	36.88	4.285	20.34	3.981	22.114
5/10/2014 15:25:00	428.17	44.97	36.73	4.821	19.75	4.598	21.463
5/10/2014 15:30:00	229.49	44.19	34.88	3.007	19.90	2.881	21.626
5/10/2014 15:35:00	421.61	42.68	36.18	4.873	19.30	4.744	20.976
5/10/2014 15:40:00	320.27	45.32	37.17	3.666	19.52	3.537	21.22
5/10/2014 15:45:00	311.90	46.67	35.93	3.800	19.75	3.630	21.463
5/10/2014 15:50:00	417.95	46.17	37.16	4.769	19.52	4.578	21.22
5/10/2014 15:55:00	408.55	43.98	36.05	4.480	19.67	4.266	21.382
5/10/2014 16:00:00	399.02	43.25	37.34	4.255	19.60	4.078	21.301
5/10/2014 16:05:00	392.12	43.58	37.53	4.035	19.45	3.909	21.138
5/10/2014 16:10:00	377.59	45.66	38.59	3.958	19.45	3.829	21.138
5/10/2014 16:15:00	377.63	45.07	36.84	4.035	19.30	3.929	20.976
5/10/2014 16:20:00	364.32	44.51	38.04	3.898	19.22	3.815	20.894
5/10/2014 16:25:00	343.65	45.09	38.27	3.626	19.37	3.527	21.057
5/10/2014 16:30:00	326.00	42.81	36.11	3.429	19.45	3.337	21.138
5/10/2014 16:35:00	317.89	42.41	36.72	3.296	19.52	3.206	21.22
5/10/2014 16:40:00	325.27	43.01	37.66	3.351	19.60	3.241	21.301
5/10/2014 16:45:00	269.58	42.85	37.49	2.775	19.75	2.686	21.463
5/10/2014 16:50:00	304.84	42.33	36.16	3.152	20.57	2.920	22.358
5/10/2014 16:55:00	316.60	41.24	35.98	3.203	20.49	2.975	22.276
5/10/2014 17:00:00	279.54	40.54	35.87	2.679	20.12	2.558	21.87
5/10/2014 17:05:00	258.86	40.33	35.71	2.580	19.97	2.484	21.707
5/10/2014 17:10:00	245.76	40.16	36.52	2.449	20.19	2.346	21.951
5/10/2014 17:15:00	225.69	40.50	36.30	2.278	20.34	2.175	22.114
5/10/2014 17:20:00	219.62	40.30	36.47	2.178	20.19	2.099	21.951
5/10/2014 17:25:00	207.64	40.65	36.85	2.069	20.27	1.989	22.033
5/10/2014 17:30:00	200.62	40.41	36.80	1.922	19.97	1.892	21.707
5/10/2014 17:35:00	143.62	41.31	37.21	1.732	20.12	1.705	21.87
5/10/2014 17:40:00	55.17	41.16	36.43	1.109	20.05	1.132	21.789
5/10/2014 17:45:00	60.05	40.32	36.65	1.112	19.52	1.167	21.22
5/10/2014 17:50:00	53.10	40.33	36.90	1.173	19.07	1.238	20.732
5/10/2014 17:55:00	52.94	40.00	36.59	1.197	19.07	1.257	20.732
5/10/2014 18:00:00	53.84	39.61	36.35	1.155	19.22	1.210	20.894
5/10/2014 18:05:00	49.42	39.41	34.96	0.647	19.07	0.725	20.732
5/10/2014 18:10:00	50.15	38.92	35.34	0.892	19.22	0.958	20.894

5/10/2014 18:15:00	50.15	38.54	35.43	0.741	19.22	0.811	20.894
5/10/2014 18:20:00	50.15	38.16	35.42	0.730	19.30	0.800	20.976
5/10/2014 18:25:00	72.19	37.87	34.88	0.486	20.79	0.526	22.602
5/10/2014 18:30:00	63.39	37.63	34.60	0.453	20.87	0.493	22.683
5/10/2014 18:35:00	48.59	37.42	34.50	0.391	20.42	0.443	22.195
5/10/2014 18:40:00	47.87	37.12	33.76	0.345	20.12	0.403	21.87
5/10/2014 18:45:00	47.11	36.79	33.61	0.268	19.97	0.330	21.707
5/10/2014 18:50:00	35.26	36.62	33.46	0.215	19.52	0.279	21.22
5/10/2014 18:55:00	28.42	36.27	33.14	0.161	19.15	0.222	20.813
5/10/2014 19:00:00	25.08	35.91	32.31	0.108	19.00	0.159	20.65
5/10/2014 19:05:00	25.08	35.55	31.85	0.042	19.15	0.067	20.813
5/10/2014 19:10:00	25.08	35.31	31.81	0.000	19.67	0.000	21.382
5/10/2014 19:15:00	25.08	34.98	31.40	0.000	18.55	0.000	20.163
5/10/2014 19:20:00	25.08	34.51	30.97	0.000	16.75	0.000	18.211
5/10/2014 19:25:00	25.08	34.09	30.74	0.000	13.31	0.000	14.472

LIST OF PUBLICATIONS

A: Journals

1. **Ali M. Humada**, Mojgan Hojabri , Saad Mekhilef , Hussein M. Hamada, Solar cell parameters extraction based on single and double-diode models: A review, *Renewable and sustainable Energy Reviews*, **56**: 494-509. **ISI journal (impact factor 6.789**).

2. **Humada Ali M. ,** Mojgan Hojabria, Nowshad Amin, Mushtaq Najeeb Ahmed, Performance assessment of two photovoltaic plant technologies and based on tropical climatic conditions: Malaysia case study, *Energies and Buildings*, 119 (2016) 233–241. **ISI journal with impact factor 2.973 (Q1).**

3. **Humada Ali M. ,** Mojgan Hojabria, Nowshad Amin, Mushtaq Najeeb Ahmed, Performance Prediction of a Grid-connected Photovoltaic System in Tropical Climate Conditions Based on Modeling, *PLoS ONE*, 11(4): e0152766. doi:10.1371/journal.pone.0152766. **ISI journal with impact factor 3.234 (Q1).**

4. **Ali M. Humada**, Mojgan Hojabri, Mohd Herwan Bin Sulaiman, Hussein M Hamad, Mushtaq N Ahmed, Modeling and Charactersation of a Grid-Connected Photovoltaic System in Tropical Climate Conditions Based on Real Results: A Case Study in Malaysia, *Renewable and sustainable Energy Reviews*, (**Revision**).

5. **Ali M. Humada**, Mojgan Hojabri, Mohd Herwan Bin Sulaiman, Hussein M Hamad, Mushtaq N Ahmed, A Five Parameters PV Modeling, Extraction and Performance Evaluation Based on Experimental Data, *Solar Energy* (**Revision**).

6. **Ali M.Humada**, Hojabri, MojganMohamed, Mortaza BSulaiman, BinHerwan, Mohd and Dakheel, Taha Hamad. 2014. A Proposed Method of Photovoltaic Solar Array Configuration under Different Partial Shadow Conditions. *Advanced Materials Research*:pp. 307-311. (**Scopus)**

7. **Ali M. Humada**, Mojgan Hojabri, Mortaza B. Mohameda, 2013, Analysis of effect external parameters on the photovoltaic solar system and its characteristics, Wulfenia, 20 (12), 179-187.

8. **Ali M. Humada,** Hojabri, Mojgan, Mohamed Mortaza B., AL-Duliamy Mushtaq N Ahmed, Sulaiman Mohd Herwan Bin and Akorede, Mudathir Funsho. Reconfiguration Method Based on DC/DC Central Converter within Different Mismatch Conditions. : Int. Jou. of Eng. Sci. and Res. Tech. (IJESRT) Vol. 2, no. 12, (2013), p. 3634.

9. AL–Duliamy MNA, M Hojabri, bin Daniyal H, **Ali M. Humada,** Simulation of Regulated Power Supply for Solar Photo-Voltaic Model: Int. Jou. of Eng. Sci. and Res. Tech. (IJESRT) Vol. 2, no. 12, (2013), p. 3607.

10. **Humada Ali M.,** M Hojabri, MB Mohamed, A NEW METHOD OF PV RECONFIGURATION UNDER PARTIAL SHADOW CONDITIONS BASED

ON DC/DC CENTRAL CONVERTER. *International Journal of Renewable Energy Resources* 4 (2014) 49-53

11. **Humada Ali M** , Mojgan Hojabria, Mushtaq Najeeb Ahmed, A Review On Photovoltaic Array Behavior, Configuration Strategies And Models Under Mismatch, Conditions , Maxwell Scientific Publications, (Scopus) (Accepted).

12. Mushtaq Najeeb Ahmed, Mojgan Hojabria, **Humada Ali M** , Hamdan bin Daniyal, Maximum Power Prediction for PV System based on P&O Algorithm, Journal of Advanced & Applied Sciences (JAAS) Volume 03, Issue 04, Pages 113-118, 2015.

B: National and International Conferences

13. **Ali M**. **Humada**, Fahmi B. Samsuri, Hojabri MojganMohamed, Mortaza B, Sulaiman, BinHerwan, Mohd and Dakheel, Taha Hamad Dakheel. Modeling of Photovoltaic Solar Array under Different levels of partial shadow Conditions. 16th International Power Electronics and Motion Control Conference and Exposition, PEMC, September 2014. (IEEE explorer).

14. **Ali M. Humad**, Mojgan Hojabria, Mortaza B. Mohamed, Mushtaq Najeeb Ahmed. A method of enhancing extracted power and efficiency improvement of PV system operates under partial shadow conditions. *National Conference on Postgraduate Studies*, Universiti Malaysia PAHANG, Kuantan, Jan 2015.

15. **Ali M**. **Humada**, Mohd Herwan Bin Sulaiman, Mojgan Hojabri, Hussein M. Hamada and Mushtaq N. Ahmed. A REVIEW ON PHOTOVOLTAIC ARRAY BEHAVIOR, CONFIGURATION STRATEGIES AND MODELS UNDER MISMATCH CONDITIONS. *International Conference On Electrical, Control And Computer Engineering* (2015), 26–28 October, Gambang Resort Hotel, , Gambang, Kuantan, Pahang, Malaysia.

C: **National and International Exhibitions**

16. **Ali M Humada**, Mojgan Hojabri, Mortaza Bin Mohamed. 2013. Maximum Power Point Tracking Techniques of Solar System Based on Mismatch weather conditions. *Creation, Innovation, Technology & Research Exposition* (CITReX), 27^{th}–28^{th} March, Universiti Malaysia Pahang, Gambang, Pahang, Malaysia (Silver Medal).

17. **Ali M Humada**, Mojgan Hojabri, Mortaza Bin Mohamed. 2014. Photovolatic Solar Array Modeling and Energy Extraction Improvement under Shadow Conditions. *Creation, Innovation, Technology & Research Exposition* (CITReX), 5^{th}–6^{th} March, Universiti Malaysia Pahang, Gambang, Pahang, Malaysia (Silver Medal).